

For Reference

NOT TO BE TAKEN FROM THIS ROOM

Ex LIBRIS
UNIVERSITATIS
ALBERTAENSIS





Digitized by the Internet Archive
in 2024 with funding from
University of Alberta Library

<https://archive.org/details/Solinas1973>

T H E U N I V E R S I T Y O F A L B E R T A

RELEASE FORM

NAME OF AUTHOR ..Marco Solinas.....

TITLE OF THESIS...The Vibrational Spectra of Hexamethylene-
.....tetramine and its Clathrate Hydrate.....
.....

DEGREE FOR WHICH THESIS WAS PRESENTED.....Ph.D......

YEAR THIS DEGREE GRANTED.....1973.....

Permission is hereby granted to THE UNIVERSITY OF
ALBERTA LIBRARY to reproduce single copies of this
thesis and to lend or sell such copies for private,
scholarly or scientific research purposes only.

The author reserves other publication rights, and
neither the thesis nor extensive extracts from it may
be printed or otherwise reproduced without the author's
written permission.

THE UNIVERSITY OF ALBERTA

THE VIBRATIONAL SPECTRA OF HEXAMETHYLENETETRAMINE AND ITS
CLATHRATE HYDRATE

BY



MARCO SOLINAS

A THESIS

SUBMITTED TO THE FACULTY OF GRADUATE STUDIES AND RESEARCH

IN PARTIAL FULFILMENT OF THE REQUIREMENTS FOR THE DEGREE

OF

DOCTOR OF PHILOSOPHY

DEPARTMENT OF CHEMISTRY

EDMONTON, ALBERTA

SPRING 1973

THE UNIVERSITY OF ALBERTA
FACULTY OF GRADUATE STUDIES AND RESEARCH

The undersigned certify that they have read,
and recommend to the Faculty of Graduate Studies and
Research, for acceptance, a thesis entitled
'THE VIBRATIONAL SPECTRA OF HEXAMETHYLENETETRAMINE AND
ITS CLATHRATE HYDRATE'
submitted by Marco Solinas in partial fulfilment of the
requirements for the degree of Doctor of Philosophy.

ABSTRACT

The infrared spectra of polycrystalline hexamethylenetetramine- h_{12} and $-d_{12}$ at 300 and 100°K have been recorded between 200 and 4000 cm^{-1} . The Raman spectra of hexamethylenetetramine- h_{12} and $-d_{12}$ in polycrystalline, single crystal and solution form have been recorded at room temperature between 50 and 4000 cm^{-1} . The existing vibrational assignments for hexamethylenetetramine- h_{12} have been modified, and the vibrational spectra of hexamethylenetetramine- d_{12} have been assigned for the first time. The assignment for the two molecules have been shown to be mutually consistent by a normal coordinate analysis on hexamethylenetetramine- h_{12} and $-d_{12}$ and an assignment based on these calculations is presented. Peaks due to the longitudinal optic components of the F_2 modes have been identified in the Raman spectra of hexamethylenetetramine- h_{12} and $-d_{12}$, and the dielectric constants of the two isotopic species have been determined using the Lyddane-Sachs-Teller relation.

The infrared spectra of the hydrates and deuterates of hexamethylenetetramine- h_{12} and $-d_{12}$ at 100°K were studied between 10 and 4000 cm^{-1} . The peaks due to the intramolecular vibrations of hexamethylenetetramine are assigned by comparison with the spectra of pure, solid hexamethylenetetramine, and the splitting of the F_2 modes

due to the reduced symmetry in the hydrate is discussed.

The spectral features due to intramolecular and intermolecular vibrations of the water molecules are discussed. Three peaks due to $\nu_{OH}(HDO)$ and $\nu_{OD}(HDO)$ were seen and their assignment is discussed in relation to the nature of the proton acceptor. The effect of intermolecular and intramolecular coupling on the shape of the $\nu_{OH}(H_2O)$ and $\nu_{OD}(D_2O)$ bands is shown to be much smaller than in ice I and this has allowed the features of the $\nu_{OH}(H_2O)$ and $\nu_{OD}(D_2O)$ bands to be assigned. The $\nu_R(H_2O)$ and $\nu_R(D_2O)$ bands were found to be richer in detail than the corresponding bands in disordered ice phases. The effect of the partial order of the water molecules on the behaviour of one of the components of the $\nu_R(H_2O)$ band is discussed.

The far infrared spectrum is discussed in terms of the theory of translational vibrations of orientationally disordered solids. The validity of the theory for partially disordered solids is experimentally established. One peak is assigned to a rotational vibration of the hexamethylenetetramine molecule. Three more are found to arise from modes to which the translational vibrations of hexamethylenetetramine contribute.

Acknowledgements

I wish to express my gratitude to Dr. J.E. Bertie whose guidance and advice made completion of this work possible.

The cooperation of various members of the Chemistry Department was invaluable. The staff of the electronics and machine shops provided prompt and competent assistance in building and maintaining the apparatus.

Students and post-doctoral fellows of Dr. Bertie's group provided the opportunity for stimulating discussions.

Mr. S. Burnie of the Department of Geology assisted in the refractive index measurements.

The patience and understanding of my wife helped and inspired me greatly during all stages of this work.

Finally I wish to acknowledge the financial assistance provided by the National Research Council of Canada and by the University of Alberta.

TABLE OF CONTENTS

	Page
Abstract	iv
Acknowledgements	vi
List of Tables.....	x
List of Figures.....	xii
<u>Chapter I. Introduction</u>	1
I.1 General Introduction	1
I.2 Vibrations in Crystals	1
I.3 The Hydrate of Hexamethylenetetramine..	17
I.4 The Structure and Spectra of the Ice Polymorphs.....	22
I.5 The Structure and Spectra of Hexamethylenetetramine	32
I.6 Aims of This work	37
<u>Chapter II. Experimental</u>	41
II.1 Chemicals and Single Crystals	41
II.2 Preparation of the Hydrate	42
II.3 Preparation of the Infrared and Raman Samples	44
II.4 Infrared Instrumentation	52
II.5 Temperature of the Infrared Samples....	54
II.6 Raman Instrumentation	56
II.7 X-Ray Methods.....	57

<u>Chapter III. The Vibrational Spectra of</u>	
<u>Hexamethylenetetramine-h₁₂ and -d₁₂..</u>	59
III.1 General.....	59
III.2 Results for HMT-h ₁₂	64
III.3 Results for HMT-d ₁₂	86
III.4 Discussion and Assignment	
for HMT-h ₁₂	100
III.5 The Transverse and Longitudinal	107
Components of the Infrared Active	
Modes of Hexamethylenetetramine-h ₁₂ ...	107
III.6 Discussion and Assignment	
for HMT-d ₁₂	114
III.7 TO-LO Splitting of HMT-d ₁₂	119
III.8 Normal Coordinate Analysis.....	122
<u>Chapter IV. Infrared Spectra of Hexamethylenetetramine</u>	
<u>Hydrate in Four Isotopic Modifications</u>	142
IV.1 General.....	142
IV.2 The Mid-Infrared Spectra.....	150
IV.3 The Far-Infrared Spectra.....	183
IV.4 X-Ray Results.....	187
<u>Chapter V. Discussion of the Infrared Spectra of</u>	
<u>Hexamethylenetetramine Hydrate.....</u>	192
V.1 The Mid-Infrared Absorptions by the Water	
Molecules.....	192

	Page
V.2 The Intramolecular Vibrations of Hexamethylenetetramine.....	204
V.2.1 Hexamethylenetetramine- h_{12}	208
V.2.2 Hexamethylenetetramine- d_{12}	215
V.2.3 Discussion.....	221
V.3 The Far-Infrared Spectra.....	225
<u>Conclusion</u>	232
<u>References</u>	235
<u>Appendix I</u>	246
<u>Appendix II</u>	254

LIST OF TABLES

<u>Table</u>		<u>Page</u>
1	Representations formed by the internal coordinates of HMT under the point group T_d .	61
2	Infrared frequencies for solid HMT- h_{12}	68
3	Raman frequencies for solid HMT- h_{12}	80
4	Raman frequencies for HMT- h_{12} in aqueous solution.....	83
5	Infrared and Raman frequencies and assignment for solid HMT- d_{12}	94
6	Raman frequencies for HMT- d_{12} in aqueous solution.....	98
7	Relation between $\nu_{LO}^2 - \nu_{TO}^2$ and the absorption intensities of the F_2 modes of HMT- h_{12}	112
8	Relation between $\nu_{LO}^2 - \nu_{TO}^2$ and the absorption intensities of the F_2 modes of HMT- d_{12}	121
9	Internal coordinates for HMT.....	124
10	Force constants for HMT.....	131
11	Potential energy distribution for HMT- h_{12} ...	132
12	Potential energy distribution for HMT- d_{12} ...	133
13	Experimental and calculated symmetry coordinate description of the normal modes of HMT- h_{12} ..	136
14	Experimental and calculated symmetry coordinates description of the normal modes of HMT- d_{12} ..	139

<u>Table</u>	<u>Page</u>
15 The frequencies of the features in the mid-infrared spectra of HMT hydrate in four isotopic modifications.....	159
16 Frequencies of the ν_{OH} (HDO) and ν_{OD}) HDO vibrations.....	182
17 Far-infrared frequencies for the hydrate of HMT in four isotopic modifications.....	185
18 Diffraction pattern of HMT-hydrate at 120°K.	190
19 Structural parameters of HMT hydrate at 253 and 120°K.....	191
20 Correlation between the frequencies of pure HMT- h_{12} and the frequencies of HMT- h_{12} in the hydrate.....	209
21 Correlation between the frequencies of pure HMT- d_{12} and the frequencies of HMT- d_{12} in the hydrate.....	216
22 Splitting and shifts of the components of the F_2 modes in the spectra of HMT hydrate.....	224
23 G matrix for HMT- h_{12}	246
24 G matrix for HMT- d_{12}	250
25 Symmetry coordinates for HMT.....	254

LIST OF FIGURES

<u>Figure</u>		<u>Page</u>
1	The cage structure of HMT hydrate.....	19
2	The HMT molecule in the crystal.....	34
3	The sample cell used for the infrared spectra.....	45
4	Apparatus for making KBr pellets.....	48
5	Apparatus for making low temperature mulls..	50
6	Scattering geometry used in the single crystal Raman study.....	63
7	Infrared spectrum of HMT-h ₁₂	66
8	The intense absorptions in the infrared spectrum of HMT-h ₁₂	67
9	Raman spectrum of a polycrystalline sample of HMT-h ₁₂	76
10	Raman spectrum of a saturated aqueous solution of HMT-h ₁₂	77
11	Raman spectrum of a single crystal of HMT-h ₁₂	78
12	Raman spectrum of a single crystal of HMT-h ₁₂	79
13	Infrared spectrum of HMT-d ₁₂	87
14	The intense absorptions in the infrared spectrum of HMT-d ₁₂	88

<u>Figure</u>	<u>Page</u>
15 Raman spectrum of a polycrystalline sample of HMT-d ₁₂	89
16 Raman spectrum of a saturated aqueous solution of HMT-d ₁₂	90
17 Raman spectrum of a single crystal of HMT-d ₁₂	91
18 Raman spectrum of a single crystal of HMT-d ₁₂	92
19 Raman spectrum of a single crystal of HMT-d ₁₂	93
20 Description of methylenic motions.....	105
21 Raman spectrum of a single crystal of HMT-h ₁₂	111
22 Plot of ($\nu_{LO}^2 - \nu_{TO}^2$) vs. the relative intensities of the infrared bands for HMT-h ₁₂ and -d ₁₂ ..	113
23 Raman spectrum of a single crystal of HMT-d ₁₂	120
24 The $\nu_{OH}(H_2O)$ band for a dried and an undried Sample of HMT-h ₁₂ ·6H ₂ O.....	143
25 The $\nu_{OD}(D_2O)$ band for a dried and an undried sample of HMT-h ₁₂ ·6D ₂ O.....	144
26 The mid-infrared spectra of HMT-h ₁₂ hydrate in three mulling agents.....	151
27 The mid-infrared spectra of HMT-h ₁₂ deuterate in the three mulling agents.....	152

<u>Figure</u>	<u>Page</u>
28 The mid-infrared spectra of HMT-d ₁₂ hydrate in three mulling agents.....	153
29 The mid-infrared spectra of HMT-d ₁₂ deuterate in three mulling agents.....	154
30 The mid-infrared spectrum of HMT-h ₁₂ ·6H ₂ O...	155
31 The mid-infrared spectrum of HMT-h ₁₂ ·6D ₂ O...	156
32 The mid-infrared spectrum of HMT-d ₁₂ ·6H ₂ O...	157
33 The mid-infrared spectrum of HMT-d ₁₂ ·6D ₂ O...	158
34 The ν _R band of HMT-h ₁₂ hydrate and of a sample of HMT-h ₁₂ hydrate containing 10% of HDO.....	173
35 The ν _R band of HMT-h ₁₂ deuterate and of a sample of HMT-h ₁₂ deuterate containing 10% of HDO.....	175
36 The ν _R band of HMT-d ₁₂ hydrate and of a sample of HMT-d ₁₂ hydrate containing 10% of HDO.....	176
37 Absorptions by ν _{OH} (HDO) and ν _{OD} (HDO) in HMT-h ₁₂ deuterate and hydrate containing 10% of HDO.....	181
38 Far-infrared spectra of HMT-h ₁₂ hydrate and deuterate and of HMT-d ₁₂ hydrate and deuterate.....	184

Chapter I. Introduction.

I.1 General Introduction.

The subjects of this thesis are the infrared and Raman spectra of hexamethylenetetramine- h_{12} and d_{12} (hereafter referred to as HMT- h_{12} and HMT- d_{12} respectively) and the infrared spectra of the hydrates of HMT- h_{12} and of HMT- d_{12} . In Section I.2 the basic principles of vibrations in crystals and their interaction with light are presented and the terms to be used later are defined. In Section I.3 the previous work on HMT hydrate is reviewed, and in Section I.4 the structures and vibrational spectra of the polymorphs of ice are discussed because the interpretation of the spectra of the hydrate draws heavily on the information gained from the spectra of the ices. In Section I.5 the previous work on the structure and vibrational spectra of HMT is reviewed. The aims of the present study are presented in Section I.6.

I.2 Vibrations in Crystals.

For the purpose of the following discussion, the symmetry elements of a crystal can be regarded as dividing into two types. One type is derived from the translational symmetry of the crystal and the second type is based on the proper or improper rotational symmetry elements (1). Because of the translational symmetry, vibrations in a crystal are usually described as displacement waves propagating through

the crystal with characteristic wavelengths and frequencies (2,3). In the directions of the axes of the Wigner-Seitz cell, which is a primitive unit cell defined in a specific way (1), the wavelengths can take certain (2,3) values between the dimension of the crystal $N_i t_i$ and twice the primitive translation $2t_i$, where N_i is the number of cells in the direction i and t_i is the primitive translation in the same direction (2,3). Usually the wave-vector of a vibration is used instead of its wavelength to describe its spatial periodicity, the direction of the vector being the propagation direction of the vibration wave, and the magnitude being the reciprocal of its wavelength (2).

If nN atoms are present in a crystal, where n is the number of atoms per unit cell and N is the number of unit cells in the crystal, the crystal has $3nN$ degrees of freedom. $3nN-3$ of these are vibrations, characterized by the fact that the center of mass of the crystal does not move during the motion and the remaining three are pure translations of the whole crystal. A graph on which the frequencies of the vibrations are plotted against their wave-vector is called a dispersion curve diagram. One such graph must be made for each propagation direction. For each value of the wave-vector there are $3n$ frequencies and thus there are $3n$ curves or branches on the dispersion curve diagram. Three of these branches have zero frequency at zero wave-vector, corresponding to the three pure translations of the crystal and are called the acoustic branches. The remaining

$3n-3$ branches have a finite frequency when the wave-vector is zero and are called optic branches. The dispersion curves can be calculated, to some approximation and with empirical help, from theoretical considerations and can be measured from inelastic neutron scattering experiments on single crystals. From the dispersion curves the density of states curve can be calculated and this curve yields the number of vibrations per unit interval of frequency.

If m p-atomic and s monoatomic species are present in a unit cell, $3m$ branches originate from rotational vibrations, $m(3p-6)$ branches are due to intramolecular vibrations and $3(m+s)$ branches, three of which are acoustic branches, are due to translational vibrations. The translational and rotational vibrations are often called intermolecular or lattice or external vibrations. The frequencies of the intermolecular vibrations are greatly dependent on the wave-vector, while those of the intramolecular vibrations are much less dependent on it.

From the periodic property of vibrations in crystals a very important set of selection rules results. These are usually called the wave-vector selection rules. It can be shown (4-6) that the interaction energy over the whole crystal between an electromagnetic wave and a displacement wave is zero unless the two waves have the same wavelength and propagate in the same direction. Therefore, in order for a vibration to be infrared active, the two waves must

have the same wave-vector i.e. $\underline{k}_l = \underline{k}_v$, where \underline{k}_l is the wave-vector of the light and \underline{k}_v is the wave-vector of the displacement wave. The wavelength of infrared light is of the order of $10,000 \text{ \AA}^\circ$, which is much greater than the size of normal unit cells. Therefore for crystals with short range forces, vibrations with $\underline{k}_l = \underline{k}_v$ have essentially the same frequencies as those with $\underline{k}_v = 0$. In the latter the displacements occurring in one unit cell are duplicated in all other cells, so one need only consider the vibrations in one unit cell to study the vibrations active in absorption. This is an approximation, but the only evidence identified to date against its validity is the fact that, in finite crystals, the longitudinal optic (LO) modes can appear in the infrared spectrum as well as the transverse optic (TO) modes. In infinite crystals only the TO modes, whose dipole moment change is parallel to the electric vector of the light, are infrared active, while the LO modes, whose dipole moment derivative is perpendicular to the electric vector of the light, are infrared inactive.

The analogous wave-vector selection rule for the Raman effect is $\underline{k}_v = \underline{k}_i - \underline{k}_s$, where \underline{k}_v is the wave-vector of the vibration, \underline{k}_i is the wave-vector of the incident light and \underline{k}_s is the wave-vector of the scattered light (6). \underline{k}_i and \underline{k}_s have magnitudes of the order of 10^{-4} \AA^{-1} , as does the difference between them, i.e. \underline{k}_v . Thus the wavelength of the Raman active vibrations is much greater than the unit

cell size, and for vibrations determined only by short range forces, the approximate rule $\underline{k}_v = 0$ can be used. For both infrared and Raman spectra these selection rules mean that the number of vibrations active as fundamental transitions is of the order of the number of atoms in one unit cell, rather than the number of atoms in the crystal.

A complication arises in the present work from the fact that the wave-vector of Raman active vibrations is not exactly zero. Vibrations that are triply degenerate at zero wave-vector and absorb and Raman-scatter light are not, in fact, triply degenerate when $\underline{k}_v \neq 0$. Long range forces, arising from the dipole moment change accompanying these vibrations, raise the frequency of the longitudinal mode above that of the doubly degenerate transverse mode which is simply due to mechanical forces in the crystal (3,4,7,8). Both the longitudinal and transverse modes are Raman active, and a doublet is seen in the Raman spectrum, provided that the frequencies of the LO and TO modes are sufficiently different to be resolved, while only a single peak is seen in the infrared spectrum (Section III. 5).

The wave-vector selection rules are not sufficient to determine whether a vibration is infrared or Raman active. Many vibrations with zero wave-vector do not cause the dipole moment or polarizability change that is required for infrared or Raman activity, respectively. To determine which vibrations do cause such changes, the vibrations of one unit cell must be analyzed using group theoretical methods. Two

approaches have been proposed to carry out a group theoretical analysis of the vibrations in a crystal. Halford (9) developed the site group approach; the factor group approach was originally proposed by Bhagavantam and Venkatarayudu (10,11,25) and was modified by Hornig (12) and by Winston and Halford (13). Both methods require a knowledge of the symmetry of the sites occupied by all species present in the crystal. The site group is the group formed by those symmetry elements which leave the site invariant. The site group of each species can be found, if a detailed crystal structure is known, by inspection of the International Tables for X-ray Crystallography (14). If the site group symmetry is not known for all species in the crystal, it can sometimes be correctly deduced from the fact that the site group must be a subgroup of the space group and of the molecular point group, and that the centers of mass of equivalent species present in the crystal must occupy complete sets of sites of a given symmetry. But one must know the space group and the number of formula units per unit cell before attempting this.

The basic assumption of the site group analysis is that only negligible interaction takes place between the vibrations of different molecules in a unit cell. The irreducible representations of the internal modes of a molecule or ion under the site group can be determined by standard methods (15). Alternatively, if the irreducible represen-

tations of the vibrations under the point group of the free species are known, the irreducible representations under the site group can easily be derived from correlation tables (15), which correlate the irreducible representations under one group with those under its subgroups. It must be emphasized that the site group analysis is an approximation of limited utility. It neglects the dynamical intermolecular coupling in the unit cell. It is also unable to analyze the intermolecular vibrations, therefore the site group analysis should be regarded only as a first step in the factor group analysis.

The term 'factor group analysis' is an unfortunate one, although very widely used, because it implies that the factor group is used in the analysis, whereas it is the unit cell group that is used whenever a meaningful distinction exists. The term arose from inconsistencies in the definition of the factor group and of the unit cell group that have recently been clarified (16,17). The factor group is usually defined as "the group formed by the cosets of the invariant subgroup of pure translations in the space group" (16). The invariant subgroup of pure translations is formed by the infinite (for an infinite crystal) number of elements which are symbolized by (E/t) . This symbolism is due to Koster (18), and t represents the infinite combinations of primitive translations and (E/t) represents the collection of operations defined as the identity operation followed by

one of the translations. The cosets of the group of primitive translations are given by $(E/t)(R_1/t')$, $(E/t)(R_2/t')$, ..., $(E/t)(R_n/t')$, where $R_1, R_2 \dots R_n$ are the proper and improper rotational symmetry elements in the space group and t' represents one element of the collection t . It is clear that the factor group is a group whose elements each contain an infinite number of elements and is of theoretical rather than practical significance in the analysis of vibrations (16,17).

The unit cell group is defined as the group formed by the elements of the space group modulo any combination of primitive translations (16,19,20). That is, if the elements of the space group are (R_1/t) , (R_2/t) , ... (R_n/t) , where R_1, R_2, \dots, R_n and t have the same meaning as above, the unit cell group is defined as the group formed by the elements (R_1/O) , (R_2/O) , ... (R_n/O) . The unit cell group is isomorphous with one of the 32 crystallographic point groups and with the factor group. The irreducible representations formed by the vibrations in a crystal can thus be determined from a knowledge of the occupied sites simply by using the character tables for the point group of the crystal class, or by using the tables which correlate the irreducible representations under the site group with those under the point group of the crystal class. Either of these procedures is commonly called factor group analysis, or, less commonly, unit cell group analysis.

The term unit cell group analysis is preferable to the term factor group analysis and will be used throughout this thesis for the following reason. When one constructs symmetry coordinates, which are symmetry-adapted linear combinations of the displacements of each molecule, for the unit cell, one must examine the relation between individual symmetry elements in one unit cell and the atomic or molecular units in the unit cell. These individual symmetry elements form the unit cell group, not the factor group, in which each element contains an infinite number of symmetry operations.

For non-symmorphic space groups (those containing screw axes and glide planes) some of the symmetry elements involve a sub-primitive translation. In such cases the unit cell group contains admixtures of elements of the type (R_i/O) with those of the type $(R_i/(a/2))$, and only forms a group modulo the appropriate primitive translations. That is, any symmetry operation which transforms the i^{th} site in one unit cell into the k^{th} site in a neighboring cell is regarded as transforming it to the k^{th} site in the original cell.

Two methods are available to carry out a unit cell group analysis of the vibrations in a crystal. The original method is due to Bhagavantam and Venkatarayudu (10,11,25). In this method the number of atoms unshifted by a given symmetry operation is multiplied by the con-

tribution for the operation (these values have been tabulated (25)). An atom is considered unshifted if the effect of the symmetry operation is to shift it into an equivalent position in any unit cell of the crystal. This procedure, which is analogous to the point group analysis of an isolated molecule, gives the characters of the reducible representations for all vibrations of zero-wavevector in the crystal. This reducible representation can be reduced in the usual (15) way to give the total irreducible representation Γ_{total} . The representation formed by the translational vibrations, $\Gamma_{\text{trans.}}$, is obtained by applying the same methods to the translational displacements of all species in the crystal. The representation, $\Gamma_{\text{rot.}}$, formed by the rotational vibrations is obtained by applying the same procedure to the rotational displacements of the polyatomic species. Finally, the representations of the intramolecular vibrations can be obtained by subtracting $\Gamma_{\text{trans.}}$ and $\Gamma_{\text{rot.}}$ from Γ_{total} .

This method is rather cumbersome because it is often difficult to visualize the effect of all symmetry operations on all particles in a unit cell. The most commonly used method is the correlation method (12,13). The representations formed by all free species under their own point group are first obtained. Next, the representations under the site group are obtained by inspection of the correlation tables (15). This step amounts to carrying out a

site group analysis. Finally, the representations under the unit cell group can be obtained by inspection of the same correlation tables. Although some good presentations of the method are available (21-24), the procedure will be illustrated by carrying out a unit cell group analysis on the tetragonal phase of adamantane.

Adamantane belongs to the point group T_d (26) and, in its low temperature modification, crystallizes in the space group $P\bar{4}2_1c, D_{2d}^4$, with two molecules in the unit cell (27). The center of gravity of each adamantane molecule occupies a site of symmetry S_4 (27,14). Under the molecular point group T_d , the intramolecular vibrations of adamantane form the representation $5A_1 + A_2 + 6E + 7F_1 + 11F_2$ (15). The translational degrees of freedom form the representation F_2 and the rotational degrees of freedom form the representation F_1 . The following correlation is therefore obtained for all possible vibrations of the two molecules in the tetragonal unit cell.

	Molecular point group	Site group	Unit Cell group
	Td	S_4	D_{2d}
Inter-molecular	Intra-molecular		
$2F_1$ (R)	$10A_1$		$19 A_1$ (1R)
	$2A_2$	A	$19 A_2$ (1R)
	$12E$	B	$19 B_1$ (1T)
	$14F_1$	E	$19 B_2$ (1T)
$2F_2$ (T)	$22F_2$		$40 E$ (2R + 2T)

The symbols in brackets designate the number of rotational (R) and translational (T) vibrations in each representation. Therefore, the above representation can be broken down as follows:

$$\begin{aligned}\Gamma_{\text{int.}} &= 18A_1 + 18A_2 + 18B_1 + 18B_2 + 36E \\ \Gamma_{\text{trans.}} &= B_1 + B_2 + 2E \\ \Gamma_{\text{rot.}} &= A_1 + A_2 + 2E\end{aligned}$$

Three of the six translational vibrations correspond to all molecules in the crystal translating in phase in the three crystallographic directions. These are the three zero-frequency, zero-wave-vector, acoustic modes. They are not genuine vibrations, and their representation, which is the representation, $B_2 + E$, of the three translational unit vectors, should be subtracted from the total representation.

The representations formed by the genuine translational vibrations are therefore:

$$\Gamma_{\text{trans.}} = B_1 + E$$

An inspection of the character table for the point group D_{2d} indicates (15,28) that the B_2 and E vibrations are active in the infrared, while the A_1 , B_1 , B_2 and E vibrations are active in the Raman effect.

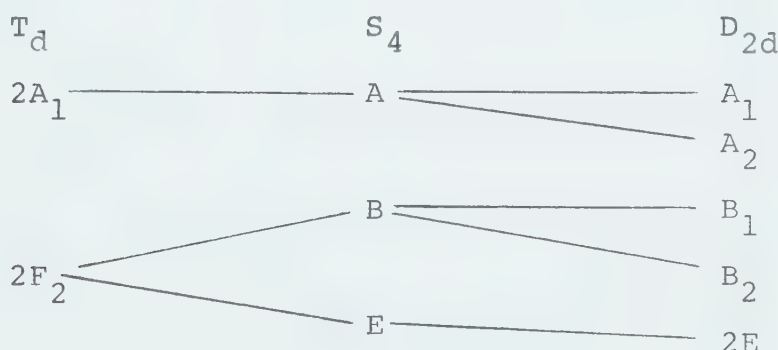
The representations formed by symmetrically complete sets of internal coordinates can also be obtained by the same method. The representations formed by the internal coordinates of adamantane under the point group

T_d are given below:

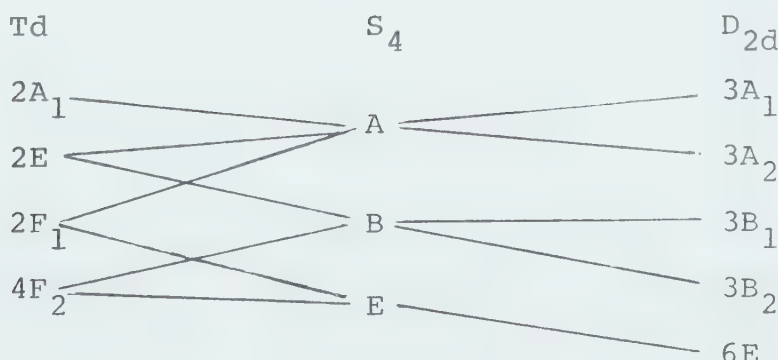
C-H stretch	$1A_1$	$+1F_2$
CH_2 stretch	$1A_1$	$+1E+1F_1+2F_2$
C-H deformation		$1E \quad 1F_1+1F_2$
CH_2 deformation	$1A_1$	$+1E \quad +1F_2$
CH_2 wag		$1F_1+1F_2$
CH_2 twist		$1A_2+1E+1F_1$
CH_2 rock		$1F_1+1F_2$
C-C stretch	$1A_1$	$+1E+1F_1+2F_2$
C-C-C deformation	$1A_1$	$+1E+1F_1+2F_2$

These representations can be correlated to the representations in the point group D_{2d} in the following way:

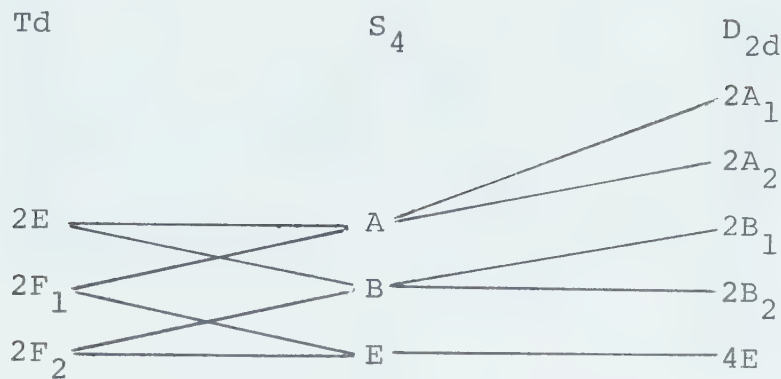
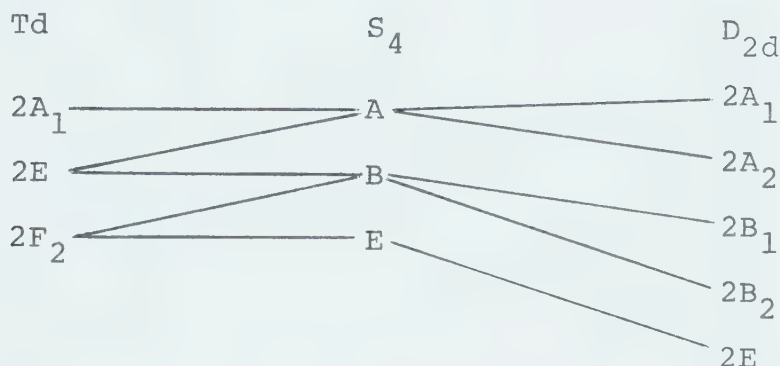
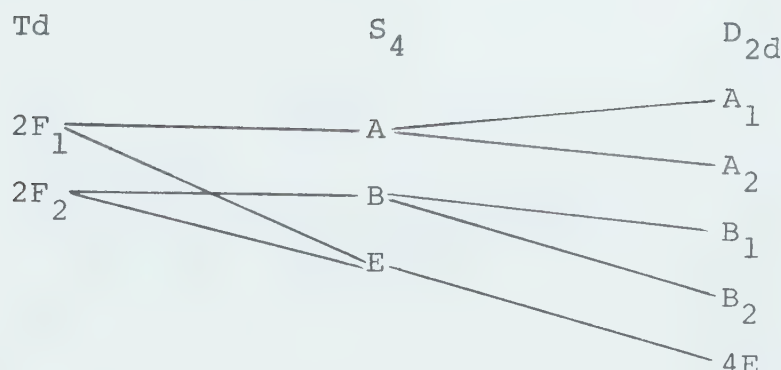
C-H stretches



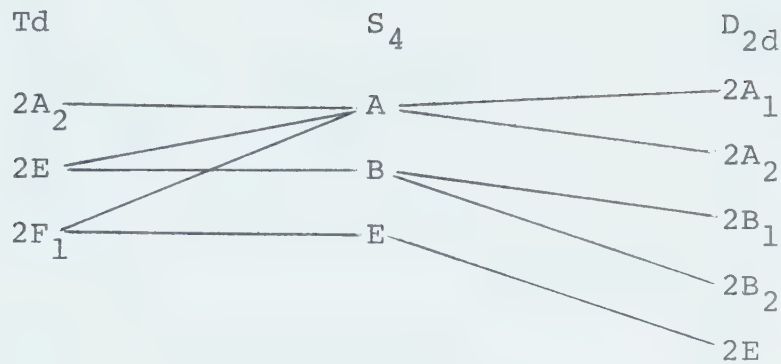
CH_2 stretch



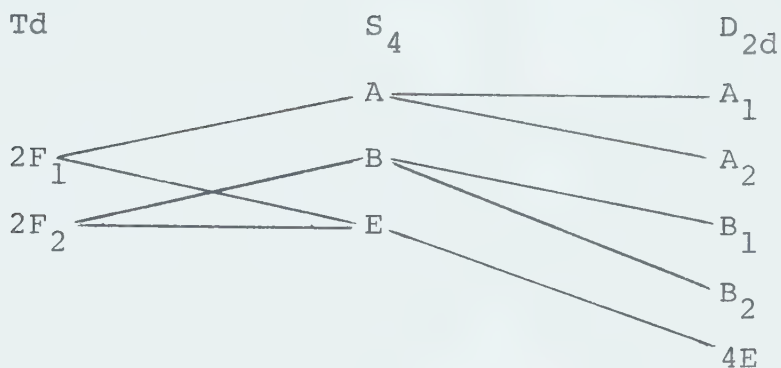
C-H deformation

CH₂ deformationCH₂ wag

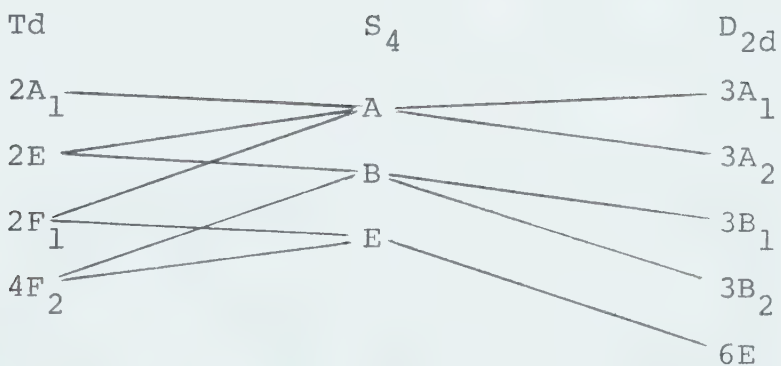
CH_2 twist



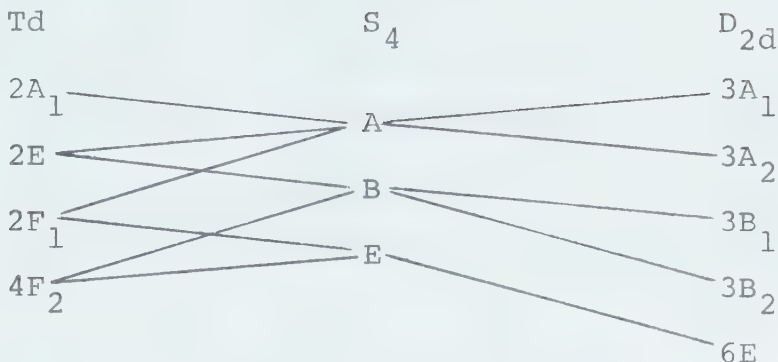
CH_2 rock



C-C stretch



C-C-C deformation



Thus, the infrared spectrum of the low temperature form of solid adamantane should contain three peaks due to the \equiv C-H stretch, nine due to the CH_2 stretch, six due to the \equiv C-H deformation, four due to the CH_2 deformation, five due to the methylenic wag, four due to the methylenic twist, five due to the methylenic rock, and eighteen due to the ring vibrations. In the Raman spectrum one should see five peaks due to the \equiv C-H stretch, fifteen peaks due to the CH_2 stretch, ten peaks due to the \equiv C-H deformation, eight peaks due to the $\equiv\text{CH}_2$ deformation, seven peaks due to the methylenic wag, eight peaks due to the methylenic twist, seven peaks due to the methylenic rock and 30 peaks due to the ring modes.

The discussion in this section has considered the activity of vibrations for fundamental transitions (29), and the strict wave-vector selection rules usually lead to the observation of sharp peaks arising from these transitions. The wave-vector selection rules are not so effective for combination transitions, in which more than one vibration changes its state of excitation and these tran-

sitions often lead to broader peaks than do fundamental transitions. The discussion has also been in terms of classical vibrations. This is valid, for the topic discussed, in the harmonic approximation because of the separability of the wave equation if the variables are normal coordinates.

I.3 The Hydrate of Hexamethylenetetramine.

Hexamethylenetetramine ($C_6H_{12}N_4$) has long been known to form a hydrate which was independently discovered by Delépine (30) and by Cambier and Brochet (31) in 1895. Delépine observed that long transparent crystals grow from a saturated aqueous solution of HMT kept at about 0°C . The crystals were found to melt with decomposition at 13.5°C . A white powder precipitated once the crystals were decomposed. The product of the decomposition was dried over sulphuric acid at -3°C and was found to consist of 44.12% water and 55.88% of dry residue. Cambrier and Brochet made essentially the same observations, but found that their crystals contained 43.50% of water and 56.50% of dry residue. The crystals were found to effloresce when they were kept in a dry atmosphere at -4 to -5°C . The conclusion common to both works was that a hydrate was formed, having the composition $C_6H_{12}N_4 \cdot 6H_2O$. This composition requires 56.45% of HMT and 43.55% of H_2O .

The phase diagram of the hydrate was determined by Evrard (32) who found the hydrate to melt with decom-

position at 13.05°C.

The crystal structure of the hydrate of HMT at -20°C was determined by Jeffrey and Mak (33,34). The primitive unit cell is rhombohedral with $a_R = 7.30 \pm 0.01 \text{ \AA}$ and $\alpha = 105.4 \pm 0.2^\circ$. The density of the hydrate ($1.209 \pm 0.010 \text{ g/cm}^3$) was found to be consistent with the value calculated for one formula unit per unit cell. The space group was found to be $R\bar{3}m(C_{3v}^5)$. Mak used a hexagonal, triply primitive unit cell with $a_H = 11.62 \text{ \AA}$ and $c_H = 8.67 \text{ \AA}$. The details of the structure are shown in Figure 1. The slightly puckered hexagonal rings formed by the water molecules are stacked along the c axis of the hexagonal cell. A guest molecule is found above and below each of the rings. The rings of neighboring columns are linked by hydrogen bonds. The HMT molecules occupy sites of C_{3v} symmetry, and the water molecules occupy sites of C_s symmetry.

The HMT molecule is hydrogen bonded to the host structure through three of its nitrogen atoms. It hangs 'bat-like' (33) with its three-fold axis coincident with the c axis of the hexagonal cell. The fourth nitrogen atom is not engaged in hydrogen bonding. The structure clearly involves the existence of the two non-equivalent kinds of oxygen atoms marked 1 and 2 in Figure 1. It is apparent from the figure that, while the oxygen atoms of type 2 are involved in four hydrogen bonds, donating two protons and accepting two, the oxygen atoms of type 1 donate two protons,

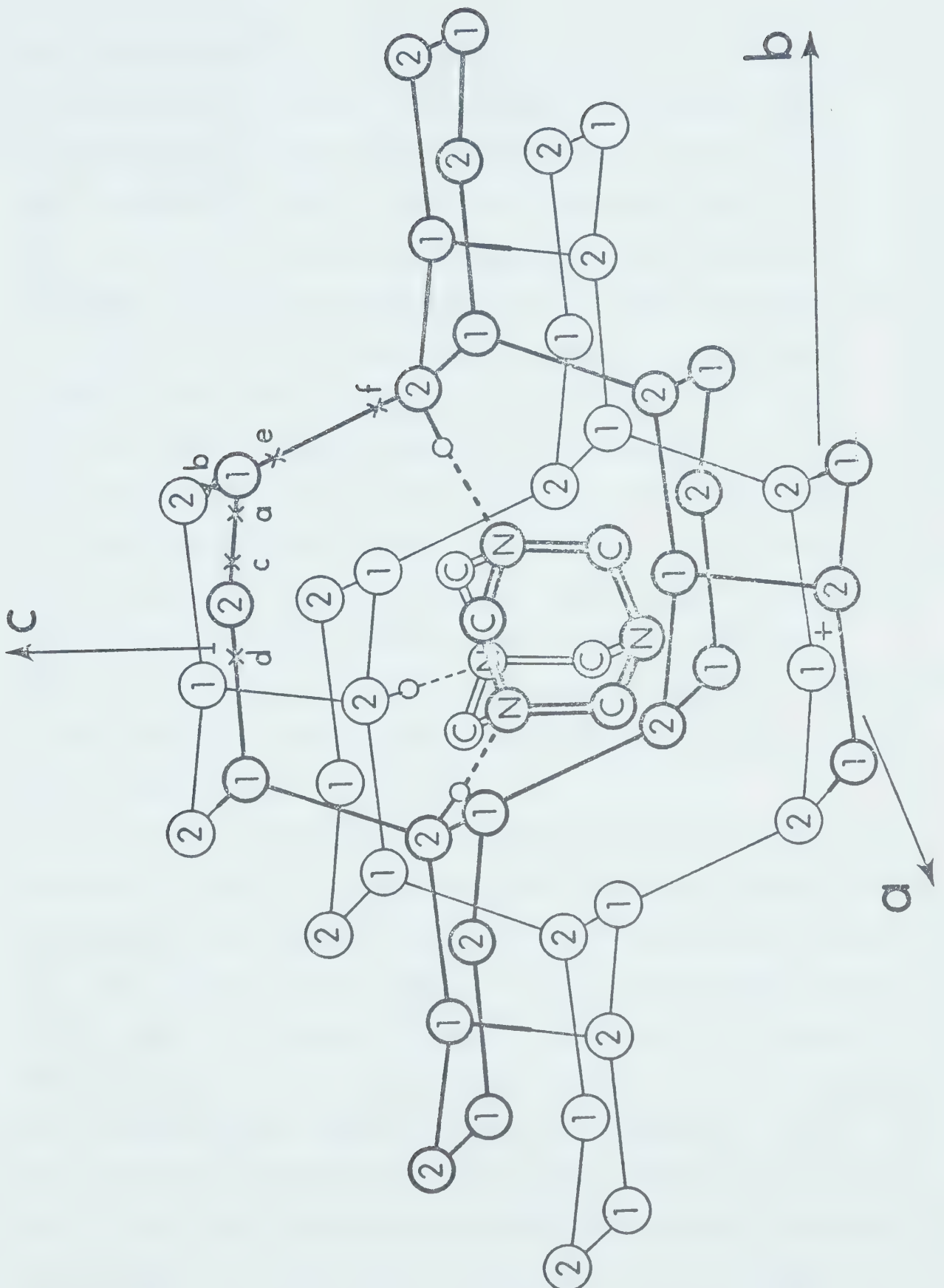


Figure 1. The Cage Structure of HMT Hydrate.

but only accept one. This leaves an electron pair in the valence shell of oxygen 1 not engaged in any bond. Two crystallographically independent types of hydrogen atoms were localized by Mak by means of a difference Fourier synthesis (34). One was seen along the O-H...N bond at a distance of 1.01\AA from the oxygen atom. The second one was localized along the hydrogen bond between two different rings, in position e of Figure 1 at a distance of 1.05\AA from the oxygen atom of type 1. The hydrogen atoms within hexagonal rings could not be localized in the x-ray study and Mak concluded that a two-fold disorder in the hydrogen positions exists within the $(\text{H}_2\text{O})_6$ rings. That is to say, while positions e and f were found to be fully occupied and fully unoccupied, respectively, positions a, b, c and d were found, on the average over the whole crystal, to be half occupied.

Mak rationalized the disorder of the hydrogen positions within a ring by saying that the only ordered configuration consistent with the crystal symmetry, requires that the hydrogen atoms engaged in the hydrogen bonds within the rings be attached to oxygen 1, while the hydrogen atoms responsible for the hydrogen bonds to the HMT molecule and between rings should be attached to oxygen 2. Since the angle $\text{O}_2-\text{O}_1-\text{O}_2$ in the rings is 126° , this would, according to Mak, lead to the energetically unfavorable situation of hydrogen bonds deviating considerably from linearity.

It is worth pointing out that, although such a large angle may lead to an energetically unfavorable situation, the existence of even larger angles in other hydrogen bonded systems is not uncommon (35).

The two crystallographically independent O...O distances were found to be 2.766 and 2.764 \AA for the bonds within a ring and between rings respectively. The O...N distance was found to be 2.816 \AA .

The molecular parameters of the HMT molecule in the hydrate were found to be appreciably altered from the values found for pure HMT.

The fact that the cage structure is reminiscent of the structure of hydroquinone clathrates, from which the concept of clathration originated (36), induced Mak to expand the concept of clathration to encompass inclusion compounds in which a bond exists between the host and the guest. Another example of a clathrate hydrate of this type is the decahydrate of trimethylamine which, however, has a different structure (37).

Davidson (38) reported a dielectric relaxation study of HMT hydrate in 1968. He found a value for the static dielectric constant of about 63 at about -53.3°C; he also found that the reorientation rate of the H_2O molecules is higher than that of ice I (39) at all temperatures. Since the number density of the water molecules in the hydrate is 0.58 of that of ice Ih, whose static dielectric con-

stant at -57°C is 114 (39) or roughly twice the value for HMT hydrate, Davidson argued that the disorder is not restricted to the hydrogen positions within individual rings because, if it were, it would lead to a low value of the dielectric constant and much lower relaxation rates than those observed. He concluded that a three-fold orientational disorder about each water molecule is required to explain the high values of the dielectric constant and of the relaxation rate in the hydrate.

Davidson also studied the dependence of the breadth of the dielectric dispersion curve on the temperature (38). The Cole-Cole width parameter (40), which is a measure of the breadth of this dispersion curve, was found to increase from 0.07 at -38°C to 0.23 at -84°C . Calculations based on first neighbor interaction showed two orientations of different energy for each water molecule. It was suggested by Davidson that the increase of the Cole-Cole width parameter with decreasing temperature may be due to the temperature dependence of the occupancy of the two possible orientations, and that this may indicate the existence of long range ordering at low temperatures.

I.4 The Structures and Spectra of the Ice Polymorphs.

Some excellent reviews of the vibrational spectra of the ice phases are available in the literature (41-46), and no attempt will be made here to cover the subject to

any great length. However an understanding of the structural and spectral features of extensively hydrogen-bonded water systems, that is, ice polymorphs and clathrate hydrates, is necessary in order to understand the spectra of the present hydrate. It is, therefore, appropriate to briefly review the literature on the subject.

Eleven polymorphs of ice are known to exist (44) and the existence of a twelfth has been suggested (47). Three of the phases whose existence has been firmly established, namely ice II, ice VIII and ice IX are orientationally ordered (48,49,50,51,52) which means that the positions of the hydrogen atoms, as well as those of the oxygen atoms, are regular over the whole crystal. Two phases, ice V and ice VI, are partially ordered (47,58), which means that some of the hydrogen atoms' positions have, on the average over the whole crystal, a degree of occupancy different from 0.5. The remaining phases (ice Ih, ice Ic, ice III, ice IV, ice VII and vitreous ice) are orientationally disordered, which means that the degree of occupancy of each hydrogen atom site is, on the average, 0.5. Of the clathrate hydrates which have so far been investigated, only the hydrate of HMT shows some degree of proton-ordering.

The infrared spectra between 4000 and 50 cm^{-1} have been reported for ice Ih and ice Ic (53,54), vitreous ice (53-57), ice II (58-59), ice V (58-59), ice IX (58-59) and ice VI (60) all at 90°K . The infrared spectrum of ice

IV has been obtained by Engelhardt and Whalley (61) and that of ice VIII was obtained by Bertie and Whalley, but neither has been published. The only clathrate hydrate of which a complete and reliable infrared spectrum has been published so far is the hydrate of ethylene oxide, whose spectrum was studied by Bertie and Othen (62,63).

Some general spectral features are common to all ice polymorphs and to ethylene oxide hydrate. The spectra of all H_2O ice phases display a very broad band centered at about 3200 cm^{-1} , due to the O-H stretching vibrations of the water molecules $\nu_{\text{OH}}(\text{H}_2\text{O})$. The O-D stretching vibrations in D_2O ices $\nu_{\text{OD}}(\text{D}_2\text{O})$, absorb over a broad region centered at about 2400 cm^{-1} . A detailed interpretation of the shapes of the $\nu_{\text{OH}}(\text{H}_2\text{O})$ and $\nu_{\text{OD}}(\text{D}_2\text{O})$ bands is not available either for the ordered or for the disordered phases of ice. Since three features are prominent in the $\nu_{\text{OH}}(\text{H}_2\text{O})$ band of ice Ih, it was common (57,64,65) to assign the three components to ν_1 , ν_3 and $2\nu_2$ where ν_1 and ν_3 refer to the crystal vibrations derived from the symmetric and asymmetric O-H stretching vibrations, respectively, and $2\nu_2$ refers to the transitions in the crystal derived from the first overtone of the angle deformation vibration of each water molecule. Bertie and Whalley (53) criticized this assignment on the grounds that the $\nu_{\text{OD}}(\text{D}_2\text{O})$ band of D_2O ice Ih contains at least six features to be accounted for, and their origin is not explained by the simple assign-

ment in terms of ν_1 , ν_3 and $2\nu_2$. They pointed out that the ν_1 and ν_3 modes of each molecule must interact with like vibrations of other molecules, and there are no symmetry restrictions to prevent interaction between ν_1 and ν_3 modes because of the disorder in the crystal. Therefore the H_2O and D_2O stretching vibrations each lead to a broad density of states curve, which may have several peaks, shoulders and inflection points on it. The spectrum corresponds to this curve multiplied by an intensity function which also may not be a smooth function of frequency. Thus the various features of the observed bands could well arise from the ν_3 and ν_1 modes and there is no need to invoke the appearance of $2\nu_2$ to explain why three gross features, and at least three less prominent features, are seen (53). It was proposed that the high frequency end of the band arises from ν_3 , and the low frequency end arises mainly from ν_1 , with mixtures of ν_3 and ν_1 contributing to the center of the band. Whalley has expressed the opinion (42) that no detailed interpretation of these bands is possible until the density of states curve is known. The same situation holds for the corresponding bands of other disordered forms of ice. Recent evidence (66) does suggest that $2\nu_2$ contributes to the O-H stretching band in the Raman spectrum of liquid water, and infrared spectra of H_2O in solution in various organic bases have indicated (67) that $2\nu_2$ becomes more intense as the hydrogen bond strength increases and

the O-H stretching frequency decreases towards 3200 cm^{-1} . Thus it seems distinctly possible that $2\nu_2$ does contribute to the $\nu_{\text{OH}}(\text{H}_2\text{O})$ and $\nu_{\text{OD}}(\text{D}_2\text{O})$ bands in the infrared spectra of the disordered ices, but the detailed interpretation of these bands is not known.

On the basis of group theory one would expect that the bands due to the $\nu_{\text{OH}}(\text{H}_2\text{O})$ and $\nu_{\text{OD}}(\text{D}_2\text{O})$ in ice II and IX would be much narrower and richer in structure than is observed. Since these phases are ordered, rather strict selection rules should apply (Section I.2). Ice II crystallizes in the space group $\text{R}\bar{3}$, C_{3i}^2 , (68) with 12 molecules per unit cell, and the unit cell group analysis predicts eight infrared active and eight Raman active O-H and O-D vibrations. Ice IX crystallizes in the space group $P4_12_12$, D_4^4 , with 12 molecules per unit cell (69), and the unit cell group analysis predicts nine infrared active and 15 Raman active $\nu_{\text{OH}}(\text{H}_2\text{O})$ and $\nu_{\text{OD}}(\text{D}_2\text{O})$ vibrations. However, for both phases the bands are just as broad as, and do not show much more structure than, those of the disordered phase. Contributions from overtones and combination transitions and transitions from excited states have been proposed to explain the broad absorption (58). It is, however, clear that the breadth is due to intermolecular coupling, because the $\nu_{\text{OH}}(\text{HDO})$ and $\nu_{\text{OD}}(\text{HDO})$ absorptions (to be discussed later in this section) are narrow.

The H-O-H deformation vibration gives rise to the

ν_2 band which is broad and featureless, and is centered near 1600 cm^{-1} in the spectra of all ice phases and ethylene oxide hydrate. This band has not been discussed to any great extent and its breadth is unexplained. A broad combination band centered at 2200 to 2300 cm^{-1} is also common to the spectra of the ices and of ethylene oxide hydrate. This band has been assigned to $3\nu_R$ and to $\nu_R + \nu_2$ where ν_R refers to the rotational vibrations of the water molecules. In the spectra of all ice phases $\nu_R(\text{H}_2\text{O})$ absorbs at about 800 cm^{-1} , and $\nu_R(\text{D}_2\text{O})$ at about 600 cm^{-1} . The bands are broad, extending from about 400 to 1000 cm^{-1} in the H_2O phases and 350 to 800 cm^{-1} in the D_2O phases, but the spectra of the different phases display important differences in detail, and the ordered and disordered phases of ice can be distinguished by the shape of their ν_R bands. In the spectra of ice II and ice IX this band consists of several very sharp features overlapping a much broader absorption (58). The sharp features are weaker in the spectra of the samples which contain a few percent of isotopic impurity than in those of the pure phases. Bertie and Whalley (58) explained these phenomena by postulating the existence of orientational order extending over at least a few unit cells in these ice phases. Some of the sharp features were said to arise from zero-wave-vector vibrations, and their weakening and broadening with the addition of isotopic impurities was said to be caused by the disorder induced in

the crystal by the random distribution of the impurities. Their hypothesis of orientational ordering in these phases was later fully confirmed (48,52). The origin of the broad absorption is, however, still unexplained. Since these phases are fully ordered (48,52), the available theory predicts that the only fundamental transitions that can be infrared active are those with zero-wave-vector, and the absorption peaks due to these vibrations are expected to be very sharp.

Other revealing differences between the spectra of ordered and disordered phases of ice are observed in the absorption peaks due to the O-H and O-D stretching vibrations of HDO molecules isolated in an environment of D₂O or H₂O molecules. These vibrations are commonly referred to as ν_{OH} (HDO) and ν_{OD} (HDO), or isolated OH and OD stretches, because they are not coupled to the vibrations of the surrounding molecules. In the spectra of the ordered phases, ice II and IX, the bands due to ν_{OH} (HDO) and ν_{OD} (HDO) are sharp, with half-widths of 10 to 18 and 4 to 8 cm⁻¹, respectively. The peaks due to the corresponding vibrations in the spectra of the disordered ice phases were found to be much broader. The half-widths found for ν_{OH} (HDO) and ν_{OD} (HDO) range from 30 and 18 cm⁻¹, respectively, for ice Ih and Ic (53) to 150 and 80 cm⁻¹, respectively, for ice V (58).

Several explanations of the factors affecting the breadth of the ν_{OH} (HDO) and ν_{OD} (HDO) bands have been dis-

cussed by Bertie and Whalley (58). Their conclusion is now widely accepted and is the following. The environment around a given oxygen atom is the same in all unit cells in the ordered phases, while it is different for each oxygen atom in the disordered phases. This causes a slight disorder in the oxygen positions and in the O...O separations. This disorder is not sufficiently large to be detected by diffraction methods, because these methods take a crystal average and because the disorder of the oxygen positions is smaller than the root mean square amplitude of the oxygen atoms, but it is sufficiently large to affect the force constant of the O-H and O-D stretching vibrations. Due to the randomness of the disorder of the hydrogen atoms a continuous distribution of O...O distances and, as a consequence, of frequencies for the isolated OH and OD stretches is expected. The result of this is the observed breadth of the ν_{OH} (HDO) and ν_{OD} (HDO) peaks in the disordered phases of ice. The ratio of the half-widths of these peaks in the spectrum of ice Ih is about equal to the square root of 2 and this, together with the fact that these peaks are much narrower in the spectra of ice II and of ice IX, strongly supports this interpretation (58). It is worth mentioning that at the time this interpretation was first proposed, the detailed structures of ice II and IX were not known, nor was it known that these phases are orientationally ordered.

The spectral region below 360 cm^{-1} , where the translational vibrations of the water molecules are found, yields the most obvious distinction between the spectra of ordered and disordered ice phases. A theory proposed by Bertie and Whalley (70) accounts well for the differences between the far infrared spectra of these phases. The observed isotope shift shows that all absorption below 360 cm^{-1} in the spectra of all ice phases is due to essentially pure translational vibrations (54,59,60). The absorption by translational vibrations in a crystal can be divided into two types, the order-allowed and the disorder-allowed absorption. The order allowed absorption arises from $(\frac{\partial \mu}{\partial Q})^2_{\text{ave.}}$ which is derived from the crystal averages of the dipole moment derivatives with respect to equivalent displacements of diffraction-equivalent sets of particles. The disorder-allowed absorption arises from $(\frac{\partial \mu}{\partial Q})^2_{\text{dis.}}$ which is derived from the difference between the actual value of the dipole moment derivative with respect to the displacement of a given particle and the crystal-average value for the diffraction-equivalent set of particles to which the particle belongs. In fully ordered crystals $(\frac{\partial \mu}{\partial Q})^2_{\text{ave.}}$ is finite, while $(\frac{\partial \mu}{\partial Q})^2_{\text{dis.}}$ is zero. Only the first type of absorption is, therefore, allowed. This absorption is only allowed if the wave-vector of the vibration is zero and a fairly small number of sharp peaks is, therefore, expected. In fully disordered crystals only the second type of ab-

sorption is allowed because $(\frac{\partial \mu}{\partial Q})^2$ ave. is zero, while the most probable value of $(\frac{\partial \mu}{\partial Q})^2$ dis. is different from zero. This absorption does not respect the zero-wave-vector selection rule and is, therefore, expected to reflect the density of vibrational states and to be broad. Bertie and Whalley showed that the absorbance is approximately proportional to the density of vibrational states times the square of the frequency (70).

The spectra of the ice phases are fully consistent with this theory. Ice II is orientationally ordered and the unit cell group analysis predicts 10 infrared active translational vibrations. Its far-infrared spectrum contains sharp lines, and nine features are clearly identified. Ice IX is also ordered and the unit cell group analysis predicts 12 infrared active translational vibrations. Eight sharp features are seen in its far-infrared spectrum. Bertie and Whalley (59) associated the sharp absorption of ice II and IX with vibrations which are infrared active under the unit cell group selection rule.

On the other hand, the far-infrared spectra of ices Ih and Ic consist of a continuous broad absorption. These two phases are orientationally disordered and Bertie and Whalley (54) interpreted the absorption as arising from vibrations made infrared active by the disorder. The features seen in the spectra, all rather broad, were assigned to features in the density of states curve. The

results of neutron scattering experiments (71,72) support this assignment. The main features of the spectra can be reproduced by calculations using a very simple force field but the absorption above 230 cm^{-1} cannot be explained in this way. There is considerable discussion in the literature over the correct explanation of this high frequency side absorption (118-120), and no interpretation appears to be generally accepted at present.

Ices V and VI are special cases in that they are partially ordered (47,48), but this was not known when their spectra were first obtained and discussed (58,59,60). Since their partial order makes them somewhat analogous to the hydrate of HMT, their spectra will be discussed in Section V.5, where the far-infrared spectrum of the Hydrate is also discussed.

I.5 The Structure and Spectra of HMT.

Many structural formulae were proposed for HMT before its crystal structure was simultaneously determined in 1923 by Dickinson and Raymond (73) and by Gonell and Mark (74) by means of X-ray diffraction methods. It was the first instance of an organic compound having its crystal structure determined by X-ray methods. Since those early days the structure has been determined many times by X-ray (75-78), neutron (79,80) and electron (81,82) diffraction methods. The molecule in the gas belongs to the point

group T_d and the following molecular parameters were determined by electron diffraction (81) from the gas:

C-N bond length $1.48 \pm 0.01 \text{ \AA}^\circ$

C-N-C angle $109.5 \pm 1^\circ$

N-C-N angle $109.5 \pm 1^\circ$

HMT was found to crystallize in a body centered cubic structure with one molecule per primitive unit cell. The space group is $I\bar{4}3m$ (T_d^3) and thus, the HMT molecule, shown in Figure 2, retains its T_d symmetry in the crystal. The cell dimension was found to be $7.021 \pm 0.009 \text{ \AA}^\circ$ at 298°K , $6.931 \pm 0.009 \text{ \AA}^\circ$ at 100°K and $6.910 \pm 0.008 \text{ \AA}^\circ$ at 34°K (78). The molecular parameters determined at room temperature by neutron diffraction are (80)

C-N bond length 1.474 \AA°

C-H bond length 1.104 \AA°

N-C-N angle 113.7°

C-N-C angle 107.3°

H-C-N angle 108.0°

The C-N bond length was found to be unaffected by temperature variations, but the temperature dependences of the other parameters was not reported (78).

Shaffer (75) explained the high enthalpy of sublimation of the crystal and the distortion of the molecule in the solid by postulating the existence of weak hydrogen

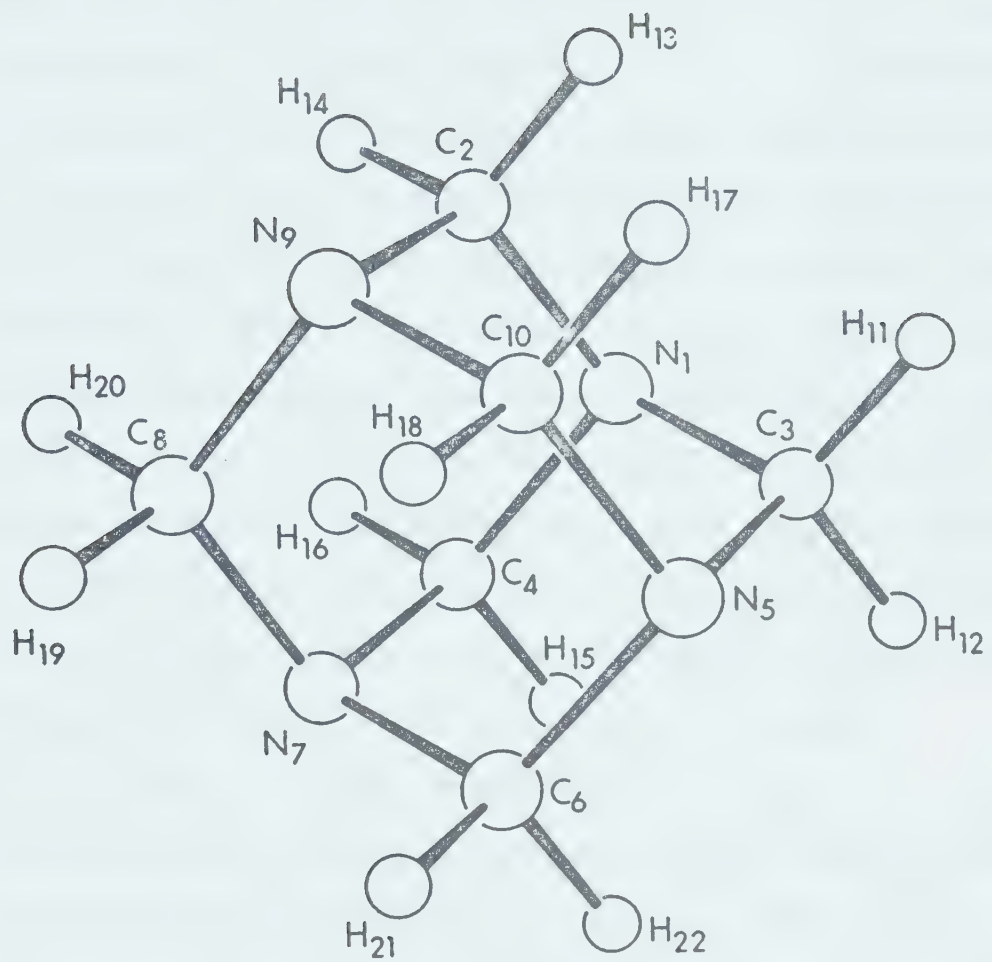


Figure 2. The HMT molecule in the Crystal.

bonds between the methylenic hydrogen atoms and the nitrogen atoms of adjacent molecules. This claim was supported by Smith (83) who found, during a proton magnetic resonance study, that HMT undergoes a phase change due to molecular reorientation at about 375°K. The energy of activation of the reorientation is about 18 Kcal/mole, while the energy of activation of a similar reorientation in adamantane is about 6 Kcal/mole (84). Smith ascribed the high energy of activation in HMT to the hydrogen bonding. However Becka and Cruickshank argued that the closest distance between hydrogen atoms and nitrogen atoms is 2.88 Å at room temperature and 2.78 Å at 34°K, which is a little greater than the sum of the normally accepted values of the van der Waals radii (1.2 and 1.5 Å). One of the normal criteria for hydrogen bonding is, therefore, not satisfied.

The infrared (85-89) and Raman spectra (90-93) of HMT have been recorded and interpreted several times. The most comprehensive Raman study was conducted by Couture-Mathieu et al (90) in 1951. This work included the study of the spectra of an oriented single crystal and of a saturated solution and enabled the authors to determine the polarization of all peaks and, therefore, the symmetry of the modes from which the peaks originate. Couture-Mathieu and her coworkers made a complete assignment of the fundamental modes of vibration. In order to make the assignment they first assigned three peaks to three ring modes on the

grounds of symmetry, frequency and intensity. Equating the frequencies of these peaks to three roots of the secular equation enabled them to calculate the force constants for the C-N stretch, the C-N-C angle deformation and the N-C-N angle deformation. The frequencies of the remaining ring modes were calculated using these force constants and, since fair agreement was obtained between the experimental and the calculated frequencies, a complete assignment of the ring modes was made. The modes due to the vibrations of the CH_2 groups were then assigned on the grounds of group frequencies. This procedure ignored any interaction between the ring modes and the vibrations of the methylenic groups, although these interactions were recognized to be important by the authors. Zijp also performed some calculations using Wilson's GF method (94), assuming the methylenic groups to be point masses and, so, ignoring the interaction between the ring modes and the CH_2 modes. His assignment of the ring modes agrees with that of Couture-Mathieu et al.

Mecke and Spiesecke (85-86) obtained and interpreted the infrared spectra of HMT in the gas phase, in solution and in polycrystalline form. They modified Couture-Mathieu's assignment of the methylenic twist, which is only Raman active; they also assigned the weak features of the infrared and Raman spectra to overtone and combination transitions and, by postulating the values for the frequencies of the inactive F_1 modes, they were able to account for all

of the features of the infrared and Raman spectra. They emphasized that the frequencies of the F_1 modes so determined were very uncertain, and suggested that those modes should become active in the spectra of addition compounds of HMT in which the site symmetry of the HMT molecule is lowered.

Cheutin and Mathieu (89) obtained and interpreted the infrared spectrum of crystalline HMT almost at the same time as Mecke and Spiesecke (85-86). Their assignment of the fundamental vibrations is largely in agreement with that of Mecke and Spiesecke, but considerable differences exist in the assignment of the weaker peaks.

Shiro et al (87) also reported and assigned the infrared spectrum of HMT. They carried out a normal coordinate calculation on the ring modes using Wilson's GF method (15) and a Urey-Bradley force field. The results of their calculations agree closely with those of Couture-Mathieu. All of the above work was carried out on HMT- h_{12} . No studies of HMT-d₁₂ appear to have been made.

I.6 Aims of this Work

This work was started with two broad aims in mind: to study the spectroscopic behaviour of the water molecules in the hydrate structure, and to investigate the effect of the reduced site symmetry and the hydrogen bonding on the spectrum of the HMT molecule.

The hydrate of HMT occupies an intermediate position between the ordered and the disordered phases of ice with respect to the orientational ordering of the water molecules. Ice V and ice VI also occupy an analogous position, but while the disorder largely dominates over the order in these two phases (47,48), the position of the hydrogen atoms in the HMT hydrates structure are predominantly ordered. In fact, if Davidson's argument is valid, and it seems reasonable to accept it, all of the hydrogen positions are, at least partially, ordered (38). At the time this work was started the spectra of water phases with partially ordered hydrogen atoms configurations were not known. The spectra of ices V and VI were known (59,60), but these phases were not known to be partially ordered, and their spectra were discussed on the assumption of complete orientational disorder. It was therefore thought that a study of the infrared spectrum of the hydrate of HMT would provide an excellent test for the theory of the translational vibrations of disordered crystals (70). This theory is completely general and is applicable to disordered, partially ordered and completely ordered crystals. The theory has briefly been reviewed in Section I.4 and its application to partially ordered systems leads to the prediction that both zero-wave-vector and non-zero-wave-vector vibrations are allowed in absorption with relative intensities that depend on the relative influence of the order and the disorder.

The hydrate of hexamethylenetetramine contains one hydrogen atom which is completely ordered (34,38) and it was thought that it would be interesting to study whether this gives rise to narrow ν_{OH} (HDO) and ν_{OD} (HDO) absorptions or whether the proton disorder in the surrounding structure broadens the width of these absorptions.

It was also thought of interest to study the spectrum of the rotational vibrations to see if the degree of ordering is sufficient to cause sharp features as were seen in the spectra of ices II and IX (58).

The interaction between the host and the guest should manifest itself in several ways:

- (a) Peaks due to the vibration of the hydrogen bonds between the water molecules and the guest molecules are expected to appear in the far-infrared region.
- (b) Because the guest molecule is held in a fixed position by the hydrogen bonds to the host cage, and because of the particular geometry of the host structure, its site symmetry (C_{3v}) is lower than the symmetry of the isolated molecule and the site symmetry of the HMT molecule in the crystal (T_d). This is expected to cause drastic changes in the spectrum of the HMT molecule in the hydrate with respect to the spectrum of pure HMT, because the triple degeneracy of the F_1 and F_2 modes is lifted under the C_{3v} site symmetry, and the A_1, E and F_1 modes, which are inactive in absorption in pure HMT, become active. The fact that one of the com-

ponents into which the F_1 modes split is active under C_{3v} symmetry is important because the F_1 modes are inactive in absorption and Raman scattering under the point group T_d and their frequencies cannot be determined directly from the spectra of pure HMT.

Chapter II. Experimental

II.1 Chemicals and Single Crystals

HMT- h_{12} was obtained from Eastman Organic Chemicals. Samples were recrystallized from water, from ethanol and from chloroform. The infrared and mass spectra of the commercial and of the recrystallized HMT were recorded, as well as those of a sample purified by sublimation and of a sample obtained from the decomposition of the hydrate. All of the above samples gave the same infrared and mass spectra and it was concluded that the commercial product was sufficiently pure. HMT- d_{12} was obtained from Merck, Sharp and Dohme of Canada Limited and used without further purification. The single crystals used in the Raman study of HMT- h_{12} were grown at room temperature by slow evaporation of the solvent from a saturated solution in chloroform. Single crystals with a volume of about 1 cm³ were obtained and used.

The isotopic purity of the D₂O used in the preparation of the hydrate was determined by NMR, using dimethylsulfoxide as an internal standard. It was found to be 99.5 ± 0.1% pure. This result was checked by measuring the intensity of the ν_{OH} (HDO) bands (Section I.4) in hydrate samples made from the 'pure' D₂O and in samples made from a 5% H₂O, 95% D₂O mixture. The details are given in Section IV.1, and it suffices to say here that the measurements confirmed that the 'pure' D₂O contained only 0.5% of

hydrogen. The H₂O used in this work was from the laboratory distilled water supply.

II.2 Preparation of the Hydrate

A saturated solution of HMT in distilled water was prepared in a glass test tube provided with a ball joint which allowed the test tube to be connected to a vacuum system. The stoppered test tube containing the solution and an excess of HMT was then placed in a cold room, whose temperature was kept at 5 ± 1°C or in a refrigerator kept at 2° to 4°C, in order to obtain a saturated solution at these temperatures; it must be remembered that the solubility of HMT increases as the temperature is lowered (95). The crystallization was then started by cooling the end of the test tube, which still contained a small excess of HMT, with liquid nitrogen. The crystallization proceeded extremely quickly and, since an amorphous mass was obtained, it was obvious that some of the mother liquor was enclosed in the hydrate. This mass was allowed to warm up until only a few very small crystals remained. The solution was then returned in the cold room or the refrigerator and was left to recrystallize for several days. The crystals grew as elongated hexagonal prisms, typically two cm long and one mm in diameter. Once about half of the solution had crystallized, the remaining solution was decanted and the crystals were transferred to a paper tissue and dried as

well as possible. They were then transferred back into the test tube, which had in the meantime been carefully wiped dry. The above operations were carried out in the cold room. When further drying of the crystals was desired, the test tube was connected to a vacuum line through its ball joint and, while kept at about 0°C with an ice bath, evacuated to a pressure of about one torr. At this point the tap to the vacuum pump was closed in order to avoid excessive decomposition of the hydrate. When the pressure in the system approached 4.5 torr (the vapor pressure of water at 0°C (96)), the tap to the vacuum pump was reopened until the pressure was lowered to one torr. This process was continued until traces of a white powder appeared on the surface of the crystals, signalling the beginning of the decomposition of the hydrate.

The crystals were then cooled in liquid nitrogen and were ground in a Spex Freezer Mill grinder. Since a considerable amount of heat was produced during the grinding, and the crystals were not in direct contact with the nitrogen, the grinding was done in five periods of one minute each, separated by five periods of about five minutes each, during which the heat produced was allowed to dissipate. The powder was placed into a glass vial which was placed into a larger vial which was stored under liquid nitrogen. Some of the ground samples were again dried under vacuum by the procedure described above.

The deuterate samples were made in the same way except that the test tube was first treated in the following way: it was initially rinsed twice with a small quantity (about 0.5 cc) of D₂O. About 0.5 cc of D₂O was then left inside the test tube overnight and finally, the test tube was rinsed once again with D₂O.

II.3 Preparation of the Infrared and Raman Samples.

The cell used for the infrared spectra was made in the machine shop of the Chemistry Department from stainless steel. A schematic diagram of the cell is given in Figure 3. It consisted of an inner part, which included a nitrogen reservoir to which a copper sample holder was soldered, and an outer jacket. The space between the inner part of the cell and the outer jacket could be evacuated through the vacuum tap. The vacuum seal was provided by two greased buna-N O-rings between the flanges of the inner and outer parts of the cell. Buna-N O-rings were also fitted between the outer jacket and windows, which were held in place by means of steel rings tightly screwed to the outer jacket. The window material was cesium iodide for the mid-infrared and polyethylene or teflon for the far infrared. When mulls or pellets were used the two halves of the cell were joined and the cell was evacuated to 10⁻² torr or less.

The inner windows containing the mulls were placed into the copper sample holder, and they were pressed together

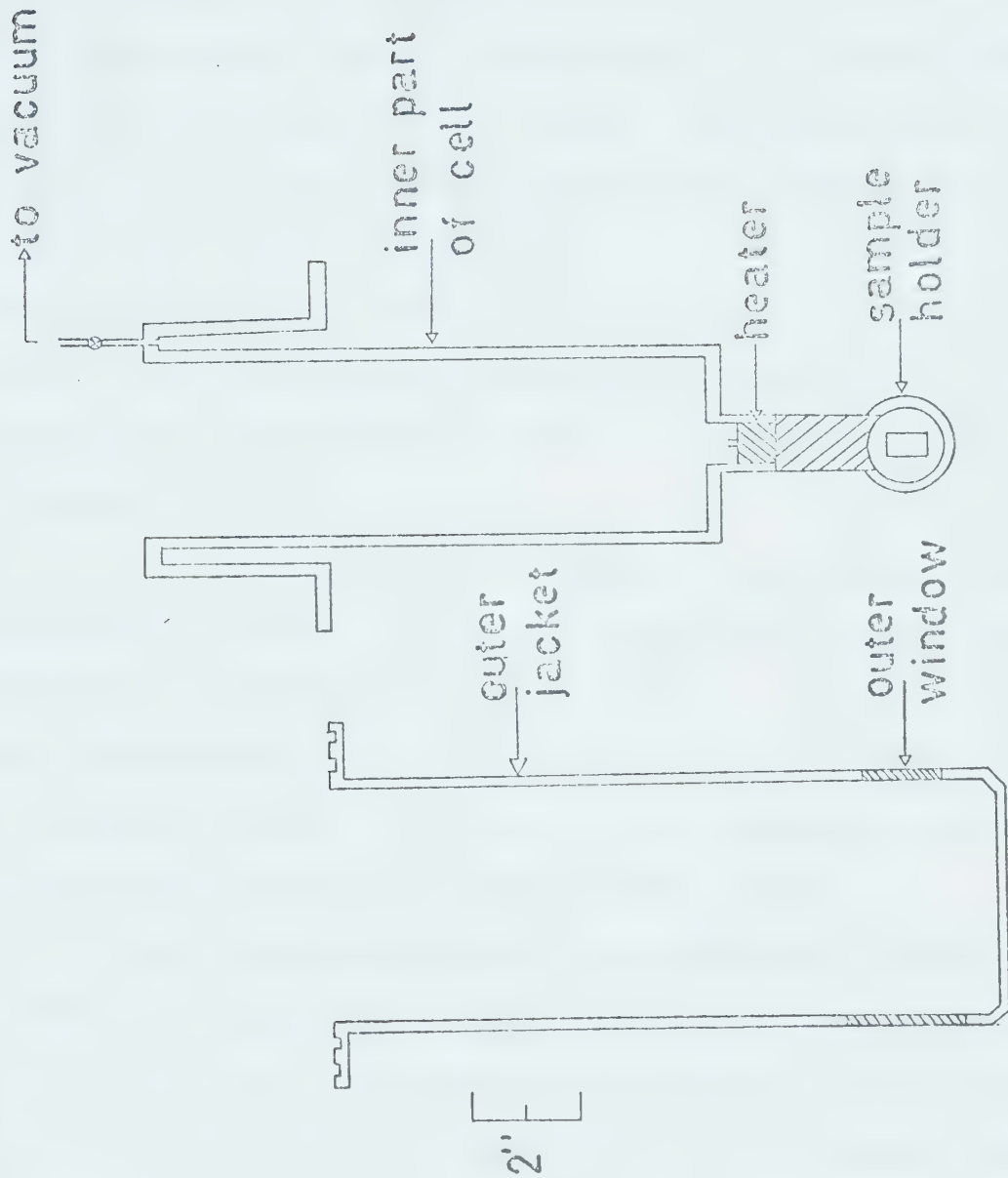


Figure 3. The sample cell used for the infrared spectra.

by means of a spring soldered to a copper ring which was screwed to the sample holder. When the polyethylene or teflon windows were used a copper spacer, 1/4" thick, with a rectangular aperture in the center, was placed between the spring and the windows. The cesium iodide windows were carefully polished in three stages using first alumina, then barnesite and finally chamois leather moistened with 98% ethanol. The polyethylene and teflon windows were conically tapered with a half angle of $3^{\circ} 26'$ in order to eliminate interference fringes.

The temperature of the copper sample holder could be monitored by means of a copper constantan thermocouple soldered to it. The temperature could also be controlled, within restricted limits (see Section II.5), by means of a small heater placed at the bottom of the nitrogen reservoir in direct contact with the copper sample holder.

The infrared samples of pure HMT were prepared by two different techniques. Nujol and Fluorolube mulls were used to investigate the regions $200 - 1300 \text{ cm}^{-1}$ and $1300 - 4000 \text{ cm}^{-1}$ respectively. KBr pellets were also used. The mulls were made by finely grinding a few milligrams of pure HMT in a small mortar for about 15 minutes; one or two drops of mulling agent were then added and the mulling was carried out for another 15 minutes. The mull was deposited in the center of one of the cesium iodide plates and the second plate was pressed against the first, causing the mull to

spread. The two windows were then placed into the cell sample holder and tightened with the spring.

The pellets were made using a piston and cylinder apparatus which was designed in collaboration with P. Tremaine and made out of hardened steel in the Department machine shop. A diagram of it is shown in Figure 4. A mixture of about 100 mg of dry KBr and two to four mg of HMT was finely ground in a mortar. The finely ground powder was placed in the piston and cylinder apparatus with the lower piston and the lower back-up ring already in place. After the powder was dispersed as evenly as possible with a spatula, the upper back-up ring and the upper piston were placed inside the cylinder, and the apparatus was transferred to a 100-ton press. Care had to be taken to place the apparatus in the center of the plattens. A pressure of between 1000 and 1500 bars was applied for about ten minutes. The pressure was then released, the pistons were removed, and the cylinder containing the pellet was placed into the cell sample holder and held in place by a copper ring screwed to the holder. Normally, perfectly transparent discs were obtained. They were firmly secured to the cylinder through the back up rings and could be cooled without difficulty.

For the Raman spectra of polycrystalline samples, crystals about 0.2 mm in size were used. They were sealed into glass melting point capillary tubes of about 1.2 mm i.d. and 1.6 - 1.8 mm o.d. The solution Raman samples were

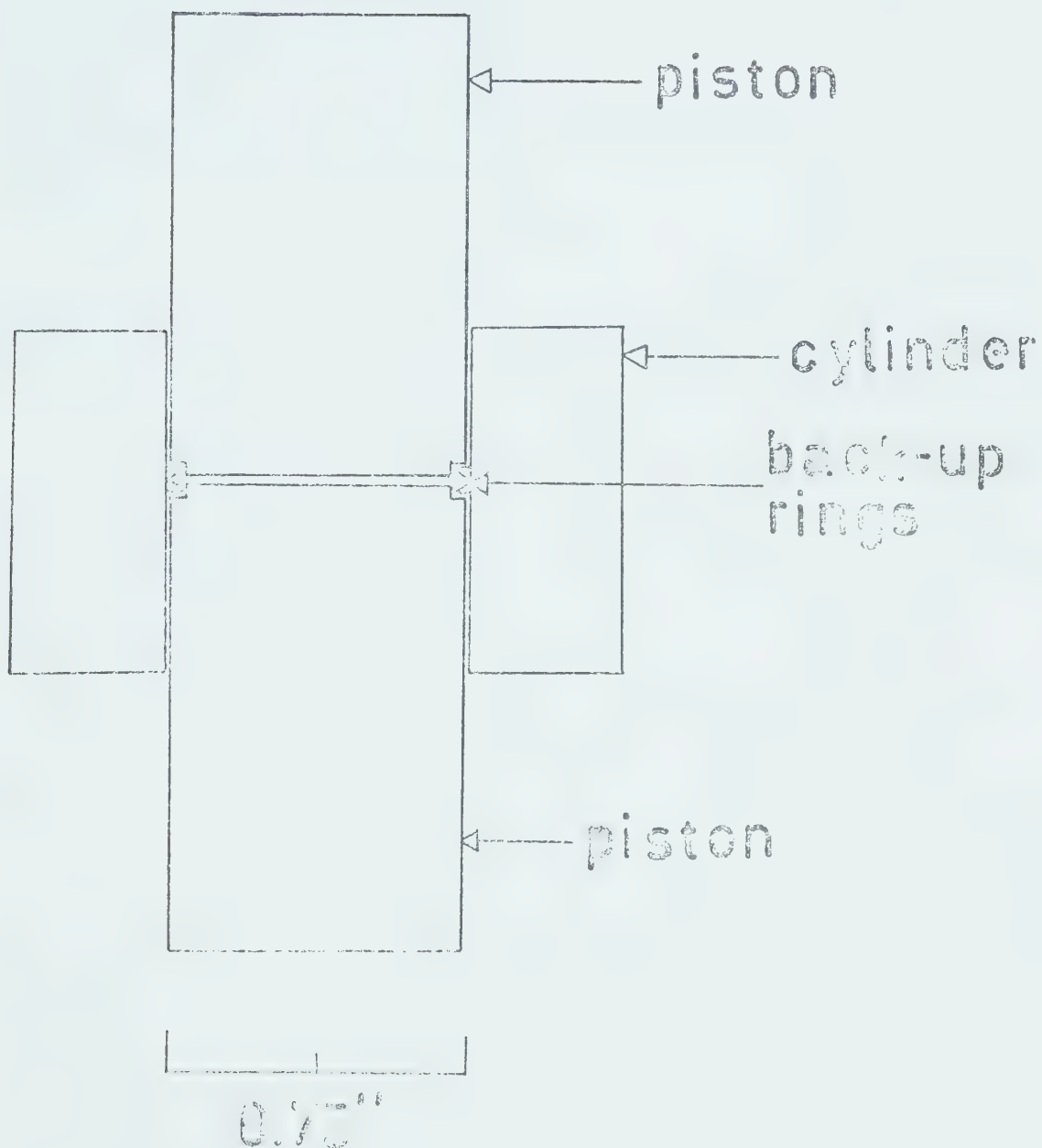


Figure 4. Apparatus for making KBr pellets.

saturated solutions of HMT in distilled water and were also sealed into similar capillary tubes. The single crystals were glued with Glyptal cement to a glass rod about 3 cm long and 2 mm thick. The glass rod was then mounted on a goniometer head which allowed the crystal to be properly oriented.

The infrared samples of the hydrate were made by a modification of the low-temperature mulling technique devised by Bertie and Whalley (97). The method is described below.

All operations were carried out in an uninsulated steel can provided with a side arm. The shape of the container, as well as the disposition of the items used in the process, is shown in Figure 5. Once the apparatus was arranged as shown in the figure, the can was filled with liquid nitrogen to about 1" below the top of the table. About half an hour was allowed for the can and the contents to cool. The sample was then taken out of the storage dewar and the inner vial was placed into its steel container inside the can, and about 1/2 cc of mulling agent was slowly condensed from a cylinder directly into the appropriate vial. The mulling agents were: propane, propylene and Freon 13 (trifluorochloromethane).

Using a long spatula, whose end had been cooled in liquid nitrogen, the desired amount of powdered sample was deposited on the window in the window holder; this varied from an estimated 5 mg for the mid-infrared to an

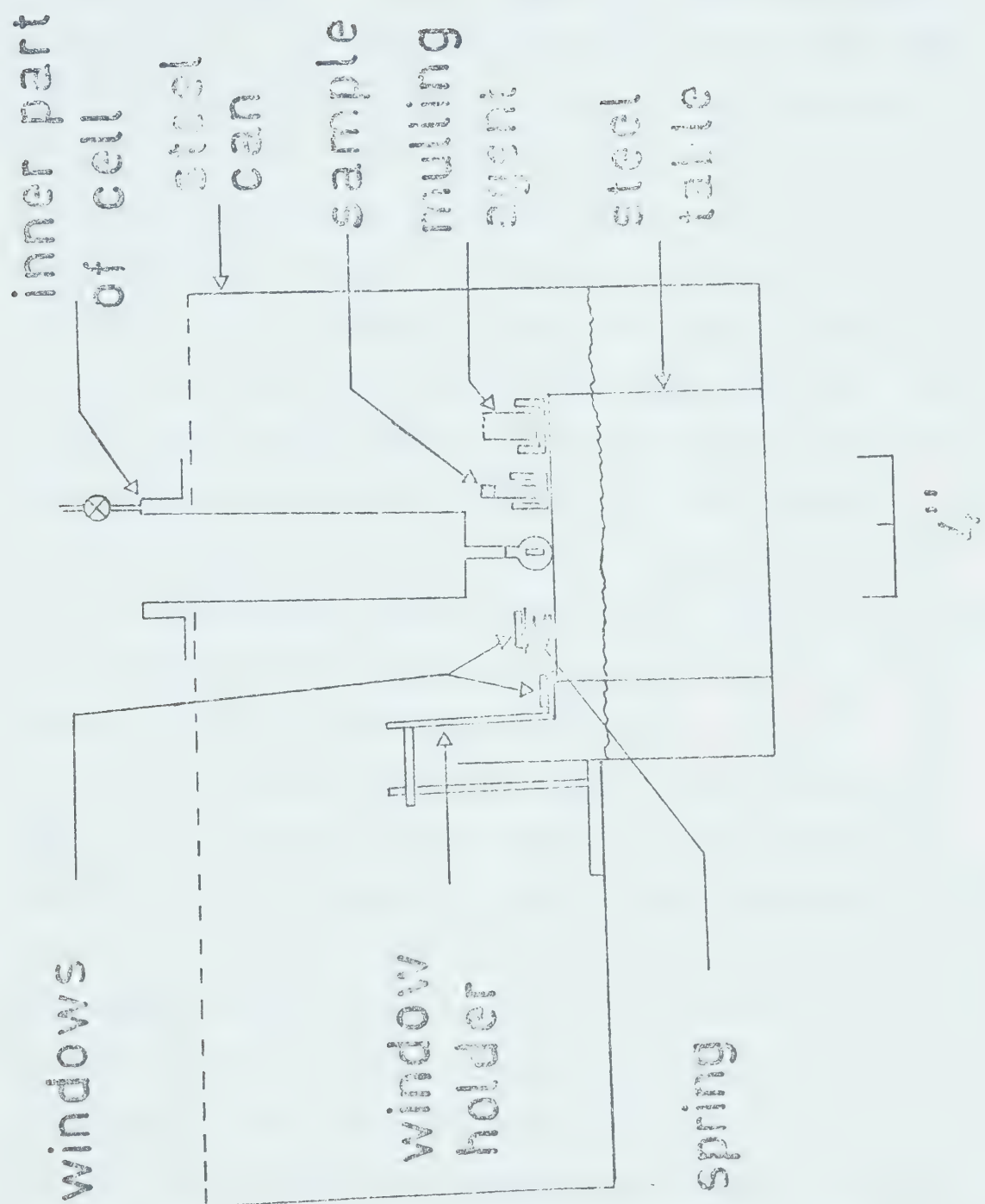


Figure 5. Apparatus for making the low temperature mulls.

estimated 100 mg for the far-infrared. Using the same spatula, one or two small drops of the mulling agent were placed on the window, where they spread on the surface. Once all the sample was slightly wet with the mulling agent, the second window which had a small dent in the center of its upper surface, was placed on top of the first one using a pair of cold, long tweezers; the window was rotated, using the same tweezers, until a clear mull was obtained. Experience alone could determine when to stop this process. When reference spectra were sought, the same procedure was followed except that only the mulling agent was placed between the windows. Once the sample was ready, the windows were transferred into the sample holder where they were pressed together by means of the spring.

When the sample was secured in the holder, the outer part of the cell, which had in the meantime been purged with dry nitrogen gas, was placed horizontally in the side arm of the can. The inner part, containing the sample and a small amount of liquid nitrogen, was joined to it, the tap opened to the vacuum, the cell brought into an upright position and the reservoir filled to the top with liquid nitrogen. When the pressure inside the cell was reduced to about 10^{-2} torr, the tap was closed and the cell was placed in the spectrometer and connected to another vacuum system. While the spectra were being recorded, the cell was continually evacuated and the liquid nitrogen

reservoir was kept full. It was found that if the pressure in the cell was less than 10^{-2} mm of Hg, the nitrogen in the cell would last for about three hours.

II.4 Infrared Instrumentation.

The spectral region between 200 and 4000 cm^{-1} was studied using a Beckman IR 12 spectrophotometer. The instrument was fitted with a fiducial marker, which marked every 25 cm^{-1} between 200 and 2000 cm^{-1} and every 50 cm^{-1} between 2000 cm^{-1} and 4000 cm^{-1} . The marks were calibrated to $\pm 0.5\text{ cm}^{-1}$ below 2000 cm^{-1} and $\pm 1\text{ cm}^{-1}$ above 2000 cm^{-1} , using gaseous water, hydrogen chloride, carbon dioxide and ammonia as frequency standards (98). While not in use the instrument was kept dry with a flow of dry air. One hour prior to use, and during use, the instrument was purged with a stream of warm, dry nitrogen, obtained by boiling liquid nitrogen. This was done in order to eliminate the interference due to carbon dioxide as well as water vapor. Whenever the baseline of the spectrum was lower than about 50% transmission the variable scale expansion facility of the instrument was used.

The region $360 - 10\text{ cm}^{-1}$ was investigated using a Beckman-RIIC FS 720 Fourier interferometer, fitted with a continuous mirror drive. Five beam splitters of different thickness and four high frequency cut-off filters were available. Each beam splitter, in combination with the

appropriate filter, permitted the study of a limited spectral region. All beam splitters were used in order to obtain the spectra between 10 and 360 cm^{-1} .

The interferograms were measured between $+x$ and $-x$ path difference (121,122). The intensities were punched onto IBM cards and were later processed using BOBS IV, a program written in FORTRAN in this laboratory by Bertie, Othen, Brooks and Sunder. The program performs a sine and cosine Fourier transformation. In order to improve the signal-to-noise ratio, the interferograms were apodized using a triangular apodization function (121). A ratio of a sample and a reference spectrum and a plot of absorbance vs. wave-number can be obtained. The program also has a provision to average several spectra, in order to further improve the signal-to-noise ratio. It was found that the average of four spectra had an acceptably low signal-to-noise ratio. In Fourier spectrometry the resolution is the reciprocal of the maximum path difference used (99). The spectra were obtained by scanning over a path difference of $\pm 0.65\text{ cm}$ which gave, before apodization, a resolution of 1.5 cm^{-1} . However, apodization lowered the resolution by 50%. The resolution was, therefore, 2.2 cm^{-1} in the region $10 - 360\text{ cm}^{-1}$. The method was calibrated several times using water vapor (100), hydrogen chloride (101) and methyl chloride (102), and was found to be accurate to 0.2 cm^{-1} .

II.5 Temperature of the Infrared Samples.

The temperature of the infrared samples could not be measured very accurately because they were held in an evacuated cell. However some indirect evidence permits the temperature of the samples to be established with some confidence. A thermocouple soldered on the copper sample holder detected a temperature of between 85 and 95°K when the reservoir of the cell contained liquid nitrogen. When propylene and Freon-13 mulls were used on cesium iodide windows, freezing of the mulling agents was sometimes observed which was signalled by clouding of the mull and by drastic changes in the spectrum. The temperature detected by the thermocouple in these cases was lower than 90°K. This temperature could be raised to 100°K by means of the electrical heater in the cell, and the mulling agents could be melted. The freezing points of propane, propylene and Freon-13 are 85, 88 and 92°K respectively (96). The agreement between the freezing points of the mulling agents and the temperature detected by the thermocouple was thus better than 3°K, and this indicates that the temperature of the mulls between cesium iodide plates was $90 \pm 5^{\circ}\text{K}$.

The temperature of the KBr pellets is more difficult to estimate. When the reservoir contained nitrogen the temperature detected by the thermocouple was 85°K, but the temperature of the pellet could not be monitored. Since little contact existed between the pellet and the

sample holder, the temperature of the pellets was probably higher than the temperature of the mulls.

Several experiments were carried out to determine the temperature of the mulls between polyethylene windows. The temperature was measured when a thermocouple was pressed between the windows, when it was pressed with some silicone grease between the windows, and when it was imbedded in one of the windows. The lowest temperature measured was 120°K. Some indirect evidence that the mulling agent had become frozen was occasionally found, but it is difficult to be sure about it. Frozen propane was found between the windows after disassembling the cell, but since very cold nitrogen gas was let into the cell it is difficult to be sure whether the propane was frozen in the evacuated cell. On several occasions the windows containing the mull were separated after the interferograms were obtained, that is 6 to 12 hours after preparation, and liquid propane was found between them. The vapor pressure of propane is 10^{-2} to 10^{-1} torr at 103°K and 10^{-5} mm of Hg at 77°K (97). Therefore, if the temperature of the mulls had been higher than 100°K the propane would probably have vaporized. It is, therefore, estimated that the temperature of the far infrared samples was lower than 100°K, but it is impossible to be more specific.

III. 6 Raman Instrumentation.

The Raman spectrometer consisted of a Carson Laboratories model 10 SP Ar⁺/Kr⁺ laser, a Spex model 1401 monochromator, a Spex model 1419 sample module, a Spex model 1420 sample illuminating chamber, a cooled FW 130 photomultiplier tube and photon-counting electronics. The 4880 Å Ar⁺ laser line was used throughout the investigation as the exciting line; the laser light was filtered to eliminate unwanted emission lines; the power of the exciting line at the sample was about 80 mW. Towards the end of the work a Coherent Radiation Laboratories Ar⁺ laser became available, and this provided an exciting line with a power of 150 mW at the sample. The Spex monochromator uses 90° excitation geometry. The linearity and the accuracy of the frequency and frequency difference ($\Delta\nu$) scales of the instrument were checked using carbon tetrachloride (103), benzene (104) and indene (105) as frequency standards. Before each spectrum was recorded, the accuracy of the $\Delta\nu$ scale was spot checked using the 455.1, 458.4 and 461.5 cm⁻¹ lines of liquid carbon tetrachloride (103). The exciting line was normally polarized with the electric vector perpendicular to the direction of the scattered light. For some spectra of the single crystal the electric vector was rotated by 90° using a quarter-wave plate. The polarization of the scattered light was selected by a polaroid analyzer, and a polarization scrambler was always placed in front of the entrance slit

of the monochromator. No correction was made for the frequency dependence of the sensitivity of the phototube.

II.7 X-ray Methods.

The hydrate samples for the X-ray studies were made in a steel can similar to that used for the low temperature mulls. A steel table was placed inside the can, and a steel container for the sample vial was placed on the table. A quartz capillary tube was placed into a hole drilled in a brass block which was also placed on the table. The can was filled with liquid nitrogen to about 1" from the top of the table, and the apparatus left to cool for about half an hour. The vial containing the sample was transferred to its container, and opened using two pairs of long tweezers whose ends had been cooled in the liquid nitrogen. The sample was extracted from the vial using a cold long spatula with a triangular end, introduced into the capillary tube with the help of a cold, very thin, steel wire and packed into the tube using the same wire. When the capillary tube was full of sample, it was introduced into the hole of a bakelite support to which it was secured by means of a small screw. On the X-ray camera, the sample was kept cold by a stream of cold nitrogen which was obtained by boiling liquid nitrogen and was conveyed to the sample through a dewar tube. A stream of warm nitrogen, coaxial to and outside of the stream of cold nitrogen, prevented condensation of

water vapor on the sample. The transfer of the sample from the preparation can to the X-ray camera was done in the following way. The capillary tube and its support were held, with a pair of tweezers, immersed in a steel scoop full of liquid nitrogen, transferred to the X-ray apparatus, where it was kept cold by the nitrogen stream, and mounted on a goniometer head which could be rotated about an axis perpendicular to the path of the X-ray beam. The capillary tube was aligned along the axis of rotation and, while the photographs were being recorded, was rotated by means of a small motor. Its temperature was monitored by means of an iron constantan thermocouple placed near the sample and a potentiometer recorder. The temperature was normally kept at $120 \pm 20^{\circ}\text{K}$.

The camera was a Jarrel-Ash precession camera used as a flat-plate powder camera. The radiation was nickel-filtered copper radiation, obtained from an Enraf-Nonius "Diffractis 601" generator. The sample to film distance was accurately calibrated by measuring the diffraction pattern of a powdered sodium chloride sample (106), and found to be 60.0 mm.

Chapter III. The Vibrational Spectra of HMT- h_{12} and d_{12} .

III.1 General.

The HMT molecule (Figure 2) belongs to the point group T_d (81). It contains 22 atoms and its 60 normal modes of vibration are a basis to the representation:

$$4A_1 + A_2 + 5E + 6F_1 + 9F_2 \quad (15).$$

The F_2 modes are infrared and Raman active, the A_1 and E modes are Raman active only and the A_2 and F_1 modes are inactive (15). The representations formed by the internal coordinates are listed in Table 1; if 72 internal coordinates are used (Table 1a), 12 redundancies are included. A comparison of these representations with the representation obtained using cartesian coordinates, which is shown above, reveals that the redundant coordinates form the representation: $2A_1 + 2E + 2F_2$. Six redundancies forming the representation $A_1 + E + F_2$ arise from the fact that the six angle deformations about each of the six carbon atoms are not linearly independent. If the six H-C-H deformations are neglected, these redundancies are eliminated. The same result is obtained if the wags, rocks and twists of the methylenic groups are selected as internal coordinates instead of the H-C-N deformation. The remaining six redundant coordinates must be associated with ring modes and

form the representation $A_1 + E + F_2$ which is the same as the representation formed by the N-C-N deformations. These last coordinates can therefore be neglected. If this procedure is followed, the representations listed in Table 1b are obtained. This method eliminates redundancies and can be used to make an assignment based on group frequencies and symmetry coordinates. However, when calculations are carried out, a force constant for the N-C-N deformations should be included. The presence of redundancies in the calculations leads to as many zero eigenvalues as there are redundancies, and the only consequent complication is that two or more of the force constants are interdependent.

HMT crystallizes in the space group $I\bar{4}3m$, T_d^3 , with one molecule per primitive unit cell (73-80). The site group symmetry of the molecule is, therefore, T_d and no site or unit cell group splitting can appear in the spectrum (21-25). The three zero-wave-vector rotational vibrations of the molecule in the crystal form the representation F_1 and are inactive, as fundamentals, in the infrared and in the Raman. The three translational vibrations of zero-wave-vector, which form the representation F_2 , have zero frequency, for they are equivalent to the translation of the crystal as a whole in the three crystallographic directions. Therefore the $3n-3$ non-zero-frequency, zero-wave-vector vibrations in the crystal form the representation:

$$4A_1 + A_2 + 5E + 7F_1 + 9F_2.$$

Table 1

- (a) Representations formed by 72 internal coordinates of HMT under the point group T_d

C-H stretch	A_1	$+E + F_1 + 2F_2$
C-N stretch	A_1	$+E + F_1 + 2F_2$
C-N-C deformation	A_1	$+E + F_1 + 2F_2$
N-C-N deformation	A_1	$+E + 2F_2$
H-C-H deformation	A_1	$+E + F_2$
H-C-N deformation	$A_1 + A_2 + 2E + 3F_1 + 3F_2$	
		$6A_1 + A_2 + 7E + 6F_1 + 11F_2$

- (b) Representations formed by 60 internal coordinates of HMT under the point group T_d

C-H stretch	A_1	$+ E + F_1 + 2F_2$
C-N stretch	A_1	$+ E + F_1 + 2F_2$
C-N-C deformation	A_1	$+ E + F_1 + 2F_2$
H-C-H deformation	A_1	$+ E + F_2$
CH_2 wag		$F_1 + F_2$
CH_2 rock		$F_1 + F_2$
CH_2 twist		$A_2 + E + F_1$
		$4A_1 + A_2 + 5E + 6F_1 + 9F_2$

Therefore nine peaks due to fundamental transitions should be seen in the infrared spectrum, 18 should be seen in the Raman spectrum.

The F_2 modes are the only ones that are infrared active. In addition, these modes transform as the xy , yz and zx components of the polarizability tensor and in the Raman spectrum of an oriented single crystal they will appear more intensely in the $x(zx)y$, $x(yz)y$ and $x(yx)y$ geometries (Figure 6) than in the $x(zz)y$ geometry in which, ideally, they are absent. The nomenclature $a(bc)d$ for the Raman scattering geometry was proposed by Damen et al (107); in this notation a indicates the propagation direction of the incident light, b indicates the direction of the electric vector of the incident light, c the direction of the electric vector of the scattered light and d is the propagation direction of the scattered light.

The A_1 and E modes are Raman active only and in the spectrum of an oriented single crystal they are expected to appear in the $x(zz)y$ geometry, and to be very weak, ideally absent, in the $x(zx)y$ geometry (108). They can be distinguished from each other because the peaks due to the A_1 modes can be polarized in the solution spectra, while those due to the E modes are not. Indeed, in the liquid phase, only peaks due to totally symmetric modes can have depolarization ratios less than $3/4$. Moreover, if the single crystal is rotated 45° about the y axis (orientation



Figure 6. Scattering geometry used in the single crystal Raman study.

M = monochromator.

x = direction of incident light.

y = direction of scattered light.

The four-fold axes of the crystal were normally along the x, y and z axes.

2b of Couture-Mathieu and Mathieu (109)), that is, if the incident light propagates along x' , which bisects the angle between x and z , and its electric vector is directed along z' , which bisects the angle between z and x , then the A_1 modes will still be strong in the $x'(z'z')y$ geometry and absent in the $x'(z'x')y$ geometry, while the E modes will be stronger in the $x'(z'x')y$ geometry than in the $x'(z'z')y$ geometry, in which they are ideally absent.

III.2 Results for HMT-h₁₂.

Infrared spectra were recorded between 4000 and 200 cm^{-1} of a finely ground polycrystalline powder dispersed in Nujol or in Fluorolube or pressed in KBr pellets. The standard slit program of the Beckman I.R. 12 instrument was used. This provided a resolution of better than two wavenumbers between 400 and 600 cm^{-1} and better than 1.3 wavenumbers between 600 and 4000 cm^{-1} . Spectra of a number of different samples held both at room temperature and at $100 \pm 10^\circ\text{K}$ were recorded.

It was found that the KBr pellets normally yielded better spectra and were easier to make. However, when using this technique, one must consider the possibility of phase changes due to the pressure treatment and of interaction between the sample and the pelleting agent. It is, therefore, necessary to check the spectra obtained against those obtained by some other sampling method. In this study, while

the possibility of phase changes could be ruled out because HMT does not have any high pressure phase in the pressure range employed to make the pellets (110), the possibility of interaction between HMT and KBr was of concern in view of the readiness with which HMT forms complexes with halogens and hydrogen halides. However, since complete agreement was found between the spectra obtained by the two methods, it was concluded that no interaction took place between HMT and KBr.

The infrared spectra of HMT- h_{12} in KBr pellets at room temperature and at 100°K are reproduced in Figures 7 and 8. The frequencies of the features are listed in Table 2. The peaks are generally sharp with half-widths of five cm^{-1} or less, the only exception being the peak at about 1000 cm^{-1} which is the resultant of several overlapping peaks and whose overall half-width is about 25 cm^{-1} . The frequencies of the sharp features are believed to be accurate to $\pm 0.5 \text{ cm}^{-1}$ in the region up to 2000 cm^{-1} and to $\pm 1 \text{ cm}^{-1}$ between 2000 and 4000 cm^{-1} , the factor limiting the accuracy being the reproducibility of the position of the frequency marks. The uncertainty in measuring the frequencies of the weak peaks and of the shoulders is obviously larger and difficult to determine; an estimated value is given for the individual features in the table. The accuracy of the frequencies previously reported was not discussed by their authors (85-94).

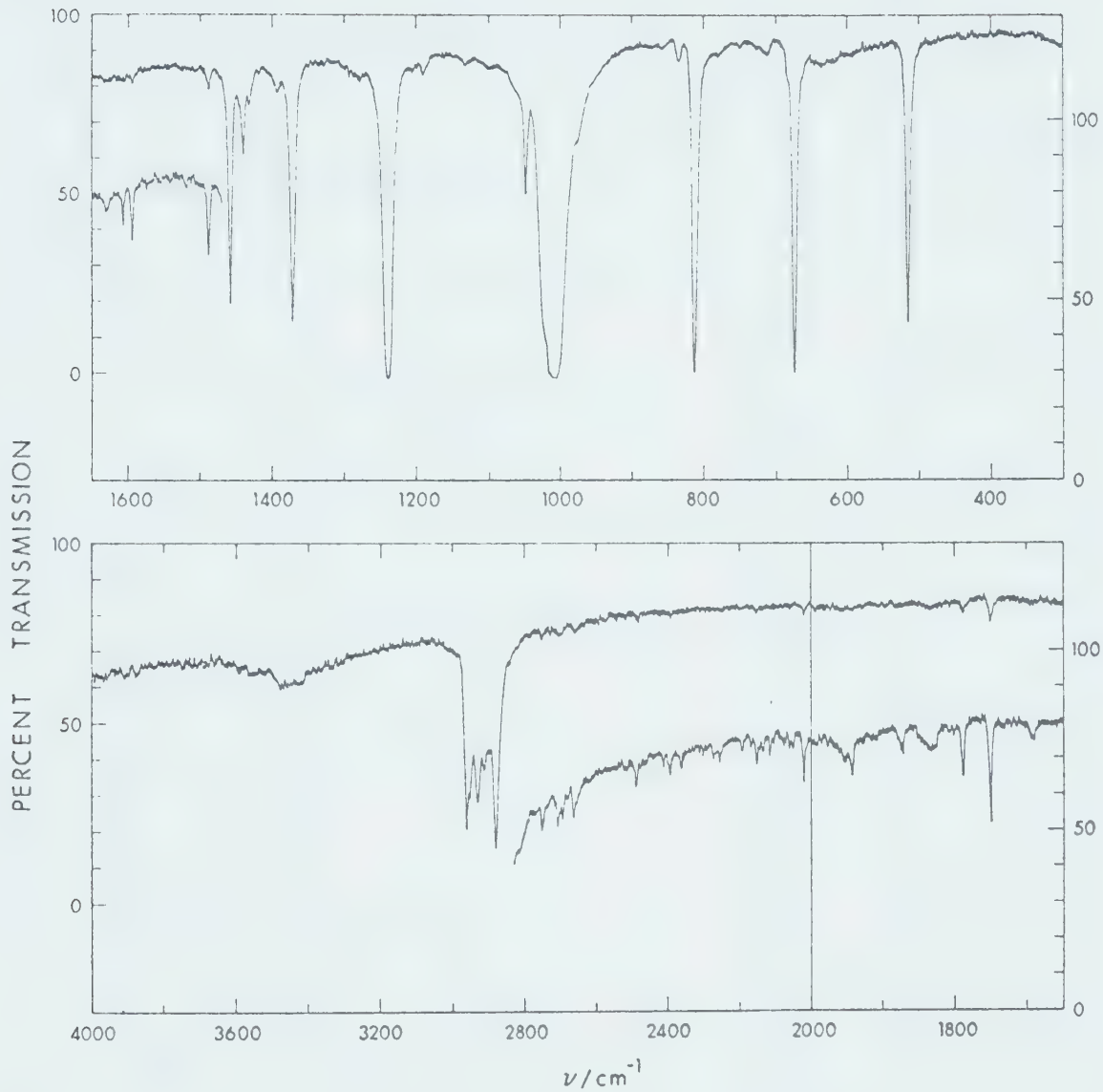


Figure 7. Infrared spectra of two samples of HMT-h₁₂ in KBr. The upper trace refers to a sample held at room temperature, the lower trace refers to a thicker sample held at 100°K. The right hand transmission scale refers to the lower trace.

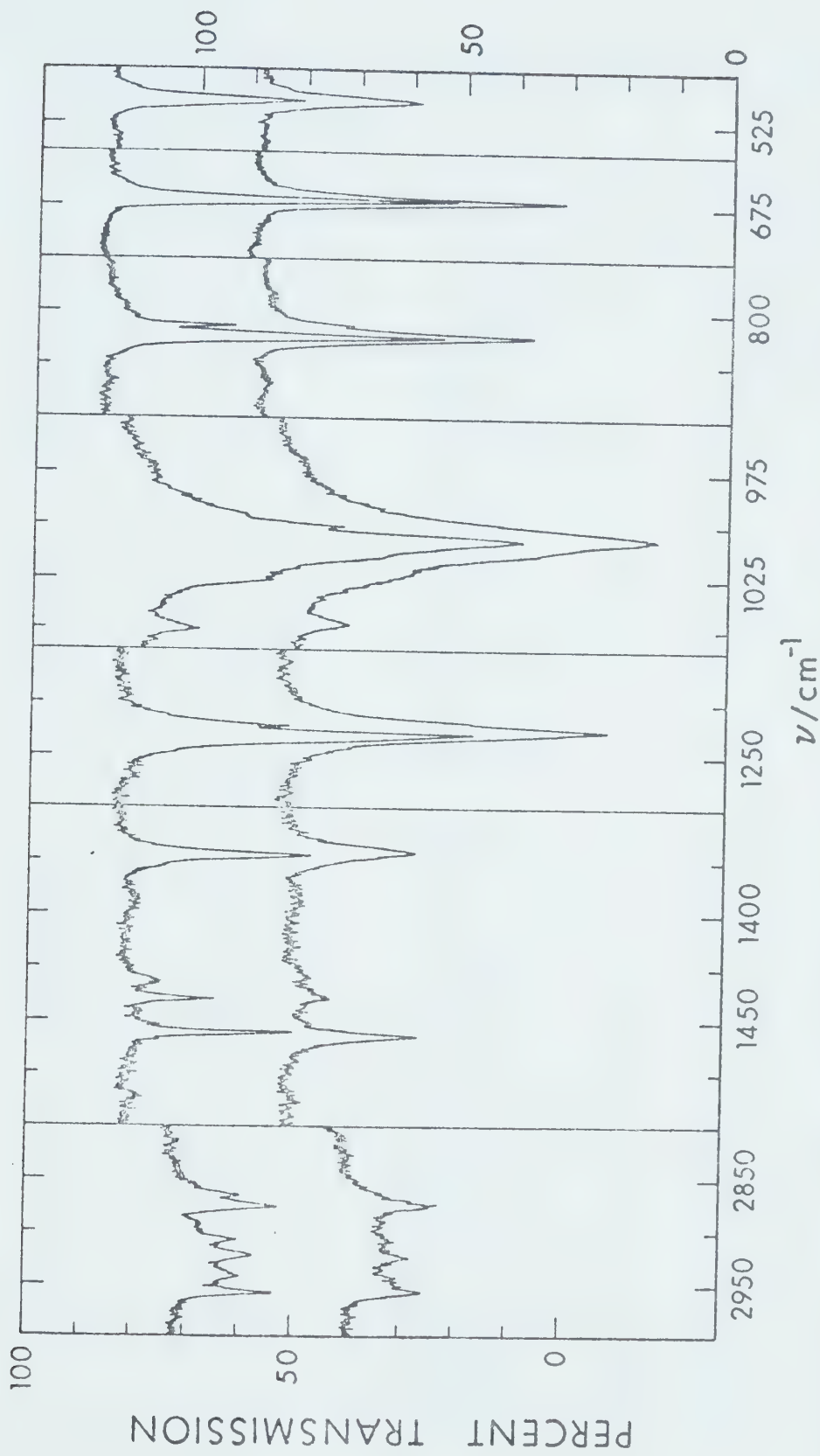


Figure 8. The intense absorptions in the infrared spectra of HMT-hL₂ in KBr, at room temperature (lower trace) and at 100°K (upper trace). The same pellet was used for both spectra. The frequency scale is uniform below 2000 cm⁻¹. The right hand transmission scale refers to the lower trace.

Table 2. Infrared Absorption Frequencies for Solid HMT-h₁₂
at 300°K and 100°K^{a,b}

Ref. 86	Ref. 89	This Work		
ν/cm^{-1}	ν/cm^{-1}	300°K		Assign.
		ν/cm^{-1}	ν/cm^{-1}	
511	513 vs	513.7(0.5) s	513.3 s	ν_{25}
		613(2)	w	613 w
630	630 w	630(1)	w	630 vw
672	674 vs	674.2(0.5) vs	673.0 vs	ν_{24}
711	711 w	712.0(1)	w	711.0 w
727		726.0(1)	w	726.0 w
	777 vw			
		807.5(1)	sh	807.2 m
812	812 vs	812.5(0.5) s	812.5 s	ν_{23}
834	835 m	833.9(1)	w	833.0 vw
855	856 w	856(2)	vw	856 vw
		872(2)	vw	872 vw
		975(3)	sh	975 sh
		992(3)	sh	994 sh
		1000(3)	sh	1000.3 s
1009	1007 vs	1006.8(1)	vw	1007.4 vs
		1013(3)	sh	1012 sh
		1020(3)	sh	1024 sh

(Table continued on next page)

Table 2 continued

Ref. 86 ν/cm ⁻¹	Ref. 89 ν/cm ⁻¹	This Work		
		300°K ν/cm ⁻¹	100°K ν/cm ⁻¹	Assign.
1048	1050 vs	1048.0(0.5) m	1049.3 m	
1134	1135 vw	1133.5(0.5) w	1133.8 w	
1190	1193 m	1191.0(0.5) m	1191.7 m	
1206		1208(2) sh	1207.5 w	
		1234(3) sh	1236.0 s	
1238	1240 vs	1238.0(0.5) vs	1240.8 vs	ν ₂₁
1275				
	1280 w	1280(2) sh	1278 sh	
1288	1293 w	1291.0(1) w	1290.0 w	
1372	1370 vs	1372.0(0.5) s	1372.9 s	ν ₂₀
1397	1393 m	1393.0(1) w	1392.0 w	
1433		1432.4(1) w	1434.1 w	
1441	1438 vs	1440.6(0.5) m	1440.5 m	
1456	1458 vs	1458.2(0.5) s	1456.6 s	ν ₁₉
1490	1493 w	1489.0(1) w	1488.6 w	
1517	1515 w	1514.0(1) vw	1518.0 vw	
1585				
1595	1593 w	1594.0(0.5) w	1593.0 w	
1608	1606 w	1608.0(0.5) w	1607.5 w	

(Table continued on next page)

Table 2 continued

Ref. 86	Ref. 89	This Work			
ν/cm^{-1}	ν/cm^{-1}	300°K		100°K	Assign.
1631	1630 w	1629.2(1)	w	1630.0	w
1692	1692 w	1690(2)	w	1690	w
1730	1730 vw				
1748	1746 m	1750.3(0.5)	m	1749.7	m
1789	1786 m	1787.1(0.5)	w	1787.0	w
1805	1800 vw	1800(2)	vw	1800	vw
1831	1829 m	1830(3)	w	1830	w
1873	1870 vw	1870(2)	w	1872	w
1945	1943 w	1940.0(1)	w	1942	w
1957	1953 w	1951(2)	w	1952	w
2024	2025 m	2022.0(1)	m	2020.4	m
2062	2064	2056(2)	vw	2065	vw
2075		2075(2)	vw	2077	vw
2114	2120 vw	2118.3(1)	vw	2115	vw
2137		2134(2)	vw	2132	vw
	2142	2139(2)	vw	2142	vw
2150		2147.0(1)	w	2150.0	w
	2156 vw				

(Table continued on next page)

Table 2 continued

Ref. 86 ν/cm^{-1}	Ref. 89 ν/cm^{-1}	This Work			
		300°K		100°K	
		ν/cm^{-1}		ν/cm^{-1}	Assign.
		2164(2)	vw	2167	vw
2193		2189(2)	vw	2192	vw
	2204 vw				
2252	2262 vw	2255(2)	vw	2254	vw
2268	2272 vw	2269(2)	vw	2271	vw
2347		2357(2)	vw	2362	vw
2387	2390 vw	2390(2)	w	2392	w
	2403 vw	2406(2)	vw	2409	vw
2481	2484 w	2482(2)	vw	2486	vw
2513	2514 vw				
2652	2654 w	2651.0(1)	w	2654.1 w	
2695		2694(2)	sh	2692	sh
	2708 m	2708(2)	w	2705	w
2744		2746(2)	w	2749	w
	2762 w				
		2815(3)	sh	2820	sh
		2840(3)	sh	2840	sh
		2864(3)	sh	2863.5 m	
		2873.5(1)	s	2876.1 s	ν_{18}

(Table continued on next page)

Table 2 continued

Ref. 86	Ref. 89	This Work		
		300°K		100°K
v/cm ⁻¹	v/cm ⁻¹	v/cm ⁻¹	v/cm ⁻¹	Assign.
2890	2884 vs	2889.5(1)	m	2892.0 s
		2906.5(1)	m	2904.3 m
		2921.6(1)	m	2919.4 m
		2941.0(1)	m	2939.5 m
2967	2948 vs	2954.7(1)	s	2955.8 s
2994		2995(3)	sh	2997.3 w
3333		3328(2)	w	3326 w
	3344 w			
3460		3465(2)	w	3465 w
	3473			
3968	3956	3965(2)	w	3965 w

(a) Values in brackets represent the experimental error of the frequencies (in cm⁻¹).

(b) vw = very weak, w = weak, m = medium, s = strong, vs = very strong, sh = shoulder.

The room temperature spectra obtained in this study are generally similar to those published by Mecke and Spiesecke (86), but considerable differences in detail exist. A careful comparison with the spectrum obtained by Cheutin and Mathieu (89) is not possible because these authors did not reproduce the spectrum in their paper, but merely listed the frequencies of the observed peaks and an approximate estimate of their relative intensities. However an examination of this list (Table 2) reveals that their spectrum differs in some detail from that obtained in the present study. The differences are probably attributable to the higher resolution achieved in this work. Unfortunately the authors of the earlier works did not give an estimate of their resolution, but, since Mecke and Spiesecke used a sodium chloride and potassium bromide instrument, their resolution could not have been very high and, in the region of 3000 cm^{-1} it was probably not better than 10 cm^{-1} . Cheutin and Mathieu also used prism instruments and their resolution was probably also low. It is also believed that the frequency accuracy of this work is higher than that of the earlier works.

The most remarkable differences between the spectra obtained at room temperature in this work and those obtained in the earlier studies occur between 2800 and 3000 cm^{-1} . Cheutin and Mathieu detected two peaks in this region, at 2884 and 2948 cm^{-1} ; Mecke and Spiesecke found three at 2890 ,

2967 and 2994 cm^{-1} . Ten peaks were located in the same region during the present study. The difference obviously reflects a difference in resolution. Only two fundamental vibrations are expected to absorb in this region and, after extensive work, as indicated in Section II.1, was carried out to ensure that the remaining peaks were not caused by impurities, it was concluded that eight of the ten peaks are due to overtones and combination transitions. Some differences of lesser importance were found in the overtone region and are obvious from the table. They will not be given any further attention. The peak which was found at 1238 and 1240 cm^{-1} in the two earlier works was found, in this work, to have a shoulder on its low frequency side. In the present work six features were located between 975 and 1020 cm^{-1} where the earlier authors reported only one peak at 1007 or 1009 cm^{-1} . The shoulder on the low frequency side of the peak at 812.5 cm^{-1} is also reported here for the first time. All differences between this and the earlier works were carefully studied and were found to be real. It is therefore believed that the spectra of HMT reported here are the most accurate spectra of HMT reported thus far.

It can be seen from the spectra in Figure 7 and 8 that considerable sharpening of the peaks occurs when the temperature of the sample is lowered. As a consequence of

this, several absorptions which appear as shoulders at room temperature become clearly resolved peaks at 100°K. This effect is particularly pronounced in the case of the shoulders on the low frequency side of the peaks at 812.5 and 1238.0 cm^{-1} , which are well resolved into sharp peaks at 100°K.

Raman spectra of a polycrystalline sample, an oriented single crystal and a saturated solution in water were obtained. The spectra are shown in Figures 9, 10, 11 and 12 and the frequencies of the observed features are listed in Tables 3 and 4 in which the results of Couture-Mathieu et al are included for comparison. The resolution was 1.5 cm^{-1} throughout the range and the accuracy of the frequencies of the sharp peaks is believed to be $\pm 1 \text{ cm}^{-1}$. The frequency of broad peaks and shoulders is less accurately known. The estimated errors for the individual features are listed in the tables. The depolarization ratios are shown for the peaks in the solution spectra. In principle, the depolarization ratios should not be larger than 0.75 (29). The values shown (Table 4) for the strong depolarized peaks are very close to this value, but those for the weak peaks sometimes exceed it. This reflects the error of measuring the intensity of weak peaks.

The single crystals used were large specimens having the morphology of a rhombic dodecahedron whose symmetry elements were clearly visible. The crystals were first roughly aligned visually, with the three four-fold

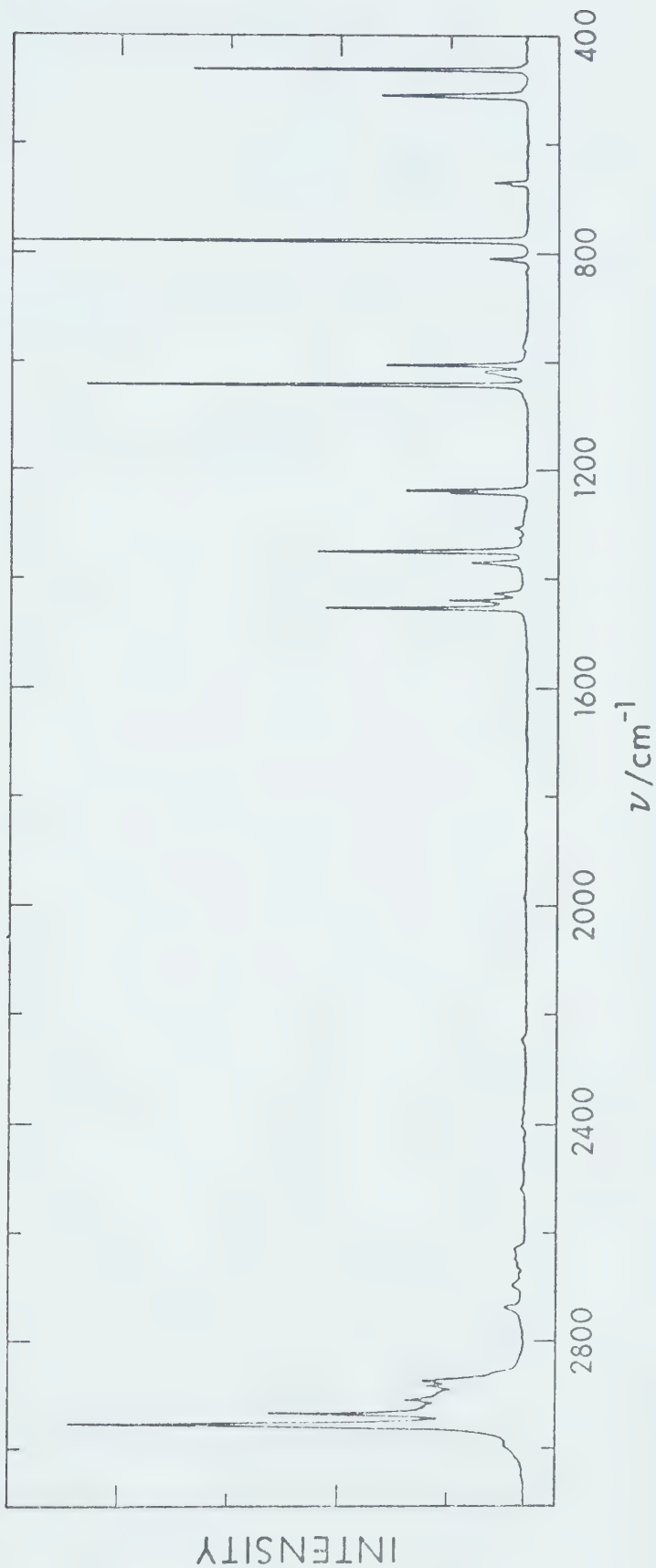


Figure 9. Raman spectrum of a polycrystalline sample of HMT-h₁₂ at room temperature.
No peaks were detected below 400 cm^{-1} .

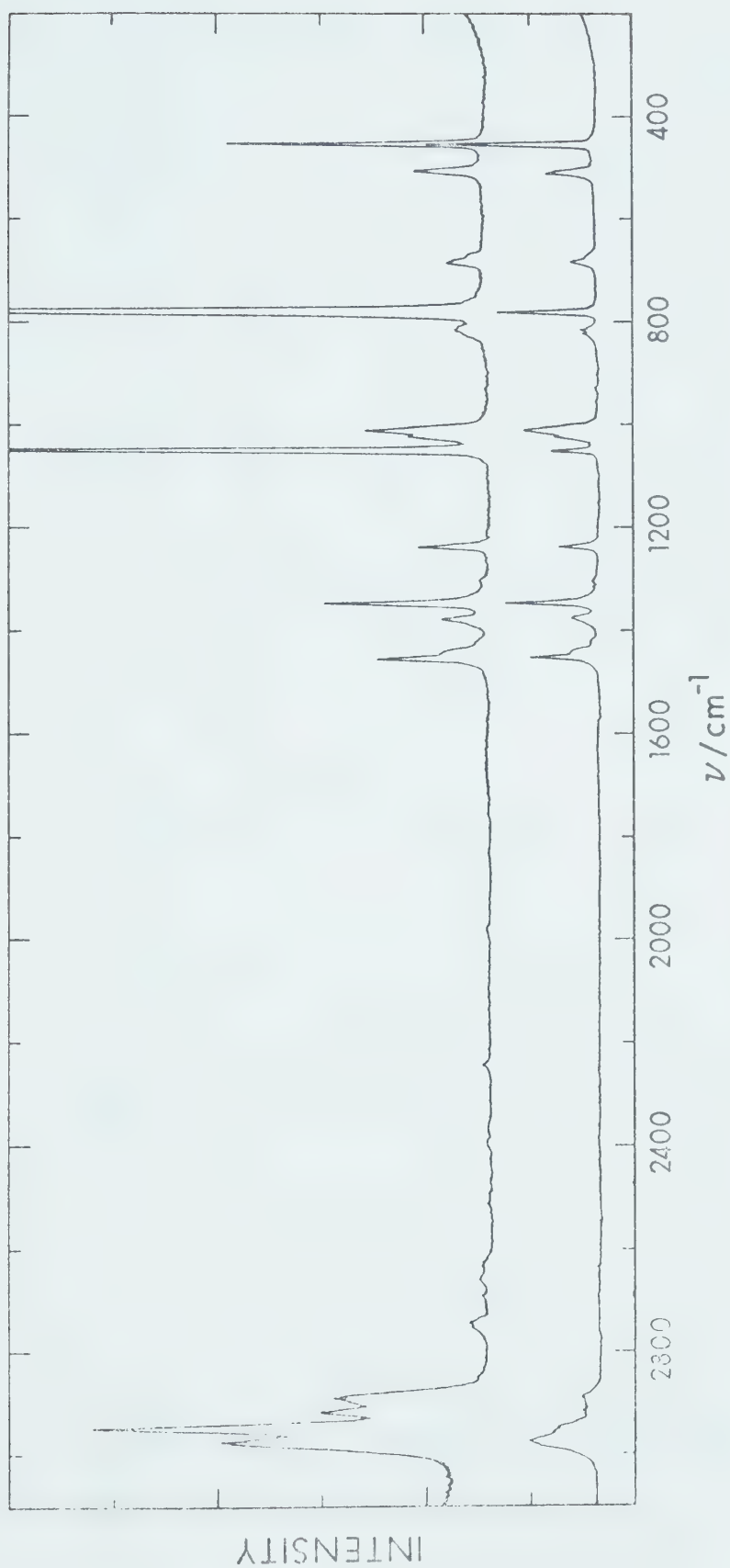


Figure 10. Raman spectra of a saturated aqueous solution of HMT-h₁₂, in parallel (upper trace) and perpendicular (lower trace) observation.

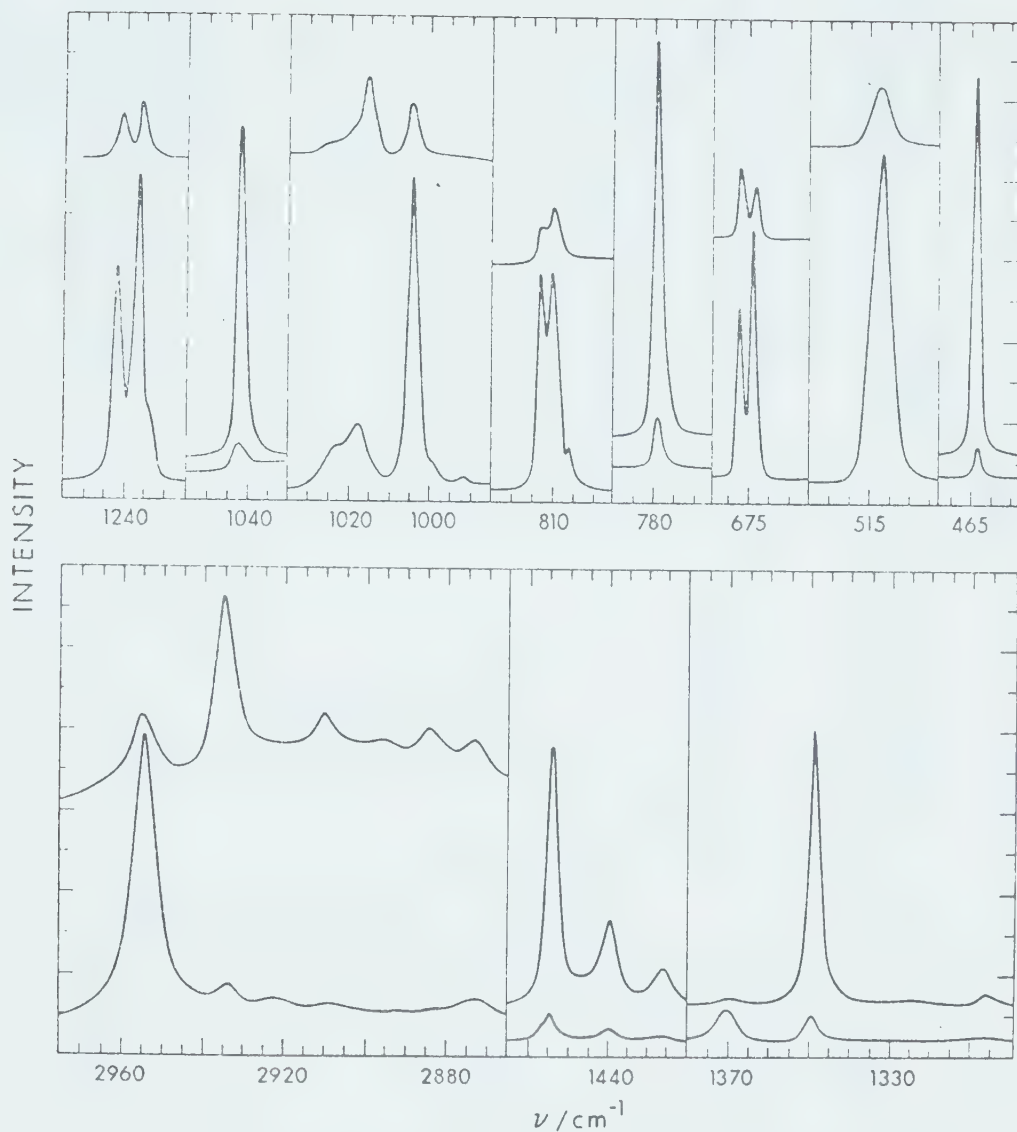


Figure 11. Raman spectra of a single crystal of HMT-h₁₂ at room temperature, under x(zz)y geometry (upper trace) and under x(zx)y geometry (lower trace).

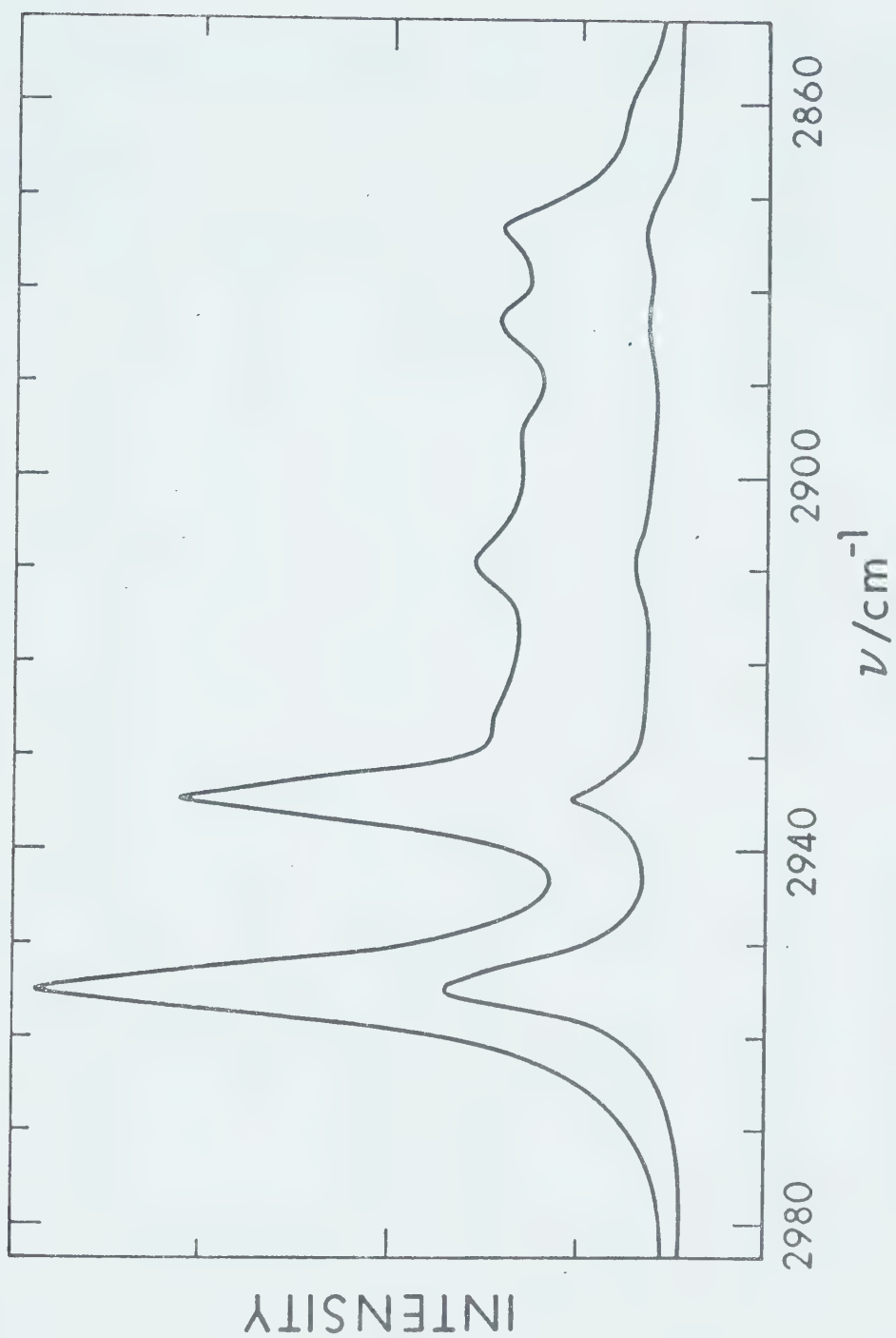


Figure 12. Raman spectra of a single crystal of HMT-h₁₂ at room temperature, under $x'(z'z')y$ geometry (upper trace) and under $x'(z'x')y$ geometry (lower trace).

Table 3. Raman Frequencies for Solid HMT-h₁₂ at 300°K^a

Reference 90			This Work			
ν/cm^{-1}	Int.	Type	ν/cm^{-1} ^b	Int.	Type	Assign.
465	8	E	463.0(1)	3.7	E	ν_{10}
513	12	F ₂	512.0(1)	1.6	F ₂	ν_{25}
586	w	-				
622	w	-				
683	2.5	F ₂	671.0(1)	0.5	F ₂	ν_{24} (TO)
			674.5(1)	0.25	F ₂	ν_{24} (LO)
696	vw	-				
710	vw	-				
756	vw	-				
782	19	A ₁	779.3(1)	10	A ₁	ν_4
812	2.5	F ₂	810.5(1)	0.5	F ₂	ν_{23} (TO)
			814.0(1)	0.25	F ₂	ν_{23} (LO)
1005	7	F ₂	1004.3(1)	1.6	F ₂	ν_{22} (TO)
			1015(3)	0.3	E	ν_9
			1017.5(1)	0.5	F ₂	ν_{22} (LO)
1020	4	E+F ₂	1024(3)	0.3	F ₂	
1041	10	A ₁	1042.0(1)	5	A ₁	ν_3
1100	vw	-				
1238	12	F ₂	1236.5(1)	1.3	F ₂	ν_{21} (TO)
			1241.8(1)	0.85	F ₂	ν_{21} (LO)
1307	vw	F ₂	1306.0(1)	0.1	E	
			1324(2)	~0.2		

(Table continued on next page)

Table 3 continued

Reference 90			This Work			
ν / cm^{-1}	Int.	Type	ν / cm^{-1}	Int.	Type	Assign.
1349	7	E	1349.2(1)	2.3	E	ν_8
1375	3.5	F_2	1370.0(1)	0.6	F_2	ν_{20}
1428	1	E	1426.9(1)	0.35	E	
1441	2.5	E	1439.6(1)	0.85	E	
1454	7	E	1454.2(1)	2.25	E	ν_7
			1457(1)	sh	F_2	ν_{19}
1989	vw	-	1987.2(1)	vw	-	
2034	w	-				
2065	2	complex				
2250	vw	-	2245	vw	-	
			2404(2)	vw	-	
2563	vw	-				
2631	w	-	2626(2)	vw	-	
			2640.2(1)	0.12	-	
2650	vw	-				
			2659(2)	0.1	-	
			2678(2)	0.1	-	
2698	w	-	2697(2)	0.1	-	
2738	w	-	2737.2(1)	0.18	-	
2786	w	-				
2828	vw	-				

(Table continued on next page)

Table 3 continued

Reference 90			This Work			
ν/cm^{-1}	Int.	Type	ν/cm^{-1}	Int.	Type	Assign.
2870	s	F_2	2861.4(1)	1.2	A_1	$\nu_1?$
			2873.6(1)	1.15	F_2	ν_{18}
			2883.0(1)	0.9	A_1	$\nu_1?$
			2895(3)	sh	-	
2933	19	A_1	2909.6(1)	0.9	A_1	
			2934.5(1)	2.8	A_1	
2953	50	F_2	2954.8(1)	5.0	F_2	ν_{17}
2994 ^c						

- (a) Intensities are in arbitrary units
- (b) Values in brackets represent the experimental error in frequency (in cm^{-1}).
- (c) This peak was not seen by Couture-Mathieu et al because of instrumental limitations. It was observed by Kahovec et al.

Table 4. Raman Frequencies for HMT-h₁₂ in Aqueous Solution^a.

Reference 90			This Work		
ν/cm^{-1}	Polarization ^b	Intensity	ν/cm^{-1} ^b	$I_{\perp}/I_{ }$	Intensity
191	P				
456	D	9	452.6(1)	0.76	3.0
509	D	3.5	508.1(1)	0.75	0.9
			670.5(1)	0.8	0.2
685	D	2.5	684.5	0.74	0.4
783	P	13	782.3	0.09	10
820	D		817.9	0.77	0.3
952	D	w			
1010	D	8	1010.0	0.73	1.4
1019	D		1022.7	0.71	0.6
1050	P	10	1048.8(1)	0.1	5.7
1237	D	5	1236.0(1)	0.70	0.8
1348	D	10	1346.5(1)	0.70	2.1
1380	D	2.5	1377.0(1)	0.71	0.6
			1422.1(1)	0.8	0.15
			1442.1(1)	0.78	0.15
1455	D	7	1452.7(1)	0.75	1.3
2890	P	w	2887.8(1)	0.16	1.7
2914	P	w	2917.2(1)	0.15	1.8
2953	P	s	2946.5(1)	0.18	4.3

(Table continued on next page)

Table 4 continued

Reference 90			This Work		
ν/cm^{-1}	Polarization ^b	Intensity	ν/cm^{-1} ^b	$I_{\perp}/I_{ }$	Intensity
2977	D	s	2975.0(1)	0.45	3.0

(a) Intensities are in arbitrary units

(b) P = polarized

D = depolarized

(c) Values in brackets represent the experimental error
of the frequency, in cm^{-1} .

axes coinciding with the x, y, and z axes as defined in Figure 6. The fine adjustment was done in the following way. Peaks were selected due to vibrations whose symmetry type was known beyond any doubt, either from the work of Couture-Mathieu et al (90) or from the spectrum of the solution or from the infrared spectrum. The peaks chosen were due to the vibration of type E at 463.0 cm^{-1} , that of type F_2 at 512.0 cm^{-1} and that of type A_1 at 779.3 cm^{-1} . The orientation of the crystal was then adjusted to maximize the ratio I_{zz}/I_{zx} for the A_1 and E vibrations, while minimizing it for the F_2 mode. This procedure gave excellent results and the polarizations measured thereafter were, in general, clearcut (Figure 11). Some of the peaks were studied (Figure 12) in the 2b orientation of Couture-Mathieu and Mathieu (109), (Section III.1). The crystal was aligned for this orientation by maximizing $I_{z'z'}/I_{z'x'}$ for the A_1 mode and minimizing it for the E mode.

With the exception of the C-H stretching region, where the presence of overtones and of combination bands gives rise to a background which is strongly polarized in the spectrum of the solution, and whose polarization is not clearcut in the spectrum of the single crystal, the symmetry type of the modes giving rise to all but the very weak peaks was determined unequivocally from their polarization behaviour. A comparison of the Raman results with the infrared spectrum, in which only the F_2 modes are active, confirms the assign-

ment of these modes. It can be seen from Tables 3 and 4 that no great differences exist between these results and those of Couture-Mathieu et al (90). A discrepancy which deserves special attention is the peak due to an F_2 mode which was found at 1457 cm^{-1} in this work and which was not seen by the earlier workers. Couture-Mathieu also reported a peak at 684 cm^{-1} , while a doublet at 671.0 and at 674.5 cm^{-1} was found in this work. The peaks previously reported at 622, 696, 1100, 2034, 2065 and 2563 cm^{-1} were not seen during this investigation.

III.3 Results for HMT-d₁₂.

Infrared spectra between 4000 and 200 cm^{-1} of a polycrystalline powder pressed into KBr pellets were recorded. Since the spectra of HMT-h₁₂ in KBr pellets were identical with those of mulls, it was thought unnecessary to check the spectrum of HMT-d₁₂ by the mulling method. The spectra were recorded with the sample held at room temperature and at 100°K . The spectra are shown in Figures 13 and 14. The frequencies of the observed features are listed in Table 5. The resolution and accuracy of the observed frequencies are the same as for the light compound. The very weak peak at 2934 cm^{-1} could be due to hydrogen impurity in the HMT. The half-widths of the bands are less than 8 cm^{-1} , with the exception of the peak at 1175 cm^{-1} which contains several overlapping peaks and whose overall

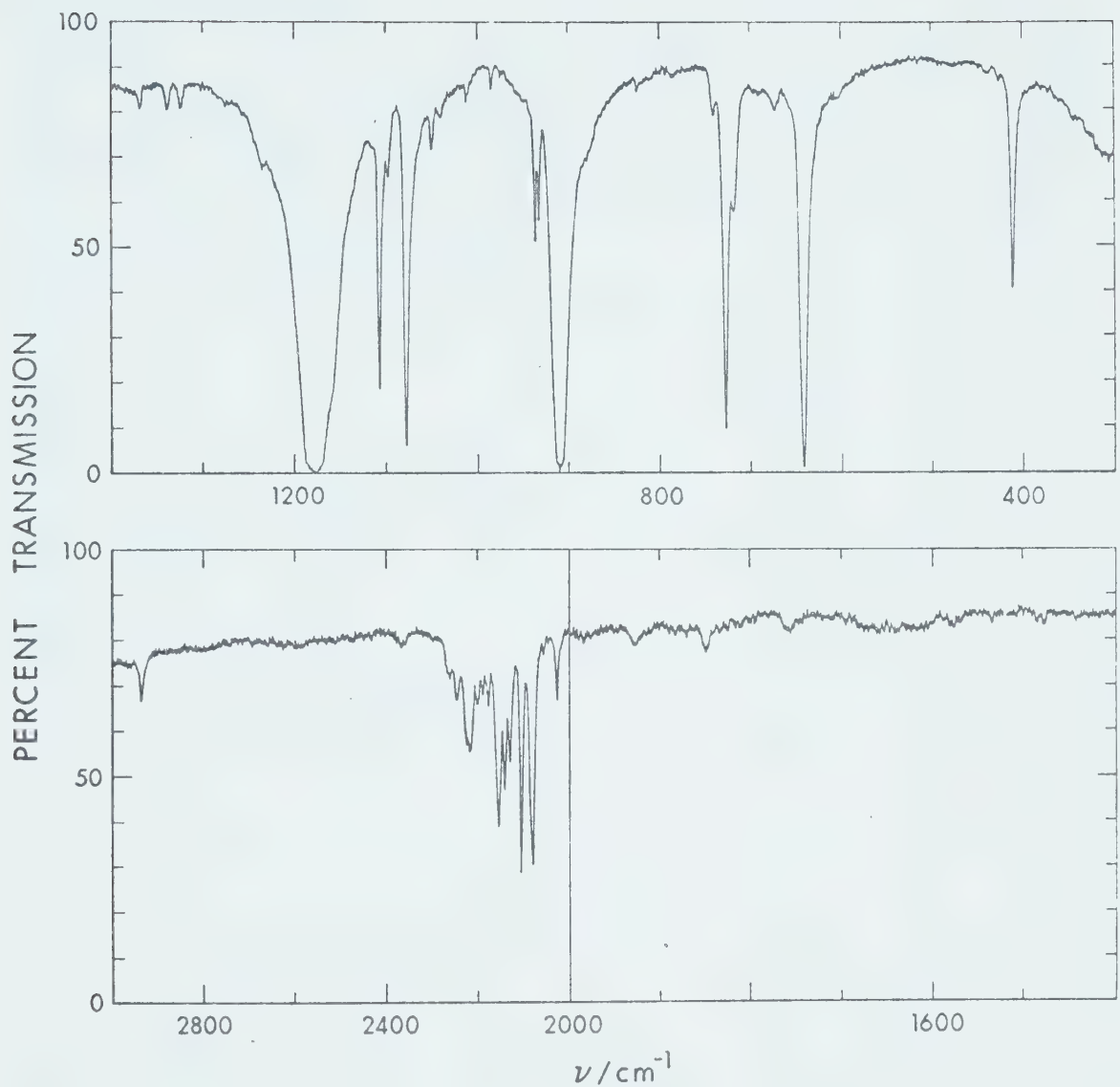


Figure 13. Infrared spectrum of a thick sample of HMT-d₁₂ in KBr at room temperature.

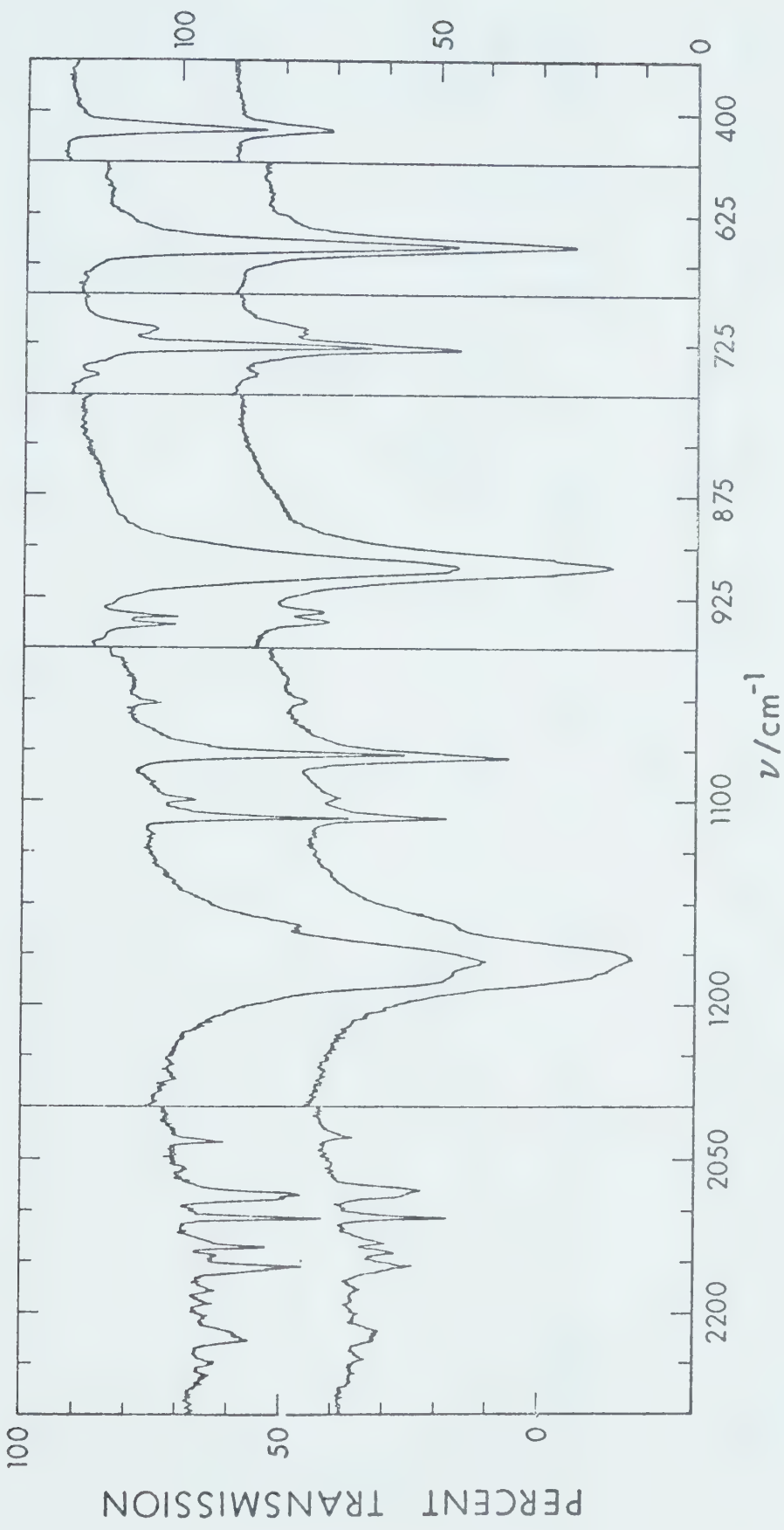


Figure 14. The intense absorptions in the infrared spectra of HMT-d₁₂ in KBr, at room temperature (lower trace) and at 100°K (upper trace). The same pellet was used for both spectra. The frequency scale is uniform below 2000 cm^{-1} . The right hand transmission scale refers to the lower trace.

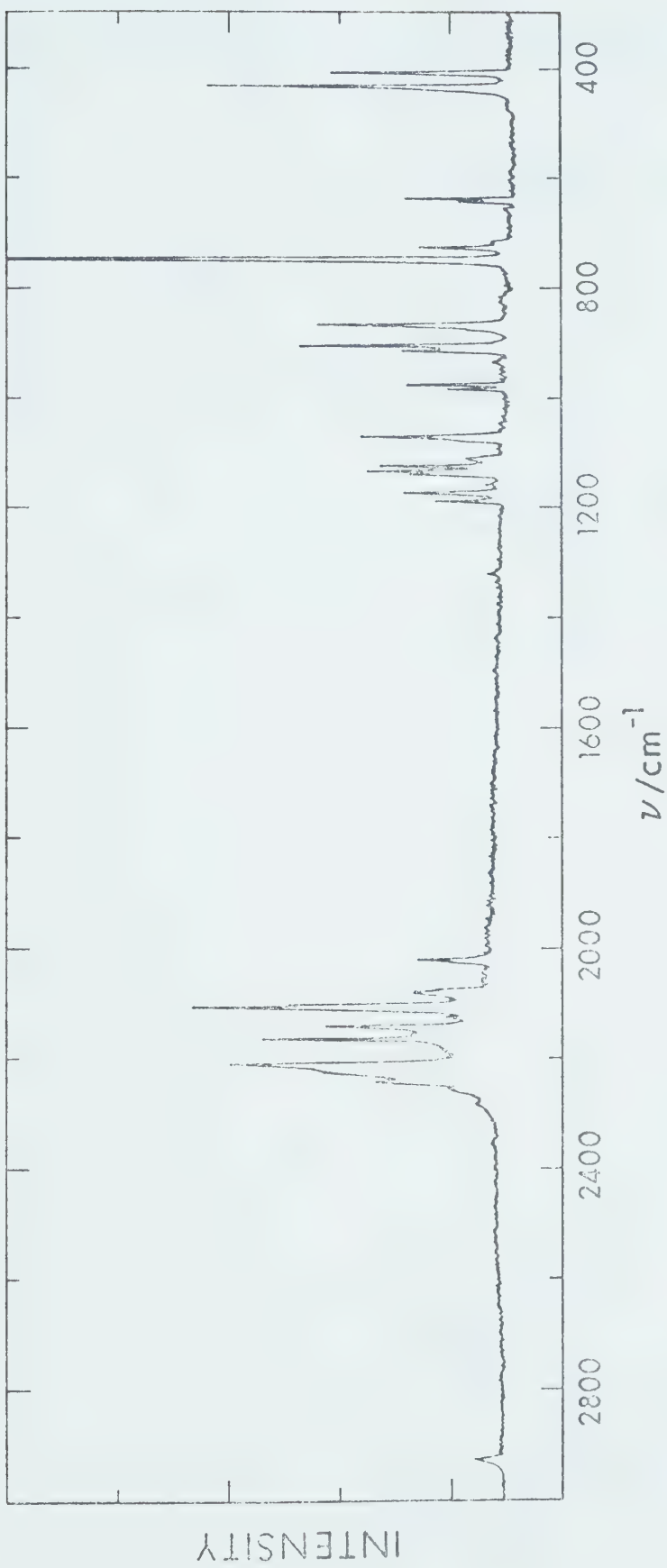


Figure 15. Raman spectrum of a polycrystalline sample of IMT-d₁₂ at room temperature.
No peaks were detected below 400 cm^{-1} .

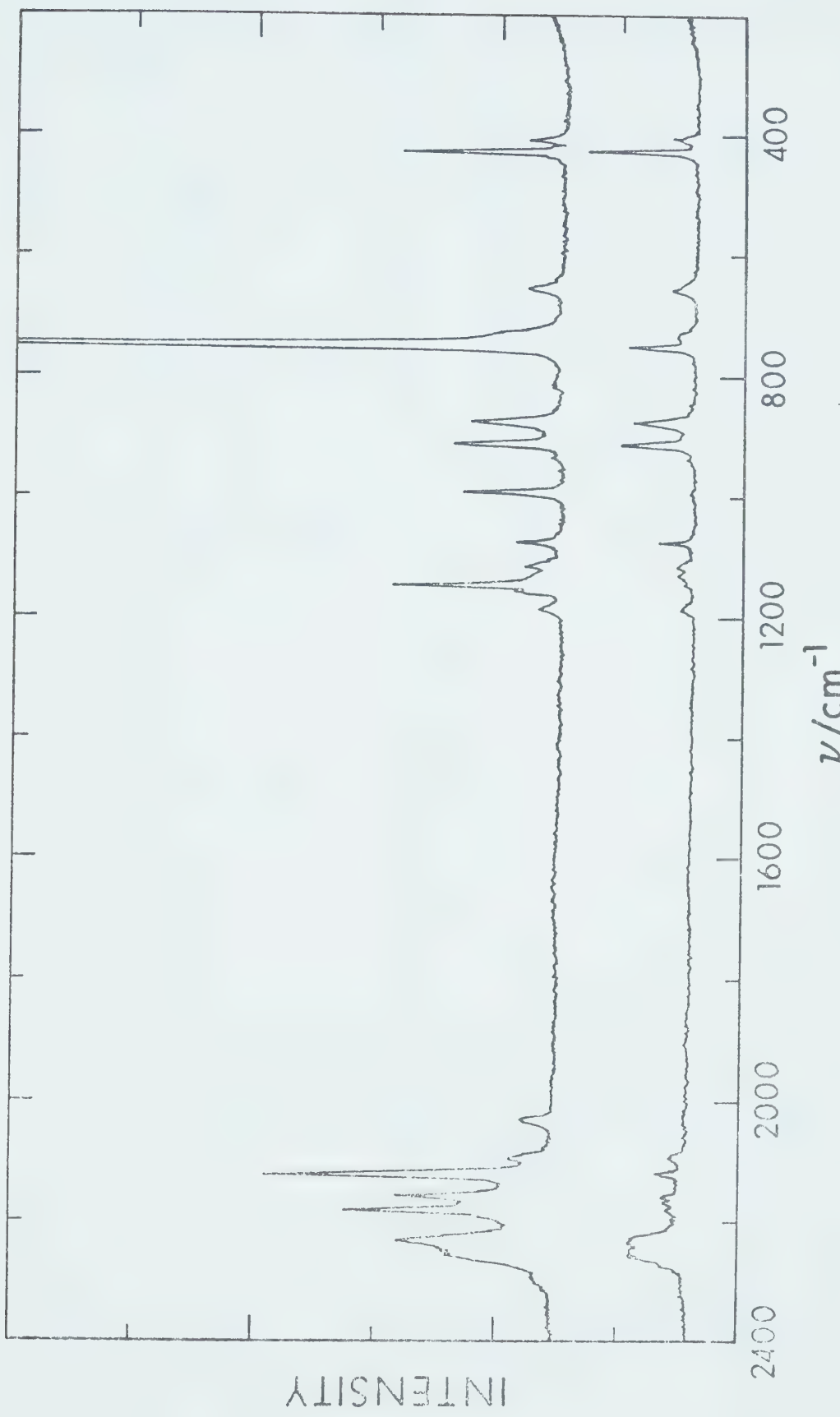


Figure 16. Raman spectra of a saturated aqueous solution of HMT-d₁₂ in parallel (upper trace) and perpendicular (lower trace) observation.

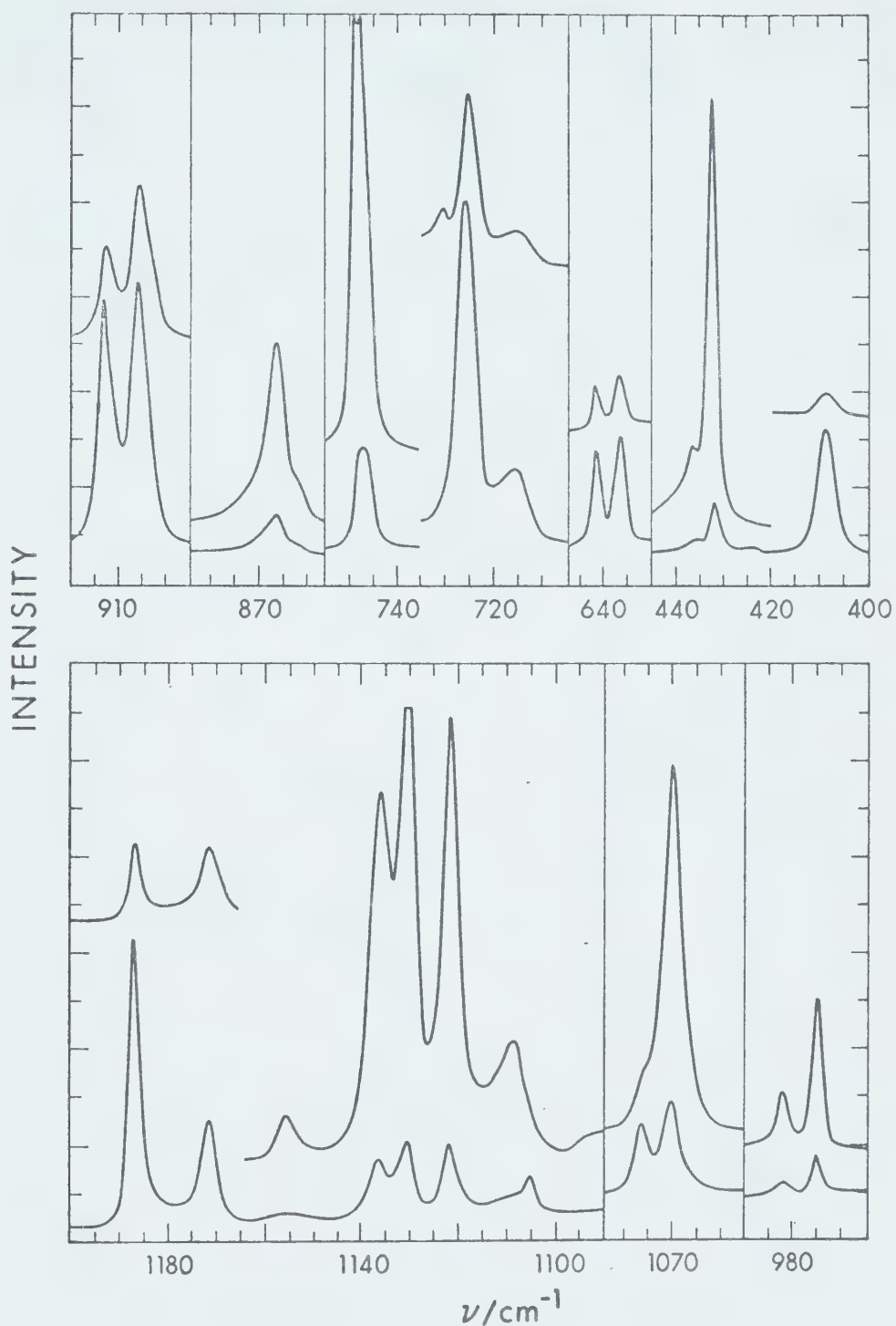


Figure 17. Raman spectra of an oriented crystal of HMT-d₁₂ at room temperature, under x(zz)y geometry (upper trace) and under x(zx)y geometry (lower trace).

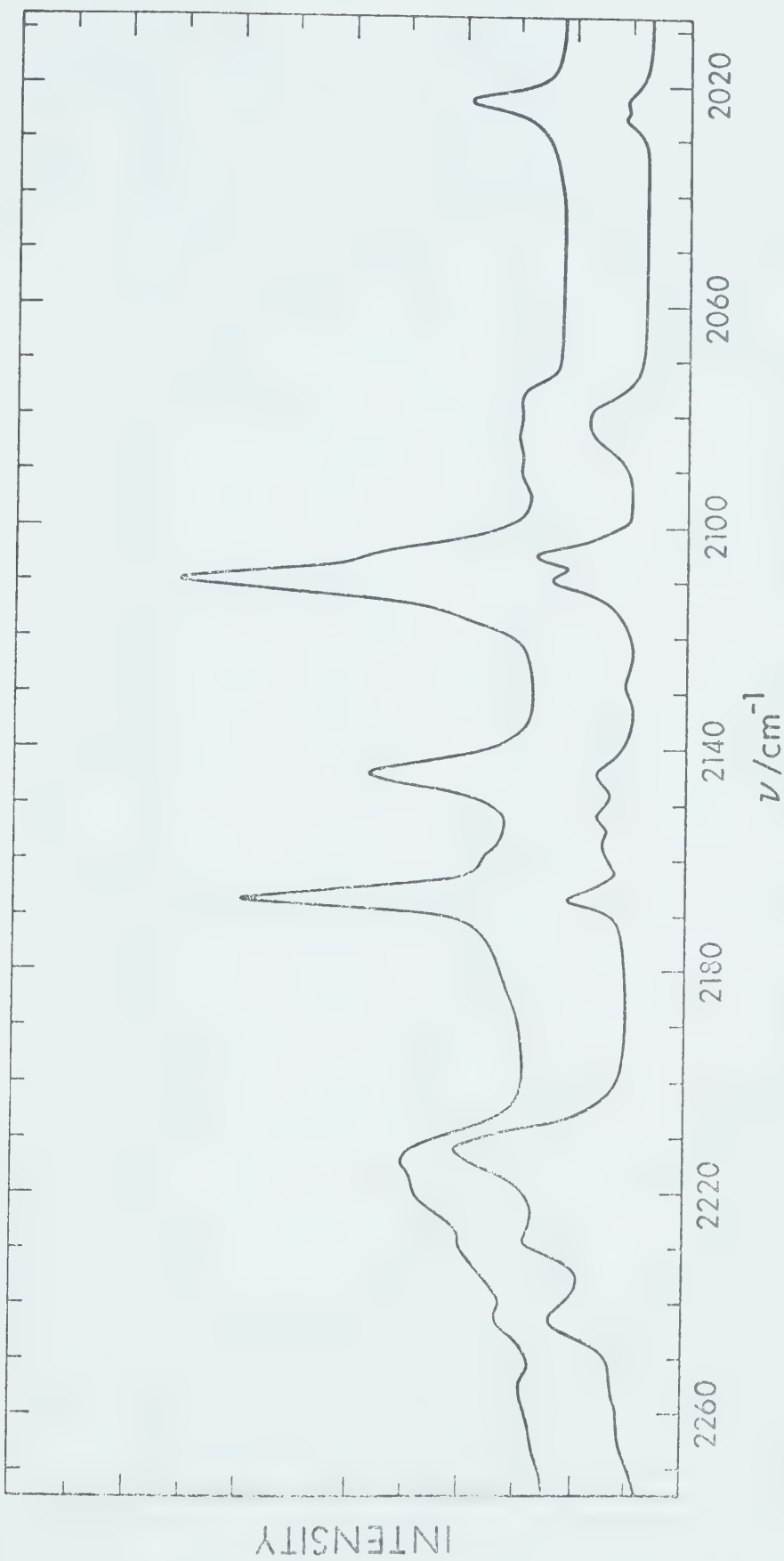


Figure 18. Raman spectra of an oriented crystal of HMT-d₁₂ at room temperature, under $x(zz)Y$ geometry (upper trace) and under $x(zx)Y$ geometry (lower trace).

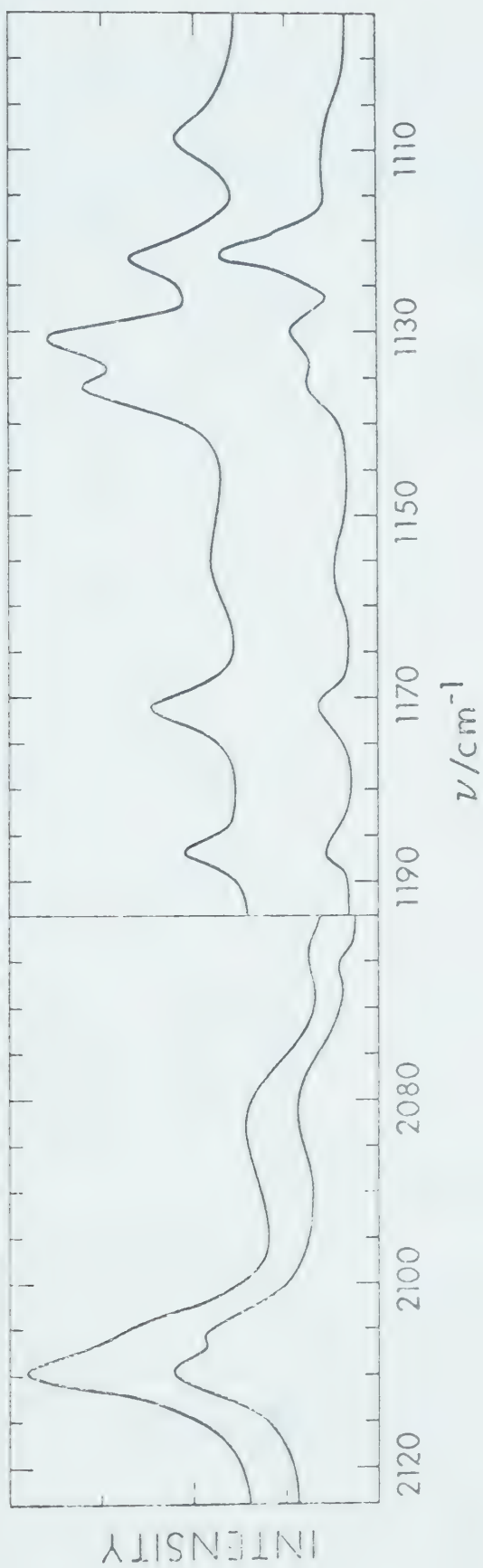


Figure 19. Raman spectra of an oriented crystal of HMT-d₁₂ at room temperature, under x' (z'z')^v geometry (upper trace) and under x' (z'x')^y geometry (lower trace).

Table 5. Infrared Absorption Frequencies (at 300 and 100°K),
Raman Shifts and Assignments for HMT-d₁₂^a.

Infrared				Raman	Type	Assign.
300°K ν/cm ⁻¹ ^b	100°K ν/cm ⁻¹ ^b			ν/cm ⁻¹ ^a	Int. ^c	
408.1(0.5) m	409.0 s			408.3(1)	0.60	F ₂ ν ₂₅
426.6(0.5) vw	424.0 vw			432.0(1)	2.50	E ν ₁₀
437.5(1) vw	439.5 vw			437.0(1)	-	-
604(2) vw	603 vw					
630(3) sh	630 sh					
640.0(0.5) s	642.3 vs			636.2(1)	0.60	F ₂ ν ₂₄ (TO)
				641.4(1)	0.28	F ₂ ν ₂₄ (LO)
673.1(1) vw	674.2 vw					
690.3(1) vw	693.0 vw					
718(2) m	719.3 m			717(2)	vw	
726.6(0.5) s	727.1 vs			725.5(1)	0.75	F ₂ ν ₂₃
739.6(1) w	740.4 w					
				748.0(1)	10	A ₁ ν ₄
825.2(0.5) vw	825.5 vw					
				863(3)	sh	
				866.5(1)	1.55	E ν ₉
908.1(0.5) vs	908.2 vs			905.7(1)	1.65	F ₂ ν ₂₂ (TO)

(Table continued on next page)

Table 5 continued

Infrared		Raman		Type	Assign.
300 °K ν/cm⁻¹ ^b	100 °K ν/cm⁻¹ ^b	ν/cm⁻¹ ^a	Int. ^c		
930.8(1)	w	932.9 m	912.8(1)	0.90	F ₂ ν ₂₂ (LO)
935.6(1)	w	937.6 m			
950 (2)	vw	950 vw	975.1(1)	0.90	A ₁ ν ₃
984(2)	vw	984.0 vw	983.1(1)	0.40	
1011.8(0.5)vw		1011.0 vw			
1039(2)	vw	1042.0 vw			
1050.0(0.5) w		1051.1 w			
			1069(1)	1.15	E ν ₈
1077.5(0.5) s		1076.2 s	1075.3(1)	0.18	F ₂ ν ₂₁
1097.2(1)	w	1098.5 w			
1107.0(0.5) m		1108.0 m	1105.0(1)	w	F ₂
			1108.8(1)	0.60	A ₁
			1121.4(1)	0.95	E ν ₇
			1131.4(1)	1.3	A ₁ ν ₂
			1137.0(1)	0.72	A ₁
1130(5)	sh	1133 sh			
			1155.5(1)	0.1	
1160(5)	sh	1162.0 s			

(Table continued on next page)

Table 5 continued

Infrared				Raman		Type	Assign.
300°K ν/cm ⁻¹ ^b		100°K ν/cm ⁻¹ ^b		ν/cm ⁻¹ ^a	Int. ^c		
1174(2)	vs	1182.1	vs	1171.2(1)	0.4	F ₂	ν ₂₂ (TO)
1184(5)	sh	1185.3	sh	1185.3(1)	0.24	F ₂	ν ₂₂ (LO)
1235.5(1)	vw	1235.0					
1322(2)	w	1322.0	w				
1339(2)	w	1340.1	w				
1368.0(1)	vw	1369.0	vw				
1476(2)	vw	1477					
1488(2)	vw	1488					
1758(2)	vw	1762	vw				
		1839.1	vw				
1850(3)	vw	1850.3	w				
		1864.8	vw				
1927(2)	vw	1928	vw				
				2022.0(1)	0.6	A ₁	or E
2026.9(1)	w	2029.5	m	2025.0(1)	sh	F ₂ ?	
2054.1(1)	vw	2059.0	vw				
2080.4(1)	m	2084.7	s	2081(3)	0.7	F ₂	
2106.6(1)	m	2108.2	s	2105.1(1)	1.7	F ₂	ν ₁₈
				2109.6(1)		A ₁	ν ₁
				2126(2)	0.2		
2130.5	w	2133.8	m				

(Table continued on next page)

Infrared		Raman		Type	Assign.	
300°K	100°K	ν/cm^{-1}	ν/cm^{-1}	ν/cm^{-1}	Int. ^c	
2140.0(1)	w	2142.0	m	2143.7(1)	1.15	A_1 or E
2153.0(1)	m	2154.3		2151(2)		
				2156(2)		
				2166.4(1)	1.9	A_1 or E
2175.1(1)	vw	2178.1	w			
		2190.0	w			
2200(2)	vw	2203.1	vw	2211.5(1)	2.2	F_2
2216(3)	w	2217	sh	2225.5(1)		A_1 or E
2226(3)	sh	2225.3	m	2228(3)	sh	F_2 ν_{17}
				2241.7(1)	1.1	F_2
2244.5(1)	vw	2246.5	w			
2262(3)	vw	2260	w			
		2269	sh			
2934.0(1)		2933.0	w	2934.2(1)	w	

(a) Values in brackets indicate experimental error of frequencies in cm^{-1} .

(b) vs = very strong; s = strong; m = medium; w = weak; vw = very weak; sh = shoulder.

(c) Intensities are in arbitrary units.

Table 6. Raman Frequencies for HMT-d₁₂ in Aqueous Solution.

ν/cm^{-1} ^a	$I_{\perp}/I_{ }$	Int. ^b
404.6(1)	0.78	0.3
425.9(1)	0.78	1.6
639 (2)	-	~0.1 (sh)
654.1(1)	0.73	0.3
735 (2)	0.70	0.5 (sh)
749.8(1)	0.05	10
873.8(1)	0.76	0.9
910.6(1)	0.71	1.0
932 (2)	-	0.05
989.5(1)	0.09	0.95
1072.5(1)	0.72	0.4
1083 (2)	-	vv
1110.7(1)	0.70	~0.2
1130 (2)	-	0.1 (sh)
1143.5(1)	0.03	1.6
1152 (2)	-	0.15 (sh)
1182.3(1)	0.73	0.2
2028 (3)	0.0	0.3
2091 (3)	0.2	3.0
2119.0(1)	0.04	2.9

(Table continued on next page)

Table 6 continued

ν/cm^{-1}	$I_{\perp}/I_{ }$	Int. ^b
2155.3(1)	0.05	1.6
2178.5(1)	0.03	2.2
2190 (3)	-	- (sh)
2227.7(1)	0.2	1.6
2252 (2)	~0.31	- (sh)
2291 (3)	-	vw

(a) Values in brackets represent experimental errors of frequencies in cm^{-1} .

(b) Intensities are in arbitrary units; sh = shoulder;
vw = very weak.

half-width is about 38 cm^{-1} , and of the peak centered at about 908 cm^{-1} whose half-width is about 15 cm^{-1} .

Raman spectra of a polycrystalline powder, a saturated aqueous solution and an oriented crystal were obtained. The spectra are shown in Figures 15 - 19. The frequencies of the observed features, their estimated errors and their polarization behaviour are listed in Tables 5 and 6. The crystal used in this investigation appeared to be single under optical examination. It was aligned by the same procedure used for the HMT- h_{12} crystal, and the symmetry properties of the vibrations causing the peaks were unambiguously obtained. The polarization data were, however, not as good as for the HMT- h_{12} single crystal. Laue X-ray diffraction photographs, obtained using unfiltered molybdenum radiation, showed that the crystal contained two regions having very nearly the same orientation, and this defect in the crystal undoubtedly accounts for the poorer polarization data.

III.4 Discussion and Assignment for HMT- h_{12} .

In this section an assignment of the infrared and Raman spectra based on the experimental evidence will be proposed. Points concerning the spectra of HMT- d_{12} (whose complete assignment is presented in Section III.5) will be used to justify some of the assignments made for the light compound.

Almost complete agreement was found between this work and the previous works with regard to symmetry. The only exception is the assignment of the weak peak at 1306 cm^{-1} to an E mode, while Couture-Mathieu et al assigned it to an F_2 mode. The results of the symmetry determinations are shown in Table 3.

With regard to the selection of the peaks due to fundamental vibrations, some disagreement exists, and this will be discussed in the appropriate parts of this section. While most fundamentals could be assigned in terms of a particular internal coordinate from considerations based on symmetry, intensity and frequency, the assignment of some modes was not possible on these grounds alone. For this reason a normal coordinate calculation was carried out to gain a better understanding of the degree of mixing of the symmetry coordinates in the normal coordinates. The details and results of these calculations are presented in Section III.8.

The C-H stretching modes. Four C-H stretching vibrations are Raman active and should be seen between 2800 and 3000 cm^{-1} ; two of them are due to F_2 modes, one to an A_1 mode and one to an E mode. The two F_2 modes are also infrared active. One of the F_2 modes is based on the asymmetric C-H stretch of the methylenic groups, while the second F_2 mode, the A_1 mode and the E mode are based on the symmetric C-H stretch. Since the different CH_2 groups

are not adjacent, very little coupling is expected between their vibrations. Consequently, the frequencies of the A_1 , E and F_2 modes based on the symmetric stretch should be very close, and should be distinctly lower than that of the F_2 mode based on the asymmetric stretch. The two peaks of medium intensity which appear in the infrared spectrum at 2873.5 and at 2954.7 cm^{-1} (Figs. 7 and 8) are almost certainly the symmetric and asymmetric F_2 methylenic stretching fundamentals respectively. The corresponding Raman peaks are seen at 2873.6 and 2954.8 cm^{-1} (Figs. 9 to 11). This agrees with the assignment of Couture-Mathieu et al. The A_1 mode was assigned by these workers to the strong Raman peak at 2933 cm^{-1} , while the E mode was not located by them. In this work the A_1 mode is assigned to one of the two peaks at 2861.4 and 2883.0 due to their proximity to the peak at 2873.6. No peaks were found whose polarization behaviour was compatible with an E type vibration. The E mode is, therefore, left unassigned. This assignment leaves the strong Raman peak at 2934.5 cm^{-1} to be assigned to an A_1 , non-fundamental transition. A possible assignment is to the first overtone of the E or F_2 methylenic deformations at 1454 and 1458 cm^{-1} , respectively.

The H-C-H deformation modes. Three peaks due to H-C-H deformation of symmetry A_1 , E and F_2 should be seen in the Raman spectrum between 1410 and 1480 cm^{-1} . The vibration of type F_2 was assigned by Cheutin and Mathieu

to the two infrared peaks at 1440 and 1458 cm^{-1} . They did not explain the reason for the splitting. It seems more reasonable to assign the peak at 1458.2 cm^{-1} to this vibration. The peak at 1440 cm^{-1} probably arises from a combination of the vibrations at 779.3 (A_1) and 674.2 cm^{-1} (F_2), as suggested by Mecke and Spiesecke.

The peak due to the A_1 mode could not be located in the Raman spectrum, while the mode of type E was assigned to the strong Raman peak at 1454.2 cm^{-1} . This agrees with the earlier assignments. The shoulder seen in the Raman spectrum of the single crystal in the $x(zx)y$ geometry at 1457 cm^{-1} (Fig. 11) is assigned to the F_2 mode, and is reported here for the first time.

The methylenic twisting modes. One peak due to the methylenic twist of type E should be seen in the Raman spectrum. In aliphatic hydrocarbons these modes are normally found between 1175 and 1310 cm^{-1} (111). Couture-Mathieu et al and Mecke and Spiesecke assigned this mode at 1441 and at 1020 cm^{-1} , respectively. These frequencies appear to be too high and too low, respectively. A third alternative is to assign the twisting mode to the peak at 1349.2 cm^{-1} which, in the earlier works was assigned to a ring mode. In the Raman spectrum of the heavy compound no peaks due to vibrations of type E were found above 1130 cm^{-1} . The 1349.2 cm^{-1} peak is, therefore, shifted by at least 20% on deuteration which is not compatible with the earlier

assignment. Therefore in this work the methylenic twist is assigned to the peak at 1349.2 cm^{-1} . This assignment leaves the strong Raman peak at 1439.6 cm^{-1} (E) to be assigned to a combination band. Mecke and Spiesecke assigned it to a combination of the F_2 fundamental at 511 cm^{-1} with an inactive F_1 vibration, for which they postulated a frequency of 925 cm^{-1} . This is compatible with the fact that in the infrared spectrum of the hydrate (Section V.) a peak is found at 934 cm^{-1} which could well arise from an F_1 mode activated in the hydrate by the C_{3v} site symmetry of the HMT molecule (34).

The methylenic wagging modes. One wagging vibration of type F_2 is expected to be infrared and Raman active. Couture-Mathieu et al assigned the peak at 1370 cm^{-1} to this mode. However their description of the wagging mode makes it clear that they really assigned this peak to what is commonly called the methylenic rock (Fig. 20). If one takes their use of the terms wag and rock to be the same as shown in Figure 20, then their assignment is acceptable.

The methylenic rocking mode. One rocking mode of type F_2 is expected to be infrared and Raman active. The earlier authors assigned this mode to the peak at 812 cm^{-1} . This assignment is maintained in this work, provided that the term rock corresponds to the description given in Figure 20.

The ring modes. Both the C-N stretches and the

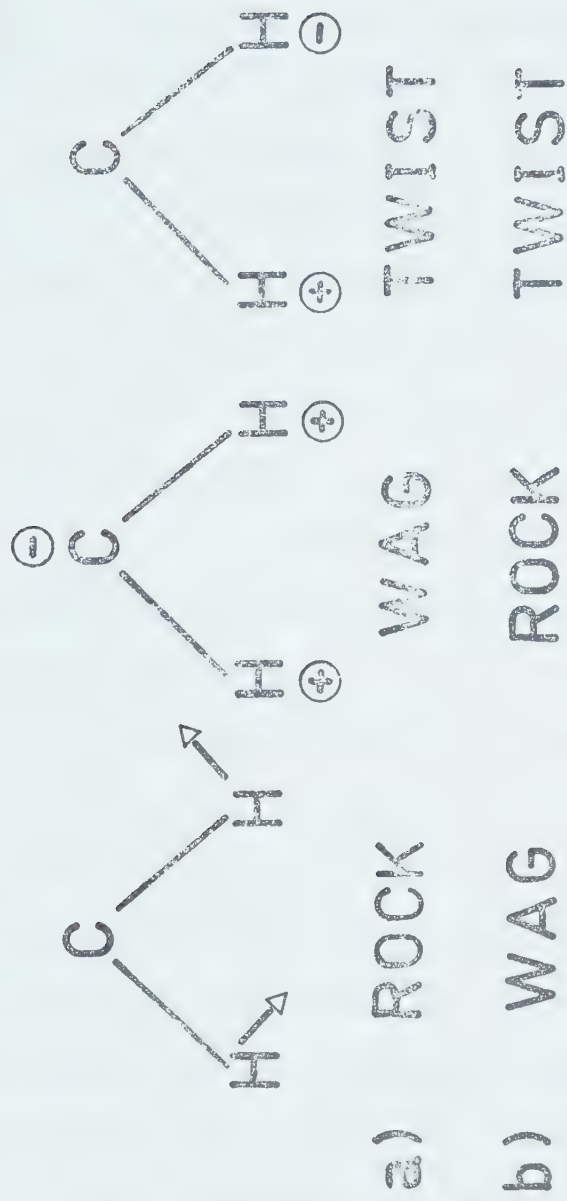


Figure 20. Description of methylenic motions according to:

- (a) This work and present day nomenclature.
- (b) Couture-Mathieu et al (90).

C-N-C deformations form the representation $A_1 + E + F_1 + 2F_2$. The two C-N stretching vibrations of type F_2 were assigned by the earlier authors to the peaks at 1238 and 1006.8 cm^{-1} . These assignments appear to be reasonable and the spectra of the heavy compound are compatible with them. The doubly degenerate C-N stretching mode is assigned at 1015 cm^{-1} , the only Raman band with the appropriate polarization behaviour between 500 and 1300 cm^{-1} . In both previous works this mode was assigned to the peak at 1350 cm^{-1} , which in this work has been assigned to the methylenic twist. The mode of type E based on the C-N-C deformation was assigned by Couture Mathieu to the peak at 463 cm^{-1} and this is undoubtedly correct.

Two peaks due to A_1 modes are found below 1100 cm^{-1} in the Raman spectrum of the crystal, at 1042.0 and 779.3 cm^{-1} . They are certainly the ring modes based on the C-N stretch and the C-N-C deformation. The peak at 779.3 cm^{-1} which is the strongest Raman peak, is assigned to the mode based on the C-N stretch (the ring breathing mode) and the peak at 1042.0 cm^{-1} is assigned to the mode based on the C-N-C deformation. This agrees with the assignment made by Couture-Mathieu et al, but Mecke and Spiesecke appear to have reversed the assignment, although they do not make their assignment of the ring modes completely clear.

The two F_2 modes based on the C-N-C deformations

were assigned in the earlier works to the peaks at 672 and 511 cm^{-1} . These assignments appear to be reasonable, subject to the possibility of mixing between the CH_2 rocking and the C-N-C deformation coordinates.

III.5 The Transverse and Longitudinal Components of the Infrared Active Modes of Hexamethylenetetramine-h₁₂₋

It is well known that, when a vibration is infrared active, the macroscopic electric field associated with the longitudinal mode (LO) causes the frequency of the LO mode to be higher than that of the transverse mode (TO). For ionic, cubic crystals with two atoms per unit cell, the frequencies of the two components are related by the Lyddane-Sachs-Teller (LST) relation (7).

$$\epsilon_0 = \epsilon_\infty (\nu_{\text{LO}} / \nu_{\text{TO}})^2 \quad \text{III.1}$$

where ϵ_0 is the static dielectric constant, ϵ_∞ is the high frequency dielectric constant and ν_{LO} and ν_{TO} are the frequencies of the longitudinal and transverse vibrations respectively. A generalization of the LST relation due to Cochran and Cowley (112) states that, for cubic crystals,

$$\prod_{i=1}^N \left[\frac{\nu_{\text{LO}}(i)}{\nu_{\text{TO}}(i)} \right] = \left(\frac{\epsilon_0}{\epsilon_\infty} \right)^{1/2} \quad \text{III.2}$$

and is applicable to a system with N infrared active normal vibrations.

The magnitude of the splitting for a given normal vibration is related to the derivative of the dipole moment with respect to the normal coordinate under consideration by the following relationship due to Haas and Hornig (113)

$$\nu_{LO}^2 = \nu_{TO}^2 + 1/3 \frac{(n^2 + 2)N}{n^2 3 \pi} \left(\frac{\partial \mu}{\partial Q} \right)^2 \quad III.3$$

where n is the refractive index at a frequency higher than the frequency of the vibration, N is the number of vibrators per unit of volume, and $(\frac{\partial \mu}{\partial Q})$ is the dipole moment change induced by the normal vibration Q and is related to the absorption intensity. The TO and LO components can manifest themselves in infrared reflection spectra and in Raman spectra (113). It is obvious from the above relation that the splitting is expected to be very large in the case of ionic crystals, which are very strong infrared absorbers, and much smaller in molecular crystals which usually absorb less strongly. However, peaks associated with longitudinal phonons have recently been identified in the Raman spectra of the molecular crystals CF_4 , HCN, DCN, ICN, and HCl (114).

Doublets were seen in the Raman spectrum of HMT-h₁₂ at frequencies close to those of the strongest infrared peaks ($671.0 - 674.5; 810.5 - 814.0 \text{ cm}^{-1}; 1004.3 - 1017.5 \text{ cm}^{-1}; 1236.5 - 1241.8 \text{ cm}^{-1}$). The hypothesis was formulated that the LO components of the F_2 modes were being observed. It was possible to test this hypothesis due to the different polarization behaviour of the transverse and longitudinal

modes.

The nonvanishing components of the polarizability derivative tensor for the point group T_d are given below (108).

$$\begin{aligned}
 \alpha' (A_1) &= \begin{pmatrix} a & a & a \end{pmatrix} & a = \alpha_{xx} = \alpha_{yy} = \alpha_{zz} \\
 \alpha' (E) &= \begin{pmatrix} b & b & b \end{pmatrix} & b = \alpha_{xx} = \alpha_{yy} = \alpha_{zz} \\
 \alpha' (F_2(x)) &= \begin{pmatrix} d & d \end{pmatrix} & d = \alpha_{yz} = \alpha_{zy} \\
 \alpha' (F_2(y)) &= \begin{pmatrix} d & d \end{pmatrix} & d = \alpha_{xz} = \alpha_{zx} \\
 \alpha' (F_2(z)) &= \begin{pmatrix} d & d \end{pmatrix} & d = \alpha_{yx} = \alpha_{xy}
 \end{aligned}$$

For the infrared and Raman active F_2 modes the (x), (y) and (z) represent the direction of polarization of vibrations. Thus the x-polarized F_2 component is observed under α_{zy} , the y polarized component under α_{xz} and the z-polarized component under α_{xy} .

If the Raman spectrum is excited by light propagating along x and is observed along y, then the wave-vector selection rule requires that the vibration observed propagates in the xy plane at about 45° to x and y (Section I.2). Thus the scattering geometry x(yx)y excites the z-polarized component of the vibration propagating in the xy plane. This is a transverse mode with the frequency ν_{TO} . The scattering geometry x(yz)y excites the x-polarized component of a vibration propagating at about 45° to the x axis, and this means that both the TO and LO components of

of the F_2 modes are excited and bands should be seen at ν_{TO} and ν_{LO} .

It can be seen in Figure 21 that the high frequency component of each of the doublets mentioned above greatly decreases in intensity in the $x(yx)y$ geometry with respect to the $x(yz)y$ geometry. They can, therefore, be assigned to the LO components of the F_2 modes. The difference $\nu_{LO}^2 - \nu_{TO}^2$ for the different F_2 modes should be proportional to their infrared relative integrated absorption intensities as shown by equation III.3. In Table 7 and Figure 22 these two quantities are related, and it can be seen that they are approximately linearly proportional. Five of the F_2 modes do not show LO-TO splitting in the Raman spectrum, which is consistent with their low infrared intensity.

On the basis of the above evidence, the Raman peaks at 674.5, 814.0, 1017.5 and 1241.8 cm^{-1} are assigned to the LO components of the F_2 modes, while the peaks at 671.0, 810.5, 1004.3 and 1236.5 cm^{-1} are assigned to the corresponding TO components.

When the above frequencies are inserted into the modified LST equation III.2, a value of 1.055 ± 0.005 is found for the ratio $\frac{\epsilon_0}{\epsilon_\infty}$. The refractive index of HMT was measured by the Becke line method (115) for sodium D light and was found to be 1.588 ± 0.002 at 22°C . The static dielectric constant of HMT is therefore found to be 2.660

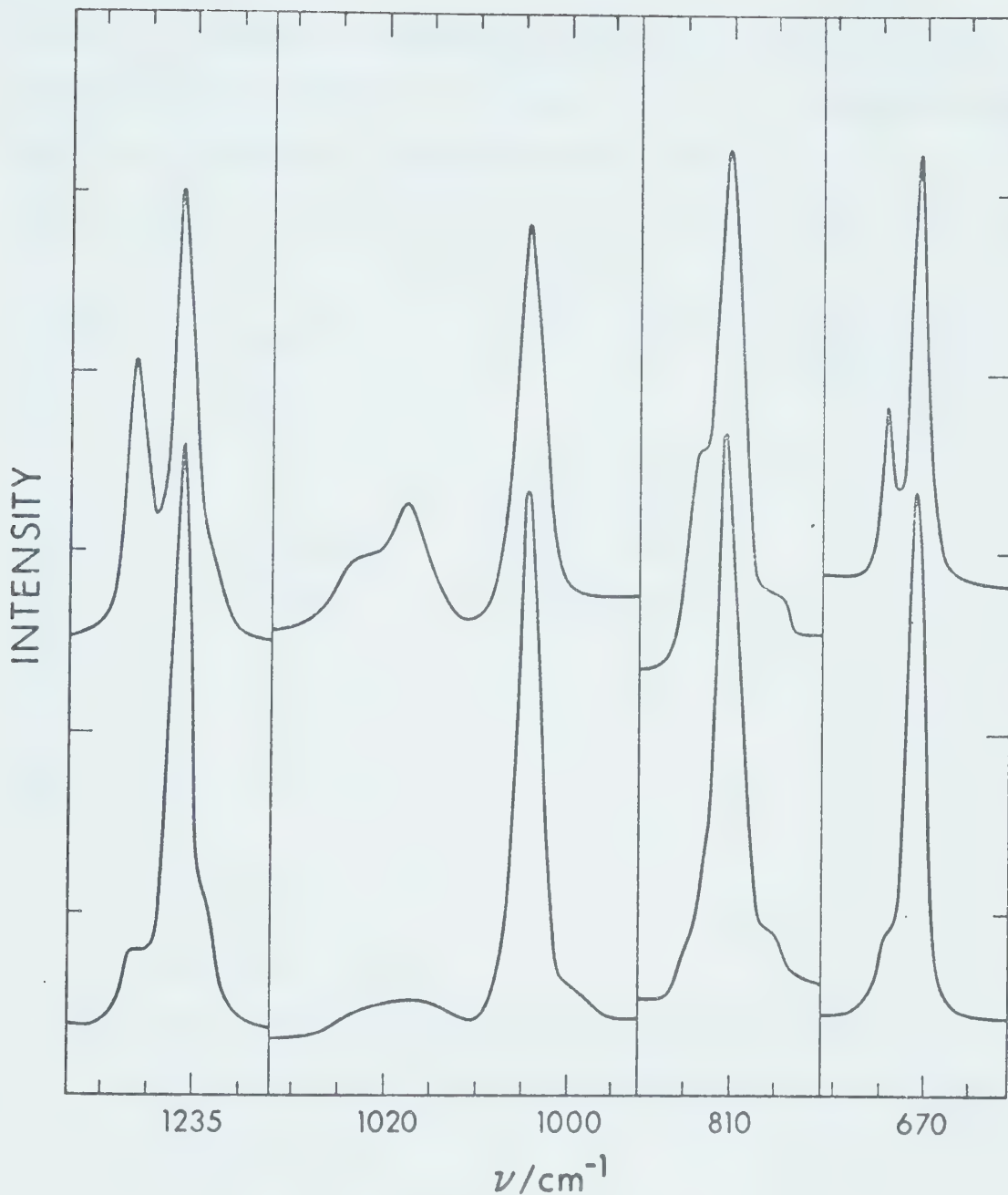


Figure 21. Raman spectra of a single crystal of HMT- h_{12} at room temperature, under $x(yz)y$ geometry (upper trace) and under $x(yx)y$ geometry (lower trace). The frequency marks are 5 cm^{-1} apart.

Table 7. Relation between the Frequencies of the Longitudinal and Transverse Components of the F_2 Modes and their Relative Integrated Intensities for HMT-h₁₂.

ν_{LO}/cm^{-1}	ν_{TO}/cm^{-1}	$\nu_{LO}^2 - \nu_{TO}^2$ a	Integrated Intensity b,c
512.0	512.0	-	0.45
674.5	671.0	1.00 \pm 0.27	1.0
814.0	810.5	1.21 \pm 0.35	1.1
1017.5	1004.3	5.67 \pm 0.42	6.2
1241.8	1236.5	2.79 \pm 0.5	2.4
1370.0	1370.0	-	0.66
1457.0	1457.0	-	0.47

(a) In $\text{cm}^{-1}/4709.25$.

(b) In arbitrary units.

(c) The error in measuring the area under a peak was found to be about 0.05 (standard deviation of three determinations).

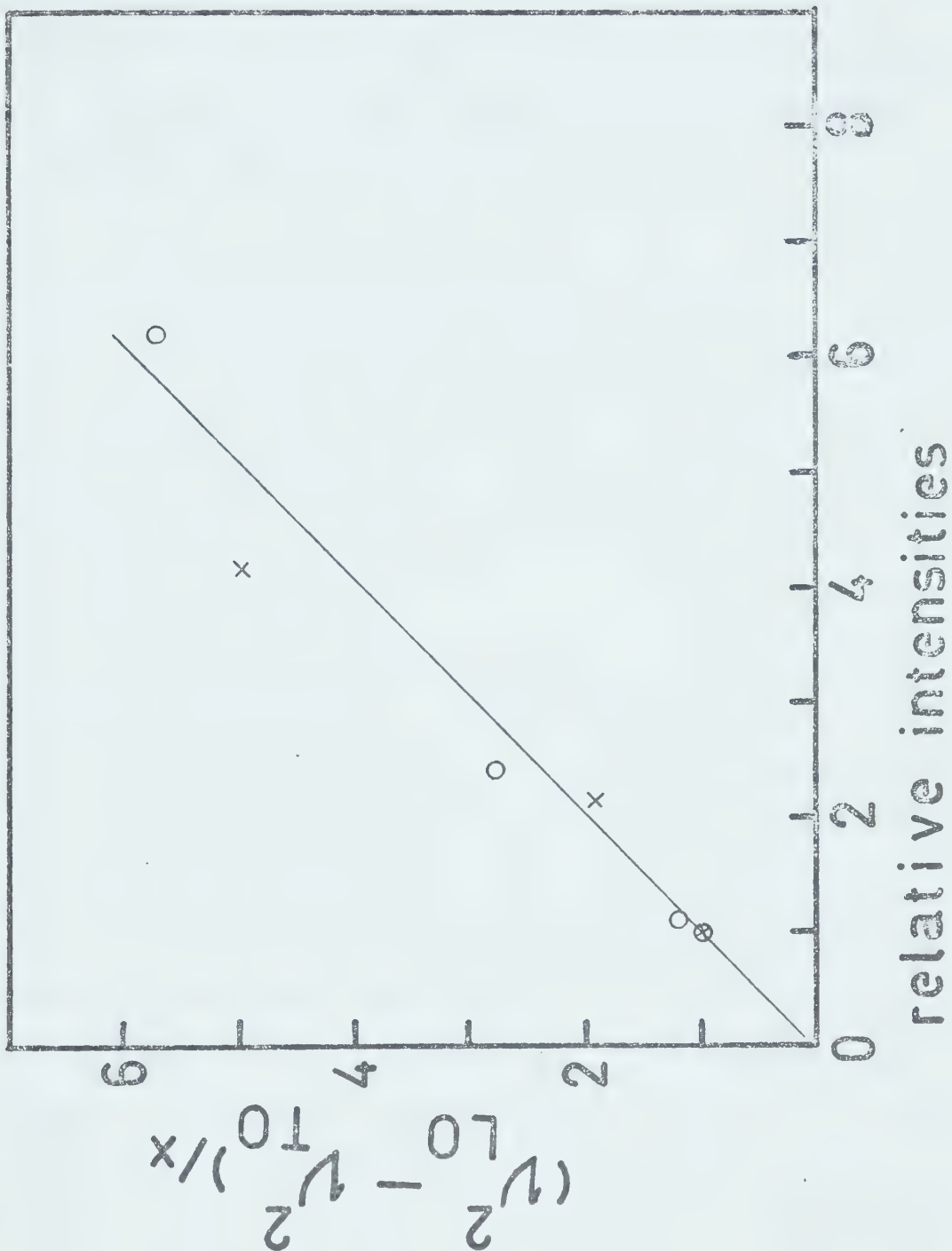


Figure 22. Plot of $(v_{LO}^2 - v_{TO}^2)/x$ vs. the relative intensities of the infrared bands, for HMT-h₁₂ (o) and HMT-d₁₂ (x).

v 's in units of cm^{-1} ; $x = 4709.25$ for HMT-h₁₂, 6644.0 for HMT-d₁₂.

± 0.008. It is, unfortunately, not possible to compare this value with the value found by dielectric methods because this value is not known.

III.6 Discussion and Assignment for HMT-d₁₂.

The polarization behavior of the oriented crystal Raman spectrum (Figures 17 and 18), the depolarization ratios of the solution Raman spectrum (Figure 16) and the infrared (Figures 13 and 14) and the Raman activity of the peaks made it possible to assign the observed spectral features to modes of specific symmetry. The results of the symmetry determinations are summarized in Table 5. The assignment of the fundamental vibrations was made on the basis of the symmetry and intensity of the spectral features. While the identification of some of the fundamental C-D stretching vibrations is subject to some doubt, the remaining fundamentals were located with little uncertainty. An assignment of the spectra in terms of internal coordinates is presented in this section. However, it must be kept in mind that a large number of modes of the same symmetry occur at frequencies between 400 and 1200 cm⁻¹, and it is most probable that the true normal coordinates are mixtures of the symmetry coordinates. Therefore the assignment given in this section is approximate, and a more detailed assignment results from the normal coordinate calculations (Section III.8).

The C-D stretches. Three medium intensity absorptions are found in the infrared spectrum at 2080.4, 2106.6 and 2153.0 cm^{-1} and one is tempted to assign two of them to the two F_2 fundamental vibrations expected in this region. But a simple calculation of the kinetic splitting between the asymmetric and symmetric C-D stretching modes, based on the diagonal force constant obtained from the assignment of the C-H stretching modes, predicts a far larger splitting than the largest separation between the above three peaks (111 cm^{-1} against the observed 73 cm^{-1}). Five bands which show the polarization properties of F_2 modes appear in the Raman spectrum of the solid, at 2081, 2105.1, 2211.5, 2228.0 and 2241.7 cm^{-1} . The breadth and the polarization behaviour of the peak at 2081 cm^{-1} suggest that it is due to a non-fundamental transition, possibly a combination of the F_2 vibrations at 1174 cm^{-1} and 908.1 cm^{-1} . The peaks at 2105.1 and 2106.6 cm^{-1} in the Raman and infrared spectra, respectively, are probably due to the fundamental F_2 mode based on the symmetric C-D stretch. The Raman peak at 2211.5 cm^{-1} does not have a counterpart in the infrared spectrum and it is a possible candidate for the asymmetric C-D stretch of type F_2 . Another possibility is to assign this mode to the peaks at 2228.0 and at 2226 cm^{-1} in the Raman and infrared spectra, respectively. The second assignment is preferred here because it would otherwise be difficult to explain why this mode does not appear in

absorption.

The polarization of the solution Raman spectrum is quite uncertain in the 2000 to 2200 cm^{-1} region, due to a strongly polarized background which makes all peaks appear at least partially polarized. In addition, no one-to-one correspondence is found between the spectra of the solution and that of the polycrystalline sample. However, the results of the polarization studies on the oriented crystal allow the A_1 fundamental to be located. The polarization of the peak at 2109.6 cm^{-1} (Figures 18 and 19) clearly identifies it as due to an A_1 transition, and its frequency is very close to that of the F_2 mode based on the symmetric stretch, as expected for the A_1 fundamental. No peaks with polarization compatible with an E mode were located in this region; it is, however, reasonable to propose that the peak due to the C-D stretch of symmetry E is overlapped by the peaks due to the corresponding A_1 and F_2 modes, and for this reason, and because of the imperfect crystal polarization data, it could not be located.

The D-C-D deformation modes. The peak due to the methylenic deformation of type A_1 is easily identified in the Raman spectrum of the solution as the polarized peak at 1143.5 cm^{-1} . Two peaks, at 1131.4 and at 1137.0 cm^{-1} , in the Raman spectrum of the oriented crystal show a polarization consistent with an A_1 mode (Figures 17 and 19). The strongest of the two, at 1131.4 cm^{-1} , is assigned to

the A_1 methylenic deformation, while the weaker one, at 1137.0 cm^{-1} , can be assigned to a combination of the F_2 modes at 725.5 and 408.3 cm^{-1} whose A_1 component is enhanced in intensity by Fermi resonance with the fundamental level at 1131.4 cm^{-1} .

Four peaks which can be assigned to F_2 modes are found in the infrared and Raman spectra between 1050 and 1200 cm^{-1} , where the CD_2 deformations are expected to occur. In addition to the F_2 CD_2 deformation, an F_2 C-N stretching mode and the F_2 methylenic wagging mode are expected in this region. By analogy with HMT- h_{12} , the ring mode is assigned to the very strong infrared band at 1174 cm^{-1} , while the Raman peak at 1185 cm^{-1} is probably due to the corresponding LO mode (Section III.7). The F_2 methylenic deformation can, therefore, be assigned either at 1105 or at 1075.3 cm^{-1} , and it is tentatively assigned at 1105.0 cm^{-1} . It is, however likely that a large degree of mixing between coordinates of the same symmetry gives rise to the normal modes which occur in this region.

The polarization behaviour of the peaks at 1121.4 and 1069.0 cm^{-1} identifies them as due to E modes. The doubly degenerate CD_2 deformation is tentatively assigned to the peak at 1121.4 cm^{-1} .

The CD_2 wagging mode. The only remaining peaks to which the F_2 CD_2 wagging mode can be assigned are at 1075.3 and 1077.5 cm^{-1} in the Raman and infrared spectra

respectively.

The CD₂ twisting mode. A peak due to an E mode occurs at 1069 cm⁻¹. This peak is assigned to the methylenic twisting mode.

The CD₂ rocking mode. The F₂ methylenic rock is assigned to the peaks at 725.5 and 726.6 cm⁻¹ in the Raman and infrared spectra respectively. This implies an isotopic shift of 11 percent, which is unusually low for a mode that essentially involves the motion of hydrogen atoms only. Since two ring modes of symmetry F₂ occur at frequencies below 650 cm⁻¹, it seems probable that considerable mixing exists between the methylenic rocking and the ring coordinates, and that the normal vibrations have different forms in the light and heavy compounds. This could account for the anomalous isotopic shifts found in this region.

The ring modes. By analogy with the assignment of HMT-h₁₂ the two ring modes of type F₂ based on the CN stretch are assigned to the very strong infrared peaks at 1174 and 908.1 cm⁻¹. The A₁ mode is unequivocally assigned to the very strong Raman peak at 748.0 cm⁻¹ (the strongest Raman peak), while the E mode is tentatively assigned at 866.5 cm⁻¹, to the only peak with the appropriate polarization behaviour between 440 and 1050 cm⁻¹.

The two F₂ modes based on the C-N-C deformations are assigned to the absorptions at 640.0 and 408.1 cm⁻¹.

The corresponding features in the Raman spectrum are the doublet at 636.2, 641.4 cm^{-1} and the peak at 408.3 cm^{-1} . The low frequency mode exhibits a shift of about 25% on deuteration which is anomalously high for a ring mode. The probable reason for this has been discussed in connection with the assignment of the methylenic rock.

By analogy with the light compound, the A_1 mode based on the C-N-C deformation is assigned to the Raman peak at 975.1 cm^{-1} and the E mode is assigned to the peak at 432.0 cm^{-1} .

III.7 TO-LO Splitting of the F_2 Modes of HMT-d₁₂.

Strong evidence exists to indicate that the longitudinal and transverse components corresponding to the infrared absorptions at 640.0, 908.1 and 1174 cm^{-1} were observed in the Raman spectra of the crystals. Unfortunately, because the crystal of HMT-d₁₂ was not perfect, the Raman evidence is not as definitive as that obtained for the light compound. The polarization behavior of the doublets at 636.2, 641.4 cm^{-1} , at 905.7, 912.8 cm^{-1} and at 1171.2, 1185.3 cm^{-1} is shown in Figure 23. In all cases the high frequency component of the doublet had lower intensity in the x(yx)y geometry than in the x(yz)y geometry, as expected for an LO mode (Section III.5). But it was found that small changes in the position of the crystal (leaving the orientation unchanged) changed the relative intensities of the two com-

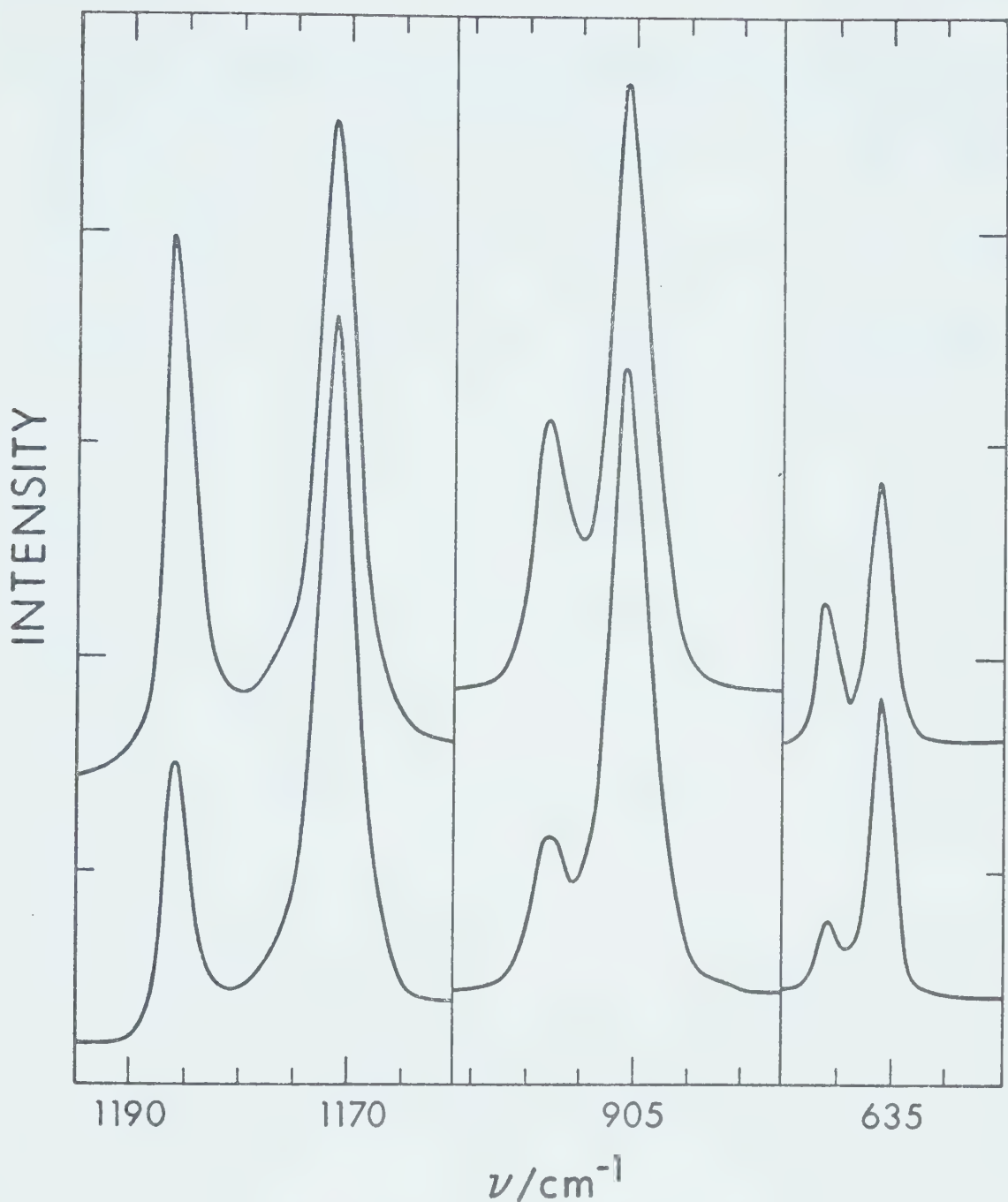


Figure 23. Raman spectra of a crystal of HMT-d₁₂ at room temperature, under x(yz)y geometry (upper trace) and under x(yx)y geometry (lower trace). The frequency marks are 5 cm^{-1} apart.

Table 8. Relation between the Frequencies of the Longitudinal and Transverse Components of the F_2 modes and their Relative Intensities for HMT-d₁₂.

ν_{TO}/cm^{-1}	ν_{LO}/cm^{-1}	$\nu_{LO}^2 - \nu_{TO}^2$ ^a	Integrated Intensity ^{b,c}
408.3	408.3	-	0.20
636.2	641.4	1.0 ± 0.2	1.0
725.5	725.5	-	0.40
905.7	912.8	1.94 ± 0.28	2.2
1075.3	1075.3	-	0.43
1107.0	1107.0	-	0.24
1171.2	1185.3	5.01 ± 0.35	4.21

(a) Units are $(\text{cm}^{-1})/6644.0$

(b) Arbitrary units.

(c) The error in measuring the area under a peak is 0.05
(standard deviation of three determinations).

ponents (although the high frequency component still had lower intensity in the $x(yx)y$ than in $x(yz)y$ geometry). This casts some doubt on the Raman polarization results, but is undoubtedly due to the fact that the crystal was not perfect. The values of $v_{LO}^2 - v_{TO}^2$ for the three Raman doublets and the relative integrated intensities of the corresponding infrared absorption peaks are tabulated in Table 8 and plotted in Figure 22. An approximately linear relation exists between the two quantities; moreover the remaining F_2 modes, which are considerably weaker in absorption, do not exhibit a splitting in the Raman spectrum. All of the above evidence indicates that the Raman peaks at 641.4, 912.8 and 1185.3 are due to the LO components of the F_2 modes, while the peaks at 636.2, 905.7 and 1171.2 cm^{-1} are due to the TO components.

If these frequencies are inserted in equation III.2, the value of $\frac{\epsilon_0}{\epsilon_\infty}$ is given as 1.057 ± 0.005 for HMT-d₁₂. The refractive index for the sodium D line was measured by the Becke line method (115) and found to be 1.584 ± 0.002 . Therefore the static dielectric constant of HMT-d₁₂ can be calculated to be 2.652 ± 0.008 .

III.8 Normal Coordinate Analysis.

Aims of the calculations.

The normal coordinate calculations were carried

out with two aims in mind. First, to test whether a single force field would reproduce the experimental frequencies and assignments for the two isotopic molecules. This would provide a test of the mutual compatibility of the two assignments and would add reliability to them. The second aim was to obtain a more accurate description of the normal vibrations in the two molecules. The assignments made in Sections III.4 and 6 can only be considered approximate. The description of a normal vibration in terms of a single symmetry coordinate, although useful because it gives a physical meaning to the assignment, can be misleading because if the frequencies of two or more symmetry coordinates in the same irreducible representation of the point groups lie close together, and if a mechanism for coupling exists, the normal vibrations of the molecule will be the resultant of this coupling and should be described as a mixture of all symmetry coordinates involved. In this particular problem a situation of this type certainly existed, especially in the case of the perdeuterated compound between 1000 and 1200 cm^{-1} and between 400 and 750 cm^{-1} , and it was thought that the unusual isotopic shifts observed could probably be explained in these terms.

Methods.

The calculations were carried out using a set of

Table 9. Internal Coordinates for Hexamethylenetetramine.

Coordinate	Number	Description ^a
r_1	1	$\nu(N_9-C_{10})$
r_2	2	$\nu(N_9-C_8)$
r_3	3	$\nu(N_9-C_2)$
r_4	4	$\nu(N_1-C_2)$
r_5	5	$\nu(N_7-C_8)$
r_6	6	$\nu(N_5-C_{10})$
r_7	7	$\nu(N_5-C_3)$
r_8	8	$\nu(N_1-C_3)$
r_9	9	$\nu(N_1-C_4)$
r_{10}	10	$\nu(N_7-C_4)$
r_{11}	11	$\nu(N_7-C_6)$
r_{12}	12	$\nu(N_5-C_6)$
α_1	13	$\delta(C_4-N_7-C_6)$
α_2	14	$\delta(C_6-N_7-C_8)$
α_3	15	$\delta(C_4-N_7-C_8)$
α_4	16	$\delta(C_3-N_1-C_4)$
α_5	17	$\delta(C_2-N_1-C_4)$
α_6	18	$\delta(C_2-N_1-C_3)$
α_7	19	$\delta(C_3-N_5-C_{10})$
α_8	20	$\delta(C_3-N_5-C_6)$

(Table continued on next page)

Table 9 continued

Coordinate	Number	Description ^a
α_9	21	$\delta(C_6-N_5-C_{10})$
α_{10}	22	$\delta(C_2-N_9-C_8)$
α_{11}	23	$\delta(C_8-N_9-C_{10})$
α_{12}	24	$\delta(C_2-N_9-C_{10})$
β_1	25	$\delta(N_1-C_2-N_9)$
β_2	26	$\delta(N_1-C_3-N_5)$
β_3	27	$\delta(N_1-C_4-N_7)$
β_4	28	$\delta(N_5-C_6-N_7)$
β_5	29	$\delta(N_7-C_8-N_9)$
β_6	30	$\delta(N_5-C_{10}-N_9)$
s_1	31	$\nu(C_3-H_{11})$
s_2	32	$\nu(C_3-H_{12})$
s_3	33	$\nu(C_2-H_{13})$
s_4	34	$\nu(C_2-H_{14})$
s_5	35	$\nu(C_4-H_{15})$
s_6	36	$\nu(C_4-H_{16})$
s_7	37	$\nu(C_{10}-H_{17})$
s_8	38	$\nu(C_{10}-H_{18})$
s_9	39	$\nu(C_8-H_{19})$
s_{10}	40	$\nu(C_8-H_{20})$
s_{11}	41	$\nu(C_6-H_{21})$

(Table continued on next page)

Table 9 continued

Coordinate	Number	Description ^a
s_{12}	42	$\nu(C_6-H_{22})$
γ_1	43	$\delta(H_{13}-C_2-H_{14})$
γ_2	44	$\delta(H_{11}-C_3-H_{12})$
γ_3	45	$\delta(H_{15}-C_4-H_{16})$
γ_4	46	$\delta(H_{21}-C_6-H_{22})$
γ_5	47	$\delta(H_{19}-C_8-H_{20})$
γ_6	48	$\delta(H_{17}-C_{10}-H_{18})$
ϵ_1	49	$\delta(H_{11}-C_3-N_1)$
ϵ_2	50	$\delta(H_{12}-C_3-N_1)$
ϵ_3	51	$\delta(H_{11}-C_3-N_5)$
ϵ_4	52	$\delta(H_{12}-C_3-N_5)$
ϵ_5	53	$\delta(H_{13}-C_2-N_1)$
ϵ_6	54	$\delta(H_{14}-C_2-N_1)$
ϵ_7	55	$\delta(H_{13}-C_2-N_9)$
ϵ_8	56	$\delta(H_{14}-C_2-N_9)$
ϵ_9	57	$\delta(H_{15}-C_4-N_1)$
ϵ_{10}	58	$\delta(H_{16}-C_4-N_1)$
ϵ_{11}	59	$\delta(H_{15}-C_4-N_7)$
ϵ_{12}	60	$\delta(H_{16}-C_4-N_7)$
ϵ_{13}	61	$\delta(H_{21}-C_6-N_5)$
ϵ_{14}	62	$\delta(H_{22}-C_6-N_5)$

(Table continued on next page)

Table 9 continued

Coordinate	Number	Description ^a
ϵ_{15}	63	$\delta(H_{21}-C_6-N_7)$
ϵ_{16}	64	$\delta(H_{22}-C_6-N_7)$
ϵ_{17}	65	$\delta(H_{19}-C_8-N_7)$
ϵ_{18}	66	$\delta(H_{20}-C_8-N_7)$
ϵ_{19}	67	$\delta(H_{19}-C_8-N_9)$
ϵ_{20}	68	$\delta(H_{20}-C_8-N_9)$
ϵ_{21}	69	$\delta(H_{17}-C_{10}-N_5)$
ϵ_{22}	70	$\delta(H_{18}-C_{10}-N_5)$
ϵ_{23}	71	$\delta(H_{17}-C_{10}-N_9)$
ϵ_{24}	72	$\delta(H_{18}-C_{10}-N_9)$

(a) v = change in length of the specified bond.

δ = change in the specified angle.

72 internal coordinates and a valence force field. The internal coordinates are defined in Table 9 with reference to Figure 2. Wilson's GF method (15) was used. The G matrix elements were calculated from the structural parameters determined by Andersen (79) and the atomic weights (96) using GMAT, a program written in FORTRAN IV by Schachtschneider (116). The values of the G matrix elements for both molecules are listed in Appendix I. A set of internal symmetry coordinates were constructed using standard methods (15). They are listed in Appendix II.

The frequencies and forms of the normal modes were calculated using the programs VSEC and EPERT written by Schachtschneider (116). The programs were modified to accept larger matrices (99×99) and were then tested by carrying out calculations on methyl fluoride and tertiary butyl bromide. The solutions obtained by Schachtschneider (116) and by Bertie and Sunder (117) were reproduced exactly.

VSEC solves the secular equation $|GF-E\lambda| = 0$ where G is the G matrix, F is the F matrix, E is a unit matrix of the same size as G and F and the λ 's are the unknown eigenvalues of the equation. This program was used in preliminary work when a reasonable force field was being sought. EPERT calculates the eigenvalues from an initial force field, then adjusts the force field, using the least squares method as a criterion for the agreement between

calculated and observed frequencies, and solves the secular equation using the adjusted force field. This procedure is followed until the eigenvalues converge and further refining does not improve the agreement.

Results.

Several diagonal force fields were tested using VSEC and, while none of them gave a satisfactory agreement between the observed and calculated frequencies of HMT-h₁₂, a force field was found which seemed a useful starting point for more complicated force fields. Several interaction force constants were then introduced, one at a time, and the force fields so obtained, including the diagonal one, were refined using FPERT to fit the frequencies of HMT-h₁₂. The diagonal force field yielded a rather poor agreement even after refinement, the average error between the observed and calculated frequencies being about 7%. A quite simple force field, which used the diagonal constants and the force constants accounting for the interactions between the C-N stretches and the H-C-N deformations (common C-N), the C-N stretches and the C-N-C' deformations and between the C-N-C and C-N-C' deformations, yielded an average error between calculated and observed frequencies of 1.7%. This was considered to be quite good, and the same force field was then used to fit the frequencies of HMT-h₁₂ and HMT-d₁₂. After refinement the frequencies of both molecules were

fitted with an overall average error of 2%. Later the interaction force constant between C-N-C and C-N-C' deformations was constrained to zero, and the force field so obtained was refined to yield an overall average error in frequencies of 2.1%.

Considerably better agreement between observed and calculated frequencies was found using more complicated force fields. In particular, a force field which included the four interaction force constants mentioned above and two more constants which accounted for the interactions between the N-C-N and N-C'-N' deformations and between the C-N-C and N-C-N' deformations, reproduced the observed frequencies within 1.09% on the average. However, the use of these complicated force fields resulted in very large contributions to the potential energy distribution from some of the interaction force constants. Whenever this is the case the physical significance of the potential energy distribution is greatly diminished.

Of particular importance is the result that the calculated assignment of the normal modes of internal coordinates, whether indicated by the potential energy distribution or the eigenvectors, was very similar for all force fields which yielded reasonable agreement. Therefore the simplest of these, which had only three interaction force constants, was selected as the most useful one to report. The force constants and the potential energy dis-

Table 10. Force Constants for Hexamethylenetetramine.

Number	Value ^a	Error	Description
1	5.087	0.18	C-N Stretch
2	1.612	0.10	C-N-C Deformation
3	1.231	0.09	N-C-N Deformation
4	4.614	0.01	C-H Stretch
5	0.590	0.007	H-C-H Deformation
6	0.819	0.012	H-C-N Deformation
7	0.447	0.04	C-N Stretch H-C-N Deformation Interaction
8	0.544	0.07	C-N Stretch C-N-C Deformation Interaction
9	0.716	0.08	C-N Stretch N-C-N Deformation Interaction

(a) Force constants 1 and 4 in units of mdynes \AA^{-1} ,
 2,3,5 and 6 in units of mdynes \AA° , all others in
 units of mdynes.

Table 11. Distribution of the Potential Energy for the Normal Modes of HMT-h₁₂ among the Force Constants Listed in Table 10.^a

Mode	Type	FREQUENCY	0.0033	0.0015	0.0020	0.9907	0.0020	0.0000	-0.0002	-0.0016	0.0023
v ₁	A ₁	FREQUENCY = 2873.2 CM-1									
v ₂	A	FREQUENCY = 1459.9 CM-1	0.0187	0.0091	0.0121	0.0028	0.7269	0.2049	-0.0383	-0.0093	0.0131
v ₃	A ₁	FREQUENCY = 1044.0 CM-1	0.0150	0.3629	0.4822	0.0049	0.0010	0.0897	0.0227	-0.0524	0.0739
v ₄	A ₁	FREQUENCY = 767.0 CM-1	1.0146	0.0383	0.0509	0.0017	0.0000	0.0081	-0.0561	0.1396	-0.1970
v ₅	A ₂	FREQUENCY = 1279.2 CM-1	0.0	0.0	0.0	0.0	0.0	1.0000	0.0	0.0	0.0
v ₆	E	FREQUENCY = 2869.3 CM-1	0.0037	0.0003	0.0013	0.9938	0.0018	0.0000	-0.0003	-0.0016	0.0005
v ₇	E	FREQUENCY = 1458.8 CM-1	0.0002	0.0073	0.0023	0.0012	0.7422	0.2431	0.0040	0.0004	-0.0006
v ₈	E	FREQUENCY = 1355.5 CM-1	0.1332	0.0139	0.0138	0.0007	0.0426	0.8582	-0.0157	-0.0263	-0.0215
v ₉	E	FREQUENCY = 1005.2 CM-1	0.9385	0.0303	0.1607	0.0034	0.0156	0.1200	0.0505	-0.2387	-0.0842
v ₁₀	E	FREQUENCY = 505.6 CM-1	0.0358	0.7588	0.2111	0.0009	0.0005	0.0451	-0.0233	0.0535	-0.0824
v ₁₁	F ₁	FREQUENCY = 2952.4 CM-1	0.0000	0.0022	0.0	0.9931	0.0	0.0046	0.0000	0.0	-0.0001
v ₁₂	F ₁	FREQUENCY = 1401.3 CM-1	0.1136	0.0377	0.0	0.0003	0.0	0.7502	0.1309	0.0	-0.0327
v ₁₃	F ₁	FREQUENCY = 1346.2 CM-1	0.3166	0.0236	0.0	0.0000	0.0	0.9943	-0.2913	0.0	-0.0432
v ₁₄	F ₁	FREQUENCY = 1174.5 CM-1	0.6814	0.0332	0.0	0.0003	0.0	0.4246	-0.0708	0.0	-0.1190
v ₁₅	F ₁	FREQUENCY = 911.4 CM-1	0.0755	0.0337	0.0	0.0059	0.0	0.8304	0.0026	0.0	0.0318
v ₁₆	F ₁	FREQUENCY = 341.3 CM-1	0.0010	0.8738	0.0	0.0004	0.0	0.1052	0.0009	0.0	0.0147
v ₁₇	F ₂	FREQUENCY = 2959.0 CM-1	0.0000	0.0071	0.0000	0.9877	0.0000	0.0053	0.0000	0.0000	-0.0001
v ₁₈	F ₂	FREQUENCY = 2370.7 CM-1	0.0036	0.0006	0.0019	0.9929	0.0019	0.0001	-0.0002	-0.0016	0.0010
v ₁₉	F ₂	FREQUENCY = 1459.4 CM-1	0.0052	0.0124	0.0049	0.0020	0.7647	0.2207	-0.0100	-0.0019	0.0030
v ₂₀	F ₂	FREQUENCY = 1368.1 CM-1	0.0850	0.0130	0.0001	0.0001	0.0043	1.1035	-0.1781	0.0006	-0.0235
v ₂₁	F ₂	FREQUENCY = 1217.0 CM-1	0.7718	0.2375	0.0453	0.0047	0.0071	0.2931	-0.0736	-0.0754	-0.2343
v ₂₂	F ₂	FREQUENCY = 1014.5 CM-1	0.2635	0.2021	0.1016	0.0056	0.0011	0.3371	0.0317	-0.0662	0.0705
v ₂₃	F ₂	FREQUENCY = 923.3 CM-1	0.9764	0.0144	0.1016	0.0022	0.0016	0.0669	0.0173	-0.1139	-0.0657
v ₂₄	F ₂	FREQUENCY = 667.7 CM-1	0.4737	0.5203	0.2131	0.0003	0.0002	0.0962	-0.0020	0.1867	-0.4095
v ₂₅	F ₂	FREQUENCY = 462.4 CM-1	0.0220	0.6714	0.0413	0.0005	0.0038	0.2967	0.0046	-0.0173	-0.0220

^aThe entries after each frequency are in the order of the force constants in Table 10.

Table 12. Distribution of the Potential Energy of the Normal Modes of HMT-d₁₂ among the Force Constants Listed in Table 10.^a

Mode	Type	FREQUENCY = 2108.8 CM-1	0.0140	0.0074	0.0099	0.9579	0.0001	-0.0008	-0.0072	0.0102	
1	A ₁	FREQUENCY = 1126.2 CM-1	0.0616	0.1414	0.1879	0.0320	0.5315	0.0542	-0.0358	-0.0661	0.0933
2	A ₁	FREQUENCY = 968.1 CM-1	0.0368	0.2488	0.3306	0.0030	0.2210	0.2468	-0.0590	0.0678	-0.0957
3	A ₁	FREQUENCY = 733.9 CM-1	0.9393	0.0142	0.0184	0.0071	0.0289	0.0016	0.0237	0.0819	-0.1156
4	A ₁	FREQUENCY = 905.0 CM-1	0.0	0.0	0.0	0.0	1.0000	0.0	0.0	0.0	
5	A ₂	FREQUENCY = 2057.6 CM-1	0.0176	0.0008	0.0078	0.9720	0.0074	0.0002	-0.0010	-0.0072	0.0019
6	E	FREQUENCY = 1131.7 CM-1	0.0546	0.0673	0.0684	0.0052	0.0011	0.3907	0.0437	-0.1300	-0.1049
7	E	FREQUENCY = 1067.5 CM-1	0.0429	0.0166	0.0309	0.0104	0.7868	0.1847	-0.0546	-0.0224	0.0107
8	E	FREQUENCY = 849.3 CM-1	0.3604	0.0025	0.0815	0.0050	0.0032	0.6130	0.0548	-0.1053	-0.0150
9	E	FREQUENCY = 474.3 CM-1	0.0359	0.7254	0.2010	0.0029	0.0052	0.0775	-0.0277	0.0522	-0.0809
10	F ₁	FREQUENCY = 2209.5 CM-1	0.0011	0.0079	0.0	0.9750	0.0	0.0166	0.0000	0.0	-0.2004
11	F ₁	FREQUENCY = 1276.7 CM-1	1.0305	0.1292	0.0	0.0016	0.0	0.1930	-0.1719	0.0	-0.1824
12	F ₁	FREQUENCY = 1054.3 CM-1	0.0360	0.0120	0.0	0.0013	0.0	1.0552	-0.1151	0.0	0.0104
13	F ₁	FREQUENCY = 888.1 CM-1	0.0311	0.0122	0.0	0.0002	0.0	0.8839	0.0383	0.0	-0.0157
14	F ₁	FREQUENCY = 759.3 CM-1	0.0402	0.1104	0.0	0.0207	0.0	0.7752	0.0202	0.0	0.0333
15	F ₁	FREQUENCY = 277.1 CM-1	0.0002	0.0025	0.0	0.0005	0.0	0.1857	0.0007	0.0	0.0064
16	F ₂	FREQUENCY = 2227.9 CM-1	0.0001	0.0271	0.0000	0.9536	0.0001	0.0196	0.0000	0.0000	-0.0005
17	F ₂	FREQUENCY = 2100.9 CM-1	0.0167	0.0026	0.0084	0.9687	0.0077	0.0003	-0.0010	-0.0072	0.0040
18	F ₂	FREQUENCY = 1190.9 CM-1	0.0666	0.2072	0.0468	0.0119	0.0000	0.2823	-0.1866	-0.0671	-0.2673
19	F ₂	FREQUENCY = 1093.5 CM-1	0.0356	0.1277	0.0391	0.0192	0.4922	0.3571	-0.0608	-0.0064	-0.0039
20	F ₂	FREQUENCY = 1071.8 CM-1	0.3131	0.0241	0.0229	0.0093	0.2100	0.7240	-0.2030	-0.0443	-0.0566
21	F ₂	FREQUENCY = 893.1 CM-1	0.0938	0.2611	0.0759	0.0286	0.0840	0.3567	0.0644	-0.0477	0.0832
22	F ₂	FREQUENCY = 735.3 CM-1	0.7003	0.0015	0.0222	0.0057	0.0051	0.1602	0.1574	-0.0820	-0.0305
23	F ₂	FREQUENCY = 644.4 CM-1	0.4409	0.5021	0.2164	0.0021	0.0013	0.0905	-0.0710	0.1812	-0.3719
24	F ₂	FREQUENCY = 352.8 CM-1	0.0337	0.5698	0.0201	0.0006	0.0040	0.4286	0.0029	-0.0159	-0.0438
25	F ₂										

^aThe entries after each force constant are in the order of the force constants in Table 10.

tribution are listed in Tables 10 and 11 and 12, respectively.

The potential energy distribution directly yields an assignment in terms of internal coordinates. However this assignment is not very specific for the H-C-N deformations, because it fails to indicate whether the normal mode in question involves the methylenic wag, rock, twist or deformation. This information is provided by the symmetrized eigenvectors, that is by the elements of the L_s matrix which relates the normal coordinate column matrix Q to the symmetry coordinate row matrix S through the matrix equation $S = L_s Q$. The elements of the j^{th} column of L_s yield the values of $\partial S_i / \partial Q_j$, which indicate the assignment of the j^{th} normal coordinate. The L_s matrix is not calculated by FPERT, so the final force field was used in the program VSEC, which does. From the results of this calculation and from the potential energy distribution the calculated assignments shown in Tables 13 and 14 were obtained.

As can be seen from Tables 13 and 14, the assignment obtained through calculations agrees well with the empirical assignment proposed in Sections III.4 and III.6. The only serious discrepancy concerns v_{23} of HMT- h_{12} and $-d_{12}$ which were described in Sections III.4 and III.6 as CH_2 and CD_2 rocking modes, while the calculations show them to be CN stretching modes. The calculated assignments are more consistent with the observed isotope shift and are

undoubtedly the correct ones. The rocking coordinate of type F₂ was found to contribute to ν_{22} and ν_{25} in HMT-h₁₂ and to ν_{22} , ν_{23} and ν_{25} in HMT-d₁₂.

A less serious discrepancy is observed in the description of ν_7 of HMT-d₁₂. This mode was tentatively described in Section III.6 as a methylenic deformation, while the calculations show it to be a mixture of the CN stretching coordinate and of the CD₂ twisting coordinate of type E. The methylenic deformation coordinate is assigned, by the calculations, to ν_8 . The calculations show some normal modes to be mixtures of several symmetry coordinates. The extent of this phenomenon is particularly pronounced for the modes of HMT-d₁₂ between 1000 and 1200 cm^{-1} (Tables 12 and 14).

Table 13. Experimental and Calculated Symmetry Coordinate Description of the Normal Modes of HMT-h₁₂.

Mode	Type	Experimental		Calculated	
		ν/cm^{-1}	Description	ν/cm^{-1}	Description
ν_1	A ₁	2861.4 or 2883.0	Symmetric CH Stretch	2873.2	Symmetric CH Stretch
ν_2	A ₁	-	-	1459.9	CH ₂ Deformation
ν_3	A ₁	1042.0	C-N-C Defor- mation	1048.0	C-N-C and N-C-N Deformation
ν_4	A ₁	779.3	C-N Stretch	767.0	C-N Stretch
ν_5	A ₂	-	-	1279.2	CH ₂ Twist
ν_6	E	-	-	2869.5	Symmetric CH Stretch
ν_7	E	1454.2	CH ₂ Deformation	1458.8	CH ₂ Deformation
ν_8	E	1349.2	CH ₂ Twist	1355.5	CH ₂ Twist
ν_9	E	1015	CN Stretch	1005.2	CN Stretch
ν_{10}	E	463.0	C-N-C Defor- mation	505.6	C-N-C, N-C-N Deformation
ν_{11}	F ₁	-	-	2952.4	Asymmetric CH Stretch
ν_{12}	F ₁	-	-	1401.3	CH ₂ Twist, Wag
ν_{13}	F ₁	-	-	1346.2	CH ₂ Twist, Wag
ν_{14}	F ₁	-	-	1179.5	CN Stretch, CH ₂ Twist

(Table continued on next page)

Table 13 continued.

Mode	Type	Experimental		Calculated	
		ν/cm^{-1}	Description	ν/cm^{-1}	Description
ν_{15}	F_1	1	-	911.4	CH_2 Rock, C-N-C Deformation
ν_{16}	F_1	-	-	341.3	C-N-C, N-C-N Deformation
ν_{17}	F_2	2954.8	Asymmetric CH Stretch	2959.0	Asymmetric CH Stretch
ν_{18}	F_2	2873.6	Symmetric CH Stretch	2870.7	Symmetric CH Stretch
ν_{19}	F_2	1458.0	CH_2 Deformation	1459.4	CH_2 Deformation
ν_{20}	F_2	1370.0	CH_2 wag	1368.1	CH_2 Wag
ν_{21}	F_2	1236.5	CN Stretch	1217.0	CN Stretch
ν_{22}	F_2	1004.3	CN Stretch	1014.5	CH_2 Rock, CN Stretch, C-N-C N-C-N Defor- mation
ν_{23}	F_2	810.5	CH_2 Rock	823.3	CN Stretch
ν_{24}	F_2	671.0	C-N-C Deformation	662.7	C-N-C Defor- mation, CN Stretch, N-C-N Deformation

(Table continued on next page)

Table 13 continued.

Experimental				Calculated	
Mode	Type	ν/cm^{-1}	Description	ν/cm^{-1}	Description
ν_{25}	F_2	512.0	C-N-C Deformation	462.4	C-N-C Deformation, CH_2 Rock

- (a) The symmetry coordinates are arranged in order of decreasing contribution to the normal mode. Only those symmetry coordinates which contribute more than 15% to a normal mode are included in the description.

Table 14. Experimental and Calculated Symmetry Coordinate Description of the Normal Modes of HMT-d₁₂.

Mode	Type	Experimental		Calculated	
		v/cm ⁻¹	Description	v/cm ⁻¹	Description
v ₁	A ₁	2109.6	Symmetric CD Stretch	2108.8	Symmetric CD Stretch
v ₂	A ₁	1131.4	CD ₂ Deformation	1126.2	CD ₂ Deformation C-N-C, N-C-N Deformation
v ₃	A ₁	975.0	C-N-C Deformation	968.1	CD ₂ Deformation N-C-N, C-N-C Deformation
v ₄	A ₁	748.0	CN Stretch	733.9	CN Stretch
v ₅	A ₂	-	-	905.0	CD ₂ Twist
v ₆	E	-	-	2097.6	Symmetric CH Stretch
v ₇	E	1121.4	CD ₂ Deformation	1131.7	CN Stretch, CD ₂ Twist
v ₈	E	1069.0	CD ₂ Twist	1067.5	CD ₂ Deformation, CD ₂ Twist
v ₉	E	866.5	CN Stretch	849.3	CD ₂ twist, CN Stretch

(Table continued on next page)

Table 14 continued

Mode	Type	Experimental		Calculated	
		ν/cm^{-1}	Description	ν/cm^{-1}	Description
ν_{10}	E	432.0	C-N-C Defor- mation	474.3	C-N-C, N-C-N Deformation
ν_{11}	F ₁	-	-	2209.5	Asymmetric CD Stretch
ν_{12}	F ₁	-	-	1276.7	CN Stretch
ν_{13}	F ₁	-	-	1058.3	CD ₂ Twist, Wag, Rock
ν_{14}	F ₁	-	-	888.1	CD ₂ Twist
ν_{15}	F ₁	-	-	759.5	CD ₂ Rock
ν_{16}	F ₁	-	-	277.1	C-N-C Defor- mation
ν_{17}	F ₂	2228.0	Asymmetric CD Stretch	2227.9	Asymmetric CD Stretch
ν_{18}	F ₂	2105.0	Symmetric CD Stretch	2100.9	Symmetric CD Stretch
ν_{19}	F ₂	1171.2	CN Stretch	1190.9	CN Stretch
ν_{20}	F ₂	1105.0	CD ₂ Defor- mation	1093.5	CD ₂ Defor- mation, CD ₂ Wag
ν_{21}	F ₂	1075.3	CD ₂ Wag	1071.8	CD ₂ Wag, CN Stretch, CD ₂ Deformation

(Table continued on next page)

Table 14 continued

<u>Experimental</u>				<u>Calculated</u>	
Mode	Type	ν/cm^{-1}	Description	ν/cm^{-1}	Description
ν_{22}	F_2	905.7	CN Stretch	893.1	CD_2 Wag, Rock, C-N-C Defor- mation
ν_{23}	F_2	725.5	CD_2 Rock	735.3	CN Stretch, CD_2 Rock
ν_{24}	F_2	636.2	C-N-C Defor- mation	644.4	C-N-C Defor- mation, CN Stretch, N-C-N Defor- mation
ν_{25}	F_2	408.3	C-N-C Defor- mation	352.8	C-N-C Defor- mation, CD_2 Rock

- (a) The symmetry coordinates are arranged in order of decreasing contribution to the normal modes. Only those symmetry coordinates which contribute more than 15 % to a normal mode are included in the description.

Chapter IV. The Infrared Spectra of Hexamethylene-tetramine Hydrate in Four Isotopic Modifications.

IV.1 General.

One of the biggest concerns in this work was to make sure that the spectra obtained were those of a hydrate whose impurity level was so low that it would not affect the spectrum. If distilled water and commercial HMT (which was shown to be pure enough for spectroscopic purposes) were used, only negligible amounts of extrinsic impurities were introduced. However, the solubility of HMT at 5°C, the temperature at which the hydrate was crystallized, is about 47% by weight (95), while the HMT accounts for 56.5% of the weight of the hydrate. Clearly, once the hydrate is formed, an excess of solution is left and the problem exists of separating the crystals from the solution as completely as possible.

In the early stages of the work the mother liquor was simply decanted and the crystals were dried on some filter paper or on paper tissues. The quality of the X-ray photographs obtained at that time was not good enough to permit the detection of ice impurity because the powder obtained by grinding the samples by hand was not fine enough. The spectra obtained from these samples, though very similar to the spectrum of ice I near 3200 cm^{-1} (curve b, Figure 24), where the absorption due to the O-H stret-

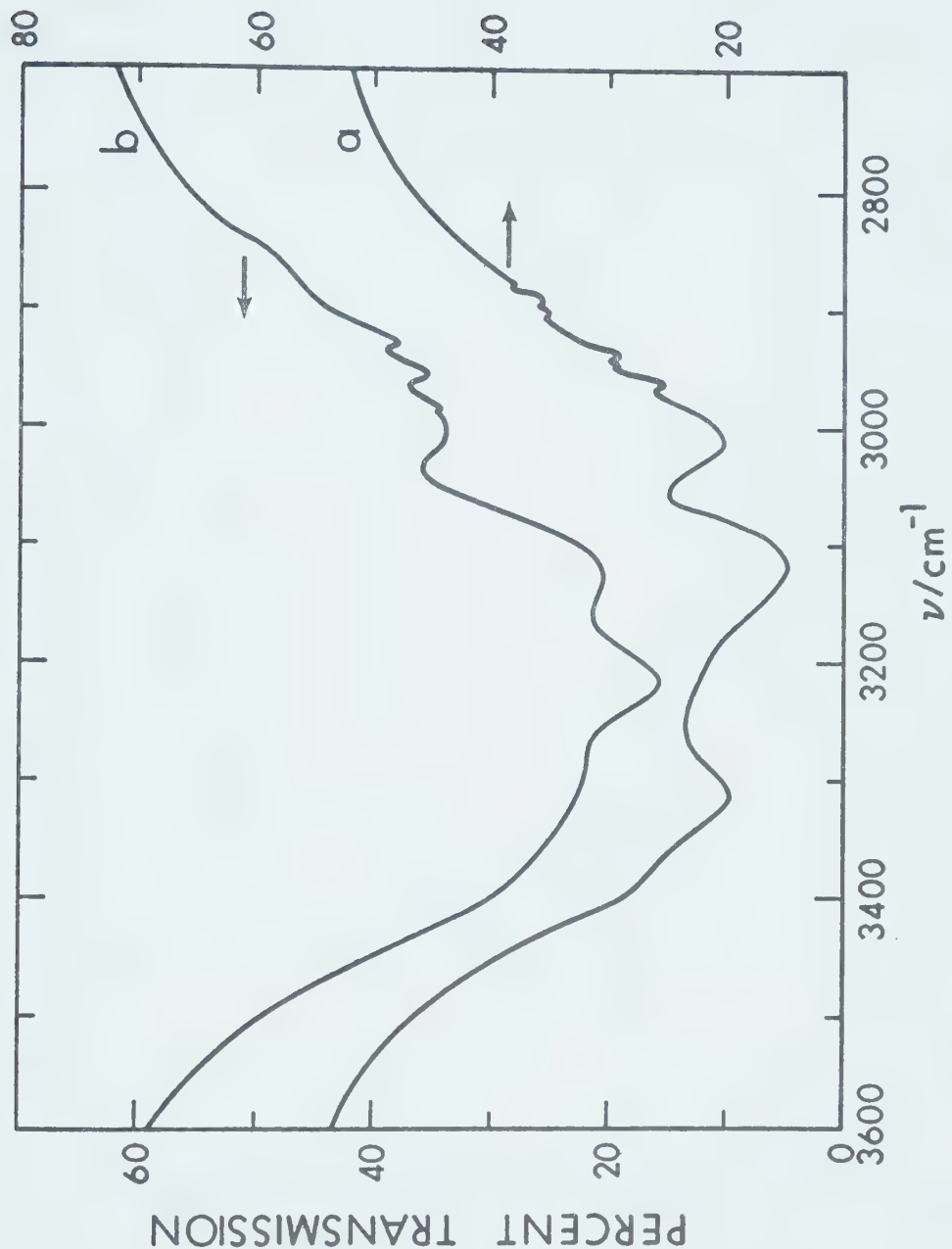


Figure 24. The ν_{OH} (H_2O) band for a dried (curve a) and an undried (curve b) sample of $\text{HMT}-\text{h}_{12}\cdot 6\text{H}_2\text{O}$.

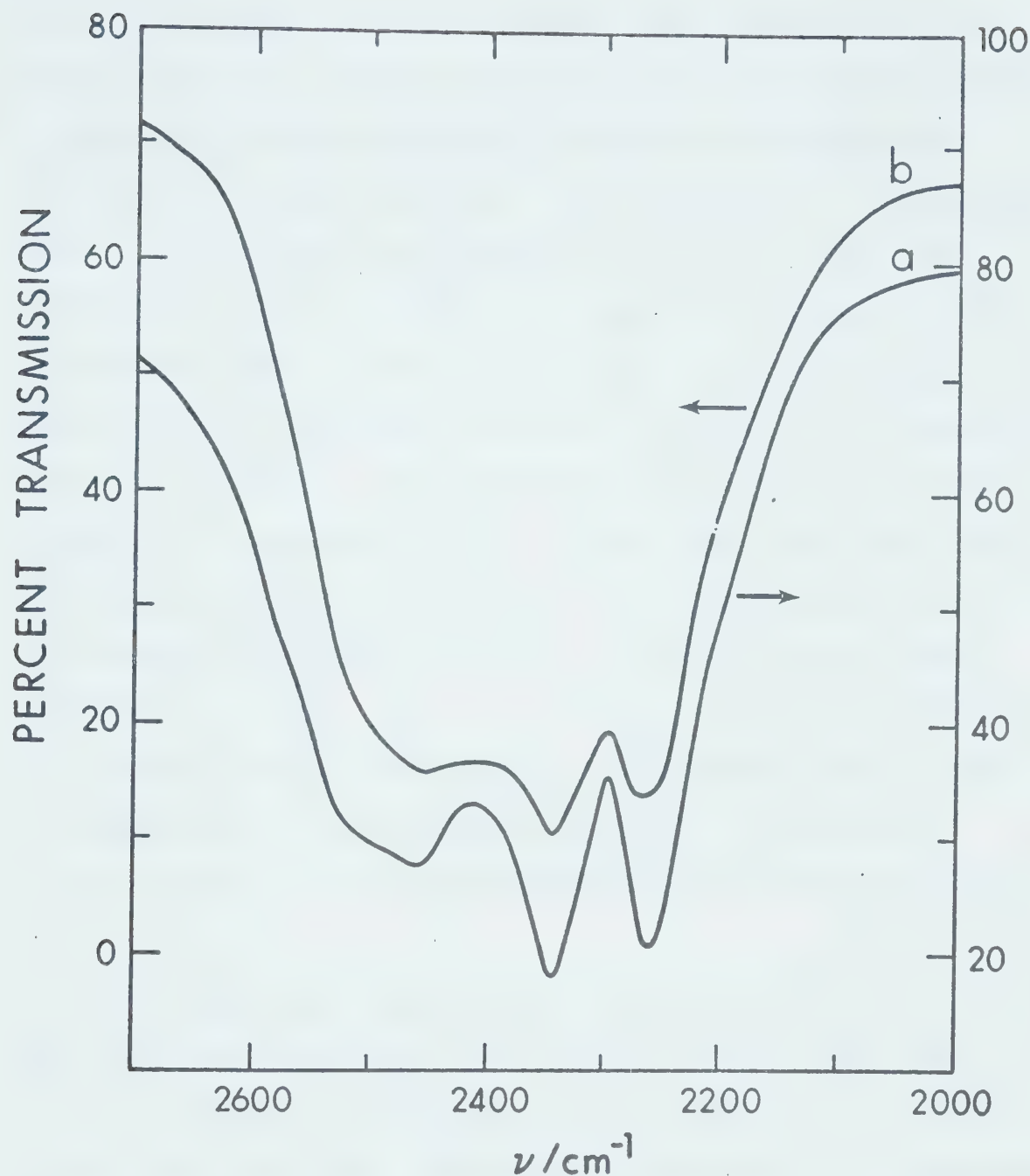


Figure 25. The $\nu_{\text{OD}}(\text{D}_2\text{O})$ band for a dried (curve a) and an undried (curve b) sample of $\text{HMT}\text{-h}_{12}\cdot 6\text{D}_2\text{O}$.

ching vibrations is found (53-60), were dramatically different from that of ice I near 800 cm^{-1} where the so called ν_R band, due to the rotational vibrations of the water molecules, is found (53-60). The spectrum of the deuterate was different from the spectrum of D_2O ice I even near 2400 cm^{-1} (curve b, Figure 25), where the O-D stretching vibrations absorb (53-60). All these facts were taken to indicate that the hydrate obtained was free of ice impurity and that, possibly, the spectrum of the hydrate was overlapped, in the region of the O-H stretching band, by the absorption by small quantities of ice which condensed on the windows while the two parts of the cell were joined together. At that time a can without the side arm (Section II.3) was being used to prepare the infrared samples, and the spectra of the deuterate and of the mulling agent always showed a peak characteristic of H_2O ice near 3200 cm^{-1} .

When the modified can with the side arm was developed, it was possible to join the two parts of the cell without any ice condensing on the windows. This was proven in the following way: the cell was handled in the same way as when the hydrate samples were prepared, but no sample, or only Freon 13 which does not absorb in the region of 3200 cm^{-1} , was placed between the windows. When the infrared spectra were recorded no trace of ice absorption was found. Having eliminated the interference from condensed

ice, it was possible to study the shape of the $\nu_{\text{OH}}(\text{H}_2\text{O})$ band of the hydrate. It was found that the shape of this band did not change appreciably when the samples were prepared avoiding condensation on the windows.

The hydrate was later made from water containing 5 atom percent of D and 95 atom percent of H, or vice versa, in order to study the O-D or O-H stretching vibrations of HDO molecules surrounded by H_2O or D_2O molecules, respectively. The samples always showed four peaks due to $\nu_{\text{OD}}(\text{HDO})$ or four peaks due to $\nu_{\text{OH}}(\text{HDO})$. The intensity of one of these peaks, at about 3277 cm^{-1} in the deuterate containing 5 atom percent of H, and at about 2420 cm^{-1} in the spectrum of the hydrate containing 5 atom percent of D, relative to that of the remaining peaks was found not to be reproducible for different samples. Since these peaks occurred at the same frequencies as the corresponding peaks in the spectra of isotopically impure light and heavy ice Ih, it was concluded that the hydrate was contaminated by small, but detectable, quantities of ice Ih. In the meantime the Spex grinder had become available (Section II.2) and X-ray photographs of much higher quality were obtained. In these photographs a weak line at a 2θ angle of 24° was identified. This line was found to be spurious because it was not consistent with the unit cell parameters determined by Mak (34). Moreover the 2θ value was in excellent agreement with a strong diffraction of ice Ih. On these

grounds the diffraction line at $2\theta = 24^\circ$ was attributed to intrinsic ice impurity. The problem of eliminating this impurity from the hydrate was solved by drying the samples under vacuum as indicated in the experimental section. The X-ray diffraction photographs showed that this treatment effectively eliminated almost all of the ice from the samples. When the samples were dried until their decomposition had just begun (Section II.2), the ice line in the photographs almost completely disappeared.

Another indication that the procedure was effective in producing a pure sample was given by the fact that the $\nu_{OH}(HDO)$ and $\nu_{OD}(HDO)$ peaks at 3277 and 2420 cm^{-1} in the spectra of the isotopically contaminated deuterate and hydrate, respectively, almost completely disappeared in the samples which had been dried under vacuum. Two samples prepared towards the end of this work yielded spectra in which the spurious peaks were absent.

Since there were indications that the hydrate had begun to decompose under vacuum, the presence of an excess of HMT in the samples was suspected, and confirmed by the presence in the x-ray photographs of a very weak line at a 2θ angle of about 17° , in good agreement with a diffraction of pure HMT (78). The spectral effects of HMT and ice impurities were then carefully investigated. For the far-infrared spectra, a sample not dried, a sample dried for only one minute and a sample dried until onset of decom-

position were used. Although the x-ray diffraction photographs of the above samples showed markedly different concentrations of ice Ih, their far-infrared spectra were identical.

The mid-infrared spectra of the isotopically pure hydrates which had been dried under vacuum were found to be dramatically different from the spectra of the earlier samples which had not been dried. The differences were, however, restricted to the $\nu_{\text{OH}}(\text{H}_2\text{O})$ band. Figure 24 shows this band for two different samples, one of which was dried under vacuum (curve a) while the other (curve b) was not. The $\nu_{\text{OD}}(\text{D}_2\text{O})$ band of the deuterate was also affected, but less dramatically; as shown in Figure 25, only the relative intensities of its three maxima were found to differ in the spectra of the pure and impure samples. No differences were found in the remaining spectral regions for the hydrate or the deuterate.

It was found that the most sensitive test for ice impurity in the hydrate or deuterate samples is the appearance of the $\nu_{\text{OH}}(\text{HDO})$ or $\nu_{\text{OD}}(\text{HDO})$ peaks at 3277 and 2420 cm^{-1} in the isotopically dilute samples. These were still visible in samples that yielded $\nu_{\text{OH}}(\text{H}_2\text{O})$ or $\nu_{\text{OD}}(\text{D}_2\text{O})$ bands which were characteristic of the pure compound (curve a of Figures 24 and 25). It is not possible to give a definitive estimate of the ice impurity concentration in the hydrate samples. If the absorptivities of the hydrate and of ice were known,

the relative intensities of the ν_{OH} (HDO) and ν_{OD} (HDO) peaks due to the hydrate and to ice could give an indication of the purity of the samples. If one assumes that the absorptivity of the strongest peak in the hydrate is the same as the absorptivity of the ν_{OH} (HDO) peak in ice, then the concentration of ice Ih in a hydrate sample dried until onset of decomposition was less than 1%. Although the above assumption is completely arbitrary, it is probably not too unrealistic.

No absorption due to pure HMT was detected in the dried samples, and the absorptions due to enclathrated HMT were identical in the spectra of dried and undried samples. It is, therefore, concluded that the level of HMT impurity obtained by drying the samples under vacuum did not affect the spectra.

In order to measure the concentration of hydrogen impurity in the 'isotopically pure' deuterate, the intensity of the ν_{OH} (HDO) peak at 3332 cm^{-1} was measured relative to that of the HMT peaks at 693.9, 812.9 and 1462.6 cm^{-1} in the spectra of 'isotopically pure' deuterate and of deuterate containing about 10% of HDO. The relative intensity of the ν_{OH} (HDO) peak was about 10 times greater in the spectrum of the sample containing 10% of HDO than in that of the 'isotopically pure' sample. This confirmed that the HDO concentration was about 1% and, therefore, that the H concentration was about 0.5% in the 'isotopically pure'

sample, as was found by NMR studies on the liquid D₂O (Section II.1). Hereafter those samples which were not deliberately contaminated with HDO will simply be referred to as the hydrate or the deuterate.

IV.2 The Mid-infrared Spectra.

The spectra of HMT-h₁₂ hydrate, HMT-h₁₂ deuterate, HMT-d₁₂ hydrate and HMT-d₁₂ deuterate mulled with propane, propylene and Freon 13 at 90°K are shown in Figures 26 - 29. These spectra represent the raw data obtained in this work, and from the spectra of each compound in the three mulling agents, the spectra of the compounds themselves were composed. These are shown in Figures 30 - 33 and the frequencies of the features are listed in Table 15. The dashed line at about 920 cm⁻¹ in Figure 32 represents an uncertainty in the spectrum due to the fact that all mulling agents absorb in that region. The spectra were obtained using the 'twice standard' slit program of the Beckman IR 12 spectrophotometer. This yielded a resolution better than 5 cm⁻¹ between 200 and 650 cm⁻¹ and better than 2.5 cm⁻¹ between 650 and 4000 cm⁻¹. The accuracy of the measured frequencies is generally worse than the accuracy of the calibration of the spectrometer, and depends on the breadth and definition of the feature concerned. An estimated error is given for each frequency in Table 15. The relative intensities of the features in Figures 30 - 33 are approximately correct,

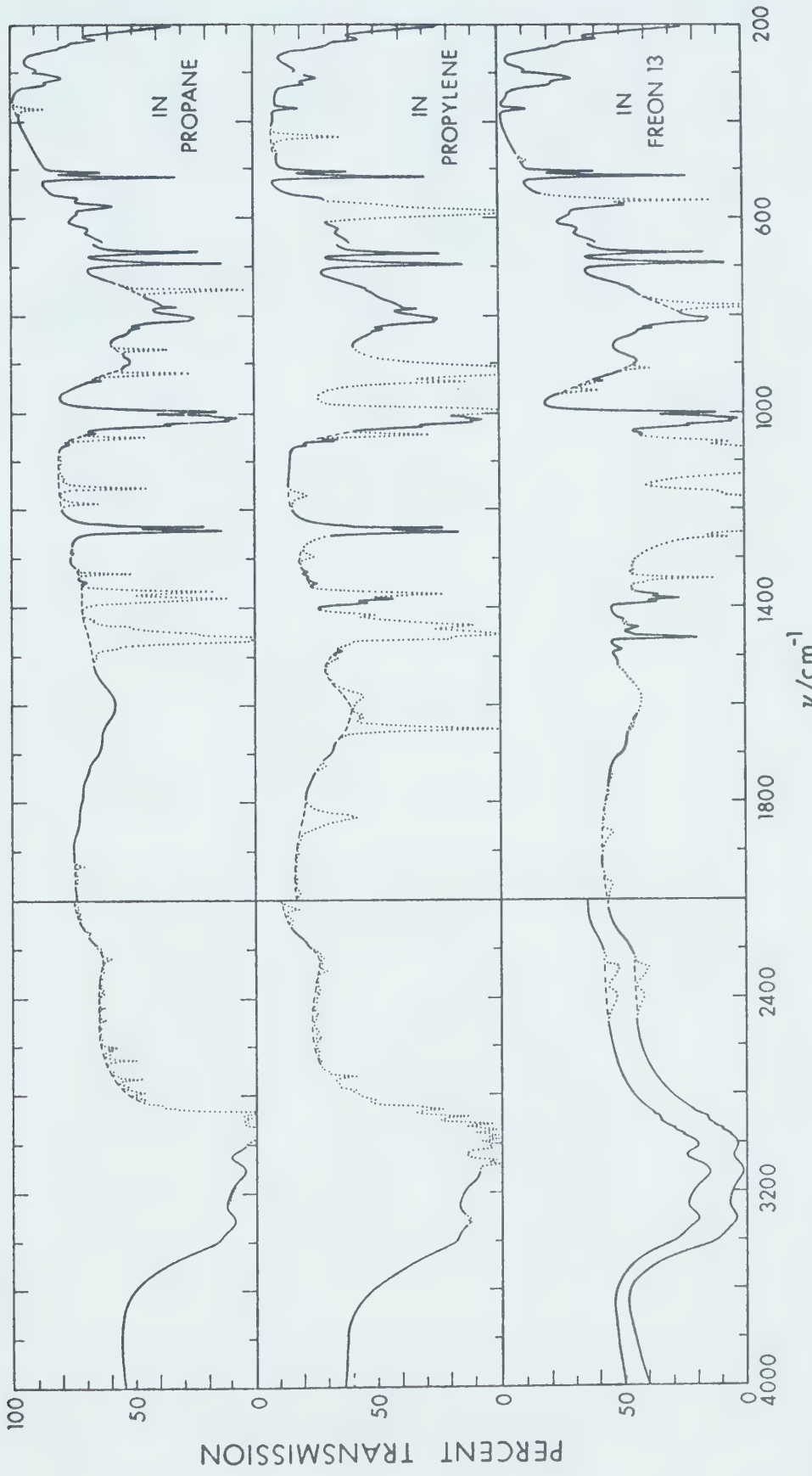


Figure 26. The mid-infrared spectra of HMT- h_{12} hydrate in the three mulling agents at 90°K. The dotted lines indicate the absorption due to the mulling agent, the dashed lines indicate the hydrate absorption in this region.

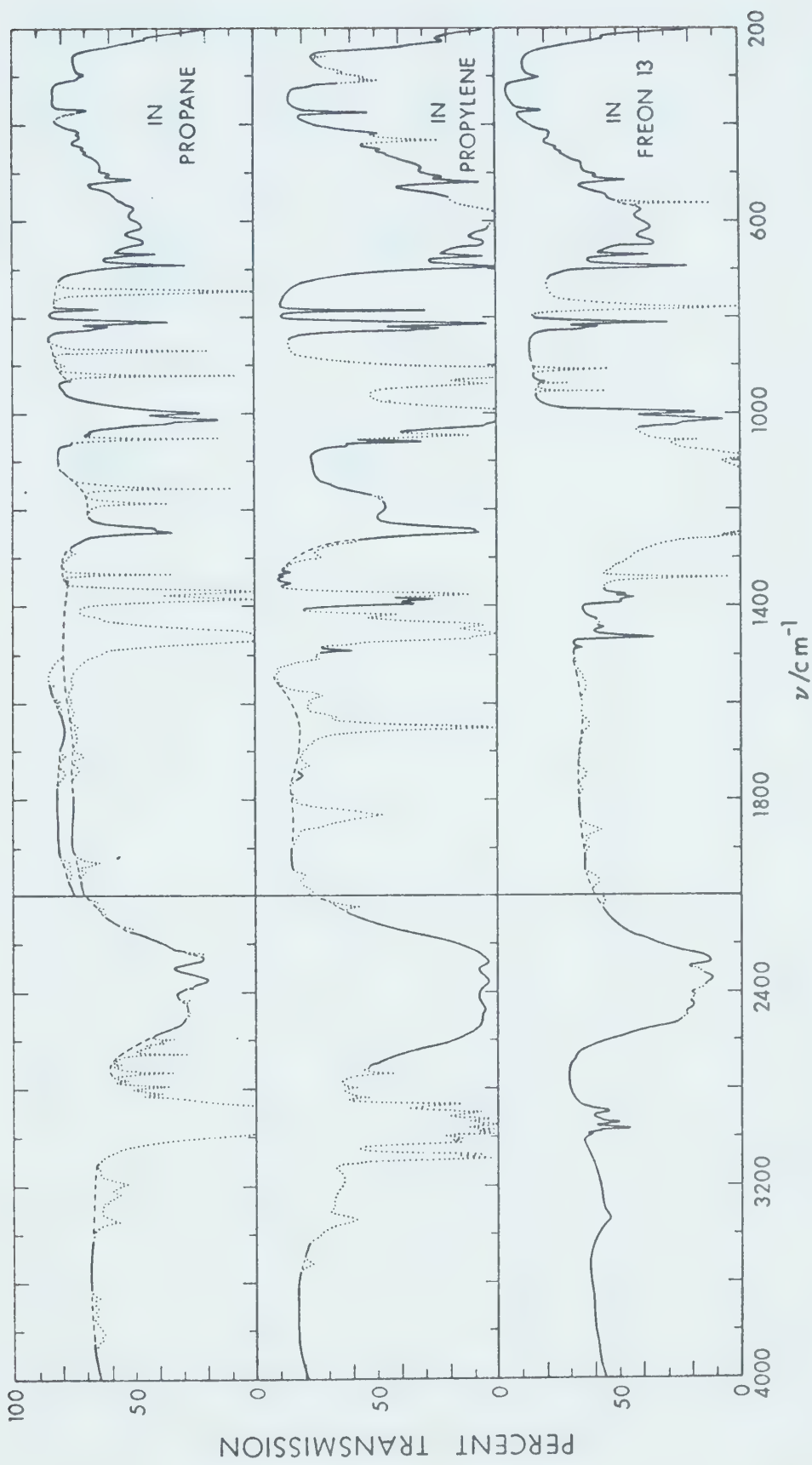


Figure 27. The mid-infrared spectra of $\text{HMT}-\text{h}_{12}\cdot 6\text{D}_2\text{O}$ in three mulling agents at 90°K . The dotted lines indicate the absorption due to the mulling agents, the dashed lines indicate the deuterate absorption in these regions.

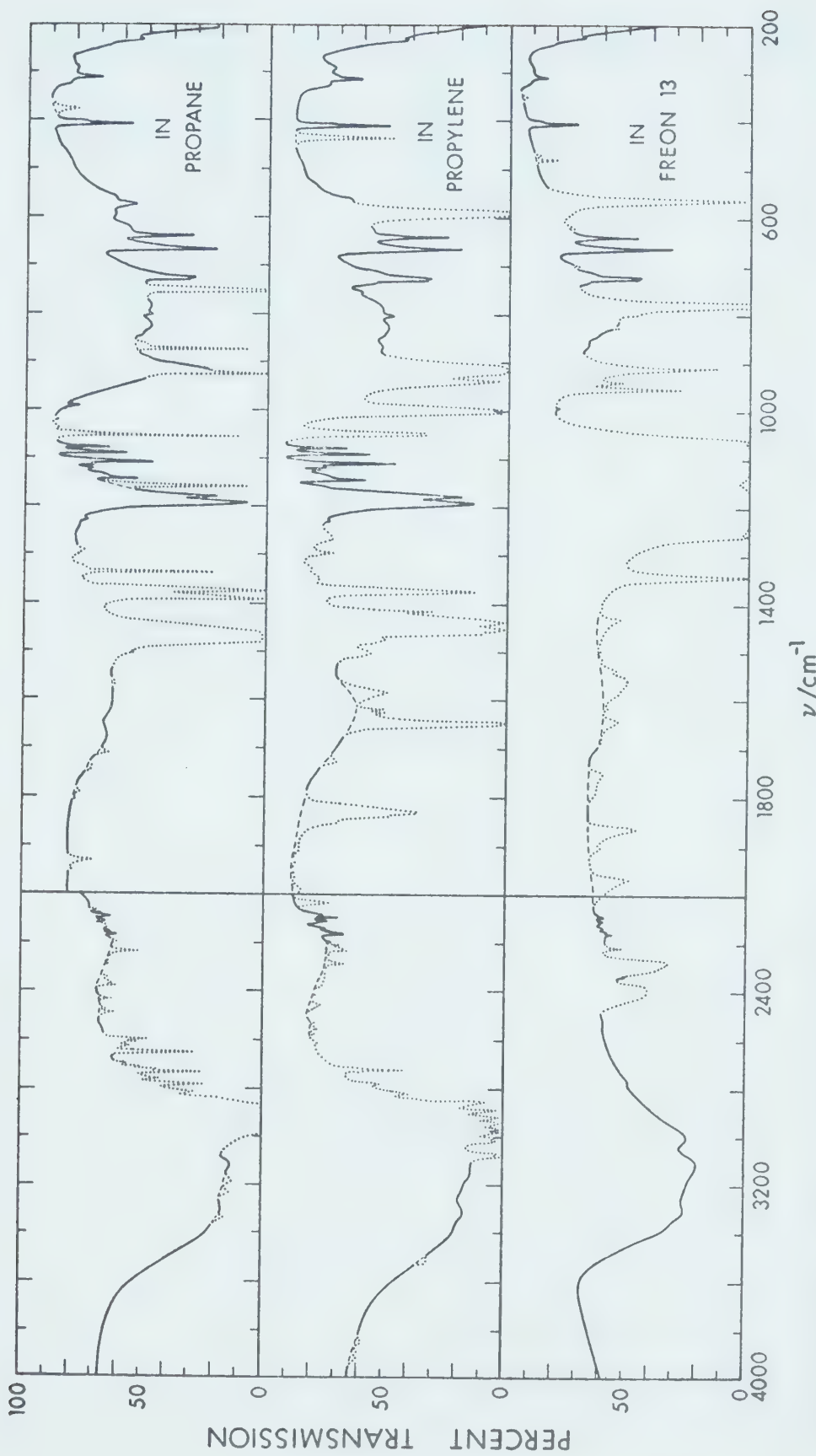


Figure 28. The mid-infrared spectra of HMT-d₁₂ · 6H₂O in three mulling agents at 90°K. The dotted lines indicate the absorption by the mulling agents, the dashed lines indicate the hydrate absorption in these regions.

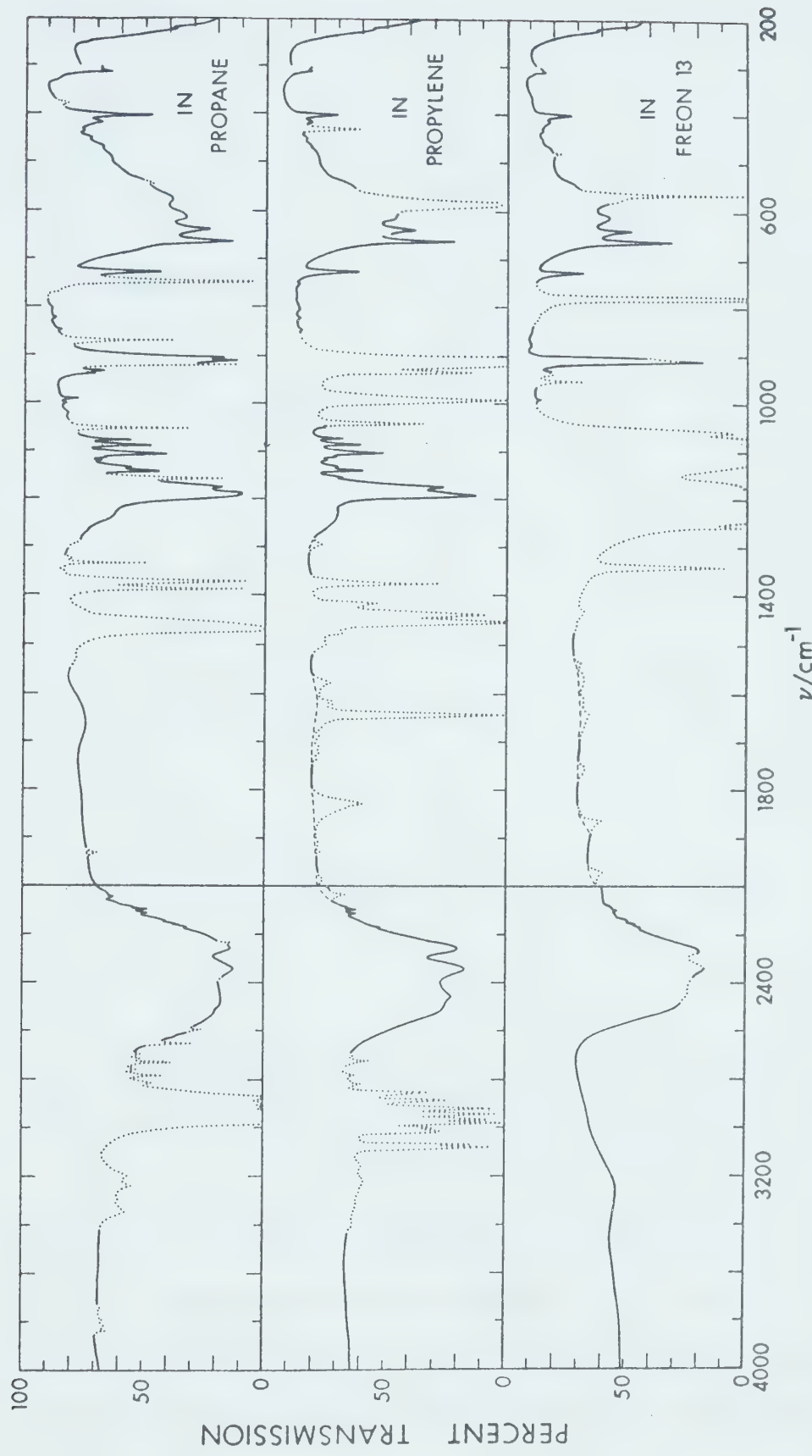


Figure 29. The mid-infrared spectra of HMT-d₁₂·6D₂O in three mulling agents at 90°K. The dotted lines indicate the absorption by the mulling agent, the dashed lines indicate the deuterate absorption in these regions.

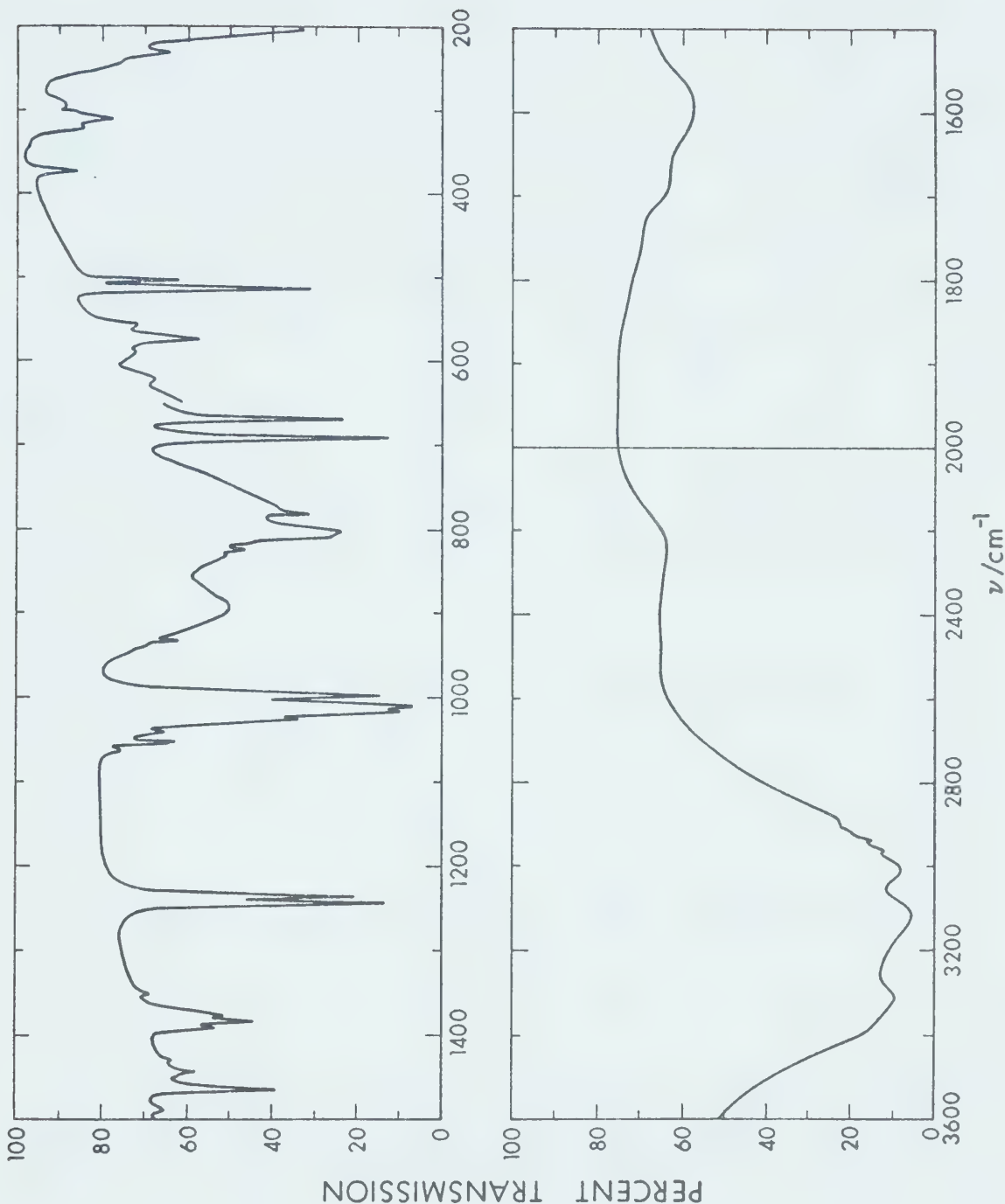


Figure 30. The mid-infrared spectrum of $\text{HMT}\text{-h}_{12}\cdot 6\text{H}_2\text{O}$ at 90°K . The spectrum was composed from spectra of three different samples each in a different mulling agent. The relative intensities of the peaks are approximately correct.

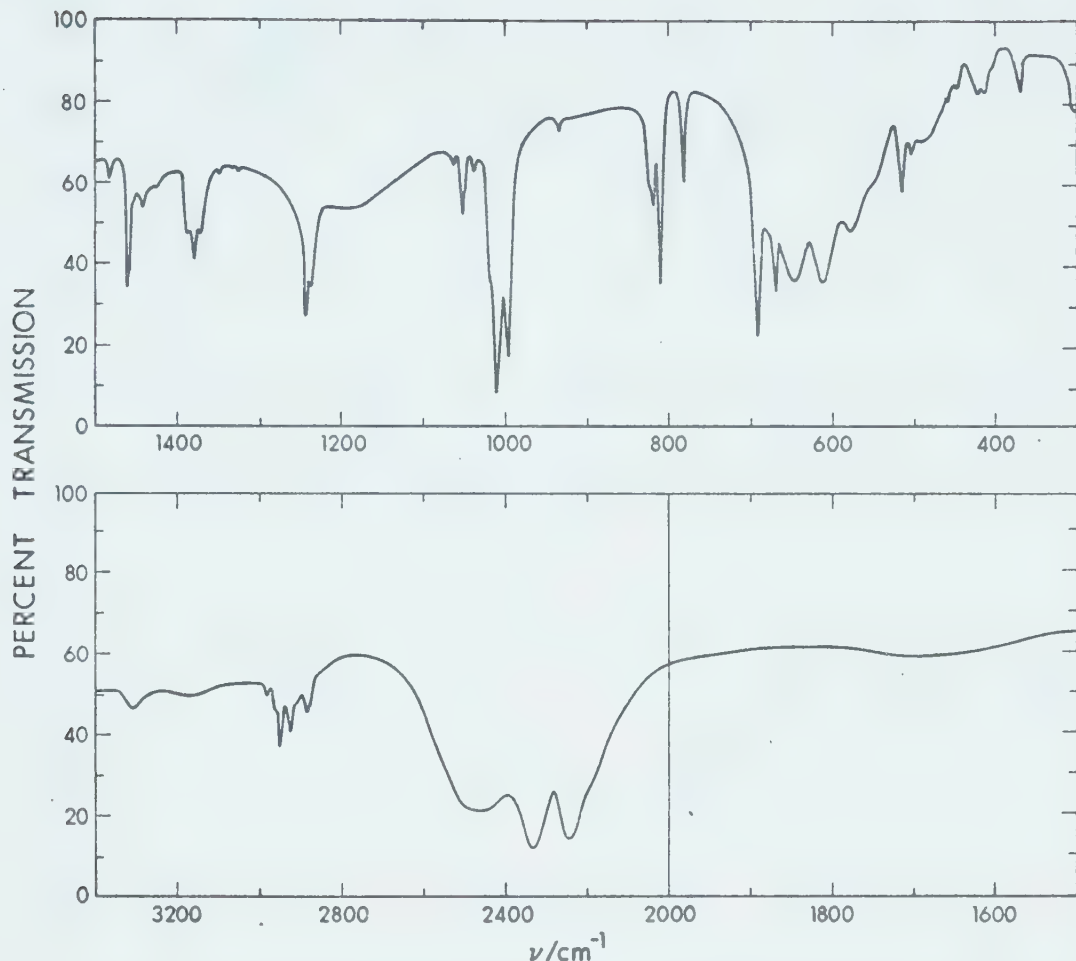


Figure 31. The mid-infrared spectrum of HMT-h₁₂·6D₂O at 90°K. The spectrum was composed from spectra of three different samples each in a different mulling agent. The relative intensities of the peaks are approximately correct.

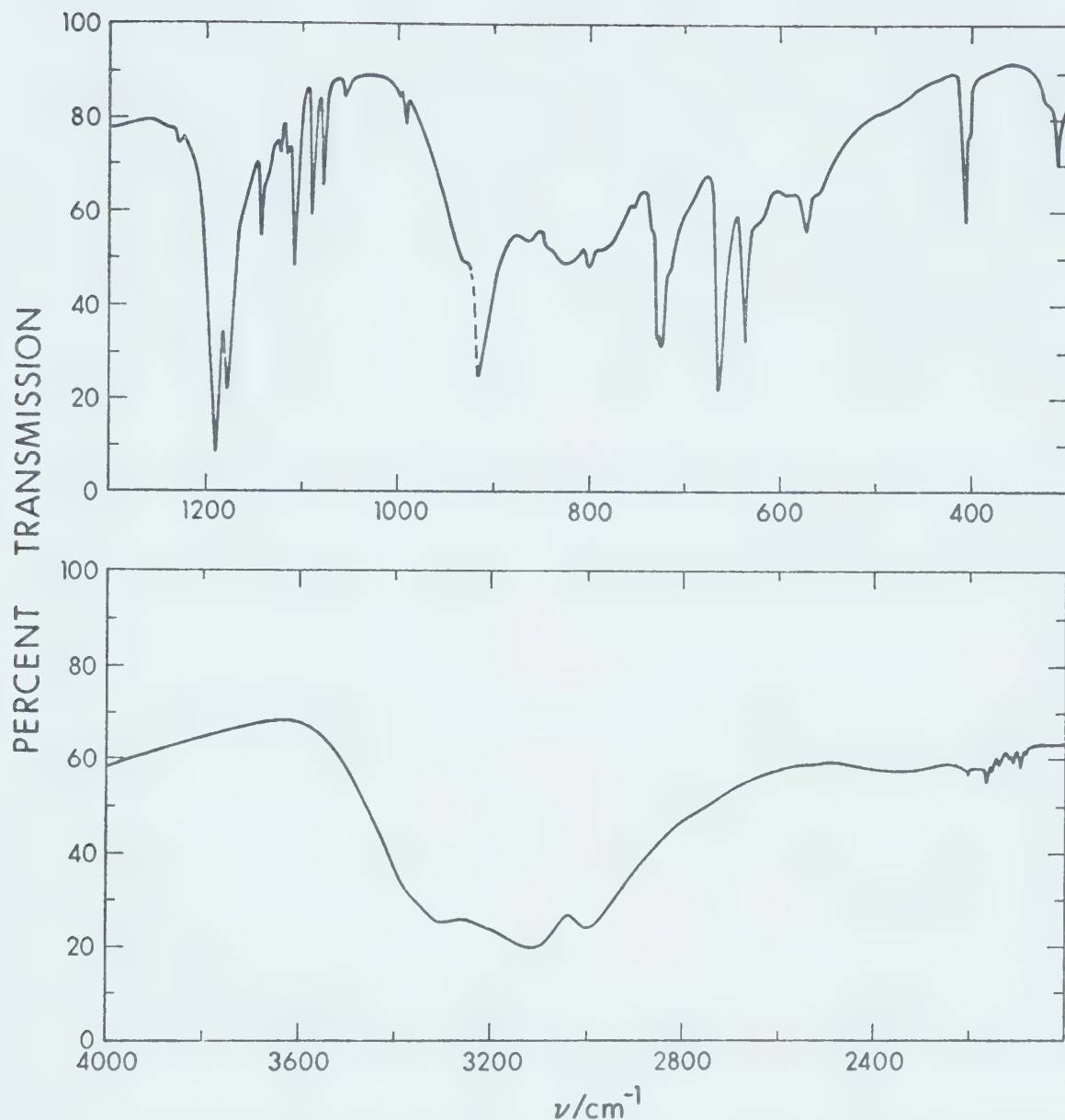


Figure 32. The mid-infrared spectrum of $\text{HMT-d}_{12} \cdot 6\text{H}_2\text{O}$ at 90°K . The spectrum was composed from the spectra of three different samples each in a different mulling agent. The relative intensities of the peaks are approximately correct. The dashed line at about 920 cm^{-1} indicates a region of uncertainty due to absorptions by the mulling agents.

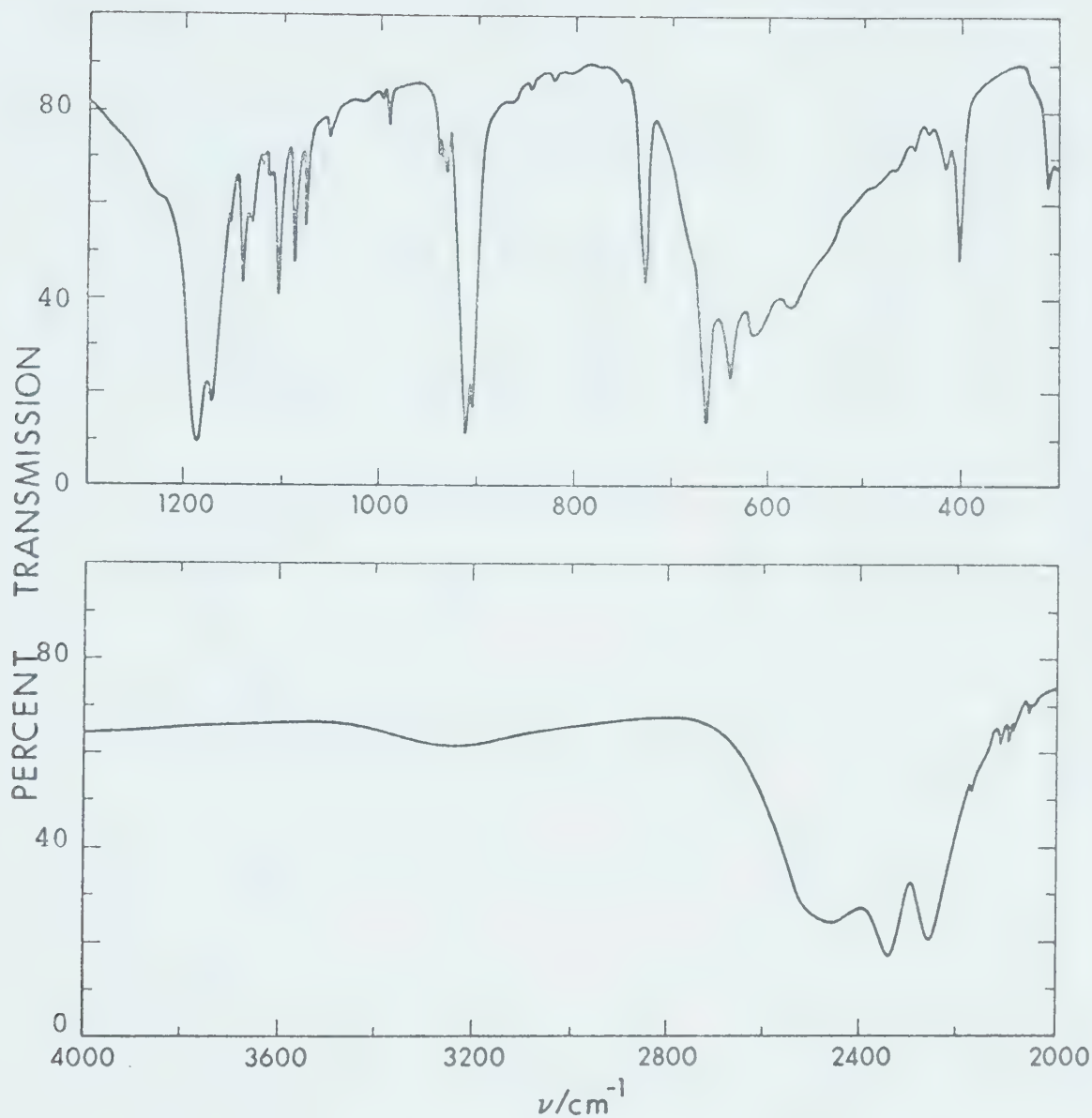


Figure 33. The mid-infrared spectrum of HMT-d₁₂·6D₂O at 90°K. The spectrum was composed from the spectra of three different samples each in a different mulling agent. The relative intensities of the peaks are approximately correct.

Table 15. The Frequencies of the Features Seen in the Mid-infrared Spectra of HMT-hydrate in Four Isotopic Modifications.

ν/cm^{-1}	HMT- $\text{h}_{12}\cdot 6\text{H}_2\text{O}$	HMT- $\text{d}_{12}\cdot 6\text{H}_2\text{O}$	ν/cm^{-1}		HMT- $\text{h}_{12}\cdot 6\text{D}_2\text{O}$	ν/cm^{-1}		HMT- $\text{d}_{12}\cdot 6\text{D}_2\text{O}$	ν/cm^{-1}
	Assig.	Assig.	ν/cm^{-1}	Assig.	Assig.	ν/cm^{-1}	Assig.	ν/cm^{-1}	Assig.
230.0 \pm 0.5 sh	H_2O	229.5 \pm 0.5 sh	H_2O	223.0 \pm 0.5	D ₂ O	222.3 \pm 1			D ₂ O
240 \pm 3 sh	H_2O	243 \pm 2 sh	H_2O	230 \pm 3 sh	D ₂ O	229 \pm 2 sh			D ₂ O
295 \pm 3 w,br	H_2O	288 \pm 2 w,br	H_2O	275 \pm 3 w,br	D ₂ O	275 \pm 2			D ₂ O
309.5 \pm 0.5 m	H_2O	309.7 \pm 0.5 m	HMT	297.4 \pm 1 m	D ₂ O	294 \pm 2 mbr			D ₂ O
319.4 \pm 0.5 m	H_2O	320.4 \pm 0.5 m	H_2O	306.6 \pm 1 m	D ₂ O	309.1 \pm 0.5 m	HMT		
372.4 \pm 0.5	HMT			371.5 \pm 0.5 m	HMT			400.5 \pm 0.5 s	HMT
			403 \pm 2 sh						
		405.7 \pm 0.5 m							
				HMT					
					415.5 \pm 1 m	D ₂ O	417.0 \pm 0.5 m	D ₂ O	
					425.0 \pm 1 m	D ₂ O			
						m	D ₂ O	435 \pm 2 w	D ₂ O
							D ₂ O	450.0 \pm 1 vw	D ₂ O

(Table continued on next page)

Table 15 continued

ν/cm^{-1}	HMT- $\text{h}_{12} \cdot 6\text{H}_2\text{O}$	Assig.	ν/cm^{-1}	HMT- $\text{d}_{12} \cdot 6\text{H}_2\text{O}$	Assig.	ν/cm^{-1}	HMT- $\text{h}_{12} \cdot 6\text{D}_2\text{O}$	Assig.	ν/cm^{-1}	HMT- $\text{d}_{12} \cdot 6\text{D}_2\text{O}$	Assig.
480	sh		456.2±1	vw	D_2O	465	vw?	D_2O ?			
502.6±0.5 m 512.6±0.5 s		HMT	474±3	sh	D_2O						
556±2	sh	H_2O	484.2±1	m	D_2O	486.0±1	sh	D_2O			
571.2±0.5 m			503.3±0.5 m 510.0±0.5 s		HMT	508.0±1	sh	D_2O			
589±2	sh		550±3	sh	D_2O	550±3	sh	D_2O			
620.0±1	w	H_2O	560±2	sh	H_2O	560	sh	D_2O			
			571.5±0.5 m		H_2O	578±2	s,br	D_2O	576±2	s,br	D_2O
			591±3	sh	H_2O						
						612±2	s,br	D_2O	610.4±2	s,br	D_2O

(Table continued on next page)

Table 15 continued

ν/cm^{-1}	Assig.	ν/cm^{-1}	Assig.	ν/cm^{-1}	Assig.	ν/cm^{-1}	Assig.
HMT-h ₁₂ ·6H ₂ O		HMT-d ₁₂ ·6H ₂ O		HMT-h ₁₂ ·6D ₂ O		HMT-d ₁₂ ·6D ₂ O	
627±3	sh	673.0±0.5 s	HMT	645±2	s,br D ₂ O	639.7±0.5 vs	HMT
		663.2±0.5 s	HMT			664.2±0.5 vs	
670.9±0.5 s	HMT			672.2±0.5 s	HMT	690	D ₂ O?
692.0±0.5 vs				693.9±0.5 vs		717±3	H ₂ O?
						722.4±1 s	HMT
						727.2±0.5 s	HMT
						734±3 sh	sh

(Table continued on next page)

Table 15 continued

ν/cm^{-1}	HMT-h ₁₂ ·6H ₂ O		HMT-d ₁₂ ·6H ₂ O		HMT-h ₁₂ ·6D ₂ O		HMT-d ₁₂ ·6D ₂ O	
	Assig.	ν/cm^{-1}		Assig.	ν/cm^{-1}	Assig.	ν/cm^{-1}	Assig.
750±10	w	H ₂ O	751±1	VW	HMT		750±1	VW
778±3	sh	H ₂ O						
783.9	0.5	w	HMT	784±5	s,br	H ₂ O	783.9±0.5	m
								HMT
				801.7±0.5	m	H ₂ O?		
							800±2	VW,br
805.2±1							812.9±0.5	HMT
810.2±1								
820	sh	HMT	822±5	m,br	H ₂ O	820.2±0.5	m	HMT
825.6±0.5	w	HMT				825±3	sh	HMT
834.0±1	sh	H ₂ O?	840±5	sh	H ₂ O			
863±3		w,br	H ₂ O				848±1	VW
								HMT

(Table continued on next page)

Table 15 continued

ν/cm^{-1}	HMT-h ₁₂ •6H ₂ O	HMT-d ₁₂ •6H ₂ O	HMT-h ₁₂ •6D ₂ O	HMT-d ₁₂ •6D ₂ O
ν/cm^{-1}	Assig.	ν/cm^{-1}	Assig.	ν/cm^{-1}
891 _{±2}	s,br H ₂ O	905 _{±3}	sh	HMT
		915 _{±3}	s	HMT
934.2 _{±0.5} w	HMT		933.4 _{±0.5} w	HMT
				932.6 _{±0.5} m
999.3 _{±0.5} vs	HMT	992.0 _{±0.5} w	HMT	HMT
				939.1 _{±0.5} m
1012.3 _{±0.5} vs	HMT		1012.6 _{±0.5} vs	HMT
				1019 _{±1}
1018.0	vs	HMT		vw
1027.3 _{±0.5} vs	HMT			HMT
1041.8 _{±0.5} m	HMT		1040.5 _{±0.5} w	HMT

(Table continued on next page)

Table 15 continued

ν/cm^{-1}	Assig.	ν/cm^{-1}	Assig.	ν/cm^{-1}	Assig.	ν/cm^{-1}	Assig.
HMT- $\text{h}_{12}\cdot 6\text{H}_2\text{O}$	HMT-d $_{12}\cdot 6\text{H}_2\text{O}$	HMT-d $_{12}\cdot 6\text{H}_2\text{O}$	HMT-h $_{12}\cdot 6\text{D}_2\text{O}$	HMT-h $_{12}\cdot 6\text{D}_2\text{O}$	HMT-d $_{12}\cdot 6\text{D}_2\text{O}$		
1054.3±0.5 m	HMT	1049±0.5 s	HMT	1054.5±1	sh	HMT	
1056.3±0.5 m	HMT			1056.8±0.5 s	HMT		
1065.0±0.5 w	HMT			1064.7±0.5 w	HMT		
		1078.8±0.5 m	HMT			1077.3±0.5	HMT
		1089.0±0.5 m	HMT			1088 m	HMT
		1107.0±0.5 m	HMT			1105.5±0.5 s	HMT
		1115.7±0.5 w	HMT				
		1122.5±0.5 w	HMT			1114.7±0.5 sh	HMT
		1139±3	sh	HMT		1120.0±0.5 w	HMT
						1133.7±0.5 m	HMT
		1142.0±0.5 m	HMT			1142.0±0.5 m	HMT
		1157	sh	HMT		1156.0±0.5 w	HMT

(Table continued on next page)

Table 15 continued

ν/cm^{-1}	Assig.	HMT-h ₁₂ •6H ₂ O	HMT-d ₁₂ •6H ₂ O	HMT-h ₁₂ •6D ₂ O	HMT-d ₁₂ •6D ₂ O
ν/cm^{-1}	Assig.	ν/cm^{-1}	Assig.	ν/cm^{-1}	Assig.
1177.7±0.5	vs	HMT			1174.2±0.5 vs HMT
1190.8±0.5	vs	HMT			1191.2±0.5 vs HMT
				1200	m,br D ₂ O
1228±1	vw	HMT			
1232±2	sh	?			
1237.0±0.5	vs	HMT		1238.3±0.5 s	
1245.3±0.5	vs	HMT			1245.5±0.5 s
1326.0	vw	HMT	1324±1	vw	sh HMT
1335.0±1	vw	HMT		1325.4±1	vw HMT
				1335	vw HMT
1351.5±0.5	w	HMT		1350.0±0.5 w	HMT
1374.6±0.5	m	HMT		1373.5±0.5 m	HMT
1382.5±0.5	s	HMT		1381.7±0.5 m	HMT

(Table continued on next page)

Table 15 continued

ν/cm^{-1}	HMT- $\text{h}_{12} \cdot 6\text{H}_2\text{O}$	HMT-d $_{12} \cdot 6\text{H}_2\text{O}$	HMT- $\text{h}_{12} \cdot 6\text{D}_2\text{O}$	HMT-d $_{12} \cdot 6\text{D}_2\text{O}$
ν/cm^{-1}	Assig.	ν/cm^{-1}	Assig.	ν/cm^{-1}
1389.2±0.5	m	HMT		
1427.0±1	vw	HMT	1388.9±0.5	m
(1434.0±0.5)vw		HMT	1423.3±1	w
1442±0.5	m	HMT	(1435±2)	vw
1446.0±1	sh	HMT	1444.0±1	m
1454.0±1	sh	HMT	1455±2	sh
1461.5±0.5	sh	HMT	1461.2±1	sh
1463.0±0.5	s	HMT	1462.6±0.5	s
1486.2±0.5		HMT	1485.2±0.5	w
1610±15	mbr	H_2O	1610±20	m,br H_2O
1690	sh	H_2O	1690	sh H_2O
1725±30	m,br	$\text{H}_2\text{O?}$	1725±20	sh H_2O
1790±10	w,br	H_2O		

(Table continued on next page)

Table 15 continued

ν/cm^{-1}	HMT-h ₁₂ •6H ₂ O	HMT-d ₁₂ •6H ₂ O	HMT-h ₁₂ •6D ₂ O	HMT-d ₁₂ •6D ₂ O
ν/cm^{-1}	Assig.	ν/cm^{-1}	Assig.	ν/cm^{-1}
1835±10	w,br H ₂ O	2086.7±1	vw	HMT
		2095.7±1	w	HMT
		2106±2	vw	HMT
		2114.2±1	w	HMT
		2122±3	w	HMT
		2145.2±1	w	HMT
		2158.5±1	w	HMT
		2170.0±1	w	HMT
		2200.0	vw	HMT
		2250±30	m,br H ₂ O	2215±20
				D ₂ O
				2256±10
				vs,br D ₂ O
				2255±10
				vs,br D ₂ O
				2341±10
				vs,br D ₂ O
				2342±10
				vs,br D ₂ O

(Table continued on next page)

Table 15 continued

ν/cm^{-1}	HMT-h ₁₂ ·6H ₂ O	HMT-d ₁₂ ·6H ₂ O	ν/cm^{-1}	HMT-h ₁₂ ·6D ₂ O	ν/cm^{-1}	HMT-d ₁₂ ·6D ₂ O
<u>Assig.</u>	<u>Assig.</u>	<u>Assig.</u>	<u>Assig.</u>	<u>Assig.</u>	<u>Assig.</u>	<u>Assig.</u>
2879±2	vw	HMT	2475±20	vs,br D ₂ O	2475±20	vs,br D ₂ O
2890±2	vw	HMT	2530±20	sh	D ₂ O	D ₂ O
2898±2	vw	HMT	2885.5±1	m	HMT	
2939±2	vw	HMT	2893.5±1	m	HMT	
2965±2	vw	HMT	2916±3	sh	HMT	
			2937.5±1	m	HMT	
			2961.5±1	m	HMT	
			2969±3	sh	HMT	
			2990.9±2	w	HMT	
3014±10	vs,br		3010±10	vs,br H ₂ O		
3120±10	vs,br		3126±10	vs,br H ₂ O		
3215±10	sh		3220±20	sh	H ₂ O	

(Table continued on next page)

Table 15 continued

ν/cm^{-1}	HMT-h ₁₂ ·6H ₂ O Assig.	HMT-d ₁₂ ·6H ₂ O ν/cm^{-1}	HMT-h ₁₂ ·6D ₂ O Assig.	HMT-d ₁₂ ·6D ₂ O ν/cm^{-1}	Assig.
3312±10	vs,br H ₂ O	3315±10	vs,br H ₂ O		
3375±20	sh H ₂ O	3380±10	sh H ₂ O		

vw = very weak, w = weak, m = medium, s = strong, vs = very strong, sh = shoulder,

br = broad

but high accuracy cannot be expected because the spectra were composed from many spectra of samples in all three mulling agents.

The features reported in Figures 30 - 33 and Table 15 were all consistently observed. The existence of some weak features was carefully investigated in order to make sure that instrumental artifacts or interference by the mulling agents were not reported as real features of the hydrate spectra. The only remaining uncertainties in the spectra arise from the interference by the mulling agents. The exact shape of the broad band at about 1600 cm^{-1} in the spectra of the deuterates could not be determined because all mulling agents absorb weakly in this region. All mulling agents also absorb at about 1430 cm^{-1} and the existence of two weak peaks in this region in the spectra of HMT- h_{12} hydrate and deuterate is very much in doubt. While the peak at about 1425 cm^{-1} is only partially overlapped by a weak absorption of Freon 13 (Figures 26 and 27), and is, therefore, a real spectral feature of the hydrate, the existence of the peak at 1435 cm^{-1} is much less certain and the frequency is reported in brackets in Table 15. A slight doubt exists about the shape of the high frequency side of the peak seen at 915 cm^{-1} in the spectrum of the hydrate of HMT- d_{12} (Figure 32) because all mulling agents absorb in this region. The remaining features are believed to be real.

The first step in the detailed interpretation of

the spectra is the distinction between the absorption by the water molecules and that by the guest molecules. The only way to positively distinguish between these two types of absorption is to study the frequencies of the features in the different isotopic modifications. The frequencies of the intramolecular and rotational vibrations of the water molecules should be about 30% lower in the spectrum of the deuterate than in that of the hydrate, while the peaks due to vibrations of the guest should remain unshifted, except for small changes due to interaction with the water modes. On the other hand any peaks which are shifted when HMT-d₁₂ is substituted for HMT-h₁₂ can be assigned to vibrations of the HMT molecule. The assignment of the various features to water or HMT is shown in Table 15.

The absorption by the water molecules. The nomenclature used below is defined in Section I.4. The $\nu_{OH}(H_2O)$ bands of HMT-h₁₂·6H₂O and HMT-d₁₂·6H₂O extend from about 2500 to about 3700 cm⁻¹ (Figures 30 and 32). Three broad maxima and two shoulders are easily identified in this region. In addition, several weak peaks are observed on the low frequency side of this band in the spectrum of HMT-h₁₂ hydrate (Figure 30). These weak peaks, which are found between 2900 and 3000 cm⁻¹, are not present in the spectrum of HMT-d₁₂ hydrate (Figure 32) and are certainly due to vibrations of the HMT molecule. The $\nu_{OD}(D_2O)$ bands of the deuterates (Figures 31 and 33) extend from about 2000 to

about 2700 cm^{-1} . Three broad maxima and two shoulders are identified. Several weak peaks which overlap the low frequency side of the band of the deuterate of HMT-d₁₂ (Figure 33), but not that of HMT-h₁₂ (Figure 31), are certainly due to vibrations of the HMT-d₁₂ molecule. The ratios of the frequencies of the three maxima at 3014, 3120 and 3312 cm^{-1} in the $\nu_{\text{OH}}(\text{H}_2\text{O})$ band to those of the corresponding maxima in the $\nu_{\text{OD}}(\text{D}_2\text{O})$ band are 1.336, 1.333 and 1.338, respectively, all ± 0.004 .

The $\nu_{\text{R}}(\text{H}_2\text{O})$ band of the hydrates extends from about 450 to about 1000 cm^{-1} (Figures 30, 32 and 34). The shape of this broad band is complicated by several sharp peaks, certainly due to absorptions by the guest, superimposed upon it. A comparison of the spectra of the hydrates of HMT-h₁₂ (Figure 30 and curve a of Figure 34) and HMT-d₁₂ (Figure 32 and curve a of Figure 36) leads to the assignment of the features due to the vibrations of the H_2O molecules. The broad maximum at about 900 cm^{-1} in the spectrum of HMT-h₁₂ hydrate can still be detected in the spectrum of HMT-d₁₂ hydrate, although in the latter it is partially obscured by an absorption of the guest. The region around 800 cm^{-1} in the spectrum of HMT-h₁₂ hydrate is greatly complicated by the presence of several peaks due to vibrations of the guest molecule. Three broad maxima and a shoulder (at 784, 822, 840 (sh) and 863 cm^{-1}) can easily be recognized in this region in the spectrum of

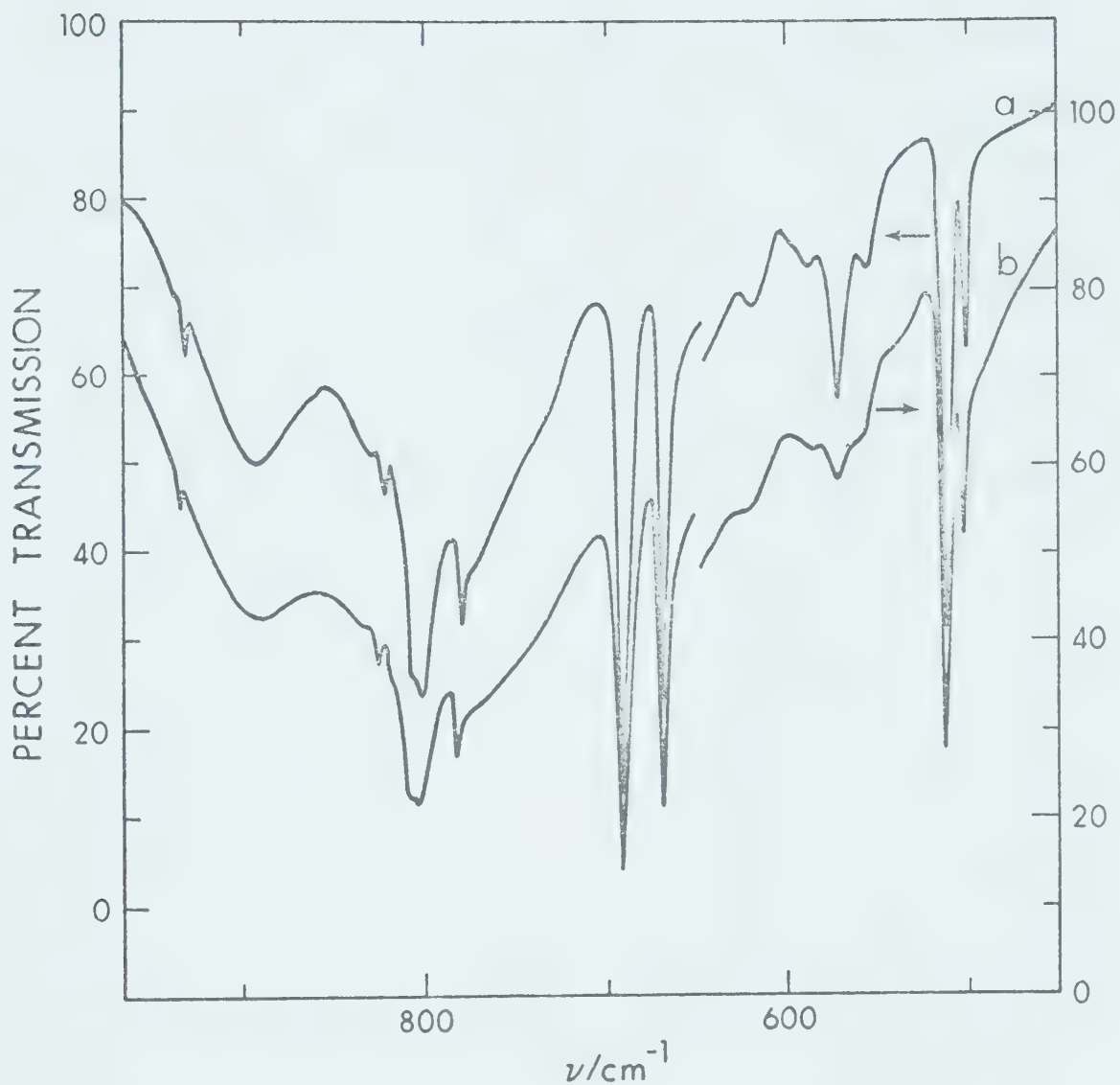


Figure 34. The ν_R band of a sample of HMT-h₁₂ hydrate (curve a) and of a sample of HMT-h₁₂ hydrate containing about 10% of HDO (curve b).

HMT-d₁₂ hydrate. The weak peak seen at 620 cm⁻¹ in the spectrum of HMT-h₁₂ hydrate appears to be still present as a shoulder in the spectrum of HMT-d₁₂ hydrate. Of particular interest are the rather sharp peaks at 556, 571 and 589 cm⁻¹ in the spectrum of HMT-h₁₂ hydrate (Figure 30 and curve a of Figure 34). These are clearly also present in the spectrum of HMT-d₁₂ hydrate (Figure 32 and curve a of Figure 36) and must arise from vibrations of the water molecules. The shift of frequencies of these peaks on deuteration is not clear, but there can be little doubt that they arise from rotational vibrations of the H₂O molecules.

The $\nu_R(D_2O)$ band of the deuterate extends from about 350 cm⁻¹ to about 750 cm⁻¹ (Figures 31, 33 and 35). The features which are common to the spectra of the deuterates of HMT-h₁₂ and -d₁₂ are: three maxima at 645 (partly obscured in the spectrum of HMT-d₁₂·6D₂O), 612 and 578 cm⁻¹, a shoulder at 550 cm⁻¹, a weak broad feature at 484 cm⁻¹ and two very weak peaks seen at 447 and 456 cm⁻¹ in the spectrum of HMT-h₁₂ deuterate and at 450 and 465 cm⁻¹ in the spectrum of HMT-d₁₂ deuterate. All these features are assigned to rotational vibrations of the D₂O molecules. In addition a broad, medium intensity peak, partly split into two components, is seen at about 420 cm⁻¹ in the spectrum of HMT-h₁₂ deuterate. Although peaks due to HMT are found at about this frequency in the spectrum of HMT-d₁₂ deuterate, there is no doubt that the doublet seen at about 420 cm⁻¹

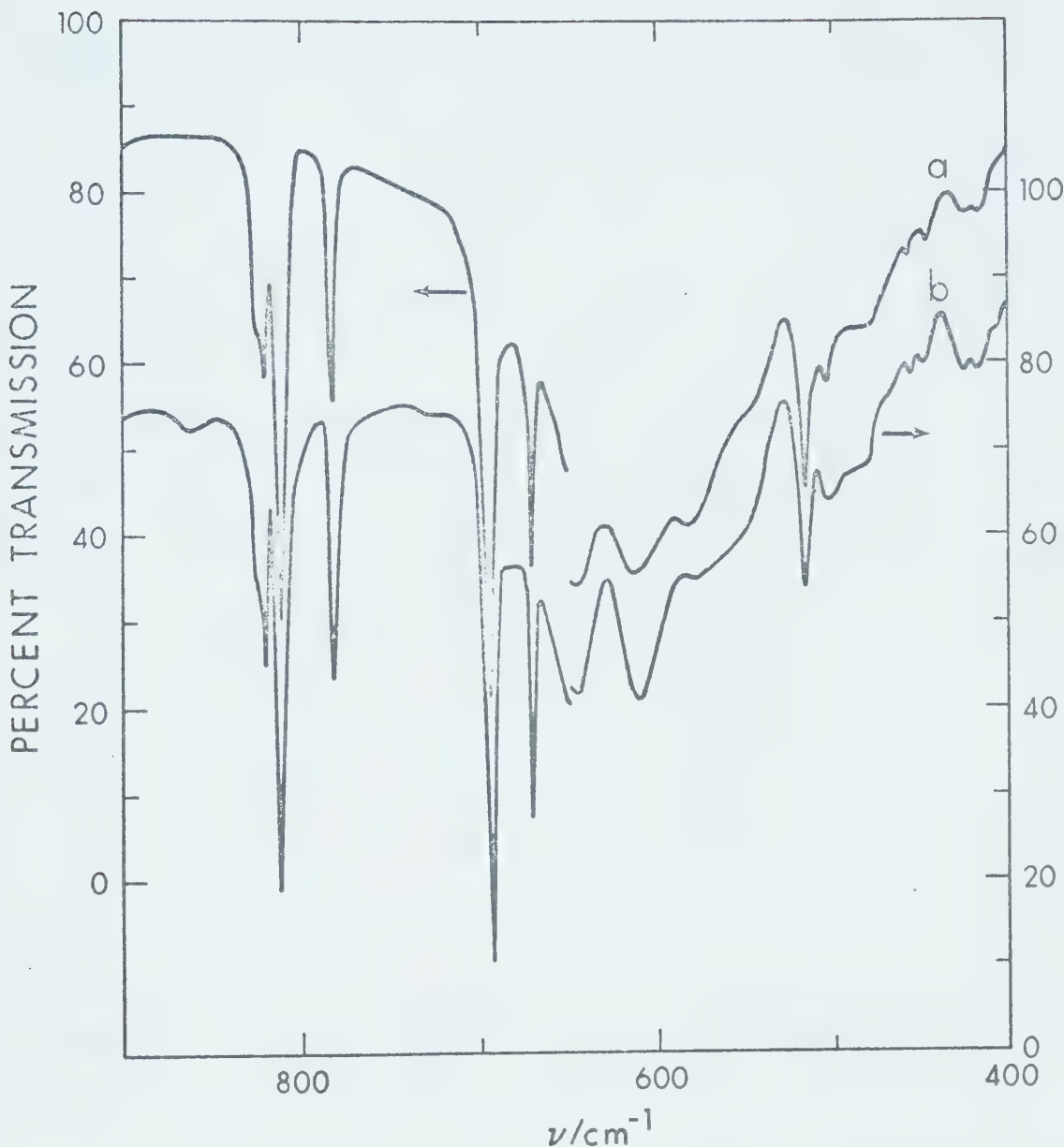


Figure 35. The ν_R band of a sample of HMT-h₁₂ deuterate (curve a) and of a sample of HMT-h₁₂ deuterate containing about 10% of HDO (curve b).

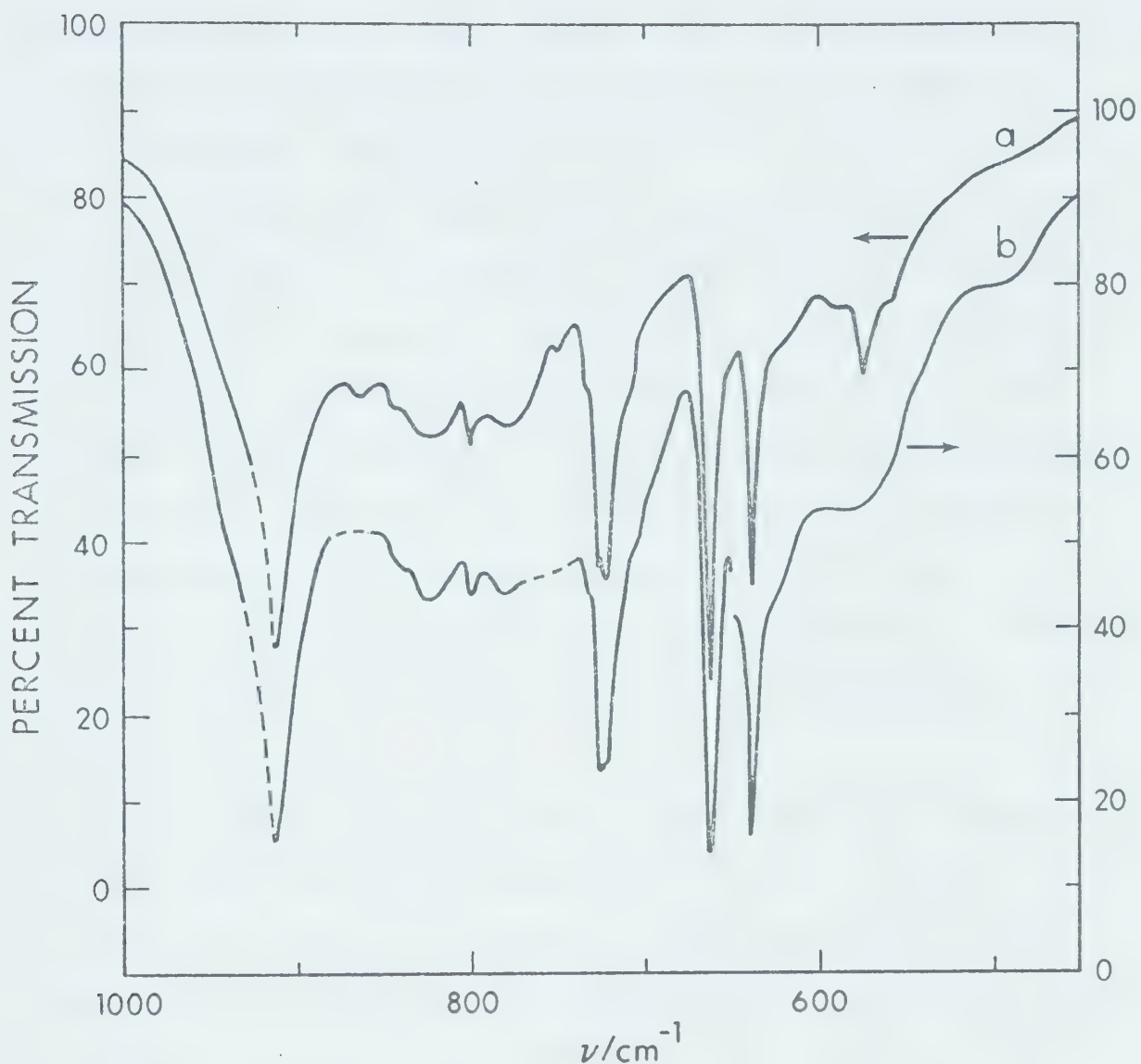


Figure 36. The ν_R band of a sample of HMT-d₁₂ hydrate (curve a) and of a sample of HMT-d₁₂ hydrate containing about 10% of HDO. The dashed lines indicate uncertainties in the spectrum due to absorptions of the mulling agent.

in the spectrum of HMT-h₁₂·6D₂O is due to rotational vibrations of the D₂O molecules, because it is not seen in the spectrum of HMT-h₁₂·6H₂O.

The ν₂(H₂O) band in the spectra of HMT-h₁₂ hydrate (Figures 26 and 30) and HMT-d₁₂ hydrate (Figure 28) shows a distinct broad maximum at 1610 cm⁻¹ and two shoulders at about 1690 and 1730 cm⁻¹. The corresponding band in the spectrum of the deuterate of HMT-h₁₂ shows a broad maximum at 1200 cm⁻¹, while its high frequency side is obscured by an absorption due to the guest molecule. This band is not clearly visible in the spectrum of HMT-d₁₂ deuterate because a broad doublet due to a vibration of HMT overlaps it extensively.

The 3ν_{R'},ν_R + ν₂ band is very broad and featureless in the spectra of both hydrates and both deuterates. Its ill-defined maximum is located at about 2250 cm⁻¹ in the spectra of the hydrates and at about 1600 cm⁻¹ in the spectra of the deuterates (Figures 26 - 32).

Absorption by the hexamethylenetetramine molecules. The absorption peaks of the guest molecules are generally sharp and well resolved. A complete discussion and assignment of these features will be presented in Section V.2. Here attention is drawn to some differences between the spectra of the hydrates and of the deuterates which are believed to be particularly significant.

In the spectrum of the deuterate of HMT-h₁₂, three

sharp peaks and a shoulder are seen at 783.0, 812.9, 820.2 and 825 cm^{-1} , respectively (Figures 31 and 35). There can be little doubt that these features are due to the guest molecule because they are absent in the spectrum of the deuterate of HMT-d₁₂ (Figure 33). The two low frequency peaks have half-widths of about five cm^{-1} , while the peak at 820 cm^{-1} is broader because a fourth peak overlaps its high frequency side, appearing as a shoulder at 825 cm^{-1} . In the spectrum of HMT-h₁₂ hydrate a weak sharp peak is seen at about 825 cm^{-1} and two badly resolved peaks are seen at 805.2 and 810.2 cm^{-1} (Figures 30 and 34). The peak at 783.9 cm^{-1} is seen in the hydrate spectrum as a peak of medium intensity overlapping the $\nu_R(\text{H}_2\text{O})$ band. In summary the spectrum of the guest molecule in this region appears to be drastically different for the hydrate and deuterate of HMT-h₁₂. More differences in the HMT absorption between the spectra of HMT-h₁₂ hydrate and deuterate are seen near 1000 cm^{-1} . Four peaks are resolved in the spectrum of the hydrate, at 999.3, 1012.3, 1018.0 and 1027.3 cm^{-1} (Figure 30). The absence of these peaks in the spectrum of the hydrate of HMT-d₁₂ (Figure 32) proves that they are due to vibrations of HMT-h₁₂. The peaks at 1018.0 and 1027.3 cm^{-1} are not seen in the spectrum of HMT-h₁₂ deuterate (Figure 31); a shoulder is instead found at about 1022 cm^{-1} . Finally, the components of the doublet at about 1240 cm^{-1} , which are very well separated in the spectrum of HMT-h₁₂

hydrate (Figure 30), are barely resolved in the spectrum of the deuterate (Figure 31), in which they overlap the $\nu_2(D_2O)$ band. The assignment to HMT- h_{12} of the two sharp doublets at about 500 and 670 cm^{-1} , of all peaks between 1300 and 1500 cm^{-1} , and of the sharp absorptions between 2880 and 3000 cm^{-1} , is immediately obvious from a comparison of the spectra of its hydrate and deuterate (Figures 30 and 31). This assignment is confirmed by the absence of these peaks in the spectra of the hydrate and deuterate of HMT- d_{12} .

The assignment of the peaks of HMT- d_{12} does not need a detailed discussion. An inspection of the spectra (Figures 32 and 33) reveals immediately which features are due to vibrations of the guest. Some significant differences between the spectra of the hydrate and of the deuterate are observed and attention will be drawn to them. A peak and a shoulder are seen at 733.6 and 736 cm^{-1} in the spectrum of the deuterate (Figure 33), while in the spectrum of the hydrate two peaks are seen at 722.4 and 727.2 cm^{-1} , with two shoulders at about 717 and 734 cm^{-1} (Figure 32). Another significant difference is found at about 400 cm^{-1} , where the spectrum of HMT- d_{12} hydrate shows a peak at 405.7 cm^{-1} and a shoulder at about 403 cm^{-1} (Figure 32), while that of HMT- d_{12} deuterate shows peaks at 400.5 and 417 cm^{-1} .

The absorption by HDO molecules. The spectra of the hydrate and deuterate containing from 2 to 10% of HDO

molecules gave three kinds of information:

- (a) Peaks were seen due to the OH and OD stretching modes, ν_{OH} (HDO) and ν_{OD} (HDO), of HDO molecules surrounded by D₂O or H₂O molecules respectively.
- (b) Peaks were seen in the region of the ν_R (H₂O) and ν_R (D₂O) which were not seen in the spectra of the pure hydrates and deuterate.
- (c) Changes were observed in one of the components of the ν_R (H₂O) band of the hydrates.

Figure 37 shows the ν_{OH} (HDO) and ν_{OD} (HDO) bands derived from the spectra of HMT-h₁₂ deuterate and hydrate, respectively, containing about 10% of HDO molecules. The frequencies and the half-widths of the bands are listed in Table 16. The very weak features at 3277 and 2420 cm⁻¹ (dotted lines in Figure 37) are due to very small amounts of ice impurity left in the sample. The ratio of the frequencies of the ν_{OH} (HDO) peaks to those of the corresponding ν_{OD} (HDO) peaks are 1.331 ± 0.009, 1.344 ± 0.005 and 1.352 ± 0.005 for the low, middle and high frequency peak, respectively. The relative intensities are approximately 1, 2 and 4 for the low, middle and high frequency peaks, respectively; their measurement is very difficult due to the difficulty of defining the baseline.

Two peaks which are not present in the spectra of the hydrate and deuterate are seen in the spectra of samples containing 10% of HDO. They are found at 500 and

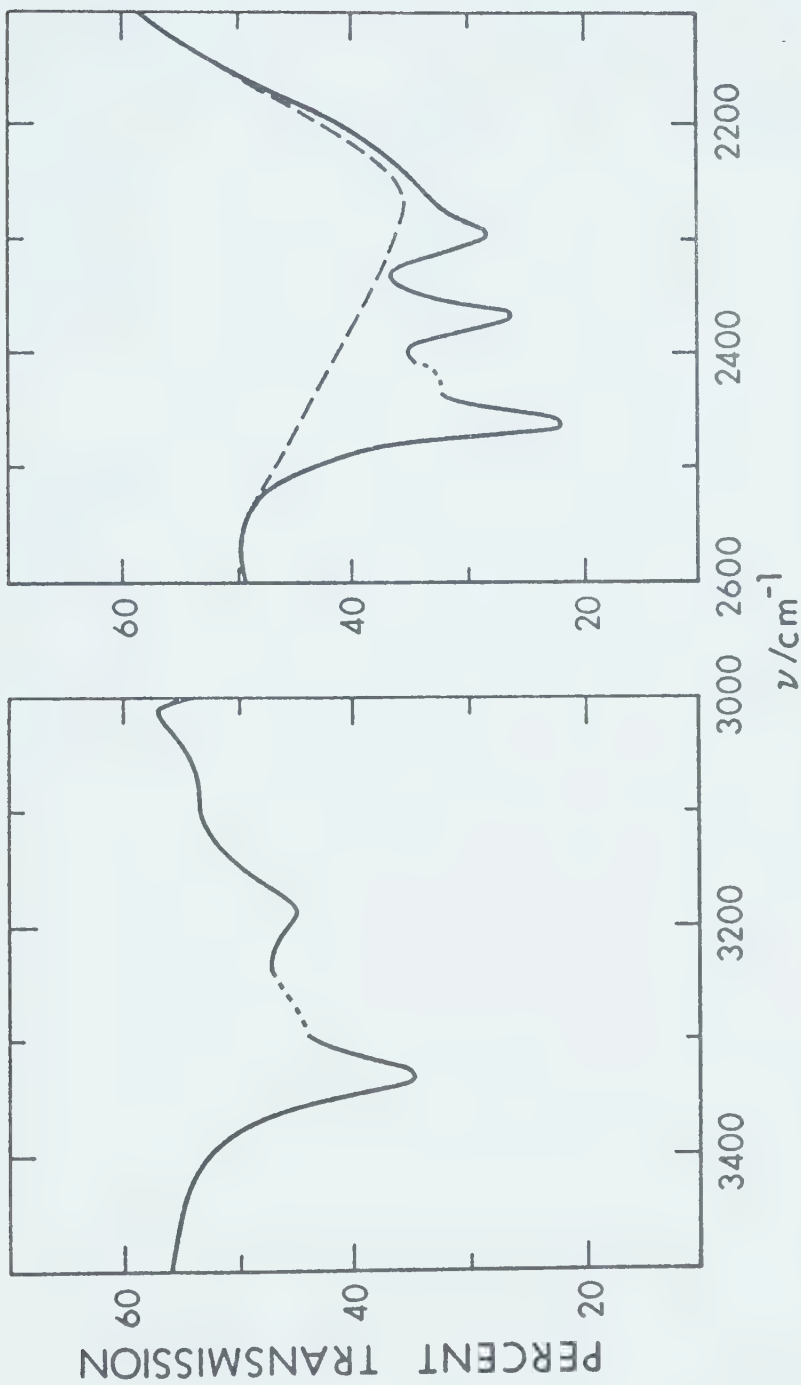


Figure 37. Absorption by ν_{OH} (HDO) in a sample of HMT-h₁₂ deuterate containing about 10% of HDO (left box) and by ν_{OD} (HDO) in a sample of HMT-h₁₂ hydrate containing about 10% of HDO.

Table 16. Frequencies of the $\nu_{\text{OH}}(\text{HDO})$ and $\nu_{\text{OD}}(\text{HDO})$ peaks.

$\nu_{\text{OH}}(\text{HDO})$ ν/cm^{-1}	Int.	Half-width/ cm^{-1}
3050 (10)	1	50 \pm 10
3184 (5)	2	50 \pm 10
3332 (5)	4	45 \pm 10
$\nu_{\text{OD}}(\text{HDO})$ ν/cm^{-1}		
2292 (5)	1	35 \pm 10
2369 (5)	2.5	35 \pm 10
2464 (5)	4.5	30 \pm 10

at 859 cm^{-1} . The first is visible as a shoulder on the low frequency side of the absorption peak at 502.6 cm^{-1} in the spectrum of HMT-h₁₂ hydrate (curve b of Figure 34), while it appears clearly in the spectrum of HMT-d₁₂ hydrate (curve b of Figure 36). The peak at 859 cm^{-1} is clearly recognizable in the spectrum of HMT-h₁₂ deuterate containing 10% of HDO (Figure 35).

The $\nu_R(\text{H}_2\text{O})$ band of HMT-h₁₂ hydrate is shown in curve a of Figure 34, while curve b shows the spectrum of a sample containing 10% of HDO. It is clear that the sharp features between 560 and 600 cm^{-1} are broad and less pronounced in the sample contaminated with HDO. Figure 36 shows the same effect, rather more pronounced, for the same band in the spectrum of HMT-d₁₂ hydrate. No comparable effect was observed in the spectra of the deuterate of HMT-h₁₂ (Figure 35).

IV.3 The Far-Infrared Spectra.

The upper box of Figure 38 shows the far-infrared spectra of HMT-h₁₂ hydrate and deuterate at 100°K , while the lower box shows those of HMT-d₁₂ hydrate and deuterate at 100°K . In both cases the hydrate spectrum is above that of the deuterate. The frequencies of the features and their estimated errors are listed in Table 17. Eleven features are clearly identified in all spectra, overlapping what appears to be a broad background absorption. The spectra

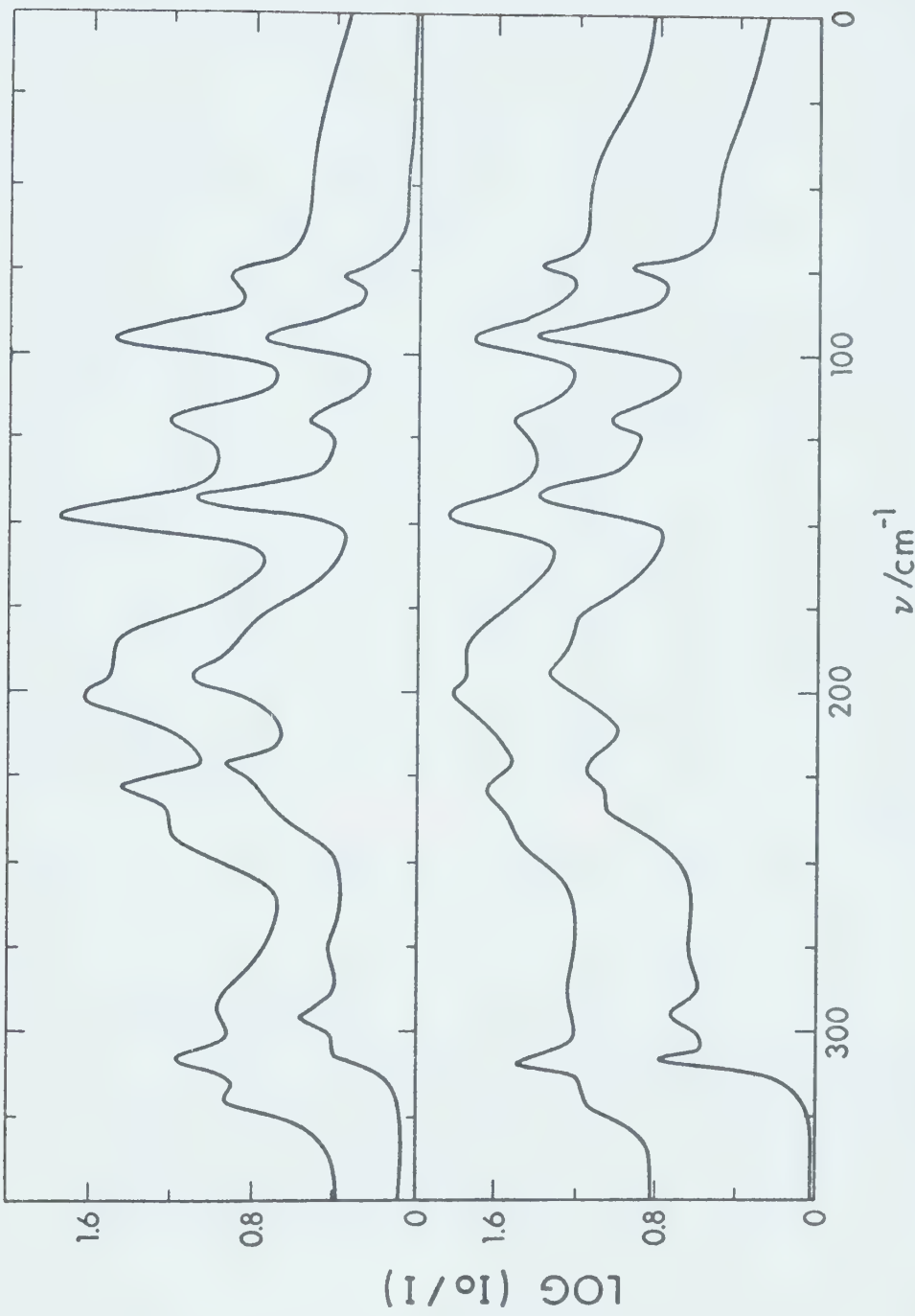


Figure 38. Far-infrared spectra of HMT-h₁₂ hydrate and deuterate (upper and lower curve respectively in the upper box), and of HMT-d₁₂ hydrate and deuterate (upper and lower curve respectively of lower box), all samples at about 100°K.

Table 17. Far-infrared Frequencies for the Hydrate of
Hexamethylenetetramine in Four Isotopic Modifications.^{a,b}

HMT-h ₁₂ ·6H ₂ O	HMT-h ₁₂ ·6D ₂ O	HMT-d ₁₂ ·6H ₂ O	HMT-d ₁₂ ·6D ₂ O
78.2(0.5) w	78.0(0.5) w	74.2(0.5) w	74.0(0.5) w
96.3(0.5) s	95.8(0.5) s	95.7(0.5) s	94.5(0.5) s
121.5(0.5) m	120.0(0.5) m	120.8(0.5) m	119.3(0.5) m
148.8(0.5) s	143.2(0.5) s	148.0(0.5) s	141.9(0.5) s
186 (3) sh	178 (3) sh	186 (3) sh	177 (3) sh
202.4(1) s	195.6(1) s	201 (2) s	194 (2) s
229.0(1) s	222.0(1) s	229.8(1) s	223 (2) s
243 (2) m	233 (3) m	242 (3) m	234 (3) m
293 (3) w	277 (3) w	287 (3) w	276 (3) w
308.5(1) m	296.0(1) m	309.0(1) m	295.5(1) m
			308.5(0.3) m
320 (2) w	307 (2) w	322 (3) w	

(a) Frequencies are in units of cm⁻¹.

(b) w = weak; m = medium; s = strong; sh = shoulder.

(c) Values in brackets represent the experimental error of the frequencies in cm⁻¹.

of the hydrate and of the deuterate of HMT-d₁₂ appear to be somewhat broader and less well defined than those of the hydrate and of the deuterate of HMT-h₁₂. This is not believed to be a real feature of the spectra, but rather to be due to the fact that the spectra of the hydrate and deuterate of HMT-d₁₂ were less extensively studied and the spectra are not of such a high quality as those of the HMT-h₁₂ compounds. The existence of the features reported is beyond any doubt, but their shapes are rather uncertain, particularly for the broad bands.

The half-widths of the four sharp peaks seen below 150 cm⁻¹ are between 10 and 12 cm⁻¹ for all compounds. It is not possible to measure them more accurately due to the uncertainty in locating the baseline. A very sharp peak is seen at 308 cm⁻¹, only in the spectrum of HMT-d₁₂·6D₂O. This peak is certainly due to an intramolecular mode of the guest molecule. The corresponding peak in the spectrum of HMT-d₁₂ hydrate is coincident with a water absorption. It is very difficult to evaluate the half-widths of the remaining peaks because they overlap very extensively. The three peaks at about 300 cm⁻¹ in the spectrum of HMT-h₁₂ hydrate are separated by 12 and 18 cm⁻¹ and are just resolved. Therefore, assuming that they have the same shape, their half-widths are probably between 12 and 18 cm⁻¹. On the same grounds the half-widths of the two peaks at 228.5 and 240 cm⁻¹ are about 11 cm⁻¹ and those of the two peaks

at about 200 cm^{-1} are about 16 cm^{-1} . It must be emphasized that the above values are to be treated with caution due to the assumptions that have been made and that the half-widths of these peaks are not necessarily physically significant. However, even a rough estimate of the half-widths is useful for the discussion of the spectra in Section V.3.

It is clear from the observed isotope shifts that a distinction between water absorption and guest absorption is not very meaningful in the far-infrared region. Some conclusions can, however, be drawn. The peaks above 180 cm^{-1} are clearly primarily due to translational vibrations of the water molecules, $\nu_T(\text{H}_2\text{O})$ and $\nu_T(\text{D}_2\text{O})$. The only peak which arises from predominantly HMT vibrations is at 78 cm^{-1} for HMT-h₁₂ and 74 cm^{-1} for HMT-d₁₂. The peak at about 148 cm^{-1} for the hydrate and 143 cm^{-1} for the deuterate arises largely from water vibrations, but appears to be influenced by HMT as well. The remaining peaks, at about 120 and 95 cm^{-1} , do not show a marked isotope shift for any single isotopic substitution, but move to lower frequencies as the molecular masses are increased. They are assigned to mixed motions of HMT and water molecules.

IV.4 X-ray Results.

The crystal structure of the hydrate was determined at 253°K (34), but the infrared spectra were obtained

at 100°K. A knowledge of the unit cell parameters at 100°K was necessary to interpret some features of the infrared spectra and, as the closest approximation attainable, this was determined from X-ray powder photographs of HMT-h₁₂ hydrate at 120°K. These photographs could readily be indexed on the basis of the unit cell determined at 253°K and this was taken as evidence that no phase transitions occur between 253 and 120°K.

The diameter of the diffraction lines of four different samples of HMT-h₁₂·6H₂O were measured to the nearest 0.01 mm and the corresponding 2θ angles and d spacings were calculated and indexed using as a guide the diffraction pattern calculated from the unit cell parameters at 253°K. The diffraction pattern observed at 120°K is reported in Table 18. The unit cell parameters at 120°K were then obtained by refining the unit cell parameters determined by Mak at 253°K to fit the diffraction pattern at 120°K. This was accomplished using DREF (132), a program written in FORTRAN IV for the University of Alberta IBM 360 computer. DREF accepts the experimental 2θ values with the appropriate indices, the wavelength of the X-ray radiation and an initial set of unit cell parameters. It then refines these parameters to fit the observed diffraction pattern, using the least square method as a criterion for a good fit. The unit cell parameters at 120°K were used to calculate the O...O and O...N bond distances

at the same temperature. Assuming that the fractional coordinates of all atoms in the unit cell remained unchanged, the values shown in Table 19 were obtained. The values found at 253°K (34) are shown in the same table for comparison.

Table 18. Diffraction Pattern of Hexamethylenetetramine Hydrate at 120°K.

Index	d spacing (in Å)
101	6.511
110	5.804
021	4.325
012	3.946
211	3.462
300	3.355
122	2.843
131	2.649
113	2.561
401	2.402
321	2.220
402	2.164

Table 19. Structural Parameters of Hexamethylenetetramine Hydrate at 253°K (34) and at 120°K.

	At 253°K	At 120°K ^a
a	$11.62 \pm 0.01 \text{ \AA}$	$11.60 \pm 0.01 \text{ \AA}$
c	$8.67 \pm 0.01 \text{ \AA}$	$8.59 \pm 0.01 \text{ \AA}$
a/c	1.340 ± 0.002	1.350 ± 0.002
O_1-O_2 (between rings)	$2.764 \pm 0.011 \text{ \AA}$	$2.74 \pm 0.01 \text{ \AA}$
O_1-O_2 (within rings)	$2.766 \pm 0.011 \text{ \AA}$	$2.76 \pm 0.01 \text{ \AA}$
O_2-N	$2.816 \pm 0.009 \text{ \AA}$	$2.79 \pm 0.01 \text{ \AA}$

^aThe wavelength of the X-ray radiation was taken as 1.5418 \AA .

Chapter V. Discussion of the Infrared Spectra of Hexamethylenetetramine Hydrate.

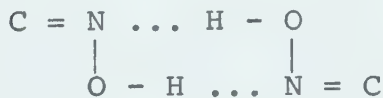
The discussion of the mid-infrared spectra and that of the far-infrared spectra will be dealt with separately. The main reason for this is that above 350 cm^{-1} little interaction takes place between the vibrations of the water molecules and those of the guest molecules and the two can, by and large, be treated separately. Below 350 cm^{-1} , on the other hand, it is much more difficult to characterize the absorptions in terms of vibrations of the host or of the guest and a different approach is needed.

V.1 The Mid-infrared Absorptions by the Water Molecules.

Before discussing the bands due to vibrations of H_2O and D_2O , the bands due to $\nu_{\text{OH}}(\text{HDO})$ and $\nu_{\text{OD}}(\text{HDO})$ will be considered. These are at 3332, 3184 and 3050 cm^{-1} for $\nu_{\text{OH}}(\text{HDO})$ and 2464, 2369 and 2292 cm^{-1} for $\nu_{\text{OD}}(\text{HDO})$ with the approximate relative intensities 4:2:1 in each case. The assignment of these peaks is not obvious. As shown in Section IV.4, two non-equivalent O...O distances are found in HMT hydrate at 120°K , one equal to 2.76 \AA and the other equal to 2.74 \AA , with multiplicities six and three respectively. Othen (123) has correlated graphically the weighted mean O...O distances with the frequencies of the isolated OD stretches of ice I, II, V, VI and IX and of the hydrate

of ethylene oxide. He obtained a rather wide spread of points, but all points referring to ice II and IX (except one) lie very close to a straight line, while all points referring to the disordered phases of ice and to ethylene oxide hydrate are within 8 cm^{-1} of a second straight line having a different slope from the first. The first straight line predicts that $\nu_{\text{OD}}(\text{HDO})$ is 2450 and 2438 cm^{-1} for O...O distances of 2.76 \AA and 2.74 \AA , respectively, while, if the second correlation is used, frequencies of about 2421 and 2403 cm^{-1} are predicted.

No reliable correlations are available of the frequencies of $\nu_{\text{OH}}(\text{HDO})$ vibrations with the O...N distances in O-D...N systems. A correlation reported by Nakamoto (124) is based on cyclic systems of the type



for which the N-O-N angle lies between 75 and 82° and the possibility exists that the proton might be associated with the nitrogen atom instead of with the oxygen atom. Such a correlation is clearly not useful to the present work. Falk (125) has studied the $\nu_{\text{OD}}(\text{HDO})$ vibration of the hydrate of trimethylamine in which an O-D...N bond has been reported (126). He found a single peak with a maximum at 2420 cm^{-1} . No features were assigned to the OD stretching vibration of the O-D...N bond. Therefore no reliable

guidelines are available to assign the $\nu_{\text{OH}}(\text{HDO})$ and $\nu_{\text{OD}}(\text{HDO})$ vibrations associated with the O-H...N bond. This complicates the assignment of the O-H...O vibrations as well.

A possible interpretation, based on the literature precedents, is to assign the peaks at 3332 and 2464 cm^{-1} to the OH and OD stretching vibrations associated with the O...O distance of 2.76 \AA , the peaks at 3184 and 2369 cm^{-1} to the OH and OD stretching vibrations associated with the O...O distance of 2.74 \AA , and the peaks at 3050 and 2292 cm^{-1} to the OH and OD stretching modes in the O-H...N and O-D...N bonds. In order to make the observed relative intensities consistent with the assignment and with the fact that there are as many O-H...N groups as there are O-H...O groups with an O...O distance of 2.74 \AA , one has to assume that the dipole moment change involved with an O-H...N vibration is half of that of an O-H...O vibration.

The frequency separation of the two nonequivalent O-D...O vibrations is difficult to reconcile with the correlation between O...O distances and OD frequencies found by Othen (123). A frequency separation of 12 or 18 cm^{-1} is predicted by the two possible correlations, while the observed frequency separation is 95 cm^{-1} . Although all correlations between O...O distances and frequencies of OH vibrations are rather crude, a discrepancy of the magnitude observed in this case is very unusual and is such as to

invalidate the assignment.

For this reason the following assignment is preferred. The evidence supporting this assignment is quite limited, but, at the present state of knowledge, it is not possible to find a more logical explanation and an alternative assignment is proposed as the simplest and most plausible hypothesis which fits the experimental data.

The assignment is based on the different coordinations of the two different types of oxygen atoms in the structure. The oxygen atoms of type 1 (Figure 1) are engaged in three hydrogen bonds, donating two protons and accepting only one, while the oxygen atoms of type 2 donate two protons and accept two. There are, therefore, two types of hydrogen bonds, that in which the proton acceptor is a three coordinated oxygen (O_1) and that in which the proton acceptor is a four coordinated oxygen (O_2). In the hydrate structure there are twice as many hydrogen bonds of the second type as there are of the first type. It seems logical to suppose that the frequency of the OH stretching vibration associated with hydrogen bonds of the first type is lower than that of the OH stretching vibration associated with hydrogen bonds of the second type. The $\nu_{OH}(HDO)$ and $\nu_{OD}(HDO)$ peaks at 3332 and at 2464 cm^{-1} can be assigned to the OH and OD stretching modes of the $O_1-\text{H}\dots O_2$ and $O_1-\text{D}\dots O_2$ bonds, respectively. The peaks at 3184 and 2369 cm^{-1} can be assigned to the $\nu_{OH}(HDO)$ and $\nu_{OD}(HDO)$ modes of the

$O_2-H\cdots O_1$ and $O_2-D\cdots O_1$ bonds, while the peaks at 3050 and 2292 cm^{-1} can be associated with the $\nu_{OH}(\text{HDO})$ and $\nu_{OD}(\text{HDO})$ vibrations of the $O-H\cdots N$ and $O-D\cdots N$ bonds. Since there are twice as many $O_1-H\cdots O_2$ bonds as $O_2-H\cdots O_1$ bonds, the relative intensities of the two higher frequency peaks are consistent with this assignment. The lowest frequency peak is half as strong as would be expected on the grounds that there are as many $O_2-H\cdots N$ bonds as there are $O_2-H\cdots O_1$ bonds. However, there is no reason why the dipole moment derivative with respect to the OH stretching vibration should be the same in the two systems. If the dipole moment derivative for an $O-H\cdots N$ vibration is half as large as that for an $O-H\cdots O$ vibration, then the observed intensities are consistent with the above assignment. On the other hand, since no unequivocal experimental data are available on the frequencies and intensities of OH stretching vibrations in hydrogen bonded systems in which the oxygen acting as a proton acceptor is three coordinated, the $\nu_{OH}(\text{HDO})$ and $\nu_{OD}(\text{HDO})$ vibrations of the $O_2-H\cdots O_1$ and $O_2-D\cdots O_1$ groups could alternatively be assigned to the peaks at 3050 and 2292 cm^{-1} and the $\nu_{OH}(\text{HDO})$ and $\nu_{OD}(\text{HDO})$ vibrations of the $O-H\cdots N$ and $O-D\cdots N$ groups could be assigned to the peaks at 3184 and 2369 cm^{-1} respectively.

Some support for the assignment of the different frequencies on the basis of the coordination of the proton acceptor is derived from a study published by Bellamy and

Pace in 1971 (127). These authors reported that the frequency of the OH stretching vibration for the 1:1 complex of phenol and dimethylacetamide in carbon tetrachloride solution is some 90 cm^{-1} lower than the corresponding frequency for the 2:1 complex. In the following discussion it will be assumed that the peaks at 3050 and 2292 cm^{-1} are due to the O-H...N and O-D...N bonds.

The width of the $\nu_{\text{OH}}(\text{HDO})$ and $\nu_{\text{OD}}(\text{HDO})$ absorptions is now discussed. These peaks in HMT hydrate are slightly broader than the corresponding peaks in the spectra of ice Ih, while they are much narrower than the corresponding peaks in the spectra of ice V (58), ice VI (60), and ethylene oxide hydrate (62). Only one crystallographically independent O-O distance is found in ice Ih (53), while seven are found in ice V, ranging from 2.766 to 2.867 \AA° (128), five are found in ice VI, ranging from 2.773 to 2.840 \AA° (129), and in the hydrate of ethylene oxide four different O-O distances range from 2.745 to 2.821 \AA° (130). The half widths reported for $\nu_{\text{OH}}(\text{HDO})$ and $\nu_{\text{OD}}(\text{HDO})$ peaks are (the values for $\nu_{\text{OD}}(\text{HDO})$ are in brackets): 30 (18), 150 (80), 120 (70), 125 (80) for ice I, ice V, ice VI and ethylene oxide hydrate, respectively. Although a quantitative correlation between the distribution of O...O bond lengths and the half widths of the $\nu_{\text{OH}}(\text{HDO})$ and $\nu_{\text{OD}}(\text{HDO})$ peaks is not available, it seems at least qualitatively established that the two quantities are related.

From the systems mentioned above, the half-width of a $\nu_{\text{OH}}(\text{HDO})$ peak arising from a single crystallographic O...O distance in a disordered phase of water is the 30 cm^{-1} observed for ice Ih. In the ordered forms of ice the corresponding half-width value is about 8 cm^{-1} . The half-widths of the $\nu_{\text{OH}}(\text{HDO})$ peaks in HMT hydrate are all about 50 cm^{-1} . The width of the two high frequency peaks may reflect the contribution to each peak by bonds 2.74 and 2.76 \AA long. This does not however explain the width of the peak assigned to the O-H...N bonds, which remains unexplained in detail.

These half-widths do not give any indication of the partial ordering of the hydrogen atoms in the HMT hydrate. In particular, the peaks due to the O-H...N and O-D...N vibrations are broad although this hydrogen position is ordered. It therefore appears that the disorder over the whole structure overcomes the order at the $\text{O}_2\text{-H...N}$ sites and causes the positions of the oxygen atoms of type 2 to be disordered, and this in turn causes a distribution of OH stretching frequencies which is responsible for the breadth of the peaks.

It has been seen in Section I.4 that no satisfactory explanation exists of the shape of the $\nu_{\text{OH}}(\text{H}_2\text{O})$ and $\nu_{\text{OD}}(\text{D}_2\text{O})$ absorption bands, either for the ordered or for the disordered phases of ice. Coupling of the OH stretching vibrations and the lack of symmetry due to the

orientational disorder were thought to be responsible for the breadth of these bands in the disordered phases. This explanation fails to account for the breadth of the corresponding bands in the spectra of the ordered ice phases. It is noticeable, however, that the $\nu_{OH}(H_2O)$ and $\nu_{OD}(D_2O)$ bands of these phases show rather more structure than those of the disordered forms (58).

The frequencies of the three maxima of the $\nu_{OH}(H_2O)$ band (at 3312, 3120 and 3014 cm^{-1}) and the $\nu_{OD}(D_2O)$ band (at 2475, 2341 and 2256 cm^{-1}) are quite close to the frequencies of the $\nu_{OH}(HDO)$ peaks (at 3332, 3184 and 3050 cm^{-1}) and $\nu_{OD}(HDO)$ peaks (at 2464, 2369 and 2292 cm^{-1}), respectively. This suggests that, following the assignment of the $\nu_{OH}(HDO)$ and $\nu_{OD}(HDO)$ peaks, the high frequency maxima of the $\nu_{OH}(H_2O)$ and $\nu_{OD}(D_2O)$ bands arise predominantly from $O_1-H...O_2$ and $O_1-D...O_2$ vibrations, the maxima at 3120 and 2341 cm^{-1} arise primarily from $O_2-H...O_1\text{ cm}^{-1}$ and $O_2-D...O_1$ vibrations, and the maxima at 3014 and 2256 cm^{-1} from $O_2-H...N$ and $O_2-D...N$ vibrations. A simple calculation shows that the splitting due to intramolecular and intermolecular coupling between different OD (or OH) oscillators, and the consequent broadening of the band, is much smaller in the hydrate of HMT than in ice Ih. This is due to the fact that the two OD stretching frequencies characteristic of the O-D oscillators on oxygen 1 are both 2464 cm^{-1} and the frequencies of the OD vibrators on oxygen 2 are 2369

and 2292 cm^{-1} . Moreover, the nearest neighbors of each water molecule are water molecules of the other type, characterized by OD stretching frequencies which are sufficiently different to severely limit the effect of intermolecular coupling.

The intramolecular coupling was estimated by a normal coordinate calculation in which no interaction force constant was used and is, thus, simply the kinetic coupling through the common oxygen atom. The force constants were calculated from the $\nu_{\text{OD}}(\text{HDO})$ frequencies and the calculations showed that the $\nu_{\text{OD}}(\text{D}_2\text{O})$ frequencies of the D_2O molecules about oxygen 2 are within 10 cm^{-1} of the $\nu_{\text{OD}}(\text{HDO})$ frequencies (5 cm^{-1} for the H_2O frequencies), while those of the D_2O molecules about oxygen 1 are about 35 cm^{-1} above and below the $\nu_{\text{OD}}(\text{HDO})$ frequency (20 cm^{-1} for the H_2O frequencies). The intermolecular coupling was estimated by a calculation on two OD oscillators with no common atom, but with an interaction force constant between the two oscillators. The value of this constant was $-0.124 \text{ mdyne } \text{\AA}^{\circ-1}$, as found for ice I by Haas and Hornig (131). The intermolecular coupling in HMT hydrate was found to change the frequencies by less than 7 cm^{-1} for OD vibrations and 8 cm^{-1} for OH vibrations, which is about eight times less than the 50 cm^{-1} for O-D and 70 cm^{-1} for O-H vibrations calculated for ice I. Therefore the calculations show that the $\text{O}_2\text{-D...N}$ and $\text{O}_2\text{-D...O}_1$

vibrations are little affected by intramolecular and intermolecular coupling, while the intramolecular coupling causes the splitting of the O_1 -D... O_2 vibrations of about the same magnitude as in ice. The intermolecular coupling is, however, eight times smaller in the hydrate than in ice. These results are consistent with the interpretation of the $\nu_{OH}(H_2O)$ and $\nu_{OD}(D_2O)$ bands proposed above. The fact that the two lower frequency maxima in each band are much narrower than the high frequency maximum is also consistent with the results of the calculations, which show that the high frequency vibrations are separated by intramolecular coupling much more than the two lower frequency vibrations.

The bands at about 2250 cm^{-1} in the hydrates and about 1600 cm^{-1} in the deuterates are clearly due to the combination and overtone transitions, $\nu_2 + \nu_R$ and $3\nu_R$, that cause similar bands in the ices and in ethylene oxide hydrate. Similarly, the bands at 1600 cm^{-1} in the hydrates and 1200 cm^{-1} in the deuterates are due to the HOH or DOD angle deformation mode, ν_2 , and, possibly, the first overtone of the ν_R vibrations, $2\nu_R$, as is the case in the ices and in ethylene oxide hydrate. The extra feature seen at about 1730 cm^{-1} in HMT hydrate may well be associated with the different types of hydrogen bonding in HMT hydrate, but no definitive interpretation of these bands can be made.

The oxygen atoms occupy sites of diffraction symmetry C_s , but the orientational disorder of the water

molecules lowers the site symmetry to C_1 . A unit cell group analysis on the proton ordered structure, in which the six water molecules in the unit cell occupy C_s sites, yields for the 18 rotational vibrations of the water molecules the representation $2A_1 + 4A_2 + 6E$ under the unit cell group C_{3v} . The A_1 and E modes are infrared and Raman active, while the A_2 modes are inactive in absorption and in the Raman effect. Eleven features have positively been assigned to H_2O or D_2O vibrations between 400 and 1000 cm^{-1} where the $\nu_R(H_2O)$ and $\nu_R(D_2O)$ vibrations are expected to occur. The isotope shift of these features identifies them as due to rotational vibrations of the water molecules but a detailed assignment can not be made. Even in the case of the ordered phases of ice many features of the spectrum of the rotational vibrations are largely unexplained (58). In the hydrate of HMT there is the additional complication of the partial proton disorder which should make all vibrations infrared active irrespective of the wave-vector. The density of vibrational states for the rotational vibrations is not known, nor is the intensity distribution function. It seems, therefore, impossible to completely distinguish between those features of the infrared spectrum which are due to zero-wave-vector vibrations and those which are made active by the disorder.

The peak seen at about 571 cm^{-1} in the spectra of the hydrates can be confidently assigned to a zero-wave-

vector rotational vibration of the H_2O molecules. This band is broader and weaker in the spectra of hydrate samples contaminated with a small quantity of deuterium. The same behaviour was observed by Bertie and Whalley for the sharp features of the $v_R(\text{H}_2\text{O})$ and $v_R(\text{D}_2\text{O})$ bands of ice II and IX (58). These authors interpreted this as being due to relaxation of the zero-wave-vector selection rule and modification of the long-range nature of the vibration by the isotopic impurities. This interpretation is probably valid for the 571 cm^{-1} peak of the present hydrate and it is of interest that this behaviour is seen even although the structure is not fully ordered. The corresponding mode of the deuterates is expected to occur at about 425 cm^{-1} . The spectrum of HMT- d_{12} deuterate is complicated in this region by HMT absorptions, but in the spectrum of HMT- h_{12} deuterate a doublet is seen which is certainly due to rotational vibrations of the D_2O molecules. This absorption was not affected by the presence of hydrogen impurity in the sample. No firm explanation was found for the fact that the 571 cm^{-1} peak of the hydrate broadened but no changes were observed in the corresponding peaks of the deuterate when isotopic impurities were added. It is possible that the form of the vibration is different in the hydrate and in the deuterate and that the rotational vibration of the H_2O molecules giving rise to the absorption at 571 cm^{-1} is essentially a zero-wave-vector vibration,

but the vibrations giving rise to the peaks at 415 and 425 cm^{-1} in the spectrum of the deuterate of HMT- h_{12} are not.

The ν_R bands in HMT hydrate and deuterate also resemble those of the ordered forms of ice in that they show far more structure, after allowing for the structure due to the HMT vibrations, than the corresponding bands in the disordered forms of ice and ethylene oxide hydrate. This can be said to reflect the partial order of the hydrogen atoms in HMT hydrate, and it is of interest that these features are present even though the hydrogen atoms are not fully ordered.

V.2 The Intramolecular Vibrations of Hexamethylenetetramine.

If the disorder of the proton positions is ignored, the HMT molecules occupy sites of C_{3v} symmetry. The correlation between the representations of the point groups T_d and C_{3v} is given below.

T_d	C_{3v}
A_1	a_1
A_2	a_2
E	e
F_1	$a_2 + e$
F_2	$a_1 + e$

Under C_{3v} symmetry the A_1 and E modes are infrared and

Raman active, while the A_2 modes are inactive in absorption and in the Raman effect. All vibrations of the HMT molecule, with the exception of the methylenic twist of type A_2 , are expected to become active under the diffraction site and unit cell groups, both of which are isomorphous with the point group C_{3v} . Each of the F_2 modes should be split into two infrared active components, while all F_1 modes should be split into an infrared active E component and an infrared inactive A_2 component.

Before the assignment of the bands due to $HMT-h_{12}$ and $HMT-d_{12}$ can be discussed, certain differences between these bands in the spectra of the hydrates and deuterates must be rationalized. These differences were briefly mentioned in Section IV.2 and must arise from interactions between the vibrations of the HMT and water molecules. The significant differences between the geometry of the HMT molecule in the hydrate and in pure, solid HMT clearly indicate that quite strong, static forces due to the surrounding water molecules act upon the HMT to lower its symmetry from T_d to C_{3v} . These forces cause the splitting predicted above, but if no other forces were present, should allow the spectrum of the hydrate to be a superposition of the spectra of HMT, under the site group symmetry, and of the water molecules. The differences between some of the HMT absorptions in the hydrate and in the deuterate clearly show that dynamic interactions also occur between the vib-

rations of the HMT and water molecules. These effects could arise from forces similar to those which cause the reduction in site symmetry, or could arise from the interaction between the vibrational dipole moment changes on the HMT and water molecules. It is not possible to determine from the present data which mechanism is the more effective and, in this situation, it seems appropriate to assign only those HMT absorptions which show the smaller effect of this dynamic interaction. In the next two paragraphs the differences between the spectra of the hydrates and deuterates are discussed in order to decide which HMT absorptions are less influenced by the dynamic interaction.

The two peaks near 1240 cm^{-1} are well resolved and 8.3 cm^{-1} apart in the spectrum of HMT- h_{12} hydrate, but are poorly resolved in HMT- h_{12} deuterate although they are still 7.2 cm^{-1} apart. It is clear that in the deuterate the HMT modes interact with the underlying $\nu_2(\text{D}_2\text{O})$ modes, more than they interact with H_2O modes in the hydrate. The HMT- h_{12} absorption between 800 and 850 cm^{-1} is quite different in the spectra of the hydrate and deuterate, and it is clear that considerable interaction between the HMT- h_{12} modes and the underlying $\nu_R(\text{H}_2\text{O})$ modes occurs in the hydrate, while the corresponding HMT- h_{12} modes are less influenced by the D_2O vibrations in the deuterate. It is less easy to understand the differences between the spectra of HMT- h_{12} hydrate and deuterate near to 1020 cm^{-1} . For

the hydrate, four peaks are seen, at 999.3, 1012.3, 1018.0 and 1027.3 cm^{-1} , while for the deuterate peaks at 998.6 and 1012.6 and a shoulder at 1022 cm^{-1} are seen. On the grounds that interaction with the modes of the partially disordered water molecules is likely to increase the breadth of the features observed, these spectra can be taken to indicate that more interaction takes place in the deuterate than in the hydrate. However, neither the H_2O or the D_2O molecules have fundamental absorption assigned in this region, although both undoubtedly absorb quite strongly through overtone and combination transitions, as is the case in ice Ih (133), and the origin of the interaction is unclear.

The spectrum of HMT-d_{12} deuterate contains peaks at 733.6 and 736 cm^{-1} , while that of HMT-d_{12} hydrate contains peaks at 722.4 and 727.2 cm^{-1} and shoulders at 717 and 734 cm^{-1} . The H_2O molecules absorb more strongly in this region than the D_2O molecules, and it is probable that the HMT-d_{12} modes are less influenced by interaction with the water molecules in the deuterate than in the hydrate. HMT-d_{12} causes peaks at 400.5 and 417 cm^{-1} in the spectrum of the deuterate, and at 405.7 with a shoulder at 403 cm^{-1} in that of the hydrate. In this case it appears that interaction with $\nu_R(\text{D}_2\text{O})$ modes increases the separation of the two HMT-d_{12} features.

In the following discussion an assignment of the

features of the infrared spectra is proposed under the assumption that the proton disorder does not disturb the selection rules or the symmetry of the vibrations appropriate to the C_{3v} diffraction unit cell group. The HMT molecules are sufficiently far apart that vibrational coupling between them should be very small. It is also assumed that the frequencies of the modes of HMT in the hydrate are very close to the frequencies of the corresponding modes in pure HMT. This assumption seems quite reasonable in view of the fact that only weak bonding exists between the water and the HMT molecules. A detailed assignment is not possible because the observed peaks cannot be assigned to HMT modes of specific symmetry under the unit cell group. The modes are therefore numbered according to the modes of pure HMT from which they are believed to derive. For clarity, upper case letters are used to designate the symmetry of the modes of pure HMT, while lower case letters are used for the modes of HMT in the hydrate.

V.2.1 Hexamethylenetetramine-h₁₂.

The assignment is summarized in Table 20, and is presented below for each type of vibration.

The CH stretching modes. These modes form the representations $3a_1 + a_2 + 4e$ in the point group C_{3v} . Of the seven modes which are in principle infrared active, $2a_1$

Table 20. Correlation Between Frequencies of Pure HMT-h₁₂
and Frequencies of HMT Vibrations in the Hydrate.

HMT-h ₁₂			HMT-h ₁₂ Hydrate		
Mode Number	Type	ν/cm^{-1}	Type	ν/cm^{-1}	
ν_{16}	F ₁	$\left\{ \begin{array}{l} 378^a \\ 341.3^b \end{array} \right.$	e	372.4	
ν_{10}	E	463.0	e	-	
ν_{25}	F ₂	512.0	a ₁ or e	$\left\{ \begin{array}{l} 502.6 \\ 512.6 \end{array} \right.$	
ν_{24}	F ₂	671.0	a ₁ or e	$\left\{ \begin{array}{l} 670.9 \\ 692.0 \end{array} \right.$	
ν_4	A ₁	779.3	a ₁	783.9*	
ν_{23}	F ₂	810.5	a ₁ + e	$\left\{ \begin{array}{l} 812.9* \\ 820.2* \\ 825 ? \end{array} \right.$	
ν_{15}	F ₁	$\left\{ \begin{array}{l} 925^a \\ 911.4^b \end{array} \right.$	e	934.2	
ν_{22}	F ₂	1004.3	a ₁ + e	$\left\{ \begin{array}{l} 999.3 \\ 1012.3 \end{array} \right.$	
ν_9	E	1015	e	1027.3	
ν_3	A ₁	1042.0	a ₁	1041.8	

(Table continued on next page)

Table 20 continued

HMT-h ₁₂			HMT-h ₁₂ Hydrate		
Mode Number	Type	v/cm ⁻¹	Type	v/cm ⁻¹	
$\nu_{16} + \nu_{24}$	$A_2 + E + F_1$ + F_2		$a_1 + 2a_2$ + 3e		$\left. \begin{array}{l} 1054.5^* \\ 1056.8^* \\ 1064.7^* \end{array} \right\}$
ν_{14}	F_1	$\left. \begin{array}{l} 1078^a \\ 1179.5^b \end{array} \right\}$	e	1232?	
ν_{21}	F_2	1236.5	a_1 or e	$\left. \begin{array}{l} 1237.0 \\ 1245.3 \end{array} \right\}$	
ν_{13}	F_1	$\left. \begin{array}{l} 1315^a \\ 1346.2^b \end{array} \right\}$	e	1335?	
ν_8	e	1349.2	e	1351.5	
ν_{20}	F_2	1370.0	a_1 or e	$\left. \begin{array}{l} 1374.6 \\ 1382.5 \end{array} \right\} ?$	
ν_{12}	F_1	1401.2 ^b	e	1389.2?	
$\nu_4 + \nu_{24}$	F_2	1440.6	$a_1 + e + f_2$	$\left. \begin{array}{l} 1427.0 \\ (1434.0) \\ 1442.0 \end{array} \right\}$	
ν_2	A_1	-	a_1	1446.0	
ν_7	E	1454.2	e	1454.0	

(Table continued on next page)

Table 20 continued

HMT-h ₁₂			HMT-h ₁₂ Hydrate		
Mode Number	Type	v/cm ⁻¹	Type	v/cm ⁻¹	
v ₁₉	F ₂	1458.0	a ₁ or e	{ 1461.5 1463.0	
v ₂₃ +v ₂₄		1490 ^c		1486.2	
v ₆	E	2869.5 ^b			{ 2885.5* 2893.5*
v ₁	A ₁	2873.2 ^b	2a ₁ + 2e		
v ₁₈	F ₂	2873.5			
-	-	2934.5	-	{ 2916* 2937.5*	
v ₁₁	F ₁	2952.4			{ 2961.5* 2969*
v ₁₇	F ₂	2954.8	a ₁ + a ₂ + 2e		
-	-	-	-	2990.9*	

(a) Determined by Mecke and Spiesecke (86) from combination transitions.

(b) Obtained from calculations (Section III.3).

(c) Assigned Mecke and Spiesecke (86).

* indicates frequencies obtained from the spectrum of the deuterated.

and 2e modes are derived from symmetric CH stretches, while 1a₁ and 2e modes are derived from asymmetric CH stretches. Seven features are seen in the spectral region between 2880 and 3000 cm⁻¹ in the spectrum of HMT-h₁₂·6D₂O. Four of these are of medium intensity and three are weaker. The two medium peaks at 2885.5 and 2893.5 cm⁻¹ are assigned to the 2a₁ and 2e modes derived from ν₁, ν₆ and ν₁₈, all of which are expected to have very similar frequencies. The peak at 2961.5 cm⁻¹ and the shoulder at 2969 cm⁻¹ are assigned to the a₁ and 2e modes derived from the assymetric CH stretches, ν₁₁ and ν₁₇. The medium intensity peak at 2937.5 cm⁻¹ can be assigned to the first overtone of a methylenic deformation mode (ν₂, ν₇ or ν₁₉).

The H-C-H deformation modes. These modes form the representation 2a₁ + 2e under the point group C_{3v}. The methylenic deformation vibrations of type E and F₂, ν₇ and ν₁₉, were observed at 1454 and 1457 cm⁻¹ respectively in the spectrum of pure HMT, while the frequency of the A₁ mode, ν₂, was calculated at 1459 cm⁻¹. Seven or eight features are seen between 1420 and 1490 cm⁻¹ in the spectra of HMT-h₁₂ hydrate and deuterate. The two strong peaks at 1461 and 1463 cm⁻¹ and the weaker features at 1454 and, possibly, at 1446 cm⁻¹ can be assigned to fundamental vibrations derived from ν₂, ν₇ and ν₁₉ of pure HMT-h₁₂. Combination transitions were observed at 1429.3 (weak) and 1440.6 cm⁻¹ (medium) in the infrared spectrum of HMT-h₁₂

and each should split into two transitions in HMT hydrate. The peaks at 1427, 1433, 1442 and, possibly, 1446 cm^{-1} can be assigned to these transitions. The weak peak at 1486.2 cm^{-1} is tentatively assigned to a combination of the vibrations at 812.9 and 672.2 cm^{-1} .

The methylenic wagging modes. The representation formed by these modes in the point group C_{3v} is $a_1 + a_2 + 2e$, so three peaks due to these modes should be seen in the infrared spectrum of the hydrate. The observed frequency of the F_2 wagging mode, ν_{20} , in pure HMT is 1370 cm^{-1} , and the F_1 coordinate was calculated to contribute to the vibrations at 1401.3, ν_{12} , and 1346.2 cm^{-1} , ν_{13} . Two of the peaks seen at 1374.6, 1382.5 and 1389.2 cm^{-1} in the spectrum of the hydrate can confidently be assigned to the a_1 and e components of ν_{20} , while the e mode derived from ν_{12} can be assigned to the third component of the triplet.

The methylenic twisting modes. These modes form the representation $2a_2 + 2e$. A peak due to a twisting mode of type e , ν_8 , was observed in the spectrum of pure HMT at 1349.2 cm^{-1} and the mode of type F_1 was calculated to contribute to the normal modes calculated at 1401.3, ν_{12} , and 1346.2 cm^{-1} , ν_{13} . The e mode derived from ν_8 is assigned to the weak peak seen at 1351.5 cm^{-1} in the spectrum of the hydrate, while the e mode derived from ν_{13} is assigned to the peak at 1335 cm^{-1} . The peaks at 1351.5 and 1335 cm^{-1} are both very weak and this is consistent with the

fact that methylenic twisting modes are normally weak in absorption (134).

The methylenic rocking modes. The representation formed by these modes in the point group C_{3v} is $a_1 + a_2 + 2e$. The e mode derived from ν_{15} (type F_1) is assigned to the peak at 934.2 cm^{-1} in the spectrum of the hydrate. It was seen in Section III.8 that no F_2 mode of $\text{HMT}-\text{h}_{12}$ could be characterized as predominantly a rocking mode, but rather the symmetry coordinate characteristic of the rocking mode contributed to ν_{22} and ν_{25} and, to a lesser extent, to ν_{23} and ν_{24} . The modes to which the rocking mode contributes appreciably are therefore assigned in the discussion of the ring modes.

The ring modes. The C-N stretching modes form the representation $3a_1 + a_2 + 4e$ under the point group C_{3v} , and additional a_1 and e modes, which are predominantly C-N stretching rather than CH_2 rocking vibrations, must be assigned. The a_1 mode derived from ν_4 is assigned to the strong peak at 783.9 cm^{-1} in the spectrum of the deuterate and the e mode due to ν_9 is assigned to the peak at 1027.3 cm^{-1} in the spectrum of the hydrate. The a_1 and e modes derived from ν_{21} , ν_{22} and ν_{23} are assigned at 1237.0 and 1245.3 cm^{-1} , 998.6 and 1012.6 cm^{-1} and 812.9 and 820.2 cm^{-1} , respectively.

The C-N-C deformation vibrations form the represen-

tation $3a_1 + a_2 + 4e$ under C_{3v} . The a_1 mode derived from ν_3 is assigned to the peak of medium intensity seen at 1041.8 cm^{-1} in the spectrum of the hydrate. A weak and a strong peak and a shoulder, at 1064.0, 1056.3 and 1054.3, remain to be assigned to this region. They are assigned to the components of the combination vibration which gives rise to the strong infrared peak seen at 1048.0 cm^{-1} in the spectrum of HMT- h_{12} . This peak was assigned to the combination of an F_1 and F_2 mode (86) and, if this assignment is correct, has A_2 , E , F_1 and F_2 components under the point group T_d . These components give rise to four infrared active transitions under the C_{3v} point group, and these can have different frequencies. The e mode arising from ν_{10} is not seen in the spectrum of the hydrate or of the deuterate. The e mode arising from ν_{16} , whose frequency was estimated to be 378 cm^{-1} by Mecke and Spiesecke (86) from the frequencies of combination bands, is assigned to the peak of medium intensity at 372.4 cm^{-1} in the spectrum of the hydrate. The a_1 and e components of ν_{24} are assigned to the doublet at 670.9 and 692.0 cm^{-1} and the components of ν_{25} are assigned to the two peaks at 502.6 and 512.6 cm^{-1} .

V.2.2 Hexamethylenetetramine-d₁₂.

The assignment is summarized in Table 21 and is presented below for each type of vibration.

Table 21. Correlation Between Frequencies of Pure HMT-d₁₂ and Frequencies of HMT-d₁₂ in the Hydrate.

HMT-d ₁₂			HMT-d ₁₂ in Hydrate	
Mode Number	Type	v/cm ⁻¹	Type	v/cm ⁻¹
v ₁₆	F ₁	277.1 ^a	e	309.1*
v ₂₅	F ₂	408.3	a ₁ or e	{ 403.2 405.7
v ₁₀	E	432.0	e	-
v ₂₄	F ₂	636.2	a ₁ or e	{ 639.7* 664.2*
v ₂₃	F ₂	725.5	a ₁ or e	{ 733.6* 736*
v ₄	A ₁	748.0	a ₁	750*
v ₁₅	F ₁	759.5 ^a	e	800*
v ₉	E	866.5	e	848*
v ₁₄	F ₁	888.1 ^a	e	-
v ₂₂	F ₂	905.7	a ₁ or e	{ 903.3* 911.3*
v ₁₆ +v ₂₅		931	a ₁ + a ₁ + 2e	932.6*
		936		{ 936* 939*

(Table continued on next page)

Table 21 continued

HMT-d ₁₂			HMT-d ₁₂ Hydrate	
Mode Number	Type	v/cm ⁻¹	Type	v/cm ⁻¹
v ₃	A ₁	975.0	a ₁	992.6*
v ₁₃	F ₁	1058.3 ^a	e	1000*?
v ₈	E	1069.0	e	1052.0*
v ₂₁	F ₂	1075.3	a ₁ or e	{ 1078.8 1089.0
v ₂₀	F ₂	1105.0	a ₁ or e	{ 1107.0 1115.7
v ₇	E	1121.4	e	1122.5
v ₂	A ₁	1131.4	a ₁	1139?
v ₁₉	F ₂	1171.2	a ₁ or e	{ 1177.7 1190.8
v ₁₂	F ₁	1276.7 ^a	e	-
v ₆	E	2097.6 ^a	e	{ 2095.7
v ₁₈	F ₂	2105.0	a ₁ or e	{ 2114.2
v ₁	A ₁	2109.6	a ₁	
v ₁₁	F ₁	2209.5	e	-
v ₁₇	F ₂	2228.0	a ₁ or e	-

(a) Obtained from calculations (Section III.8)

* These frequencies were obtained from the spectrum of the deuterated, all others from the spectrum of the hydrate.

The CD stretching modes. The considerations presented for the CH stretching modes also apply to the CD stretching vibrations. One would therefore expect to see four peaks near 2100 cm^{-1} due to the $2a_1$ and $2e$ modes based on the symmetric CD stretches and three peaks near 2225 cm^{-1} due to the a_1 and $2e$ modes based on the asymmetric CD stretches. However, no peaks due to vibrations of HMT-d₁₂ are seen above 2200 cm^{-1} in the spectra of HMT-d₁₂ hydrate and deuterate and the asymmetric CD stretching modes presumably absorb too weakly to be observed. This is consistent with the fact that the asymmetric CD stretching mode is very weak in the infrared spectrum of HMT-d₁₂. Even the assignment of the CD symmetric stretching modes is far from obvious. Several peaks, none of which is particularly prominent, are seen between 2085 and 2200 cm^{-1} . The peaks at 2095.7 and 2114.2 are tentatively assigned to fundamental vibrations because they are the most intense peaks close to the frequencies of the fundamentals in pure HMT.

The D-C-D deformation vibrations. ν_2 was observed at 1131.4 cm^{-1} in the Raman spectrum of pure HMT-d₁₂. Either the shoulder at 1139 cm^{-1} in the spectrum of the hydrate or the peak of medium intensity at 1142 cm^{-1} in the spectra of the deuterate and hydrate can be assigned to the a_1 vibration derived from ν_2 . The e mode derived from ν_8 is assigned to the strong peak at 1052 cm^{-1} in the spectrum of the hydrate. This is about 20 cm^{-1} lower than

in the Raman spectrum of HMT-d₁₂, but the only alternative is to assign it to the medium intensity peak at about 1078 cm⁻¹, which is far more likely to be due to a wagging mode, as discussed below. ν₂₀ of pure HMT-d₁₂ is predominantly a methylenic deformation (Section III.8) and was observed at 1107 cm⁻¹. The two peaks seen at about 1107 and 1115 cm⁻¹ in the spectra of the hydrate and deuterate are assigned to the a₁ and e components of ν₂₀.

The methylenic wagging modes. The assignment of the infrared active e component of ν₁₃ is very dubious. The frequency of ν₁₃ in pure HMT-d₁₂ is not known from experiment, but was calculated to be 1058.3 cm⁻¹. Its e component is tentatively assigned to the weak peak at 1000 cm⁻¹ in the spectrum of HMT-d₁₂ deuterate, and the large frequency difference may reflect errors in the calculated value. The a₁ and e components of ν₂₁, which was observed at 1075.3 cm⁻¹ in pure HMT-d₁₂, are assigned to the peaks at 1078.8 and 1089.0 cm⁻¹ in the spectrum of the hydrate.

The methylenic twisting modes. ν₉, predominantly a twisting mode, was observed at 866.5 cm⁻¹ in the Raman spectrum of HMT-d₁₂. The very weak peak at 848 cm⁻¹ in the spectrum of the deuterate is assigned to this mode. The frequency of the F₁ twisting mode, ν₁₄, of pure HMT-d₁₂ was calculated to be 888.1 cm⁻¹ (Section III.8). No peaks which can be assigned to the e component of this mode are seen in the spectra of the hydrate or deuterate near to

this frequency. The very weak peak at 800 cm^{-1} in the spectrum of HMT-d₁₂ deuterate could be assigned to this mode, but it is so far away from the calculated frequency that this mode is best left unassigned.

The methylenic rocking modes. The calculated frequency of the F₁ rocking mode, ν_{15} , (Section III.8) is 759.5 cm^{-1} . Its e component is tentatively assigned to the peak at 800 cm^{-1} in the spectrum of the deuterate. The F₂ rocking vibration contributes to ν_{22} , ν_{23} , ν_{24} and ν_{25} in HMT-d₁₂ and none of these modes can be characterized as predominantly a methylenic rock. The modes to which the F₂ rocking vibration contributes are therefore assigned in the discussion of the ring modes.

The ring modes. The A₁ CN stretching vibration (ν_4) was seen at 748 cm^{-1} in the Raman spectrum of pure HMT-d₁₂; the a₁ mode derived from it is tentatively assigned to the very weak peak at 750 cm^{-1} in the spectrum of the deuterate. If this assignment is correct, it is somewhat surprising that the absorption is so weak compared to the peak at 783.9 cm^{-1} in HMT-h₁₂ deuterate which was assigned to the corresponding mode of HMT-h₁₂. This casts some doubt on the assignment, but no plausible alternative is available. The e mode derived from ν_7 is assigned to the very weak peak at 1122.5 cm^{-1} in the spectrum of the hydrate. The a₁ and e components of ν_{19} and ν_{23} are

assigned at 1177.7 and 1190.8 cm^{-1} in the spectrum of the hydrate and 733.6 and 736 cm^{-1} in the spectrum of the deuterate, respectively.

The A_1 C-N-C deformation mode, ν_3 , is at 975 cm^{-1} in pure HMT-d₁₂, so the a_1 component of this mode is assigned to the weak peak at 992.6 cm^{-1} in the spectrum of the deuterate. No peak is seen in the hydrate or deuterate spectra that lies at a frequency close to that of ν_{10} , so this mode is left unassigned as was the corresponding mode of the hydrate and deuterate of HMT-h₁₂. The peak at 309 cm^{-1} in the spectrum of HMT-d₁₂ deuterate can confidently be assigned to the e component of ν_{16} , by analogy with the assignment of the hydrate and deuterate of HMT-h₁₂ on the grounds that the frequency of ν_{16} was calculated to be 277 cm^{-1} (Section III.8). The a_1 and e components of ν_{24} , which occurs at 636.2 cm^{-1} in the spectrum of pure HMT-d₁₂, are confidently assigned to the peaks seen at 639.7 and 664.2 cm^{-1} in the spectrum of the deuterate. The a_1 and e components of ν_{25} can be assigned at 403 and 405.7 cm^{-1} in the hydrate and 400.5 and 417 cm^{-1} in the deuterate.

V.2.3 Discussion.

All the prominent peaks and most of the weaker peaks due to HMT-h₁₂ and HMT-d₁₂ were logically assigned, on the grounds that their frequencies lie close to the

frequencies of corresponding modes in pure HMT. Conversely, the great majority of the modes expected under the C_{3v} site group were assigned. Both facts make the assignment internally consistent and support it. The most uncertain assignments are those in the CH and CD stretching regions.

For HMT-h₁₂ and HMT-d₁₂ no peaks could be found in the hydrate or deuterate spectra which could reasonably be assigned to the e mode, ν_{10} , the doubly degenerate C-N-C deformation mode found at 463 and 432 cm^{-1} in pure HMT-h₁₂ and -d₁₂, respectively. This mode also appears to be weak or missing in addition compounds with iodine and bromine. Weak peaks were assigned to this mode by Shiro et al (87), but were not reported by Bowmaker and Hannan (135,136). It is reasonable to suppose that the absorption by this mode in HMT hydrate and deuterate is masked by the water absorption. A CD₂ twisting mode of symmetry e under C_{3v} , derived from the F₁ twisting mode of pure HMT, was also left unassigned. This may be due to its low intensity or may indicate that the calculated frequency for this mode in pure HMT-d₁₂ is in error.

No attempt was made to characterize the components arising from the splitting of the F₂ modes by their symmetry type. Calculations carried out by Shiro et al (87) on molecular complexes of HMT with bromine and iodine indicate that the a₁ components are always to the high frequency side of the e components, but, since no exper-

imental evidence for this was provided and since there is no obvious theoretical reason why this should be the case, it is preferred here to leave the question of the symmetry of the modes open to further experimental work. The Raman polarization behaviour that can be obtained from the study of the Raman spectrum of an oriented single crystal should make it possible to characterize the vibrations according to their symmetry type.

Some comments can be made about the separation of the two components derived from the F_2 modes, but only those peaks which can confidently be attributed to this source and whose separation is clear will be discussed. For each of these doublets, Table 22 shows the separation between the components, the separation divided by the frequency of the corresponding mode in pure HMT, the mean frequency and the frequency of the corresponding mode in pure HMT. For each isotope the mean frequency in the hydrate and deuterate is higher than the corresponding frequency in the pure compound except for ν_{25} for which the mean frequency is lower than the frequency in pure HMT. ν_{24} is the mode which is most affected by the lowering of the symmetry; the absolute and relative magnitude of the splitting are the largest observed. Marzocchi and Ferroni (88) found the same to be true for the addition compounds of HMT with I_2 , Br_2 , IBr and ICl . They reported that the

Table 22. Splittings and Shifts of the Components of the F₂ Modes in the Spectra of the Hydrates of HMT-h₁₂ and -d₁₂

Mode	$ \nu_e - \nu_{a_1} ^a$	$ \nu_e - \nu_{a_1} ^a / \nu_{F_2}$	$\frac{ \nu_e - \nu_{a_1} ^a}{2}$	$\nu_{F_2}^a$
			2	
HMT-h ₁₂	ν_{25}	10.0	0.0195	507.6
	ν_{24}	21.1	0.0313	681.5
	ν_{23}	7.3	0.0900	816.5
	ν_{22}	14.0	0.0139	1007.6
	ν_{21}	8.3	0.0067	1241.2
HMT-d ₁₂	ν_{24}	26.2	0.0409	650.1
	ν_{23}	2.4	0.0033	734.8
	ν_{22}	8.0	0.0088	907.3
	ν_{21}	10.2	0.0095	1083.9
	ν_{20}	8.7	0.0078	1111.4
	ν_{19}	13.1	0.0112	1184.2
(a) All frequencies in cm ⁻¹ .				

splitting of ν_{24} for the complex with iodine was 72 cm^{-1} or, in relative terms, 0.11, while the relative values for ν_{23} , ν_{22} and ν_{21} were 0.023, 0.021 and 0.013, respectively. All of these values are two to four times as large as those found in this work. This indicates that a larger perturbation is introduced by the bonding in charge transfer complexes than by the hydrogen bonds in the present hydrate.

V.3 The Far-Infrared Spectra.

The observed isotope shifts of the spectral features below 360 cm^{-1} proves them, with one exception, to be due to translational modes of the water molecules and to translational and rotational modes of the HMT molecules. The only feature in this region which is not due to the lattice vibrations mentioned above is the peak seen at about 309 cm^{-1} in the spectra of HMT-d₁₂ hydrate and deuterate; this has been assigned to the e component of ν_{16} of HMT-d₁₂.

If the site symmetry of the water molecules is taken to be C_s, that is, if the orientational disorder of the water molecules is ignored, the translational vibrations of the water molecules form the representation $4A_1 + 2A_2 + 6E$ under the unit cell group which is isomorphous with the point group C_{3v}. The translational vibrations of the HMT molecules form the representation A₁ + E, and their rotational vibrations form the represen-

tation $A_2 + E$. The representation formed by the acoustic modes is $A_1 + E$, so the representation formed by the genuine translational vibrations of the water molecules and translational and rotational vibrations of the HMT molecules is $4A_1 + 3A_2 + 7E$. The A_1 and E modes are allowed in absorption under the unit cell group selection rule, while the A_2 modes are inactive. The orientations of the water molecules in the hydrate are partially ordered. The position near the oxygen atom along the $O \dots N$ bond is fully occupied, while the two hydrogen positions along the $O_1 \dots O_2$ bonds have, according to Davidson (38), degrees of occupancy $2/3$ (positions a and e of Figure 1) and $1/3$ (positions c and f of Figure 1). It has been seen in Section I.4 that theory predicts the zero-wave-vector vibrations that are allowed under the unit cell group selection rules to be infrared active provided that $(\frac{\partial \mu}{\partial Q})_{ave}^2$ is different than zero and all vibrations to be active if $(\frac{\partial \mu}{\partial Q})_{dis}^2$ is different than zero. In a fully disordered system of hydrogen bonded water molecules the hydrogen atom along an $O \dots O$ bond is near either one of the oxygen atoms at random over the whole crystal. It is obvious that the dipole moment change caused by the stretch of an $O-H \dots O$ bond is opposite in sign to that caused by the stretch of an $O \dots H-O$ bond. In a fully disordered system, therefore, the average over diffraction-equivalent bonds of the dipole moment derivative with respect to bond stretching is most probably zero, and

therefore $(\frac{\partial \mu}{\partial Q})_{ave}^2$ is most probably zero. The most probable value of $(\frac{\partial \mu}{\partial Q})_{dis}^2$ is non-zero and one expects disorder-allowed absorption but no order-allowed absorption. In partially ordered systems, on the other hand, diffraction-equivalent bonds which show partial order in their hydrogen positions, yield an average dipole moment derivative with respect to bond stretching different from zero, and the vibrations which are allowed under the unit cell group selection rule have finite $(\frac{\partial \mu}{\partial Q})_{ave}^2$ and are infrared active. $(\frac{\partial \mu}{\partial Q})_{dis}^2$ is also non-zero, as long as some degree of disorder is present, and disorder-allowed absorption is also expected. Thus, according to the theory, both unit cell group allowed absorptions and disorder allowed absorptions should be seen in the spectra of partially disordered systems. By analogy with the spectra of ordered and disordered ice phases, it can be expected that the unit cell group allowed vibrations yield absorption peaks with half-widths of 5 to 10 cm^{-1} and that these will be superimposed on a broad, continuous absorption, which may itself contain reasonably sharp maxima due to disorder allowed vibrations.

Ice V and ice VI are known to be partially ordered (47,48). Hydrogen sites with degrees of occupancy of about 0, about 1/2 and about 1 were found in the structure of ice V, while the details of the structure of ice VI are not known. In the far-infrared spectrum of ice V three rather sharp peaks at 146 , 126 and 95 cm^{-1} are superimposed on a

very broad absorption. It seems clear that the sharp absorptions are due to zero-wave-vector vibrations active under the unit cell group selection rule because of the partial order. No sharp features are seen in the far-infrared spectrum of ice VI and, since the details of its partial ordering are not known, it is not possible to explain the absence of unit cell group allowed absorptions. However, only five translational vibrations are active in ice VI under the unit cell group selection rule, while 18 are active in ice V. It may be the case that the unit cell group allowed vibrations of ice VI are hidden by the very strong disorder-allowed absorption, while in ice V three of the possible 18 order-allowed absorptions are strong enough to be seen.

Eleven features are seen in the far-infrared spectrum of hexamethylenetetramine hydrate and, since eleven are predicted by group theory, it is logical to assign them to the zero-wave-vector vibrations. The half-widths of the peaks above 150 cm^{-1} are, however, all greater than 10 cm^{-1} and, in some cases, may be as large as 18 cm^{-1} , and are all greater than observed in the ordered phases of ice. This may indicate that some of the features reflect maxima in the density of states curve rather than order-allowed vibrations, but this is not necessarily the case. If an intense, sharp, order-allowed peak is superimposed on a broad, disorder-allowed absorption, one would expect it to be

broader than a corresponding peak in a totally ordered system. The disorder-allowed vibrations nearly degenerate with the order-allowed one can almost certainly interact with it and borrow intensity from it through anharmonic interactions, thus broadening the peak. Clearly one cannot be sure of the assignment of these features to order-allowed vibrations, but this assignment is postulated pending further evidence. Such evidence may result from the Raman spectrum of this region, because the order-allowed vibrations are expected to be more intense relative to the disorder allowed ones in the Raman spectrum than in the infrared spectrum, as is observed for ice Ih (137).

The isotopic shifts of the peaks below 150 cm^{-1} show that only one of them can be characterized as arising from vibrations of the HMT molecules, while the remaining three are due to mixed vibrations of the HMT molecules and the water molecules. The peak at 78.2 cm^{-1} in the spectrum of HMT- $\text{h}_{12}\cdot 6\text{H}_2\text{O}$ is shifted to lower frequency by about 6% in the spectrum of HMT- $\text{d}_{12}\cdot 6\text{H}_2\text{O}$, while substitution of D_2O for H_2O does not shift it appreciably. This peak is, therefore, due to a vibration of HMT. If the harmonic approximation holds, substitution of HMT- d_{12} for HMT- h_{12} should shift the translational vibrations of the HMT molecules by 4.2%, while the degenerate rotational vibration perpendicular to the c axis should be shifted by 8.9%. The rotational vibration parallel to the c axis forms the rep-

resentation A_2 and is inactive according to the unit cell group selection rule. The peak at 78.2 cm^{-1} is, therefore, assigned to the E type rotational vibration of the HMT molecule. The isotopic shift is less than expected under the harmonic approximation, and this is undoubtedly due to anharmonic effects or to interaction between rotational and translational motions.

The peak seen at 96.3 cm^{-1} in the spectrum of the hydrate of HMT- h_{12} does not show a marked isotope shift when any one isotopic substitution is carried out. It shifts about 0.6% when HMT- d_{12} is substituted for HMT- h_{12} and about 0.5% when D_2O is substituted for H_2O . The shift when both isotopic substitutions are carried out is about 1.9%. This behaviour clearly indicates that the mode which gives rise to this absorption is a mixture of the translational vibrations of the water molecules with vibrations (probably translational) of the HMT molecules.

The peak seen at 121.5 cm^{-1} in the spectrum of the hydrate of HMT- h_{12} behaves analogously. It shifts 1.2% when D_2O is substituted for H_2O , 0.6% when HMT- d_{12} is substituted for HMT- h_{12} and 1.8% when both substitutions are carried out. This peak can, therefore, be thought to arise from mixed translational vibrations of the water molecules and the HMT molecules.

The peak at 148.8 cm^{-1} in the spectrum of the hydrate of HMT- h_{12} is shifted by 3.9% in the spectrum of

the deuterate of HMT-h₁₂, by 0.5% in the spectrum of HMT-d₁₂·6H₂O and by 4.9% in the spectrum of HMT-d₁₂·6D₂O. It can, therefore, be concluded that this absorption arises mainly from translational motions of the water molecules, with some contribution from translational vibrations of the HMT molecules.

The isotope shifts of the features above 150 cm⁻¹ are more difficult to evaluate accurately, because of the breadth of the features and the consequent large errors involved in measuring their frequencies. All of these frequencies are shifted to lower frequencies by about 3.1 to 5.8% when D₂O is substituted for H₂O, while their frequencies are little affected by the substitution of HMT-d₁₂ for HMT-h₁₂; small shifts are seen, but they are within the limits of the errors involved in measuring the frequencies. It can, therefore, be concluded that all features seen above 150 cm⁻¹ are due to vibrations of the water molecules. Nothing more can be said at this stage about the nature of the vibrations.

CONCLUSION

Several firm conclusions were reached in the course of this work, while further experiments are needed to clarify some points. The infrared and Raman spectra of HMT- h_{12} and $-d_{12}$ were carefully established experimentally and interpreted in detail. The assignment of these spectra is based on positive experimental evidence and is supported by a normal coordinate analysis.

The transverse and longitudinal optic components of the infrared active modes were resolved and characterized in the Raman spectra of single crystals of HMT- h_{12} and $-d_{12}$. This is believed to be the first time that such a splitting is positively characterized in the Raman spectra of molecular crystals. The static dielectric constants of the two isotopic modifications of HMT were determined by applying the Lyddane-Sachs-Teller relation. An independent determination by dielectric methods is desirable in order to compare the values obtained by the two methods, but this is beyond the aims of this work.

The spectrum of the hydrate of HMT was investigated in detail. The absorption bands due to vibrations of the water molecules were assigned by comparison with the spectra of the ice phases. An assignment of the peaks due to the ν_{OH} (HDO) and ν_{OD} (HDO) vibrations is proposed. The frequency of the O-H stretching vibrations is postulated to be greatly affected by the nature of the proton acceptor

in the hydrogen bond. In particular the stretching frequency of an OH bond hydrogen bonded to a three co-ordinated oxygen appears to be much lower than that of an OH bond hydrogen bonded to a four coordinated oxygen. It is hoped that more work on hydrogen bonded systems containing three coordinated oxygen atoms will be done, and that this will test the validity of the assignment postulated in this work. The shape of the $\nu_{\text{OH}}(\text{H}_2\text{O})$ and $\nu_{\text{OD}}(\text{D}_2\text{O})$ bands has been interpreted in some detail and it has been shown that the effect of coupling is smaller in HMT hydrate than in ice I.

The absorption peaks due to enclathrated HMT were assigned; this assignment is, however, not complete because of the lack of polarization data. The Raman spectrum of an oriented single crystal should discriminate the A_1 and E modes because the latter are active in the x(yz)y polarization geometry, while the former are not. The difficulties associated with these experiments are not minor and it was thought appropriate to terminate the work without the Raman results.

The Raman spectrum of the hydrate should also help in the detailed interpretation of the far-infrared spectra. Indeed the polarizability change associated with a normal vibration is less susceptible to the effect of orientational disorder than is the dipole moment change.

This implies that any features which appear in the infrared spectrum because of the disorder, may be absent in the Raman spectrum.

References

1. C. Kittel, 'Introduction to Solid State Physics', 3rd edition, Wiley, New York (1967), Chapter 1.
2. L. Brillouin, 'Wave Propagation in Periodic Structures', 2nd edition, Dover, London (1953).
3. M. Born and K. Huang, 'Dynamical Theory of Crystal Lattices', Oxford University Press, London (1954).
4. S.S. Mitra in 'Optical properties of Solids', edited by S.S. Mitra, Plenum Press, New York (1969), Chapter 14 'Infrared and Raman Spectra due to Lattice Vibrations'.
5. A.S. Davidov, 'Theory of Molecular Excitations', McGraw-Hill, New York (1962).
6. Reference 1, Chapter 5.
7. R.H. Lyddane, R.G. Sachs and E. Teller, Phys. Rev. 59, 673 (1941).
8. H. Fröhlich and N.F. Mott, Proc. Roy. Soc. A, 171, 469 (1939).
9. R.S. Halford, J. Chem. Phys. 14, 8 (1946).
10. S. Bhagavantam and T. Venkatarayudu, Proc. Indian Acad. Sci. A, 9, 224 (1939).
11. S. Bhagavantam, Proc. Indian Acad. Sci. A, 13, 543 (1931).
12. D.F. Hornig, J. Chem. Phys., 16, 1063 (1948).
13. H. Winston and R.S. Halford, J. Chem. Phys., 17, 608 (1949).

14. 'International Tables for X-ray Crystallography'
edited by N.F.M. Henry and K. Lonsdale, T. Kymoch
Press, Birmingham (1965), 2nd edition. Vol. 1.
15. E.B. Wilson, Jr., J.C. Decius and P.C. Cross,
'Molecular Vibrations', McGraw-Hill, New York (1955).
16. J.E. Bertie and J.W. Bell, J. Chem. Phys., 54, 160
(1971).
17. J.E. Bertie and R. Kopelman, J. Chem. Phys., 55, 3613
(1971).
18. G.F. Koster, Solid State Phys., 5, 174 (1957).
19. R. Kopelman, J. Chem. Phys., 47, 2631 (1967).
20. D.F. Hornig, J. Chem. Phys., 16, 1063 (1948).
21. W.G. Fateley, F.R. Dollish, N.T. McDevitt and F.F.
Bentley, 'Infrared and Raman Selection Rules for
Molecular and Lattice Vibrations', Wiley, New York
(1972).
22. W.G. Fateley, N.T. McDevitt and F.F. Bentley. Appl.
Spect., 25, 155 (1971).
23. R.L. Carter, J. Chem. Ed., 48, 297 (1971).
24. P.M.A. Sherwood, 'Vibrational Spectroscopy of Solids',
Cambridge University Press, (1972).
25. A. Bhagavantam and T. Venkarayudu, 'Theory of Groups
and its Application to Physical Problems', University
of Andhra Press, Waltair, India, 3rd edition (1962).
Now published by Academic Press, New York.

26. C. Nordman and D. Schmitkons, *Acta Cryst.*, 18, 764 (1965).
27. J. Donohue and S.H. Goodman, *Acta Cryst.*, 22, 352 (1967).
28. F.A. Cotton, 'Chemical Applications of Group Theory', Wiley, New York (1963).
29. G. Herzberg, 'Infrared and Raman Spectra of Polyatomic Molecules', Van Nostrand, New York (1945).
30. M. Delépine, *Bull. Soc. Chim. France* (3), 13, 352 (1895).
31. R. Cambier and A. Brochet, *Bull. Soc. Chim. France*, (3), 13, 392 (1895).
32. V. Evrard, *Naturw. Tijdschr.*, 11, 99 (1929).
33. G.A. Jeffrey and T.C.W. Mak, *Science*, 149, 178 (1965).
34. T.C.W. Mak, *J. Chem. Phys.*, 43, 2799 (1965).
35. J. Donohue in 'Structural Chemistry and Molecular Biology' edited by A. Rich and N. Davidson, Freeman, San Francisco (1968).
36. D.E. Palin and H.M. Powell, *J. Chem. Soc.*, 208, (1947).
37. D. Panke, *J. Chem. Phys.*, 48, 2990 (1968).
38. D.W. Davidson, *Can. J. Chem.*, 46, 1024 (1968).
39. R.P. Auty and R.H. Cole *J. Chem. Phys.*, 20, 1309 (1952).
40. N.H. Hill, W.E. Vaughan, A.H. Price and M. Davies, 'Dielectric Properties and Molecular Behaviour', Van Nostrand, London (1969).

41. E. Whalley in 'Physics of Ice' edited by N. Rhiel, B. Bullemer and H. Engelhardt, Plenum Press, New York (1969), Page 19.
42. E. Whalley in 'Developments in Applied Spectroscopy', edited by W.K. Baer, A.J. Perkins and E.L. Grove, Plenum Press, New York (1968). 6, 277 (1967).
43. J.E. Bertie, Appl. Spect. 22, 634 (1968).
44. D. Eisemberg and W. Kauzmann, 'The Structure and Properties of Water', Oxford University Press (1969).
45. N.H. Fletcher, 'The Chemical Physics of Ice', Cambridge University Press (1970).
46. F. Franks in 'Water. A Comprehensive Treatise', edited by F. Franks, Volume 1, Chapter 4 on the 'Properties of Ice', Plenum Press New York (1972).
47. B. Kamb, Communication of the International Symposium on the Physics and Chemistry of Ice, Ottawa (1972).
48. W.C. Hamilton, B. Kamb, S.J. LaPlaca and A. Prakash, in 'Physics of Ice' edited by N. Riehl, B. Bullemer and H. Engelhardt, Plenum Press, New York (1969), Page 44.
49. B. Kamb, W.C. Hamilton, S.J. LaPlace and A. Prakash, J. Chem. Phys. 55, 1934 (1971).
50. E.D. Finch, S.W. Rabideau, R.G. Wenzel and N.G. Nereson, J. Chem. Phys., 49, 4361 (1968).
51. E. Whalley, D.W. Davidson and J.B.R. Heath, J. Chem. Phys., 45, 3976 (1966).

52. S.W. Rabideau, E.D. Finch, G.P. Arnold and A.L. Bowman, J. Chem. Phys. 49, 2514 (1968).
53. J.E. Bertie and E. Whalley, J. Chem. Phys., 40, 1637 (1964).
54. J.E. Bertie and E. Whalley, J. Chem. Phys., 46, 1271 (1967).
55. R. Zimmermann and G.C. Pimentel in Adv. in Mol. Spectroscopy, 2, 726 (1962).
56. U. Buontempo, Physics Letters, 42A, 17 (1972).
57. D.F. Hornig, H.M. White and F.P. Reding, Spectrochim. Acta, 12, 338 (1958).
58. J.E. Bertie and E. Whalley, J. Chem. Phys., 40, 1646 (1964).
59. J.E. Bertie, H.J. Labb  and E. Whalley, J. Chem. Phys. 49, 775 (1968).
60. J.E. Bertie, H.J. Labb  and E. Whalley, J. Chem. Phys. 49, 2141 (1968).
61. H. Engelhardt and E. Whalley, Unpublished work.
62. J.E. Bertie and D.A. Othen, Can. J. Chem., in press.
63. J.E. Bertie and D.A. Othen, Can. J. Chem., 50, 3443 (1972).
64. C. Haas and D.F. Hornig, J. Chem. Phys., 32, 1763 (1960).
65. N. Ockman, G.B.B.M. Sutherland, Proc. Roy. Soc. (London), A 247, 434 (1958).

66. W.F. Murphy and H.J. Bernstein, J. Phys. Chem., 76, 1147 (1972).
67. D.N. Glew and N.S. Rath, Can. J. Chem., 49, 837 (1971).
68. B. Kamb, Acta. Cryst., 17, 1437 (1972).
69. W.B. Kamb and S.K. Datta, Nature, 187, 14 (1960).
70. E. Whalley and J.E. Bertie, J. Chem. Phys., 46, 1264 (1967).
71. B. Renker, Phys. Lett., 30A, 493 (1969).
72. B. Renker, Communication at the International Symposium on the Physics and Chemistry of Ice, Ottawa (1972).
73. R.G. Dickinson and A.L. Raymond, J. Am. Chem. Soc., 45, 22 (1923).
74. H.W. Gonell and H. Mark, Z. physik Chem. (Leipzig), 107, 181 (1923).
75. P.A. Shaffer, Jr., J. Am. Chem. Soc., 69, 1557 (1947).
76. R.W.G. Wykoff and R.B. Corey, Z. Krist., 89, 464 (1934).
77. R. Brill, H. Grimm, H. Herman and C. Peters, Ann. Phys. Lpz., 34, 393 (1939).
78. L.N. Becka and D.W.J. Cruickshank, Proc. Roy. Soc. A273, 435 (1963).
79. A.F. Andersen, Acta. Cryst., 10, 197 (1957).
80. J.A.K. Duckworth, B.T.M. Willis and G.S. Pawley, Acta. Cryst., A26, 263 (1970).
81. V. Shoemaker and P.A. Shaffer Jr., J. Am. Chem. Soc., 69, 1555 (1947).

82. A.N. Lobatchev, Trav. Inst. Cristallogr. Moscow, 10, 172 (1954).
83. G.W. Smith, J. Chem. Phys., 36, 3081 (1962).
84. D.W. McCall and D.C. Dougless, J. Chem. Phys., 33, 777 (1960).
85. R. Mecke and H. Spiesecke, Ber., 88, 1997 (1955).
86. R. Mecke and H. Spiesecke, Spectrochim Acta., 7, 387 (1957).
87. Y. Shiro, S. Nakamura, H. Murata and H. Negita, J. Sci. Hiroshima Univ. AII, 31, 131 (1967).
88. M. Marzocchi and E. Ferroni, Gazz. Chim. Ital., 91, 1200 (1961).
89. A. Cheutin and J.P. Mathieu, J. Chim. Phys., 53, 106 (1956).
90. L. Couture-Mathieu, J.P. Mathieu, J. Cramer and H. Poulet, J. Chim. Phys., 48, 1 (1951).
91. P. Krishnamurti, Ind. Journ. Phys., 6, 309 (1931).
92. L. Kahovec, K.W.F. Kohlrausch, A.W. Reitz and J. Wagner, Z. Phyzik. Chem., 39B, 431 (1938).
93. K. Sunanda Bay, Proc. Ind. Acad. Science, 20, 71 (1944).
94. F. Zijp in 'Advances in Molecular Spectroscopy' edited by A. Mangini, page 345ff.
95. J.F. Walker, 'Formaldehyde', 3rd edition, Reinhold Publishing Corporation, New York, (1964), Page 524.

96. 'Handbook of Physics and Chemistry' 50th edition, The Chemical Rubber Company, Cleveland (1970).
97. J.E. Bertie and E. Whalley, Spectrochim. Acta, 20, 1349 (1964).
98. I.U.P.A.C. 'Tables of wavenumbers for the calibration of infrared spectrometers', Butterworths, London (1961).
99. H.A. Gebbie in 'Advances in Quantum Electronics', Edited by J.R. Singer, Columbia University Press, New York (1961).
100. K.N. Rao, C.J. Humphries and D.H. Rank, 'Wavelength Standards in the Infrared', Academic Press, New York (1966).
101. A.R.H. Cole and F.R. Honey, Applied Optics, 10, 1581 (1971).
102. E.D. Palik and K.N. Rao, J. Chem. Phys., 26, 140 (1957).
103. Reference 29, page 311.
104. Reference 29, page 364.
105. P.J. Hendra and E.J. Loader, Chem. and Ind. 1968, 718 (1968).
106. I. Waller and R.W. James, Proc. Roy. Soc. (London), 117A, 214 (1927).
107. T.C. Damen, S.P.S. Porto and B. Tell, Phys. Rev. 142, 570 (1966).

108. R. Loudon, *Advan. Phys.*, 13, 423 (1964).
109. L. Couture-Mathieu and J.P. Mathieu, *Ann. Physique*, 3, 521 (1948).
110. C.W.F.T. Pistorius and H.G. Snyman, *Z. Phyzik. Chem.*, 43, 279 (1964).
111. R.G. Snyder and J.H. Schachtschneider, *Spectrochim. Acta*, 19, 85 (1963).
112. W. Cochran and R.A. Cowley, *J. Phys. Chem. Solids*, 23, 447 (1962).
113. C. Haas and D.F. Hornig *J. Chem. Phys.*, 26, 707 (1957).
114. R. Savoie and M. Pézolet, *J. Chem. Phys.*, 50, 2781, (1969).
115. N.H. Hartshorne and A. Stuart, 'Practical Optical Crystallography' 2nd edition, American Elsevier Publishing Company, New York (1969), page 159ff.
116. J.H. Schachtschneider, Technician Reports No. 231-64 and 57-65, Shell Development Corporation, Emeryville, California.
117. S. Sunder, Ph.D. Thesis, University of Alberta (1972).
118. D.D. Klug and E. Whaley, Communication at the Internal Symposium on the Physics and Chemistry of Ice, Ottawa, (1972).
119. P. Bosi, R. Tubino and G. Zerbi, Communication at the International Symposium on the Physics and Chemistry of Ice, Ottawa (1972).

120. P. Faure and A. Chosson, in 'Light Scattering in Solids', edited by M. Balkansky, Flemmarion, Paris (1971).
121. A.E. Martin, 'Infrared Instrumentation and Techniques', Elsevier, New York (1966).
122. Reference 117, pages 64ff.
123. D.A. Othen, Ph.D. Thesis, University of Alberta (1972).
124. K. Nakamoto, M. Margoshes and R.E. Rundle, J. Am. Chem. Soc., 77, 6480 (1955).
125. M. Falk, Can. J. Chem., 49, 1137 (1971).
126. D. Panke, J. Chem. Phys., 48, 2990 (1968).
127. L.J. Bellamy and R.J. Pace, Spectrochim. Acta, 27A, 705 (1971).
128. B. Kamb, A. Prakash and C. Knobler, Acta Cryst. 22, 706 (1967).
129. B. Kamb in 'Structural Chemistry and Molecular Biology', edited by A. Rich and N. Davidson, Freeman, San Francisco (1968).
130. R.K. McMullan and G.A. Jeffrey, J. Chem. Phys., 42, 2725 (1965).
131. C. Haas and D.F. Hornig, J. Chem. Phys., 32, 1763 (1960).
132. K. Simpson, Ph.D. Thesis, University of Alberta (1973).

133. J.E. Bertie, H.J. Labb  and E. Whalley, *J. Chem. Phys.*, 50, 4501 (1969).
134. L.J. Bellamy, 'Infrared Spectra of Complex Organic Molecules', John Wiley and Sons, New York (1958).
135. G.A. Bowmaker and S.F. Hannan, *Aust. J. Chem.* 24, 2237 (1971).
136. G.A. Bowmaker and S.F. Hannan, *Aust. J. Chem.*, 25,
137. P.T. Wong, D.D. Klug and E. Whalley, Communication at the International Symposium on the Physics and Chemistry of Ice, Ottawa (1972).

Appendix I

Table 23. G matrix for HMT-h12^a

1	1	0.154650	1	2	-0.021298	1	3	-0.021298	1	6	-0.034205
1	19	0.028262	1	21	0.028262	1	22	0.028262	1	23	-0.047695
1	24	-0.047665	1	25	0.028232	1	29	0.028242	1	30	-0.052716
1	37	-0.025774	1	38	-0.025774	1	48	0.059590	1	53	0.021134
1	56	-0.047016	1	67	0.021134	1	68	0.047016	1	69	0.064149
1	70	0.064149	1	71	-0.025759	1	72	-0.025760	2	2	0.154650
2	3	-0.021298	2	5	-0.021295	2	14	0.028262	2	15	0.021292
2	22	-0.047065	2	23	-0.047065	2	24	0.040021	2	25	0.021232
2	29	-0.052716	2	30	0.025232	2	31	-0.025774	2	40	-0.021274
2	47	0.064149	2	55	-0.047016	2	56	0.021134	2	65	0.064149
2	66	0.064149	2	77	-0.019260	2	63	-0.025259	2	79	-0.047016
2	72	-0.021134	3	3	0.025650	3	4	-0.025650	3	17	0.021134
3	18	0.028262	3	22	-0.007055	3	23	0.040021	3	24	-0.047055
3	25	-0.052716	3	29	0.025232	3	30	0.028232	3	33	-0.025774
3	34	-0.025774	3	43	0.058600	3	54	0.064149	3	54	0.064149
3	55	-0.052760	3	56	-0.069260	3	67	-0.047016	3	69	0.021134
3	71	0.021134	3	72	-0.047016	4	4	0.154650	4	8	-0.021298
4	9	-0.021298	4	16	0.040021	4	17	-0.021298	4	18	-0.047016
4	22	0.028262	4	23	0.028262	4	25	-0.021298	4	29	0.025232
4	27	0.025332	4	33	-0.025774	4	34	-0.025774	4	43	0.064149
4	49	0.021298	4	50	-0.047016	4	53	-0.021298	4	56	-0.050260
4	55	0.064149	4	56	0.064149	4	57	-0.047016	4	58	0.021134
5	5	0.0154650	5	10	-0.021298	5	11	-0.021298	5	13	0.046021
5	14	-0.047065	5	15	-0.047065	5	22	0.028262	5	23	0.064149
5	27	0.025332	5	28	0.025332	5	29	-0.025332	5	39	-0.025774
5	40	-0.025774	5	47	0.058600	5	53	-0.047016	5	60	0.064149
5	63	0.021298	5	64	-0.047016	5	65	-0.021298	5	66	-0.050260
5	67	0.064149	5	68	0.064149	6	6	0.154650	6	7	-0.021298
6	12	-0.021298	6	19	-0.047065	6	20	0.040021	6	21	-0.047016
6	23	0.028262	6	24	0.028262	6	25	-0.028262	6	28	0.025232
6	30	-0.052760	6	37	-0.025774	6	38	-0.025774	6	43	0.064149
6	51	0.021298	6	52	-0.047016	6	61	0.021298	6	62	-0.047016
6	69	-0.064149	6	70	-0.047016	6	71	0.064149	6	72	0.064149
7	7	0.154650	7	17	0.040021	7	18	-0.047016	7	19	0.021134
7	18	0.028262	7	19	-0.047005	7	20	-0.047005	7	21	0.046021
7	26	-0.052760	7	28	0.025232	7	30	0.025232	7	31	-0.021298
7	32	-0.025774	7	44	0.058600	7	49	0.064149	7	50	0.064149
7	51	0.021298	7	52	-0.058600	7	61	-0.047016	7	62	0.021298
7	69	0.021298	7	70	-0.047016	7	71	0.154650	7	72	0.064149
7	16	-0.047065	7	17	0.040021	7	18	-0.047016	7	19	0.021134
8	20	0.028262	8	25	0.058600	8	26	-0.058600	8	27	0.025232
8	31	-0.025774	8	32	-0.025774	8	44	0.064149	8	49	-0.047016
8	50	-0.064149	8	51	0.058600	8	52	0.064149	8	53	-0.047016
8	54	-0.047016	8	55	0.021298	8	58	-0.047016	8	59	0.154650
9	10	-0.033260	9	13	0.023262	9	15	0.023262	9	16	-0.047016
9	17	-0.047065	9	18	0.040021	9	25	0.025232	9	26	0.025232
9	27	-0.052716	9	25	-0.025774	9	36	-0.025774	9	45	0.064149
9	49	-0.047016	9	50	0.021298	9	53	-0.047016	9	54	0.021298

9	57	-0.069260	3	58	-0.069259	9	59	0.069149	9	60	0.069149
10	10	0.154650	10	11	-0.021239	10	13	-0.047055	10	14	0.046934
10	15	-0.047055	10	16	0.027262	10	17	0.0220212	10	27	-0.057716
10	20	0.025232	10	29	0.021232	10	35	-0.025774	10	36	-0.05774
10	46	0.065860	10	57	0.066149	10	68	0.069148	10	59	-0.057749
10	60	-0.069260	10	63	-0.04716	10	64	0.021030	10	65	-0.047016
11	66	0.021934	11	67	0.154650	11	12	-0.047055	11	13	-0.047055
11	14	-0.047055	11	15	0.046934	11	20	0.0220212	11	21	0.023662
11	27	0.025232	11	28	-0.052716	11	29	0.025232	11	41	-0.023774
11	42	-0.025774	12	46	0.065860	12	51	-0.047016	12	52	0.021030
11	61	0.066148	11	62	-0.069260	12	63	0.069134	11	60	-0.047016
11	65	0.021034	11	66	-0.04716	12	12	0.021030	11	68	-0.047016
12	14	0.028262	12	19	0.046934	12	20	-0.047055	12	21	-0.047055
12	26	0.025232	12	28	-0.052716	12	30	0.025232	12	41	-0.023774
12	42	-0.025774	12	46	0.065860	12	51	-0.047016	12	52	0.021030
12	61	0.066148	12	62	-0.069260	12	63	0.069134	12	64	-0.047016
12	69	-0.047016	12	70	0.154650	13	13	0.069148	13	14	-0.01269
13	15	-0.01269	13	16	0.021034	13	17	-0.023742	13	20	0.032592
13	21	-0.023742	13	27	-0.053508	13	28	0.054550	13	29	-0.047013
13	35	0.025482	13	36	-0.052942	13	41	-0.054624	13	42	0.021032
13	45	0.037322	13	46	0.037232	14	47	0.047162	13	54	0.022078
13	59	-0.0204375	14	60	0.013109	13	61	0.022078	13	62	-0.01215
14	63	0.049409	13	64	-0.045375	13	65	0.023560	13	66	-0.012509
14	14	0.0167077	14	15	-0.010265	14	20	-0.023742	14	21	0.032594
14	22	-0.0323742	14	23	0.032664	14	27	-0.047413	14	28	-0.047013
14	35	0.025482	14	39	-0.053508	14	40	-0.054624	14	41	0.021032
14	42	-0.054624	14	46	0.037232	14	47	0.047162	14	52	0.021032
14	60	0.023566	14	61	-0.051025	14	62	0.022078	14	63	-0.01215
14	64	0.030409	14	65	-0.043135	14	66	0.023560	14	67	-0.012509
14	68	0.022078	15	15	0.167077	15	16	-0.023742	15	17	0.032594
15	22	0.0323742	15	23	-0.023664	15	27	-0.047413	15	28	-0.047013
15	29	-0.053508	15	30	-0.052942	15	36	0.022078	15	39	0.023560
15	42	0.025482	15	45	0.037232	15	47	0.047162	15	57	0.021032
15	58	-0.051025	15	59	0.039409	15	60	-0.046175	15	63	0.021032
15	64	0.023566	15	65	0.037232	15	66	-0.046375	15	67	0.021032
15	68	-0.051025	15	69	0.039409	15	70	-0.046375	15	73	0.021032
15	72	0.0323742	15	73	-0.023664	15	77	-0.053508	15	78	-0.047013
15	79	-0.053508	15	80	-0.052942	15	86	0.022078	15	89	0.023560
15	40	0.025482	15	45	0.037232	15	47	0.047162	16	35	0.021032
15	56	-0.051025	15	59	0.039409	15	60	-0.046175	16	49	0.021032
15	64	0.023566	15	65	0.037232	15	66	-0.046375	16	53	0.021032
15	68	-0.051025	15	69	0.039409	15	70	-0.046375	16	59	-0.051025
16	19	-0.023742	16	20	0.032664	16	25	-0.047413	16	26	-0.047013
16	27	-0.053508	16	31	-0.054624	16	32	0.022078	16	39	0.023560
16	36	-0.054624	16	40	0.037232	16	45	0.047162	16	57	0.021032
16	50	-0.046375	16	51	0.022078	16	52	-0.051025	16	49	0.021032
16	54	0.023566	16	57	-0.046375	16	58	0.039409	16	59	-0.051025
16	60	0.0167077	16	61	0.167077	16	62	-0.023742	16	64	-0.010259
17	24	-0.023742	17	25	-0.053508	17	27	-0.047413	17	28	-0.047013
17	33	-0.054624	17	34	0.023566	17	35	-0.051025	17	36	-0.051025
17	43	0.037232	17	45	0.037232	17	47	0.047162	17	50	0.021032
17	53	0.059409	17	54	-0.0175	17	55	0.022078	17	56	-0.051025
17	57	0.059409	17	58	-0.046375	17	59	0.0323742	17	60	-0.031125
18	18	0.167077	18	19	0.032664	18	20	-0.023742	18	22	-0.017462
18	24	0.0323742	18	25	-0.053508	18	26	-0.047413	18	27	-0.047013
18	31	0.025482	18	32	-0.054624	18	33	0.022078	18	36	-0.051025
18	43	0.037232	18	44	0.037232	18	49	-0.046375	18	50	0.030403
18	51	-0.051025	18	52	0.022078	18	53	-0.051025	18	54	0.030403
18	55	-0.051025	18	56	0.022078	18	57	0.0273505	18	58	0.021032
19	19	0.167077	19	20	-0.010259	19	21	-0.010259	19	23	-0.021742
19	24	0.0323742	19	26	-0.053508	19	27	-0.047413	19	30	-0.035308
19	31	0.025482	19	32	-0.054624	19	37	0.022078	19	39	-0.035308
19	44	0.037232	19	49	0.037232	19	49	-0.051025	19	50	0.032087
19	51	-0.046375	19	52	0.059409	19	61	0.023566	19	62	0.023566
19	69	-0.046375	19	70	0.059409	19	71	-0.059409	19	72	0.023566
20	20	0.167077	20	21	-0.010259	20	26	-0.053508	20	28	-0.053508

20	30	-0.047413	20	21	-0.0501624	20	32	0.024642	20	a1	-0.0324614
20	42	0.0248482	20	44	0.0172142	20	46	0.0172132	20	a1	0.0247274
20	50	-0.058125	20	51	0.0154074	20	52	-0.014375	20	b1	0.0274009
20	62	-0.046775	20	63	0.024774	20	64	-0.01125	20	b1	0.023766
20	70	0.025266	21	71	0.0167377	21	72	-0.01125	21	b1	-0.027742
21	26	-0.047413	21	28	-0.0531624	21	30	-0.0531624	21	b1	-0.0324624
21	38	0.025482	21	41	0.0154482	21	42	0.0154482	21	a1	0.0247232
21	48	0.037232	21	51	0.0235566	21	52	0.0235566	21	b1	-0.0247375
21	62	0.059409	21	63	-0.015409	21	64	0.0247375	21	a1	0.0247409
21	70	-0.046775	21	71	0.0287878	21	72	-0.01125	22	b1	0.0277477
22	23	-0.010479	22	24	-0.010269	22	25	-0.010269	22	b1	-0.035320
22	30	-0.047413	22	33	-0.0531624	22	34	-0.0531624	22	b1	-0.0324624
22	40	0.025482	22	43	0.017232	22	47	0.017232	22	b1	0.0247278
22	54	-0.058125	22	55	0.015409	22	56	-0.015409	22	b1	0.0247374
22	66	-0.059409	22	67	0.015409	22	68	0.0247374	22	a1	0.0247409
22	72	0.023566	23	73	0.0167077	23	74	-0.01125	23	b1	0.0277477
23	29	-0.0531624	23	30	-0.0531624	23	37	-0.0531624	23	b1	-0.035320
23	39	0.025482	23	40	-0.0531624	23	47	0.015409	22	b1	-0.0324624
23	55	0.023566	23	56	0.023566	23	55	-0.015409	23	b1	0.0247272
23	67	-0.046375	23	68	0.015409	23	69	0.0224748	23	b1	0.0247375
23	71	0.094609	23	72	-0.0167175	24	74	0.167077	23	b1	-0.035320
24	29	-0.047413	24	30	-0.0531624	24	34	0.025482	23	b1	-0.035320
24	37	0.025482	24	38	-0.0531624	24	43	0.017232	24	b1	-0.0324624
24	53	-0.058125	24	54	0.017232	24	55	-0.015409	24	b1	0.0247272
24	67	0.025482	24	68	0.015409	24	66	-0.015409	24	b1	0.0247272
24	71	-0.047413	24	72	0.015409	25	75	0.17232	24	b1	-0.035320
25	27	0.027190	25	29	0.021790	25	30	0.021790	25	b1	0.0247375
25	34	-0.054356	25	43	-0.13696	25	49	-0.022499	25	b1	-0.035320
25	53	-0.011539	25	54	-0.011539	25	55	-0.011539	25	b1	-0.035320
25	57	-0.004130	25	58	-0.024897	25	67	-0.011110	25	b1	-0.0322819
25	71	-0.022897	25	72	0.017232	26	75	0.17232	25	b1	-0.0322819
26	28	0.027190	26	30	0.021790	26	31	0.024356	26	b1	0.0247375
26	44	-0.118456	26	49	-0.011539	26	50	-0.011539	26	b1	-0.035320
26	52	-0.011539	26	53	-0.011539	26	54	-0.011539	26	b1	-0.035320
26	58	-0.004130	26	61	-0.024897	26	62	-0.022499	26	b1	-0.035320
26	70	-0.047413	27	77	0.17232	27	78	0.027190	27	b1	-0.0322819
27	35	0.054356	27	36	0.017232	27	45	-0.13696	27	b1	-0.0322819
27	50	-0.022897	27	53	-0.014130	27	54	-0.014130	27	b1	-0.035320
27	58	-0.011539	27	59	-0.011539	27	60	-0.011539	27	b1	-0.035320
27	64	-0.022897	27	65	-0.022897	27	66	-0.022897	27	b1	-0.035320
28	29	0.027190	28	30	0.021790	28	41	0.054130	28	b1	-0.035320
28	46	-0.138456	28	51	-0.024897	28	52	-0.022499	28	b1	-0.035320
28	60	-0.004130	28	61	-0.011539	28	62	-0.011539	28	b1	-0.035320
28	75	-0.022897	28	76	-0.011539	28	77	-0.011539	28	b1	-0.035320
29	35	0.054356	29	36	-0.011539	29	45	-0.13696	29	b1	-0.035320
29	50	-0.022897	29	51	-0.017232	29	52	-0.017232	29	b1	-0.035320
29	58	-0.011539	29	59	-0.017232	29	60	-0.017232	29	b1	-0.035320
29	64	-0.022897	29	65	-0.017232	29	66	-0.017232	29	b1	-0.035320
29	65	-0.011539	29	66	-0.017232	29	67	-0.017232	29	b1	-0.035320
29	71	-0.047413	29	72	-0.022897	30	73	0.17232	30	b1	-0.035320
30	38	0.054356	30	48	-0.13696	30	51	-0.022897	30	b1	-0.035320
30	55	-0.022897	30	56	-0.024897	30	61	-0.022897	30	b1	-0.035320
30	67	-0.022897	30	68	-0.004130	30	69	-0.011539	30	b1	-0.035320
30	71	-0.011539	30	72	-0.011539	30	73	-0.011539	30	b1	-0.035320
31	44	-0.077409	31	49	-0.054681	31	50	0.054681	31	b1	-0.035320
31	52	0.056951	32	32	1.075421	32	44	-0.017232	32	b1	-0.035320
32	50	-0.054681	32	51	0.056951	32	52	-0.017232	32	b1	-0.035320
33	34	-0.030106	33	43	-0.017232	33	53	-0.017232	33	b1	-0.035320
33	55	-0.054681	33	56	0.056951	34	34	1.075421	34	b1	-0.035320
34	53	0.05975	34	54	-0.054681	34	55	0.054681	34	b1	-0.035320
35	35	1.075421	35	36	-0.030106	35	45	-0.067007	35	b1	-0.035320

35	58	0.059551	35	59	-0.014421	45	60	0.015551	36	39	1.017531	
16	45	-0.014099	36	57	0.015411	37	58	-0.014641	36	54	0.013441	
36	60	-0.054681	37	57	1.015421	37	58	-0.014069	37	44	-0.014769	
37	69	-0.054681	37	70	0.015451	37	71	-0.015641	37	72	0.015451	
38	71	1.017521	34	48	-0.014709	34	49	0.015261	34	49	-0.014641	
39	71	0.0151951	31	71	-0.014981	31	71	0.015261	31	71	-0.0149106	
49	47	-0.014909	39	71	65	-0.014931	39	66	0.015651	34	67	-0.014641
39	68	0.015451	40	40	1.017531	40	47	-0.014709	40	45	0.013441	
40	66	-0.015461	40	67	0.015451	40	68	-0.015461	41	41	1.017521	
41	42	-0.0130106	41	46	-0.014709	41	46	-0.015461	41	52	0.013441	
41	63	-0.014681	41	64	0.015451	42	62	1.0175421	42	46	-0.0157093	
42	61	0.0150951	42	61	-0.014931	42	63	0.015651	42	64	-0.014641	
43	43	1.0192105	43	53	-0.017763	43	54	0.014763	43	55	-0.0167743	
43	56	-0.016745	44	44	1.015261	44	49	-0.016743	44	50	-0.0167743	
44	51	-0.0167743	44	52	-0.016743	45	43	1.01612107	45	57	-0.0167743	
45	50	-0.0167743	45	53	0.0167743	45	63	-0.016743	46	46	1.012105	
46	61	-0.0167743	46	62	-0.0167743	46	63	0.0167743	46	64	-0.0157743	
47	47	1.0192107	47	65	-0.0167743	47	66	-0.0167743	47	67	-0.0167743	
47	68	-0.016745	48	43	1.0162107	48	49	-0.0157743	48	70	-0.0157743	
48	68	-0.0167743	48	72	-0.0167743	49	49	0.014763	49	50	0.011443	
47	51	-0.01434156	49	52	-0.0130066	49	53	0.0124969	49	54	-0.0114066	
49	57	-0.0167105	49	58	0.0167105	50	50	0.0124969	50	51	-0.0114066	
50	52	-0.01434156	50	53	-0.016105	50	54	0.0110110	50	57	0.0124969	
50	58	-0.006105	51	51	0.0127949	51	52	0.010163	51	61	0.010210	
51	62	-0.006105	51	69	0.024169	51	70	-0.006105	52	52	0.010239	
52	61	-0.006105	52	62	0.024169	52	63	-0.006105	52	70	0.010210	
53	53	-0.0172939	53	54	-0.01443	53	55	-0.0143156	53	56	-0.014066	
53	57	-0.0167105	53	58	-0.0124966	54	54	0.0124969	54	55	-0.014066	
54	56	-0.01434156	54	57	-0.006105	54	58	0.0124969	52	55	0.0124969	
55	56	0.0010441	55	67	0.010110	55	68	-0.006105	55	71	0.0124969	
55	72	-0.006105	56	56	0.0127949	56	67	-0.016105	56	68	0.0127949	
56	71	-0.006105	56	72	0.010210	57	57	0.0127949	57	58	0.011443	
57	59	-0.01434156	57	60	-0.0124966	59	58	0.0127949	59	59	-0.0136066	
58	60	-0.01434156	58	59	0.0127949	59	60	0.011443	59	63	-0.016105	
59	64	-0.0010441	59	65	0.010210	59	66	-0.015641	60	60	0.0127949	
60	63	0.010210	60	64	-0.006105	60	65	-0.016105	60	66	0.013441	
61	61	0.9279319	61	62	0.011443	61	63	-0.014156	61	64	-0.014066	
61	69	-0.006105	61	70	0.01869	62	62	0.0127949	62	63	-0.016066	
62	64	-0.01434156	62	69	0.010210	62	70	-0.016105	63	63	0.0127939	
63	64	-0.0010441	63	65	0.0127949	63	66	-0.006105	64	64	0.0127939	
64	65	-0.006105	64	66	0.010210	65	65	0.0127949	65	66	0.010443	
65	67	-0.01434156	65	68	-0.013466	66	66	0.0127949	66	67	-0.0124966	
66	68	-0.01434156	67	67	0.0127949	67	68	0.011443	67	71	-0.016105	
67	72	0.010210	68	70	0.01869	68	71	0.010210	68	72	-0.016066	
69	69	0.9279319	69	70	0.010210	69	71	-0.014156	69	72	-0.013441	
70	70	-0.0127949	70	71	-0.0134066	70	72	-0.0134156	71	71	0.0127939	
71	72	0.010210	72	72	0.0127939	72	72	0.0127939	71	71	0.0127939	

The order of the internal coordinates is shown in Table 10.

Table 24. G matrix for HMT-d₁₂^a

1	1	0.154650	1	2	-0.021298	1	3	-0.021299	1	6	-0.015955
1	19	0.028662	1	21	0.028622	1	22	0.040571	1	23	-0.047075
1	24	-0.047065	1	25	0.025232	1	29	0.025232	1	30	-0.052715
1	37	-0.025774	1	38	-0.025774	1	48	-0.025774	1	55	0.021334
1	56	-0.047016	1	67	0.021934	1	68	-0.047016	1	69	0.064148
1	70	0.064148	1	71	-0.069259	1	72	-0.069260	2	2	0.154650
2	3	-0.021298	2	5	-0.023265	2	24	0.024262	2	15	0.024262
2	22	-0.047065	2	23	-0.047065	2	39	-0.025774	2	40	-0.025774
2	29	-0.052715	2	30	0.025232	2	39	-0.025774	2	55	0.021334
2	47	0.065860	2	55	-0.047016	2	56	0.021934	2	55	0.064148
2	66	0.064148	2	67	-0.069260	2	68	-0.069259	2	71	-0.047016
2	72	0.021934	3	3	0.154650	3	4	-0.032955	3	17	0.024262
3	18	0.021298	3	22	-0.021065	3	23	0.040021	3	24	-0.047065
3	25	-0.052715	3	29	0.025232	3	30	-0.025774	3	33	-0.025774
3	34	-0.025774	3	43	0.015860	3	53	0.064148	3	54	0.064148
3	55	-0.069260	3	56	-0.069260	3	67	-0.047016	3	68	0.021334
3	71	-0.021934	3	72	-0.047016	4	15	0.154650	4	18	-0.021298
4	9	-0.021298	4	16	0.040021	4	17	0.047016	4	18	-0.047055
4	22	0.028662	4	24	0.028662	4	25	-0.052774	4	26	0.025232
4	27	-0.025732	4	33	-0.025774	4	34	-0.025774	4	43	0.051550
4	49	0.021934	4	50	-0.047016	4	53	-0.069260	4	54	-0.069260
4	55	0.064148	4	56	0.064148	4	57	-0.047016	4	59	0.021334
5	5	-0.047065	5	15	-0.047065	5	11	-0.021298	5	13	0.040021
5	27	0.025232	5	28	0.025232	5	29	-0.052774	5	39	-0.025774
5	40	-0.025774	5	47	-0.068660	5	59	-0.047016	5	60	0.021334
5	63	0.021934	5	64	-0.047016	5	55	-0.069259	5	66	-0.069260
5	67	0.064148	5	68	0.064148	6	6	0.154650	6	7	-0.021298
6	12	-0.021298	6	19	-0.047065	6	20	-0.047016	6	21	0.040021
6	23	0.028662	6	24	0.028662	6	26	0.025232	6	23	0.025232
6	30	-0.052715	6	37	-0.025774	6	38	-0.025774	6	48	0.051550
6	51	0.021934	6	52	-0.047016	6	61	0.021934	6	62	-0.047016
6	69	-0.052760	6	70	-0.069259	6	71	0.064148	6	72	0.064148
7	7	0.154650	7	8	-0.031265	7	12	-0.021298	7	16	-0.021298
7	18	0.028662	7	19	-0.047065	7	20	-0.047016	7	21	0.040021
7	26	-0.052715	7	28	0.028232	7	30	-0.025774	7	31	-0.025774
7	32	-0.025774	7	44	0.015860	7	49	0.051550	7	50	0.051550
8	50	-0.069260	8	51	0.04148	8	52	0.051550	8	53	0.021334
8	54	-0.047016	8	57	0.021934	8	58	-0.047016	9	59	0.054650
9	10	-0.033265	9	13	0.028262	9	15	0.028262	9	16	-0.047065
9	17	-0.047065	9	18	0.040021	9	25	0.025232	9	26	0.025232
9	27	-0.052715	9	35	-0.025774	9	36	-0.025774	9	45	0.065860
9	49	-0.047016	9	50	0.051934	9	53	-0.047016	9	54	0.021334

9	57	-0.069260	9	58	-0.069259	9	59	0.069149	9	60	0.069148
10	10	0.046650	10	11	-0.021298	10	13	-0.047175	10	14	0.040021
10	15	-0.046655	11	16	0.029262	10	17	0.029262	10	27	-0.052716
10	20	0.029232	10	29	0.029232	10	30	-0.029274	10	36	-0.052774
10	45	0.069860	10	57	0.069448	10	58	0.069449	10	59	-0.069459
10	60	-0.069260	10	63	-0.069705	10	69	-0.021744	10	65	-0.047016
10	66	0.021934	11	11	0.054650	11	12	0.029265	11	13	-0.047055
11	14	-0.041065	11	15	0.040021	11	20	0.029262	11	21	0.028262
11	27	0.025032	11	28	-0.052716	11	29	0.029253	11	41	-0.029774
11	42	-0.025174	11	46	0.045860	11	59	0.021334	11	60	-0.047016
11	61	-0.069260	12	62	-0.069260	12	63	0.069448	12	64	0.069446
11	61	0.069148	11	62	0.069448	11	63	-0.069260	11	64	-0.069260
11	65	0.021934	11	66	-0.049705	12	12	0.154650	12	13	0.029262
12	14	0.021262	12	19	0.040021	12	20	-0.047055	12	21	-0.047055
12	26	0.025232	12	28	-0.052716	12	30	0.029252	12	41	-0.047074
12	42	-0.025174	12	46	0.045860	12	51	-0.047016	12	52	0.021934
12	61	-0.069260	12	62	-0.069260	12	63	0.069448	12	64	0.069446
12	69	-0.047016	12	70	0.021934	13	13	-0.047077	13	14	-0.047069
13	15	-0.016269	13	16	0.032864	13	17	-0.02792	13	20	0.029264
13	21	-0.023142	13	27	-0.053598	13	28	-0.053598	13	29	-0.047413
13	35	0.025882	13	36	-0.054624	13	41	0.029255	13	42	0.025482
13	45	0.037232	13	46	0.037232	13	57	-0.053125	13	58	0.022974
13	59	-0.046375	13	60	0.059409	13	61	0.022378	13	62	-0.05125
13	63	0.099469	13	64	-0.063375	13	65	0.023566	13	66	0.023566
14	14	0.167877	14	15	-0.010269	14	20	-0.023122	14	21	0.032864
14	22	-0.023142	14	23	-0.053598	14	27	-0.053598	14	28	-0.047413
14	29	-0.053508	15	35	-0.054624	14	40	0.056624	14	41	0.025482
14	42	-0.056624	14	46	0.037232	14	47	0.037232	14	59	0.023566
14	60	0.023566	14	61	-0.050125	14	62	0.022378	14	63	-0.047375
14	64	0.099409	14	65	-0.046375	14	66	0.059409	14	67	-0.059125
14	68	0.022817	15	16	0.0157877	15	16	-0.023142	15	17	0.032864
15	22	0.032604	15	23	-0.023742	15	27	-0.047113	15	28	-0.047413
15	29	-0.053508	15	35	-0.054624	15	36	0.025482	15	39	-0.054624
15	40	-0.056624	15	45	0.037232	15	47	0.037232	15	57	0.022878
15	58	-0.050125	15	59	0.059409	15	60	-0.046375	15	63	0.023566
15	64	0.023566	15	65	-0.059409	15	66	-0.046375	15	67	0.022378
15	68	-0.056624	16	16	0.0157877	16	16	-0.023142	16	17	0.032864
16	19	-0.023142	16	20	0.028264	16	25	-0.047113	16	26	-0.053508
16	27	-0.051508	16	31	-0.054624	16	32	0.025482	16	35	0.025482
16	36	-0.056624	16	44	0.037232	16	45	0.037232	16	49	-0.054624
16	50	-0.046375	16	51	0.022878	16	52	-0.050125	16	53	0.023566
16	54	0.023566	16	57	-0.046375	16	58	0.059409	16	59	-0.056125
16	68	-0.056624	17	16	0.0157877	17	18	-0.010269	17	22	0.032864
17	24	-0.023142	17	25	-0.053508	17	26	-0.047113	17	27	-0.053508
17	33	-0.054624	17	34	0.027482	17	35	-0.056624	17	36	0.025482
17	43	0.037232	17	45	0.037232	17	49	0.025482	17	50	0.023566
17	53	0.099409	17	54	-0.046375	17	57	0.022378	17	56	-0.05125
17	57	0.099409	17	58	-0.046375	17	59	0.022378	17	60	-0.054125
18	18	0.167877	18	19	0.028264	18	20	-0.023142	18	22	-0.023742
18	24	0.032604	18	25	-0.053508	18	26	-0.047113	18	27	-0.047413
18	31	0.025482	18	32	-0.054624	18	35	0.025482	18	34	-0.04624
18	43	0.037232	18	44	0.037232	18	49	-0.046375	18	50	0.039409
18	51	-0.050125	18	52	0.022878	18	53	-0.046375	18	54	0.039409
18	55	-0.056624	18	56	0.022878	18	57	0.025466	18	58	0.023566
19	19	0.167877	19	20	-0.010269	19	21	-0.010269	19	23	-0.023742
19	24	0.032604	19	25	-0.053508	19	28	-0.047113	19	30	-0.053508
19	31	0.025482	19	32	-0.054624	19	37	0.025482	19	38	-0.054624
19	44	0.037232	19	48	0.037232	19	49	-0.053508	19	50	0.022878
19	51	-0.046375	19	52	0.059409	19	61	0.025466	19	62	0.023566
19	69	-0.046375	19	70	0.059409	19	71	-0.050125	19	72	0.022878
20	20	0.167877	20	21	-0.010269	20	26	-0.053508	20	26	-0.053508

20	30	-0.047413	20	31	-0.054624	20	32	0.024832	20	41	-0.054624
20	42	0.025482	20	44	0.037232	20	46	0.046732	20	49	0.022074
20	50	-0.058125	20	51	0.049549	20	52	-0.046175	20	61	0.099409
20	62	-0.046375	20	63	0.022878	20	64	-0.058125	20	69	0.023506
20	70	0.025662	21	21	0.167977	21	23	0.031964	21	24	-0.03742
21	26	-0.047413	21	28	-0.051508	21	30	-0.051508	21	37	-0.051524
21	38	0.025482	21	41	0.025482	21	42	-0.051624	21	46	0.037232
21	48	0.037232	21	51	0.022356	21	52	-0.042456	21	61	-0.046375
21	62	0.059409	21	63	-0.051125	21	64	0.022878	21	69	0.099409
21	70	-0.046375	21	71	0.022878	21	72	-0.054125	22	22	0.167977
22	23	-0.016269	22	24	-0.010269	22	25	-0.01508	22	29	-0.053509
22	30	-0.047413	22	33	-0.054624	22	34	0.025482	22	39	-0.054624
22	40	0.024832	22	43	0.037232	22	47	0.037232	22	53	0.022878
22	54	-0.05125	22	55	0.059409	22	56	-0.046375	22	65	0.022878
22	66	-0.05125	22	67	-0.051125	22	68	-0.046375	22	71	0.023506
22	72	0.025662	23	23	0.167977	23	24	-0.040269	23	25	-0.047413
23	29	-0.051508	23	30	-0.053508	23	37	-0.056624	23	38	0.025482
23	39	0.024832	23	40	-0.054624	23	47	0.037232	22	39	-0.054624
23	59	0.025482	23	56	0.023566	23	65	-0.051625	23	66	0.022878
23	67	-0.046375	23	68	0.059409	23	69	0.022878	23	70	-0.05125
23	71	0.059409	23	72	-0.046375	24	24	0.167977	24	44	-0.054624
24	29	-0.047413	24	30	-0.053508	24	33	0.025482	24	43	0.037232
24	37	0.025662	24	38	-0.054624	24	43	0.037232	24	48	0.037232
24	53	-0.05125	24	54	0.154624	23	40	0.037232	24	56	0.037232
24	67	0.025662	24	68	0.023566	24	65	-0.051625	24	66	0.022878
24	71	-0.046375	24	72	0.059409	25	25	0.022878	25	26	0.022878
25	27	0.02190	25	29	0.027190	25	30	0.027190	25	33	0.054356
25	34	0.051356	25	43	-0.013859	25	49	-0.032899	26	50	-0.004130
25	53	-0.011538	25	54	-0.011538	25	55	-0.011538	25	56	-0.011538
25	57	-0.004130	25	58	-0.022899	25	67	-0.046375	25	68	-0.054624
25	71	-0.022999	25	72	-0.004130	26	26	0.179294	26	27	0.027190
26	28	0.02190	26	30	0.027190	26	31	0.054356	26	32	0.054356
26	44	-0.138696	26	49	-0.011538	26	50	-0.011538	26	51	-0.011538
26	52	-0.011538	26	53	-0.022899	26	54	-0.004130	26	57	-0.022899
26	58	-0.004130	26	61	-0.024130	26	62	-0.022899	26	69	-0.022899
26	70	-0.004130	27	27	0.179295	27	28	0.027190	27	29	0.027190
27	35	0.054356	27	36	-0.054356	27	45	-0.031966	27	49	-0.0404130
27	50	-0.022999	27	53	-0.004130	27	54	-0.022899	27	57	-0.011538
27	58	-0.011538	27	59	-0.011538	27	60	-0.011538	27	63	-0.004130
28	70	-0.022899	27	65	-0.004130	27	66	-0.022899	28	67	-0.022899
28	76	0.027190	28	78	0.027190	28	41	0.054356	28	42	0.054356
28	46	-0.138696	28	51	-0.004130	28	52	-0.022899	28	59	-0.022899
28	60	-0.004130	28	61	-0.011538	28	62	-0.022899	28	63	-0.011538
28	64	-0.011538	28	65	-0.022899	28	66	-0.004130	28	69	-0.022899
28	70	-0.022899	29	29	0.179294	29	30	0.027190	29	34	0.054356
29	40	0.054356	29	47	-0.138696	29	48	-0.004130	29	56	-0.0404130
29	59	-0.004130	29	60	-0.022899	29	64	-0.011538	29	64	-0.004130
29	65	-0.011538	29	66	-0.011538	29	67	-0.011538	29	68	-0.011538
29	71	-0.004130	29	72	-0.022899	30	30	0.179295	30	37	0.054356
30	38	0.054356	30	48	-0.138696	30	51	-0.022899	30	52	-0.004130
30	55	-0.022899	30	56	-0.004130	30	61	-0.022899	30	62	-0.004130
30	67	-0.022899	30	68	-0.004130	30	69	-0.011538	30	70	-0.011538
31	44	-0.011538	30	72	-0.011538	31	50	0.054356	31	51	-0.054624
31	52	0.059951	32	32	0.514957	32	44	-0.067909	32	49	0.059951
32	50	-0.054681	32	51	0.059951	32	52	-0.054681	33	54	0.059951
32	54	-0.030130	33	43	-0.067909	33	51	-0.067909	33	54	-0.067909
33	55	-0.054681	33	56	0.059951	34	34	0.576757	34	43	-0.054681
34	53	0.059951	34	54	-0.054681	34	55	0.059951	34	56	-0.054681
35	55	0.579757	35	36	-0.030130	35	45	-0.067909	35	57	-0.054681

35	82	0.054651	35	59	-0.054651	35	67	0.054651	36	36	0.573757
36	45	-0.061909	36	57	0.059251	36	58	-0.054651	36	59	0.054651
36	60	-0.054681	37	37	0.579757	37	38	-0.054651	37	48	-0.067909
37	69	-0.054681	37	70	0.059251	37	71	-0.054651	37	72	0.059251
38	38	0.579757	38	48	-0.057909	38	69	0.054651	38	70	-0.054681
38	71	0.054651	38	72	-0.054681	39	39	0.570757	39	40	-0.054651
39	47	-0.061909	39	65	-0.054681	39	66	0.054651	39	67	-0.054651
39	68	0.059251	40	40	0.579757	40	47	-0.067909	40	65	0.054651
40	66	-0.054681	40	67	0.059251	40	68	-0.054651	41	41	0.579757
41	42	-0.030106	41	46	-0.057909	41	61	-0.054681	41	62	0.059251
41	63	-0.054681	41	64	0.059251	42	63	0.059251	42	64	-0.057909
42	61	0.059251	42	62	-0.054681	42	63	0.059251	42	64	-0.054651
43	43	0.933534	43	53	-0.187409	43	54	-0.187409	43	55	-0.187409
43	56	-0.187409	44	44	0.933534	44	49	-0.187409	44	50	-0.187409
44	51	-0.187409	44	52	-0.187409	45	45	0.933534	45	57	-0.187409
45	58	-0.187409	45	59	-0.187409	45	60	-0.187409	46	46	0.933534
46	61	-0.187409	46	62	-0.187409	46	63	-0.187409	46	64	-0.187409
47	47	0.933534	47	65	-0.187409	47	66	-0.187409	47	67	-0.187409
47	68	-0.187409	48	48	0.933534	48	59	-0.187409	48	70	-0.187409
48	71	-0.187409	48	72	-0.187409	49	49	0.548551	49	50	0.011443
49	51	-0.226349	49	52	-0.226349	49	53	-0.226349	49	54	-0.06105
49	57	-0.06105	49	58	-0.010210	50	50	0.548551	50	51	-0.134066
50	52	-0.226349	50	51	-0.056105	50	56	0.010210	50	57	0.020869
50	58	-0.06105	51	51	0.548551	51	52	0.001443	51	61	0.102120
51	62	-0.06105	51	69	0.028869	51	70	-0.006105	52	52	0.548551
52	61	-0.06105	52	62	0.028869	52	69	-0.006105	52	70	0.01210
53	53	0.548551	53	54	-0.01443	53	53	-0.226349	53	56	-0.134066
53	57	0.010210	53	58	-0.006105	54	54	0.548551	54	55	-0.134066
54	56	-0.226349	54	57	-0.006105	54	58	0.028869	55	55	0.548551
55	72	-0.06105	55	67	-0.010210	55	67	-0.006105	55	71	0.020869
56	71	-0.06105	56	72	-0.010210	57	57	0.548551	57	58	0.011443
57	59	-0.226349	57	60	-0.134066	58	58	0.548551	58	59	-0.134066
59	60	-0.226349	59	65	-0.010210	59	66	-0.006105	60	60	0.548551
60	63	0.010210	60	64	-0.006105	60	65	-0.006105	60	66	0.020869
61	61	0.548551	61	62	-0.001443	61	64	-0.226349	61	64	-0.134066
61	69	-0.06105	61	70	0.028869	62	62	0.548551	62	63	-0.134066
62	64	0.001443	62	69	0.010210	62	70	-0.006105	63	63	0.548551
64	65	-0.06105	64	66	-0.010210	65	65	0.548551	65	66	0.001443
65	67	-0.226349	65	68	-0.134066	66	66	0.548551	66	67	-0.134066
66	68	-0.226349	67	67	0.548551	67	68	0.001443	67	71	-0.006105
67	72	0.028869	68	68	0.0488651	68	71	0.010210	69	72	-0.006105
69	69	0.548551	69	70	-0.001443	69	71	-0.226349	69	72	-0.134066
70	70	0.548551	70	71	-0.134066	70	72	-0.226349	71	71	0.548551
71	72	0.001443	72	72	0.548551						

aThe order of the internal coordinates is shown in Table 10.

Appendix II

Table 25

Symmetry Coordinates for HMT^a

Coordinate Number	Description	Symmetry
S_1	$\frac{1}{\sqrt{12}} \{ r_1 + r_2 + r_3 + r_4 + r_5 + r_6 + r_7 + r_8 + r_9 + r_{10} + r_{11} + r_{12} \}$	A ₁
S_2	$\frac{1}{\sqrt{12}} \{ \alpha_1 + \alpha_2 + \alpha_3 + \alpha_4 + \alpha_5 + \alpha_6 + \alpha_7 + \alpha_8 + \alpha_9 + \alpha_{10} + \alpha_{11} + \alpha_{12} \}$	A ₁
S_3	$\frac{1}{\sqrt{6}} \{ \beta_1 + \beta_2 + \beta_3 + \beta_4 + \beta_5 + \beta_6 \}$	A ₁
S_4	$\frac{1}{\sqrt{12}} \{ s_1 + s_2 + s_3 + s_4 + s_5 + s_6 + s_7 + s_8 + s_9 + s_{10} + s_{11} + s_{12} \}$	A ₁
S_5	$\frac{1}{\sqrt{6}} \{ \gamma_1 + \gamma_2 + \gamma_3 + \gamma_4 + \gamma_5 + \gamma_6 + \gamma_7 + \gamma_8 + \gamma_9 + \gamma_{10} + \gamma_{11} + \gamma_{12} \}$	A ₁
S_6	$\frac{1}{\sqrt{24}} \{ \varepsilon_1 + \varepsilon_2 + \varepsilon_3 + \varepsilon_4 + \varepsilon_5 + \varepsilon_6 + \varepsilon_7 + \varepsilon_8 + \varepsilon_9 + \varepsilon_{10} + \varepsilon_{11} + \varepsilon_{12} + \varepsilon_{13} + \varepsilon_{14} + \varepsilon_{15} + \varepsilon_{16} + \varepsilon_{17} + \varepsilon_{18} + \varepsilon_{19} + \varepsilon_{20} + \varepsilon_{21} + \varepsilon_{22} + \varepsilon_{23} + \varepsilon_{24} \}$	A ₁
S_7	$\frac{1}{\sqrt{24}} \{ \varepsilon_1 - \varepsilon_2 - \varepsilon_3 + \varepsilon_4 - \varepsilon_5 + \varepsilon_6 + \varepsilon_7 - \varepsilon_8 + \varepsilon_9 - \varepsilon_{10} - \varepsilon_{11} + \varepsilon_{12} + \varepsilon_{13} - \varepsilon_{14} - \varepsilon_{15} + \varepsilon_{16} + \varepsilon_{17} - \varepsilon_{18} - \varepsilon_{19} + \varepsilon_{20} + \varepsilon_{21} - \varepsilon_{22} - \varepsilon_{23} + \varepsilon_{24} \}$	A ₂
S_8	$\frac{1}{\sqrt{24}} \{ -r_1 - r_2 + 2r_3 + 2r_4 - r_5 - r_6 - r_7 - r_8 - r_9 - r_{10} + 2r_{11} + 2r_{12} \}$	E(a)

(Table continued on next page)

Table 25 continued

Coordinate Number	Description	Symmetry
s_9	$\frac{1}{\sqrt{24}}$ $\{-\alpha_1 - \alpha_2 + 2\alpha_3 + 2\alpha_4 - \alpha_5 + 2\alpha_7 + 2\alpha_7 - \alpha_8 - \alpha_9 - \alpha_{10} + 2\alpha_{11} - \alpha_{12}\}$	$E(a)$
s_{10}	$\frac{1}{\sqrt{12}}$ $\{2\beta_1 - \beta_2 - \beta_3 + 2\beta_4 - \beta_5 - \beta_6\}$	$E(a)$
s_{11}	$\frac{1}{\sqrt{24}}$ $\{-s_1 - s_2 + 2s_3 + 2s_4 - s_5 - s_6 - s_7 - s_8 - s_9 - s_{10} + 2s_{11} + 2s_{12}\}$	$E(a)$
s_{12}	$\frac{1}{\sqrt{12}}$ $\{2\gamma_1 - \gamma_2 - \gamma_3 + 2\gamma_4 - \gamma_5 - \gamma_6\}$	$E(a)$
s_{13}	$\frac{1}{\sqrt{48}}$ $\{-\varepsilon_1 - \varepsilon_2 - \varepsilon_3 - \varepsilon_4 + 2\varepsilon_5 + 2\varepsilon_6 + 2\varepsilon_7 + \varepsilon_8 - \varepsilon_9 - \varepsilon_{10} - \varepsilon_{11} - \varepsilon_{12}$ $+ 2\varepsilon_{13} + 2\varepsilon_{14} + 2\varepsilon_{15} + 2\varepsilon_{16} - \varepsilon_{17} - \varepsilon_{18} - \varepsilon_{19} - \varepsilon_{20} - \varepsilon_{21} - \varepsilon_{22} - \varepsilon_{23} - \varepsilon_{24}\}$	$E(a)$
s_{14}	$\frac{1}{4}$ $\{\varepsilon_1 - \varepsilon_2 - \varepsilon_3 + \varepsilon_4 - \varepsilon_9 + \varepsilon_{10} + \varepsilon_{11} - \varepsilon_{12} + \varepsilon_{17} - \varepsilon_{18} - \varepsilon_{19} + \varepsilon_{20} - \varepsilon_{21} +$ $\varepsilon_{22} + \varepsilon_{23} - \varepsilon_{24}\}$	$E(a)$
s_{15}	$\frac{1}{\sqrt{8}}$ $\{-r_1 + r_2 + r_5 - r_6 + r_7 + r_8 - r_9 - r_{10}\}$	$E(b)$
s_{16}	$\frac{1}{\sqrt{8}}$ $\{-\alpha_1 + \alpha_2 - \alpha_5 + \alpha_6 + \alpha_8 - \alpha_9 + \alpha_{10} - \alpha_{12}\}$	$E(b)$
s_{17}	$\frac{1}{2}$ $\{\beta_2 - \beta_3 + \beta_5 - \beta_6\}$	$E(b)$

(Table continued on next page)

Table 25 continued

Coordinate Number	Description	Symmetry
s_{18}	$\frac{1}{\sqrt{8}}$ $\{s_1 + s_2 - s_5 - s_6 - s_7 - s_8 + s_9 + s_{10}\}$	E(b)
s_{19}	$\frac{1}{2}$ $\{\gamma_2 - \gamma_3 + \gamma_5 - \gamma_6\}$	E(b)
s_{20}	$\frac{1}{4}$ $\{\varepsilon_1 + \varepsilon_2 + \varepsilon_3 + \varepsilon_4 - \varepsilon_9 - \varepsilon_{10} - \varepsilon_{11} - \varepsilon_{12} + \varepsilon_{17} + \varepsilon_{18} + \varepsilon_{19} + \varepsilon_{20}$ $- \varepsilon_{21} - \varepsilon_{22} - \varepsilon_{23} - \varepsilon_{24}\}$	E(b)
s_{21}	$\frac{1}{\sqrt{48}}$ $\{-\varepsilon_1 + \varepsilon_2 + \varepsilon_3 - \varepsilon_4 - 2\varepsilon_5 + 2\varepsilon_6 + 2\varepsilon_7 - 2\varepsilon_8 - \varepsilon_9 + \varepsilon_{10} + \varepsilon_{11} + 2\varepsilon_{13} -$ $2\varepsilon_{14} - 2\varepsilon_{15} + 2\varepsilon_{16} - \varepsilon_{17} + \varepsilon_{18} + \varepsilon_{19} - \varepsilon_{20} - \varepsilon_{21} + \varepsilon_{22} + \varepsilon_{23} - \varepsilon_{24}\}$	E(b)
s_{22}	$\frac{1}{4}$ $\{-r_1 + r_2 - r_5 + r_6 + r_7 - r_8 + r_9 - r_{10} + 2r_{11} - 2r_{12}\}$	F ₁ (a)
s_{23}	$\frac{1}{4}$ $\{-\alpha_1 - \alpha_2 + 2\alpha_3 - \alpha_5 + \alpha_6 - 2\alpha_7 + \alpha_8 + \alpha_9 - \alpha_{10} + \alpha_{12}\}$	F ₁ (a)
s_{24}	$\frac{1}{4}$ $\{s_1 - s_2 - 2s_3 + 2s_4 + s_5 - s_6 + s_7 - s_8 + s_9 - s_{10}\}$	F ₁ (a)
s_{25}	$\frac{1}{4}$ $\{\varepsilon_1 - \varepsilon_2 - \varepsilon_3 + \varepsilon_4 + \varepsilon_9 - \varepsilon_{10} - \varepsilon_{11} + \varepsilon_{12} - \varepsilon_{17} + \varepsilon_{18} + \varepsilon_{19} - \varepsilon_{20} -$ $\varepsilon_{21} + \varepsilon_{22} + \varepsilon_{23} - \varepsilon_{24}\}$	F ₁ (a)

(Table continued on next page)

Table 25 continued

Coordinate Number	Description	Symmetry
S_{26}	$\frac{1}{\sqrt{32}}$ $\{-\varepsilon_1 - \varepsilon_2 + \varepsilon_3 + \varepsilon_4 + \varepsilon_9 + \varepsilon_{10} - \varepsilon_{11} - \varepsilon_{12} - 2\varepsilon_{13} - 2\varepsilon_{14} + 2\varepsilon_{15} + 2\varepsilon_{16}$ $- \varepsilon_{17} - \varepsilon_{18} + \varepsilon_{19} + \varepsilon_{20} + \varepsilon_{21} + \varepsilon_{22} - \varepsilon_{23} - \varepsilon_{24}\}$	$F_1(a)$
S_{27}	$\frac{1}{\sqrt{32}}$ $\{-\varepsilon_1 + \varepsilon_2 - \varepsilon_3 + \varepsilon_4 + 2\varepsilon_5 - 2\varepsilon_6 + 2\varepsilon_7 - 2\varepsilon_8 - \varepsilon_9 + \varepsilon_{10} - \varepsilon_{11} + \varepsilon_{12}$ $- \varepsilon_{17} + \varepsilon_{18} - \varepsilon_{19} + \varepsilon_{20} - \varepsilon_{21} + \varepsilon_{22} - \varepsilon_{23} + \varepsilon_{24}\}$	$F_1(a)$
S_{28}	$\frac{1}{\sqrt{52}}$ $\{-r_1 + 3r_2 - 2r_3 + 2r_4 - 3r_5 + r_6 - r_7 + r_8 - 3r_9 + 3r_{10}\}$	$F_1(b)$
S_{29}	$\frac{1}{\sqrt{48}}$ $\{-3\alpha_1 + 3\alpha_2 + 2\alpha_4 + \alpha_5 - 3\alpha_6 + \alpha_8 - \alpha_{10} - 2\alpha_{11} + 3\alpha_{12}\}$	$F_1(b)$
S_{30}	$\frac{1}{\sqrt{48}}$ $\{3s_1 - 3s_2 + s_5 - s_6 - 3s_7 + 3s_8 - s_9 + s_{10} - 2s_{11} + 2s_{12}\}$	$F_1(b)$
S_{31}	$\frac{1}{\sqrt{48}}$ $\{-\varepsilon_1 + \varepsilon_2 + \varepsilon_3 - \varepsilon_4 - 2\varepsilon_5 + 2\varepsilon_6 + 2\varepsilon_7 - 2\varepsilon_8 + \varepsilon_9 - \varepsilon_{10} - \varepsilon_{11} + \varepsilon_{12} - 2\varepsilon_{13}$ $+ 2\varepsilon_{14} + 2\varepsilon_{15} - 2\varepsilon_{16} + \varepsilon_{17} - \varepsilon_{18} - \varepsilon_{19} + \varepsilon_{20} - \varepsilon_{21} + \varepsilon_{22} + \varepsilon_{23} - \varepsilon_{24}\}$	$F_1(b)$

(Table continued on next page)

Table 25 continued

Coordinate Number	Description	Symmetry
S_{32}	$\frac{1}{\sqrt{96}}$ $\{\varepsilon_1 + \varepsilon_2 - \varepsilon_3 - \varepsilon_4 + 2\varepsilon_5 + 2\varepsilon_6 - 2\varepsilon_7 - 2\varepsilon_8 - 3\varepsilon_9 - 3\varepsilon_{10} + 3\varepsilon_{11} + 3\varepsilon_{12} - 3\varepsilon_{17}\}$ $-3\varepsilon_{18} + 3\varepsilon_{19} + 3\varepsilon_{20} + \varepsilon_{21} + \varepsilon_{22} - \varepsilon_{23} - \varepsilon_{24}\}$	$F_1(b)$
S_{33}	$\frac{1}{\sqrt{96}}$ $\{3\varepsilon_1 - 3\varepsilon_2 + 3\varepsilon_3 - 3\varepsilon_4 + \varepsilon_9 - \varepsilon_{10} + \varepsilon_{11} - \varepsilon_{12} - 2\varepsilon_{13} + 2\varepsilon_{14} - 2\varepsilon_{15}$ $+ 2\varepsilon_{16} - \varepsilon_{17} + \varepsilon_{18} - \varepsilon_{19} + \varepsilon_{20} - 3\varepsilon_{21} + 3\varepsilon_{22} - 3\varepsilon_{23} + 3\varepsilon_{24}\}$	$F_1(b)$
S_{34}	$\frac{1}{\sqrt{6}}$ $\{-\mathbf{r}_1 + \mathbf{r}_3 - \mathbf{r}_4 + \mathbf{r}_6 - \mathbf{r}_7 + \mathbf{r}_8\}$	$F_1(c)$
S_{35}	$\frac{1}{\sqrt{6}}$ $\{-\alpha_4 + \alpha_5 + \alpha_8 - \alpha_9 - \alpha_{10} + \alpha_{11}\}$	$F_1(c)$
S_{36}	$\frac{1}{\sqrt{6}}$ $\{\mathbf{s}_5 - \mathbf{s}_6 - \mathbf{s}_9 + \mathbf{s}_{10} + \mathbf{s}_{11} - \mathbf{s}_{12}\}$	$F_1(c)$
S_{37}	$\frac{1}{\sqrt{24}}$ $\{-\varepsilon_1 + \varepsilon_2 + \varepsilon_3 - \varepsilon_4 + \varepsilon_5 - \varepsilon_6 - \varepsilon_7 + \varepsilon_8 + \varepsilon_9 - \varepsilon_{10} - \varepsilon_{11} + \varepsilon_{12} + \varepsilon_{13}$ $- \varepsilon_{14} - \varepsilon_{15} + \varepsilon_{16} + \varepsilon_{17} - \varepsilon_{18} - \varepsilon_{19} + \varepsilon_{20} - \varepsilon_{21} + \varepsilon_{22} + \varepsilon_{23} - \varepsilon_{24}\}$	$F_1(c)$
S_{38}	$\frac{1}{\sqrt{12}}$ $\{\varepsilon_1 + \varepsilon_2 - \varepsilon_3 - \varepsilon_4 - \varepsilon_5 - \varepsilon_6 + \varepsilon_7 + \varepsilon_8 + \varepsilon_{21} + \varepsilon_{22} - \varepsilon_{23} - \varepsilon_{24}\}$	$F_1(c)$

(Table continued on next page)

Table 25 continued

Coordinate Number	Description	Symmetry
S ₃₉	$\frac{1}{\sqrt{12}}$ $\{\epsilon_9 - \epsilon_{10} + \epsilon_{11} - \epsilon_{12} + \epsilon_{13} - \epsilon_{14} + \epsilon_{15} - \epsilon_{16} - \epsilon_{17} + \epsilon_{18} - \epsilon_{19} + \epsilon_{20}\}$	$F_1(c)$
S ₄₀	$\frac{1}{\sqrt{12}}$ $\{-r_1 - r_2 + r_3 + r_4 - r_5 - r_6 + r_7 + r_8 + r_9 + r_{10} - r_{11} - r_{12}\}$	$F_2(a_-)$
S ₄₁	$\frac{1}{\sqrt{12}}$ $\{-\alpha_1 + \alpha_2 - \alpha_3 + \alpha_4 + \alpha_5 + \alpha_6 - \alpha_7 - \alpha_8 + \alpha_9 - \alpha_{10} + \alpha_{11} - \alpha_{12}\}$	$F_2(a)$
S ₄₂	$\frac{1}{\sqrt{6}}$ $\{\beta_1 + \beta_2 + \beta_3 - \beta_4 - \beta_5 - \beta_6\}$	$F_2(a)$
S ₄₃	$\frac{1}{\sqrt{6}}$ $\{-r_3 + r_4 - r_7 + r_8 + r_9 - r_{10}\}$	$F_2(a)$
S ₄₄	$\frac{1}{\sqrt{6}}$ $\{-\alpha_2 + \alpha_4 + \alpha_5 + \alpha_6 - \alpha_9 - \alpha_{11}\}$	$F_2(a)$
S ₄₅	$\frac{1}{\sqrt{12}}$ $\{-s_1 - s_2 - s_3 - s_4 - s_5 - s_6 + s_7 + s_8 + s_9 + s_{10} + s_{11} + s_{12}\}$	$F_2(a)$
S ₄₆	$\frac{1}{\sqrt{6}}$ $\{s_7 - s_8 - s_9 + s_{10} - s_{11} + s_{12}\}$	$F_2(a)$
S ₄₇	$\frac{1}{\sqrt{6}}$ $\{-\gamma_1 - \gamma_2 - \gamma_3 + \gamma_4 + \gamma_5 + \gamma_6\}$	$F_2(a)$

(Table continued on next page)

Table 25 continued

Coordinate Number	Description	Symmetry
S_{48}	$\frac{1}{\sqrt{24}}$ $\{-\varepsilon_1 - \varepsilon_2 - \varepsilon_3 - \varepsilon_4 - \varepsilon_5 - \varepsilon_6 - \varepsilon_7 - \varepsilon_8 - \varepsilon_9 - \varepsilon_{10} - \varepsilon_{11} - \varepsilon_{12} + \varepsilon_{13}$ $+ \varepsilon_{14} + \varepsilon_{15} + \varepsilon_{16} + \varepsilon_{17} + \varepsilon_{18} + \varepsilon_{19} + \varepsilon_{20} + \varepsilon_{21} + \varepsilon_{22} + \varepsilon_{23} + \varepsilon_{24}\}$	$F_2(a)$
S_{49}	$\frac{1}{\sqrt{12}}$ $\{\varepsilon_1 + \varepsilon_2 - \varepsilon_3 - \varepsilon_4 + \varepsilon_5 + \varepsilon_6 - \varepsilon_7 - \varepsilon_8 + \varepsilon_9 + \varepsilon_{10} - \varepsilon_{11} - \varepsilon_{12}\}$	$F_2(a)$
S_{50}	$\frac{1}{\sqrt{12}}$ $\{\varepsilon_{13} - \varepsilon_{14} + \varepsilon_{15} - \varepsilon_{16} + \varepsilon_{17} - \varepsilon_{18} + \varepsilon_{19} - \varepsilon_{20} - \varepsilon_{21} + \varepsilon_{22} - \varepsilon_{23} + \varepsilon_{24}\}$	$F_2(a)$
S_{51}	$\frac{1}{\sqrt{24}}$ $\{r_1 + r_2 + 2r_3 + 2r_4 + r_5 + r_6 - r_7 - r_8 - r_9 - r_{10} - 2r_{11} - 2r_{12}\}$	$F_2(b)$
S_{52}	$\frac{1}{\sqrt{24}}$ $\{\alpha_1 - \alpha_2 - 2\alpha_3 + 2\alpha_4 - \alpha_5 - \alpha_6 - 2\alpha_7 + \alpha_8 - \alpha_9 + \alpha_{10} + 2\alpha_{11} + \alpha_{12}\}$	$F_2(b)$
S_{53}	$\frac{1}{\sqrt{12}}$ $\{2\beta_1 - \beta_2 - \beta_3 - 2\beta_4 + \beta_5 + \beta_6\}$	$F_2(b)$
S_{54}	$\frac{1}{\sqrt{48}}$ $\{-3r_1 - 3r_2 - 2r_3 + 2r_4 + 3r_5 + 3r_6 + r_7 - r_8 - r_9 + r_{10}\}$	$F_2(b)$
S_{55}	$\frac{1}{\sqrt{48}}$ $\{3\alpha_1 + \alpha_2 + 2\alpha_4 - \alpha_5 - \alpha_6 + 3\alpha_8 + \alpha_9 - 3\alpha_{10} - 2\alpha_{11} - 3\alpha_{12}\}$	$F_2(b)$

(Table continued on next page)

Table 25 continued

Coordinate Number	Description	Symmetry
S_{56}	$\frac{1}{\sqrt{24}}$ $\{s_1 + s_2 - 2s_3 - 2s_4 + s_5 + s_6 - s_7 - s_8 - s_9 - s_{10} + 2s_{11} + 2s_{12}\}$	$F_2(b)$
S_{57}	$\frac{1}{\sqrt{48}}$ $\{-3s_1 + 3s_2 + 3s_5 - 3s_6 - s_7 + s_8 + s_9 - s_{10} - 2s_{11} + 2s_{12}\}$	$F_2(b)$
S_{58}	$\frac{1}{\sqrt{12}}$ $\{-2\gamma_1 + \gamma_2 + \gamma_3 + 2\gamma_4 - \gamma_5 - \gamma_6\}$	$F_2(b)$
S_{59}	$\frac{1}{\sqrt{48}}$ $\{\varepsilon_1 + \varepsilon_2 + \varepsilon_3 + \varepsilon_4 - 2\varepsilon_5 - 2\varepsilon_6 - 2\varepsilon_7 - 2\varepsilon_8 + \varepsilon_9 + \varepsilon_{10} + \varepsilon_{11} + \varepsilon_{12} + 2\varepsilon_{13}$ $- 2\varepsilon_{14} + 2\varepsilon_{15} + 2\varepsilon_{16} - \varepsilon_{17} - \varepsilon_{18} - \varepsilon_{19} - \varepsilon_{20} - \varepsilon_{21} - \varepsilon_{22} - \varepsilon_{23} - \varepsilon_{24}\}$ $\{-\varepsilon_1 - \varepsilon_2 + \varepsilon_3 + \varepsilon_4 + 2\varepsilon_5 + 2\varepsilon_6 - 2\varepsilon_7 - 2\varepsilon_8 - \varepsilon_9 - \varepsilon_{10} + \varepsilon_{11} + \varepsilon_{12} + 3\varepsilon_{17}$ $+ 3\varepsilon_{18} - 3\varepsilon_{19} - 3\varepsilon_{20} + 3\varepsilon_{21} + 3\varepsilon_{22} - 3\varepsilon_{23} - 3\varepsilon_{24}\}$	$F_2(b)$
S_{60}	$\frac{1}{\sqrt{96}}$	
S_{61}	$\frac{1}{\sqrt{8}}$ $\{3\varepsilon_1 - 3\varepsilon_2 + 3\varepsilon_3 - 3\varepsilon_4 - 3\varepsilon_9 + 3\varepsilon_{10} - 3\varepsilon_{11} + 3\varepsilon_{12} + 2\varepsilon_{13} - 2\varepsilon_{14}$ $+ 2\varepsilon_{15} - 2\varepsilon_{16} - \varepsilon_{17} + \varepsilon_{18} - \varepsilon_{19} + \varepsilon_{20} + \varepsilon_{21} - \varepsilon_{22} + \varepsilon_{23} - \varepsilon_{24}\}$ $\{r_1 - r_2 - r_5 + r_6 + r_7 + r_8 - r_9 - r_{10}\}$	$F_2(b)$ $F_2(c)$
S_{62}	$\frac{1}{\sqrt{8}}$	
S_{63}	$\frac{1}{\sqrt{8}}$ $\{-\alpha_1 - \alpha_2 + \alpha_5 - \alpha_6 + \alpha_8 + \alpha_9 + \alpha_{10} - \alpha_{12}\}$	$F_2(c)$

(Table continued on next page)

Table 25 continued

Coordinate Number	Description	Symmetry
s_{64}	$\{\beta_2 - \beta_3 - \beta_5 + \beta_6\}$	$F_2(c)$
s_{65}	$\{r_1 - r_2 + r_5 - r_6 - r_7 + r_8 - r_9 + r_{10} + r_{11} - 2r_{12}\}$	$F_2(c)$
s_{66}	$\{\alpha_1 + \alpha_2 + 2\alpha_3 + \alpha_5 - \alpha_6 - 2\alpha_7 - \alpha_8 - \alpha_9 + \alpha_{10} - \alpha_{12}\}$	$F_2(c)$
s_{67}	$\{-s_1 - s_2 + s_5 + s_6 - s_7 - s_8 + s_9 + s_{10}\}$	$F_2(c)$
s_{68}	$\{-s_1 + s_2 - 2s_3 + 2s_4 - s_5 + s_6 - s_7 + s_8 - s_9 + s_{10}\}$	$F_2(c)$
s_{69}	$\{-\gamma_2 + \gamma_3 + \gamma_5 - \gamma_6\}$	$F_2(c)$
s_{70}	$\{-\varepsilon_1 - \varepsilon_2 - \varepsilon_3 - \varepsilon_4 + \varepsilon_9 + \varepsilon_{10} + \varepsilon_{11} + \varepsilon_{12} + \varepsilon_{17} + \varepsilon_{18} + \varepsilon_{19} + \varepsilon_{20} - \varepsilon_{21} - \varepsilon_{23} - \varepsilon_{24}\}$	$F_2(c)$
s_{71}	$\frac{1}{\sqrt{32}} \{ \varepsilon_1 + \varepsilon_2 - \varepsilon_3 - \varepsilon_4 - \varepsilon_9 - \varepsilon_{10} + \varepsilon_{11} + \varepsilon_{12} - 2\varepsilon_{13} - 2\varepsilon_{14} + 2\varepsilon_{15} + 2\varepsilon_{16} + \varepsilon_{17} + \varepsilon_{18} - \varepsilon_{19} - \varepsilon_{20} - \varepsilon_{21} - \varepsilon_{22} + \varepsilon_{23} + \varepsilon_{24} \}$	$F_2(c)$

(Table continued on next page)

Table 25 continued

Coordinate Number	Description	Symmetry
s_{72}	$\frac{1}{\sqrt{32}}$ $\{-\varepsilon_1 + \varepsilon_2 - \varepsilon_3 + \varepsilon_4 - 2\varepsilon_5 + 2\varepsilon_6 - 2\varepsilon_7 + 2\varepsilon_8 - \varepsilon_9 + \varepsilon_{10} - \varepsilon_{11} + \varepsilon_{12}$ $- \varepsilon_{17} + \varepsilon_{18} - \varepsilon_{19} + \varepsilon_{20} - \varepsilon_{21} + \varepsilon_{22} - \varepsilon_{23} + \varepsilon_{24}\}$	$F_2(c)$

(a) In terms of the internal coordinates given in Table 10.

B30057